R. L. Myklebust

ELECTRON PROBE ANALYSIS
SOCIETY of AMERICA

PROCEEDINGS
FOURTH NATIONAL CONFERENCE
on
ELECTRON MICROPROBE ANALYSIS

PASADENA, CALIFORNIA
JULY 16-18, 1969

Additional copies of these Proceedings may be obtained for $5.00 per copy, prepaid, from:

A. A. Chodos
Caltech - Geology
Pasadena, California 91109

Make checks payable to "The Electron Probe Analysis Society of America" or EPASA. Payment must accompany order, we will not invoice.

FOURTH NATIONAL CONFERENCE ON ELECTRON MICROPROBE ANALYSIS

PRESENTED BY

THE ELECTRON PROBE ANALYSIS SOCIETY OF AMERICA

JULY 16 - 18, 1969

HUNTINGTON-SHERATON HOTEL

PASADENA, CALIFORNIA

THE ELECTRON PROBE ANALYSIS SOCIETY OF AMERICA

INCORPORATED ON JANUARY 1, 1968

—NATIONAL OFFICERS - 1969—

PRESIDENT

K. F. J. Henrich
National Bureau of Standards

PRESIDENT-ELECT

R. E. Ogilvie
Massachusetts Institute of Technology

SECRETARY

T. O. Ziebold
Massachusetts Institute of Technology

TREASURER

A. A. Chodos
California Institute of Technology

MEMBERS AT LARGE

H. Yakowitz
National Bureau of Standards

C. A. Andersen
Applied Research Laboratories

John Colby
Bell Telephone Laboratories

THE ELECTRON PROBE ANALYSIS SOCIETY OF AMERICA

—SUSTAINING MEMBERS—

Anaconda American Brass Company
Waterbury, Connecticut

Applied Research Laboratories
Glendale, California

Canberra Industries
Middletown, Connecticut

Consolidated Electrodynamics Corporation
Monrovia, California

Corning Glass Works
Corning, New York

Engis Equipment Company
Morton Grove, Illinois

JEOLCO (U.S.A.), Inc.
Medford, Massachusetts

Materials Analysis Company
Palo Alto, California

Ortec, Inc.
Oak Ridge, Tennessee

Perkin-Elmer Corporation
Norwalk, Connecticut

Philips Electronic Instruments
Mount Vernon, New York

Siemens America, Inc.
New York, New York

FOURTH NATIONAL CONFERENCE ON ELECTRON MICROPROBE ANALYSIS

— INVITED SPEAKERS —

Quantitative Microanalysis

J. HENOC

National Bureau of Standards
Washington, D.C.

Electron Spectroscopy

B. HENKE

University of Hawaii
Honolulu, Hawaii

Chemical Bonding Studies Through X-ray Analysis

E. W. WHITE

Pennsylvania State University
University Park, Pennsylvania

Non-Dispersive Analysis

R. FITZGERALD

University of California
San Diego, California

Scanning Electron Microscopy

T. E. EVERHART

University of California
Berkeley, California

FOURTH NATIONAL CONFERENCE ON ELECTRON MICROPROBE ANALYSIS

— GENERAL PROGRAM —

TUESDAY, July 15, 1969

7:00 p.m.	Registration in the foyer of the Georgian Room until 10:00 p.m.
7:00 p.m.	Exhibits open in the Georgian Room and East Room.

WEDNESDAY, July 16, 1969

8:00 a.m.	Registration in the foyer of the Georgian Room.
	All Technical Presentations will be held in the Viennese Room.
8:30 a.m.	Welcome by D. B. Wittry, Conference Chairman.
8:35 a.m.	Opening address by EPASA President, K. F. J. Heinrich.
8:45 a.m.	Invited paper by J. Henoc.
9:35 a.m.	Technical session: Quantitative Electron Probe Microanalysis I.
1:25 p.m.	Technical session: Quantitative Electron Probe Microanalysis II.
5:00 p.m.	EPASA Business meeting: K. F. J. Heinrich presiding.
6:30 p.m.	Reception on the Pool Terrace.

THURSDAY, July 17, 1969

TECHNICAL SESSION A - San Marino Room
TECHNICAL SESSION B - Viennese Room

8:45 a.m.	Invited paper by B. L. Henke - Viennese Room.
9:35 a.m.	Technical session A: New Methods and Instrumentation I.
9:35 a.m.	Technical session B: New Methods and Instrumentation II.
10:30 a.m.	Technical session A: Solid State Materials.
1:15 p.m.	Invited paper by E. White - Viennese Room.
2:05 p.m.	Technical session A: Geological Applications.
2:05 p.m.	Technical session B: Metallurgical Applications.
3:40 p.m.	Technical session A: Biological Applications.
7:30 p.m.	Banquet at the Pool.

FRIDAY, July 18, 1969

All Technical Presentations will be held in the Viennese Room.

8:45 a.m.	Invited paper by R. Fitzgerald.
9:35 a.m.	Technical session: New Methods and Instrumentation III.
1:15 p.m.	Invited paper by T. E. Everhart.
2:05 p.m.	Technical session: Scanning Electron Microscopy.
3:40 p.m.	Technical session: New Methods and Instrumentation IV.
5:40 p.m.	Conference closing.

PREFACE

The success of a technical conference can depend either on the hard work of a few key people or on the collective efforts of many people. In the present case, we have been fortunate in having both factors working toward a successful meeting. A large number of "microprobers" in Southern California contributed to organizing the program and the exhibits. The Program Chairman, C. A. Andersen, and Exhibits Chairman, E. L. Miller, put in some long hours at critical times during the planning.

Particular mention must be made of the tireless efforts of the Arrangements Chairman, A. A. Chodos. He not only handled arrangements, but served on the program committee, coordinated the exhibits, served as conference secretary, conference treasurer, proceedings chairman, and often as conference typist. It is largely due to Art's willingness to tackle unpleasant and time consuming jobs that the organization of this meeting proceeded very smoothly.

Acknowledgement must also be made to the organizers of previous conferences, particularly D. R. Beaman, and to the Executive Council of the Electron Probe Analysis Society for advice and suggestions.

It was very gratifying that the financial support provided by exhibitors was even greater this year than in previous years. Without this support, it would not have been possible to maintain the same registration fee.

Finally, acknowledgment should be made to the authors of the contributed and invited papers which have made it possible to plan what we hope will be an outstanding technical program.

David B. Wittry
General Chairman

FOURTH NATIONAL CONFERENCE ON ELECTRON MICROPROBE ANALYSIS

—CONFERENCE ORGANIZERS—

GENERAL CHAIRMAN . . . . . D. B. Wittry, University of Southern California

ARRANGEMENTS CHAIRMAN . . A. A. Chodos, California Institute of Technology

PROGRAM CHAIRMAN . . . . . C. A. Andersen, Applied Research Laboratories

Program	C. A. Andersen, Chairman E. Wolf, T. West, R. Fitzgerald, A. Baird, A. Chodos, W. Robison, D. Wittry
Exhibitors	E. Miller, Chairman J. Moskal, J. Shaffer, W. Shequen
Audio Visual	J. Nicholson, Chairman R. Jones
Registration	R. Jones, Chairman R. Nolder, L. Cooper, L. Moudy, J. Ogren, J. Donner, A. VanCouvering
Publicity & Entertainment	R. Abelmann, Chairman L. Cooper, R. Herfert
Ladies Program	L. Moudy, Chairman Mrs. D. Wittry, Mrs. E. Davidson, Mrs. A. Chodos

FOURTH NATIONAL CONFERENCE ON ELECTRON MICROPROBE ANALYSIS

—PROGRAM—

TUESDAY, JULY 15

1:30 PM Executive Council of the Electron Probe Analysis Society of America meets in Parlor 237.

7:00 PM Registration begins in the foyer to the Georgian Room. Registration will continue until 10:00 PM.

7:00 PM Exhibits will open in the Georgian Room and the East Room.

WEDNESDAY, JULY 16

8:00 AM Registration in the foyer to the Georgian Room.

All Technical Presentations will be held in the Viennese Room.

8:30 AM Welcome by D. B. Wittry, Conference Chairman.

8:35 AM Opening address by K. F. J. Heinrich, President of the Electron Probe Analysis Society of America.

TECHNICAL SESSION

Quantitative Electron Probe Microanalysis I.
K. F. J. Heinrich, Chairman

8:45 AM INVITED PAPER. Quantitative Microanalysis; J. Henoc.

1 9:35 AM Mass Absorption Coefficients for Au, Pb and Bi; J. B. Woodhouse.

2 9:55 AM Measurement of the X-Ray Continuum from Thick Targets; T. S. Rao-Sahib and D. B. Wittry.

10:15 AM Coffee Break

3 10:30 AM Measurement and Calculation of Absolute X-Ray Intensities: The Effect of K and L Cross Sections; D. B. Brown and J. V. Gilfrich.

4 10:50 AM Density Effect of X-Ray Emission for Porous Specimens; T. Ichinokawa.

5 11:10 AM Depth Distribution of Fe-Al Characteristic X-Rays in EPMA Targets of Fe-Al Alloys; R. Shimizu, K. Murata and M. Fujiwara.

6	11:30 AM	Depth Distribution of Cu and Au Characteristic X-Rays in Inclined EPMA Targets of Au-Cu Alloy; R. Shimizu, K. Murata and N. Gennai.
7	11:50 AM	Effect of Electron Bombardment on the Microscopical Structure of Target Materials; G. Shinoda, M. Seki and M. Kita.
	12:10	Lunch - Authors, invited speakers and session chairmen.

TECHNICAL SESSION

Quantitative Electron Probe Microanalysis II.
D. B. Wittry, Chairman

8	1:25 PM	The Influence of Target Absorption on the Reliability of Quantitative Chemical Analysis; V. G. Macres.
9	1:45 PM	The Effect of Electron Beam Angle of Incidence in Quantitative Microprobe Analysis; J. W. Colby, D. R. Wonsidler and D. K. Conley.
10	2:05 PM	Absorption Correction by the Use of Dual Take-Off Angle Spectrometers; P. S. Ong.
11	2:25 PM	Continuum Fluorescence: Is It Important?; J. D. Brown.
12	2:45 PM	Atomic Number Correction Uncertainty; K. F. J. Heinrich and H. Yakowitz.
13	3:05 PM	The Source and Nature of Deadtime in Electron Microprobe Analysis; D. R. Beaman, J. A. Isasi, and R. Lewis.
	3:25 PM	Coffee Break.
14	3:40 PM	Quantitative Analysis of Oxygen in Oxides; T. Shiraiwa and N. Fujino.
15	4:00 PM	Standard Reference Materials for Quantitative Electron Probe Microanalysis; K. F. J. Heinrich.
16	4:20 PM	A Critical Examination of Computer Programs Used in Quantitative Electron Microprobe Analysis; D. R. Beaman and J. A. Isasi.
17	4:40 PM	An Investigation of the Atomic Number Effect in Cu-Ni Alloys; R. M. Ingersoll, H. R. MacQueen and J. L. Solomon.
	5:00 PM	BUSINESS MEETING

The Electron Probe Analysis Society of America; K. F. J. Heinrich presiding.

6:30 PM RECEPTION

Pool Terrace.

THURSDAY, JULY 17

TECHNICAL SESSIONS A & B

The Invited Paper will be in the Viennese Room as will Session B. Session A will be in the San Marino Room.

8:45 AM INVITED PAPER. Electron Spectroscopy; B. L. Henke.

TECHNICAL SESSION A

New Methods and Instrumentation I.
A. A. Chodos, Chairman

18 9:35 AM Imaging Properties of the Secondary Ion Emission Microanalyzer; R. Lewis and A. Cambey.

19 9:55 AM Analytic Methods for the Ion Microprobe Mass Analyzer, Part II; C. A. Andersen.

10:15 AM Coffee Break.

Solid State Materials
D. Kyser, Chairman

20 10:30 AM Electron Beam Modulated Optical Properties of Semiconductors; J. H. McCoy and D. B. Wittry.

21 10:50 AM Analysis of $GaAs_xP_{1-x}$ Grown from Ga-GaAs-GaP Ternary System: Quantitative Correction and Solid Solubility Isotherms; C. K. Kim.

22 11:10 AM Effect of Substrate Condition on the Nucleation and Growth of TbGe Films; M. A. Wilkov and W. D. Stewart.

23 11:30 AM Quantitative Analysis of Ternary and Quaternary Semiconducting Alloys; M. C. Finn.

24 11:50 AM The Use of an Interactive Computing System in Quantitative Electron Microprobe Spectroscopy; W. Reuter.

12:10 Lunch.

TECHNICAL SESSION B

New Methods and Instrumentation II.
R. E. Ogilvie, Chairman

25 9:35 AM A Computer-Operated Microprobe; M. Bayard.

26 9:55 AM X-Ray Emission Spectra for the Analysis of Insulating Films in the Microprobe Analyzer; J. W. Colby, D. R. Wonsidler and A. Andreshuck.

10:15 AM Coffee Break.

27 10:30 AM A Small Computerized On-Line Data Gathering System for the Electron Microprobe; F. D. Ingram.

28 10:50 AM MANIP: A Computer Program for Processing X-Ray Intensity Data on Punched Paper Tape from the Electron Probe Microanalyzer; G. L. Fisher and W. G. Wickersty, Jr.

29 11:10 AM Spatial Concentration Display and Mapping; J. L. Solomon.

30 11:30 AM Technique for In-Situ Characterization of Surface Scales; C. J. Spengler.

31 11:50 AM Automated Stepping System for Carbon Analysis; J. S. Duerr, J. Adario and R. E. Ogilvie.

12:10 AM Lunch.

TECHNICAL SESSIONS A & B

The Invited Paper will be in the Viennese Room as will Session B. Session A will be in the San Marino Room.

1:15 PM INVITED PAPER. Chemical Bonding Studies through X-Ray Analysis; E. White.

TECHNICAL SESSION A

Geological Applications
K. Keil, Chairman

32 2:05 PM Semiquantitative Electron Microprobe Determination of Fe^{+2}/Fe^{+3} and Mn^{+2}/Mn^{+3} in Oxides and Silicates and its Application to Petrologic Problems; A. L. Albee and A. A. Chodos.

33 2:25 PM Quantitative Procedure in Electron Probe Analysis of Silicate Series; R. Coy-yll and J. Soudiere.

34 2:45 PM Characterisation of Pyroclastic Units - a Stratigraphic Application of the Microprobe; D. G. W. Smith, J. A. Westgate and M. C. Tomlinson.

35 3:05 PM Mineral Inclusions and Microstructure of Carbonado Diamond; L. F. Trueb and C. G. Henderson.

3:25 PM Coffee Break.

Biological Applications
W. L. Robison, Chairman

36 3:40 PM Study of Distribution of Diffusible Ions in Biological Tissues Using a Secondary Ion Emission Micro-Analyzer; P. Galle, G. Blaise and G. Slodzian.

37 4:00 PM Electron Microprobe Analysis of Thyroidal Iodine in the White-Throated Sparrow; D. C. Zeigler, W. H. Zeigler, J. E. Harclerode and E. W. White.

38 4:20 PM The Distribution of Strontium in the Rat Femur as Determined by Electron Microprobe Analysis; A. R. Johnson.

39 4:40 PM Electron Micro-probe Analysis and Scanning Electron Microscopy of Human Teeth; J. D. Eick, W. A. Miller, M. E. Neiders, J. W. Leitner and C. H. Anderson.

40 5:00 PM Scanning Electron Microscopy of Dental Caries Enzymatically Simulated In-Vitro; S. N. Kreitzman, A. J. Saffir, R. S. Harris and R. E. Ogilvie.

6:30 PM Bar facilities open in the Pool area.

7:30 PM BANQUET

TECHNICAL SESSION B

Metallurgical Applications
T. O. Ziebold, Chairman

41 2:05 PM Microprobe Measurements of the Direct Field Force on Impurity Atoms in Metals; T. Hehenkamp.

42 2:25 PM Microprobe Analysis of Diffusion in Thin Bi-Metal Films of Au-Cu; E. I. Alessandrini and J. D. Kuptsis.

43 2:45 PM Electronprobe Microanalysis of Cylindrical Electrodeposited Magnetic Films; A. Baltz.

44 3:05 PM Electron Microprobe Analysis of the Ternary Alloy System Fe-Ni-P; A. S. Doan, Jr. and J. I. Goldstein.

3:25 PM Coffee Break.

45 3:40 PM Equilibrium Phase Studies in Fast-Reactor Fuel Alloys; D. R. O'Boyle, D. E. Busch and J. E. Sanecki.

46 4:00 PM Microanalysis of Highly Radioactive Reactor Fuels; R. Natesh, B. J. Koprowski and E. M. Butler.

47 4:20 PM Diffusion Behavior in Uranium-Plutonium Oxide Fuel Irradiated in a Fast Neutron Flux; R. Natesh, D. R. O'Boyle and E. M. Butler.

48 4:40 PM Combined Scanning Electron Microscopy and X-Ray Microanalysis in Metallurgical Nuclear Applications; L. Meny and M. Champigny.

49 5:00 PM Scanning Electron Microscopy of Spall Fracture in Armco Iron; F. I. Grace and J. V. Foltz.

50 5:20 PM Microprobe Analysis of Light Elements in Multi-Phase Alloys; G. W. Bruno and S. H. Moll.

FRIDAY, JULY 18

All Technical Presentations will be held in the Viennese Room.

TECHNICAL SESSION

New Methods and Instrumentation III.
L. S. Birks, Chairman

8:45 AM INVITED PAPER. Non-Dispersive X-Ray Analysis; R. Fitzgerald.

51 9:35 AM An Evaluation of a Solid-State X-Ray Detection System for Microprobe Analysis; E. Lifshin.

52 9:55 AM Qualitative and Semi-Quantitative Analysis with Non-Dispersive X-Ray Detectors; R. L. Myklebust and K. F. J. Heinrich.

10:15 AM Coffee Break.

53 10:30 AM Simultaneous Multi-Element Analysis with a Single X-Ray Spectrometer; A. J. Saffir, R. E. Ogilvie, R. S. Harris.

54 10:50 AM Selection of Optimum Pulse Height Analysis Window; L. V. Sutfin, R. E. Ogilvie and R. S. Harris.

55 11:10 AM Characteristics of Multilayer Soap Films Depending on the Number of Layers; S. Kimoto, H. Hashimoto and I. Ando.

56 11:30 AM Small Angle X-Ray Reflection; L. Marton.

57 11:50 AM A Geometric Method for the Location of the Center of Kossel Patterns; W. D. Donnelly.

12:10 PM Lunch.

TECHNICAL SESSION

Scanning Electron Microscopy
E. D. Wolf, Chairman

1:15 PM INVITED PAPER. Scanning Electron Microscopy; T. E. Everhart.

58 2:05 PM The Scanning Electron Microscopy of Periodic Ultrasonic Fields; R. S. Gvosdover, G. V. Spivak, A. E. Lukianov, M. V. Bicov and G. V. Saparin,

59 2:25 PM Scanning Electron Microscopy of Crystallographic Defects in Silicon; E. K. Brandis and G. H. Schwuttke.

60 2:45 PM Specimen Heating Device for Scanning Electron Microscope; S. Kimoto, H. Hashimoto, T. Kosuge and A. Mogami.

61 3:05 PM Computer Controlled Scanning Electron Microscope; D. Yankovich, R. E. Ogilvie, R. E. Warren and P. C. Reist.

3:25 PM Coffee Break.

New Methods and Instrumentation IV.
E. D. Wolf, Chairman

62 3:40 PM The Application of Some New Instrumental Techniques to Electron Microprobe Analysis and Scanning Electron Microscopy; J. P. Smith and L. R. Reid.

63 4:00 PM An Electron Spectrometer for the Scanning Electron Microscope; R. E. Ogilvie, J. Adario and G. Sheldon.

64 4:20 PM A High Resolution Electron Microscope with Efficient X-Ray Microanalysis Facilities; C. J. Cooke and I. K. Openshaw.

65 4:40 PM The Observation of High Resolution Electron Images in the Hitachi Electron Probe Microanalyzer; H. Okano, S. Hosoki and T. Tomura.

66 5:00 PM A New Scanning Electron Microscope with X-Ray Micro-Analytical Capability; R. Buchanan and N. Yew.

67 5:20 PM A New Microprobe; P. S. Ong, C. D. Rudd, N. Galetta and A. Juner.

Conference Closes.

SATURDAY, JULY 19

9:00 AM Post mortem meeting of Executive Council, planners of past meetings, planners of 1970 and 1971 meetings and other interested parties. Parlor 237.

FOURTH NATIONAL CONFERENCE ON ELECTRON MICROPROBE ANALYSIS

—LIST OF EXHIBITORS—

Applied Research Laboratories, P.O. Box 129, Sunland, California 91040

Bell & Howell, Consolidated Electrodynamics Corporation, Analytical Instruments Division, 1500 S. Shamrock, Monrovia, California 91016

Canberra Industries, 50 Silver Street, Middletown, Connecticut

Engis Equipment Company, 8035 Austin Avenue, Morton Grove, Illinois 60053

The Harshaw Chemical Company, 1945 East 97th Street, Cleveland, Ohio 44106

Isomet Corporation, 433 Commercial Avenue, Palisades Park, New Jersey 07650

JEOLCO (U.S.A.), Incorporated, 477 Riverside Avenue, Medford, Massachusetts 02155

Kevex Corporation, Nuclear Physics Division, 898 Mahler Road, Burlingame, California 94010

Materials Analysis Company, 1060 East Meadow Circle, Palo Alto, California 94303

Nuclear Diodes, Incorporated, P.O. Box 135, Prairie View, Illinois 60069

Nuclear Equipment Corporation, 931 Terminal Way, San Carlos, California 94070

ORTEC Incorporated, an EG&G Company, 100 Midland Road, Oak Ridge, Tennessee 37830

The Perkin-Elmer Corporation, Norwalk, Connecticut 06852

Philips Electronic Instruments, 750 South Fulton Avenue, Mount Vernon, N.Y. 10550

Siemens America, Incorporated, 350 Fifth Avenue, New York, New York 10001

MEETING

FIFTH NATIONAL CONFERENCE ON ELECTRON PROBE ANALYSIS

This meeting is to be held at the Waldorf-Astoria Hotel, New York, New York (USA) July 22-24, 1970.

The sponsor of the meeting will be the Electron Probe Analysis Society of America.

For general information pertaining to this meeting contact:

Mr. Paul Lublin
General Telephone and Electronics Lab
208-20 Willets Point Boulevard
Bayside, New York 11630

The topics of the technical sessions will include:

Electron Microprobe X-Ray Analysis, Techniques, Methodology, Instrumentation. Principles of Electron Scattering and X-Ray Generation, Quantitative Correction Procedures, Soft X-Ray Emission and Micro-Analysis, Computer Applications to Microprobe data, Kossel Techniques, Scanning Electron Microscopy, New Methods and Instrumentation in Micro-Analysis, Applications.

The number of papers to be presented is estimated to be between 50 to 100. Attendance at the meeting is estimated to be between 400 and 500. There will be no restrictions on attendance.

Contributed papers will be considered and a "call for papers" will be issued through direct mailing and meeting announcements six or eight months in advance of meeting. Everyone is invited to contribute papers. Abstracts must be submitted in English and sent to:

Mr. J. W. Colby
Bell Telephone Labs, Inc.
555 Union Boulevard 22-01041
Allentown, Pennsylvania 18103

Abstracts will be available in the program at the time of the meeting. The abstracts will be printed in English. The papers will not be available.

Exhibitors should contact:

Dr. Gordon Fisher
International Nickel Company
Paul D. Mercia Research Lab.
Suffern, New York 10901

SUMMARIES OF PAPERS

An index of authors and their affiliations follows these papers.

MASS ABSORPTION COEFFICIENTS FOR Au, Pb AND Bi

John B. Woodhouse
University of Illinois, Urbana, Illinois

The experimental determination of mass absorption coefficients for wavelengths from 2Å to 10Å which are reported in the paper were the first new measurements at these wavelenghts since the work of Andrews (1938; Au, 2Å - 10Å)[1] and Schulz (1936; Pb, for wavelengths up to 2Å)[2]. These heavy elements were chosen because it was thought that their low melting points would allow the use of simple apparatus to produce foils suitable for use in the experimental setup of the earlier work of Hughes and his coworkers [3]. The foil thicknesses required for these experiments needed to be about 2 microns. A simple apparatus was evolved for the even deposition of these metals onto a polyester film base. The uniformity was tested by their attenuation of x-ray monochromatic beams, and was found to be about 1% over a few square centimeters, the superficial density by weighing and measuring.

The results of these measurements are compared to the earlier experimental data. There is good agreement with the low wavelength range of Andrews' data; that is, up to the first M edge. Andrews' data from the first to the fifth M edges is rather sparse and the present work supplies a more precise definition of this region. On the long wavelength side of the fifth M edge there is a 10% discrepancy between the old and new measurements, the new ones being the lower.

The results for Pb above 2Å and all those for Bi were new data, never reported previously. The form of these three elements' absorption curves, as outlined by these experiments, indicate that the main changes in absorption occur in the third, fourth, and fifth edges, the first and second edge jumps are relatively small.

---

1. C. L. Andrews, Phys. Rev. 54, 994-999 (1938).

2. K. Schulz, Ann. Phys. 27, 1-14 (1936).

3. G. D. Hughes, J. B. Woodhouse, and I. A. Bucklow, Brit, J. Appl. Phys. (J. Phys. D.) 1, Ser. 2, 695-706 (1968).

MEASUREMENT OF THE X-RAY CONTINUUM FROM THICK TARGETS *

T. S. Rao-Sahib and D. B. Wittry
University of Southern California, Los Angeles, California

According to the theoretical consideratuon by Kramers[1] of the continuous X-ray spectrum produced by electron bombardment of a thick target, the energy between frequencies υ and $\upsilon + d\upsilon$ radiated per electron impact is given by[2]

$$I_\upsilon \, d\upsilon = \frac{8\pi}{3\sqrt{3}\ell} \frac{e^2 h}{mc^3} Z(\upsilon_o - \upsilon) \, d\upsilon \qquad (1)$$

using cgs units. In equation (1) e is the electronic charge, m the electron mass, h is Planck's constant, c is the velocity of light, Z the atomic number of the specimen, $\upsilon_o = V_o e/h$ where V_o is the accelerating voltage, and ℓ is a numerical constant.

Equation (1) was only roughly confirmed by early results using X-ray tubes[3], where the correction for backscattered electrons is not very important, and target absorption corrections could not be made accurately. If the intensity of the X-ray continuum as produced and measured in an electron probe microanalyser is found to verify equation (1) after correction for absorption and atomic number effects, then this would provide additional confidence in the commonly accepted values of mass absorption coefficients and the general procedures for applying corrections to experimentally observed intensities. Such a verification would also provide a means of adjusting the mass absorption coefficient for any element whose corrected X-ray continuum intensity deviates from that predicted by equation (1).

In the present study, an EMX was used, with an X-ray take-off angle of 52.5°. Beam voltage was kept constant at 30 kV, and X-ray intensities were measured at a fixed wavelength of 2.000 Å. This value of wavelength was chosen since it avoided the peaks of the characteristic lines of the elements which were examined. Beam current as measured with a Faraday cage was kept constant at 0.3 μA.

Under these conditions, equation (1) reduces to

$$I_\upsilon \sim Z \qquad (2)$$

Absorption and atomic number effect corrections were made under the following assumptions:

1) The cross-section Q for production of the continuum is independent of the energy of the electrons.

2) The spatial distribution of excitation for the X-ray continuum is the same as for the characteristic X-rays.

3) The mass absorption coefficient is known. (Values of μ/ρ used were those for the Sm $L\beta_1$ line[4] which has a wavelength of 1.998 Å).

---

* Research sponsored by the Air Force Office of Scientific Research, Office of Aerospace Research, United States Air Force, under Grant # AF-AFOSR-68-1414.

4) Duncumb and Shields' voltage dependence of $f(\chi)$[5] is used, with Heinrich's coefficient for voltage[6].

5) The atomic number correction is calculated from equation (10) of Duncumb and Reed[7] using E_k = 6.2 keV (corresponding to λ = 2.000 Å), together with assumption (1) above and Bishop's data[8] for backscatter coefficient η .

6) Background from the instrument due to backscattered electrons or current collected by apertures is negligible.

7) Contributions to the intensity at λ = 2.000 Å due to higher order reflections are negligible.

The results obtained for 17 elements ranging in atomic number from 12 to 83 are shown in figure 1. With the exception of Mn and Fe, the intensities from the remaining elements can be seen to follow equation (2) quite closely. This also confirms the validity of the assumptions made above. The high intensity from Fe may be due to the proximity of the Fe K $\alpha_1\alpha_2$ line which has its peak at 1.9373 Å. No ready explanation can be given for the low intensity from Mn. It may be pointed out, however, that λ = 2.000 Å lies close to the region of the K absorption edge for Mn. As mentioned earlier, the technique suggested by this study might be used to estimate μ/ρ for any particular wavelength. The accuracy of this procedure is limited mainly by assumption (2) and presumably could be improved by independent measurements of $f(\chi)$ for the continuum, for example by Green's method[9].

---

1. H. A. Kramers, Phil. Mag. 46, 836 (1923).

2. A. H. Compton and S. K. Allison, "X-Rays in Theory and Experiment", Van Nostrand Co., New York (1935), p. 105.

3. H. Kulenkampff, Ann. d. Phys. 69, 548 (1922).

4. Mass absorption data of K. F. J. Heinrich in "The Electron Microprobe", John Wiley & Sons, New York (1966), p. 368.

5. P. Duncumb and P. K. Shields, "The Electron Microprobe", John Wiley & Sons, New York (1966), p. 287.

6. K. F. J. Heinrich, Proc. 2nd National Conf. on Microprobe Analysis, Boston, Mass.

7. P. Duncumb and S. J. B. Reed, "Quantitative Electron Probe Microanalysis", NBS Spec. Publ. 298.

8. H. E. Bishop, "Optique des Rayons X et Microanalyse", Hermann, Paris (1967), p. 158.

9. M. Green, "X-Ray Optics and X-Ray Microanalysis", Academic Press, New York (1963), p. 361-77.

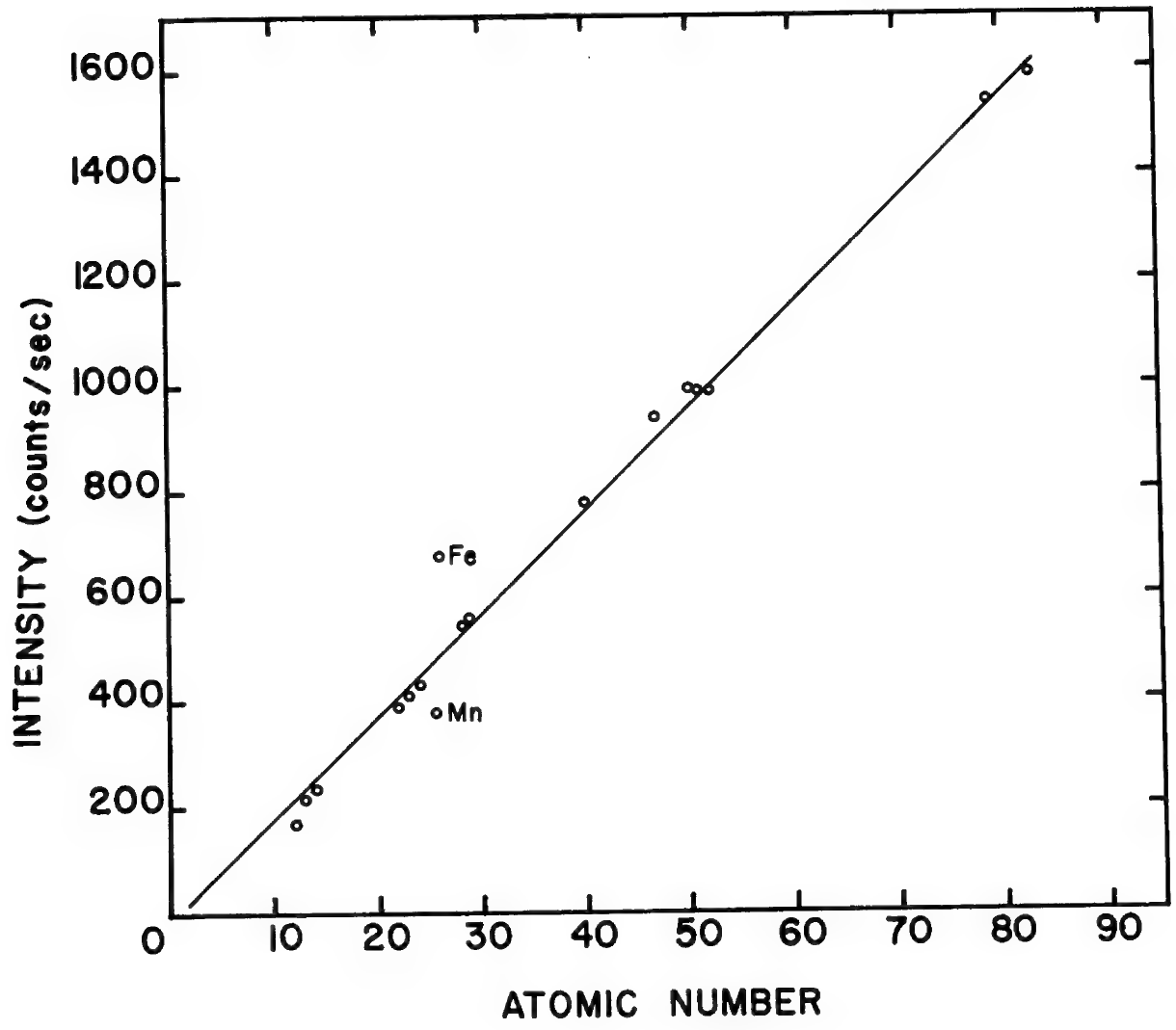

Figure 1. X-ray continuum intensity at 2.000 Å plotted as a function of atomic number.

MEASUREMENT AND CALCULATION OF ABSOLUTE X-RAY INTENSITIES: THE EFFECT OF K AND L CROSS SECTIONS

D. B. Brown and J. V. Gilfrich
Naval Research Laboratory, Washington, D. C.

Objectives: This work had two principal objectives, 1.) to test the ability of the electron transport method to calculate absolute x-ray intensities as determined by comparison with measured values, 2.) to check the absolute magnitudes of the K and L ionization cross sections.

Background: K and L ionization cross sections are necessary for accurate fluorescent corrections in quantitative electron probe analysis. Theoretical estimates of Burhop[1] are not in good agreement with other work.[2] Green's measurements of the cross sections used in conjunction with the fluorescent-yield recommendations of Fink et al.[3] suggested that the Burhop values for K, L_I and L_{II} should be raised by about 1.2 times and for L_{III} they should be about doubled.

Values of the cross sections may be tested by comparing calculated and measured values of absolute x-ray intensities. A previous comparison[4] using an approximation method to estimate K cross sections gave a standard deviation of 37 % for measured and calculated K lines but no calculations of L lines was possible.

Measurements: The absolute output of commercial x-ray tubes was measured using a LiF crystal spectrometer,[5] as shown in Figure 1. Corrections were made for crystal diffraction, detector efficiency, and geometry. Experimental conditions are listed in Table 1.

Calculations: The electron transport method[6] was used to calculate the absolute intensities of the same characteristic lines as those measured in the x-ray tubes. In this computer program, the transport of electrons in the anode is handled with the aid of a numerical solution of the Boltzmann transport equation. Allowance was made for fluorescence by the continuum and for Coster-Krönig transitions. Cross sections for K and L ionization were initially scaled to match the quantum mechanical values of Burhop but the agreement was unsatisfactory. Then they were scaled to match the larger values recommended by Green and agreement improved.

Results and Discussion: Results are shown in Table 2. Agreement between calculated and measured values is better than 20 % relative for K lines and 35 % relative for L lines except the $\gamma_1\gamma_2$ doublet for tungsten where both the theoretical and experimental difficulties are considerable. In the case of K lines the calculated values are all lower than the experimental values but it is difficult at present to elucidate the reasons for this.

---

1. E. H. S. Burhop, Proc. Camb. Phil. Soc. 36, 43 (1940).

2. M. Green, Ph.D. Thesis, University of Cambridge, 1962;
W. Hink, Zeit. Phys. 177, 424 (1964); Zeit. Phys. 182, 227 (1965),
M. Green and V. E. Cosslett, Brit. J. Appl. Phys. 1, 425 (1968).

3. R. W. Fink, et al., Rev. Mod. Phys. 38, 513 (1966).

4. L. S. Birks, et al., J. Appl. Phys. 36, 699 (1965).

5. J. V. Gilfrich and L. S. Birks, Anal. Chem. 40, 1077 (1968).

6. D. B. Brown and R. E. Ogilvie, J. Appl. Phys. 37, 4429 (1966).
D. B. Brown, et al., J. Appl. Phys., to be published.

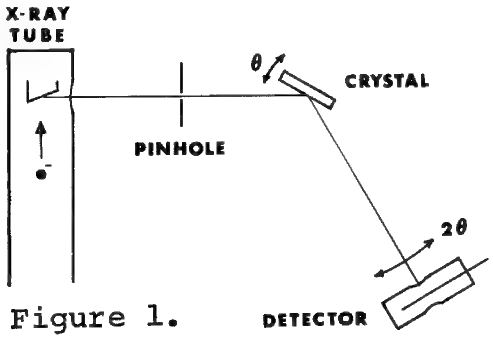

Figure 1.

TABLE 1

Target	kV	ma		Incidence Angle	Takeoff Angle
Au	25	8.6	Siemens Spectroscopy	84°	6°
"	45	9.2	" "	"	"
W	"	5	Machlett OEG-50	70°	20°
Mo	"	5	" "	"	"
Cu	"	2	" "	"	"
Cr	"	5	" "	"	"

TABLE 2

Element	Edge	Line	kV	Calc. Intensity*	Meas. Intensity*
Au	L_{III}	L_α	25	19	17
"	"	"	45	43	~~58~~ 57
W	"	"	"	63	~~59~~ 55
"	L_{II}	$L_{\beta 1}$	"	43	~~50~~ 49
"	L_I	$L_{\gamma 1,\gamma 2}$	"	0.9	1.3
Mo	K	K_α	"	55.7	59.3
Cu	"	"	"	202	~~234~~ 215
Cr	"	"	"	313	~~376~~ 302

* (photons/sec./sterad./ma.) x 10^{-10}

DENSITY EFFECT OF X-RAY EMISSION FOR POROUS SPECIMENS

Takeo Ichinokawa
Waseda University, Tokyo, Japan

Density effect of X-ray emission was measured for tablet specimens of various densities. Graphite, Cr_2O_3, CuO and ZnS, of which particle sizes were less than 1 μm, were used as specimens. The specimen density was changed from about 1 to 4 g/cm^3. X-ray intensities of those specimens were measured by electron probe microanalyzers of which take-off angles are 90 and 10 degrees. Electron probes were focused on the specimen surface to a diameter of about 10 μm.

An example is shown in Fig. 1 for graphite specimens of various densities. The relative X-ray intensity of carbon K-radiation increased with the increasing of the specimen density and that of the lowest density (ρ = 1.4) was 70% compared with a single crystal graphite specimen (ρ = 2.25).

To examine the depth distribution of X-ray production for various densities, $F(\chi)$ curves were experimentally measured by Green's method. By means of the theory of electron probe microanalysis, $F(\chi)$ can be separated into two factors, i.e. F(0) and $f(\chi)$. F(0) values and $f(\chi)$ curves were obtained for various specimen densities from the curves of experimental $F(\chi)$. The results show that experimental $f(\chi)$ curves scarcely depend on the specimen density as shown in Fig. 2, but F(0) remarkably depends on it.

Thus, the density effect of X-ray emission on porous specimens should be attributed as an effect of the atomic number correction. Hence, the back scattering factors R were obtained for various densities from the measurements of the specimen current with applying the specimen bias. The results as shown in Fig. 3 show that the back scattering factor R is not concerned with the specimen density, whereas the secondary electron emission remarkably depends on it. Similar results were obtained for other samples of various densities. Therefore, it is concluded that the stopping power S of electrons in porous specimens plays an important role of the density effect.

The author supposes that the difference of X-ray emission due to the specimen density is caused by the difference of electron energy loss mechanisms in the specimen, because small energy losses due to the secondary electron emission or surface plasma may contribute to the stopping power. Therefore, recent theories of electron probe microanalysis, which do not include the specimen density, are not applicable for porous specimens.

A correction procedure on the density effect will be discussed in the conference.

1. P. Duncumb and P. Shields: "The Electron Microprobe", John Wiley & Sons, New York (1964), p. 284.

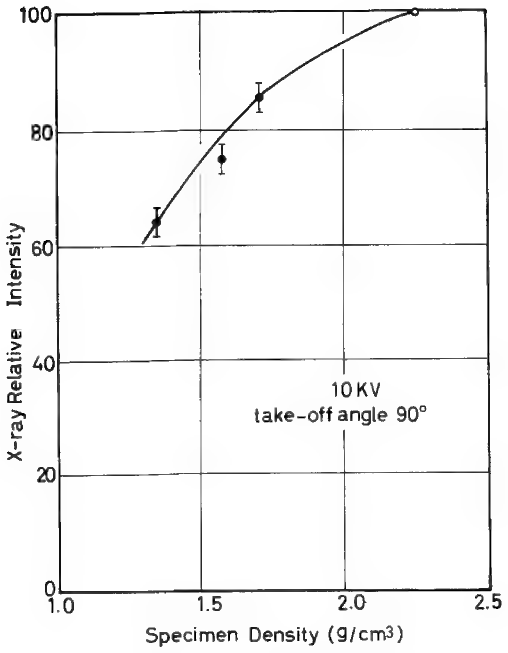

Fig. 1 Relation between relative X-ray intensity of carbon K-radiation and specimen density for graphite specimens.

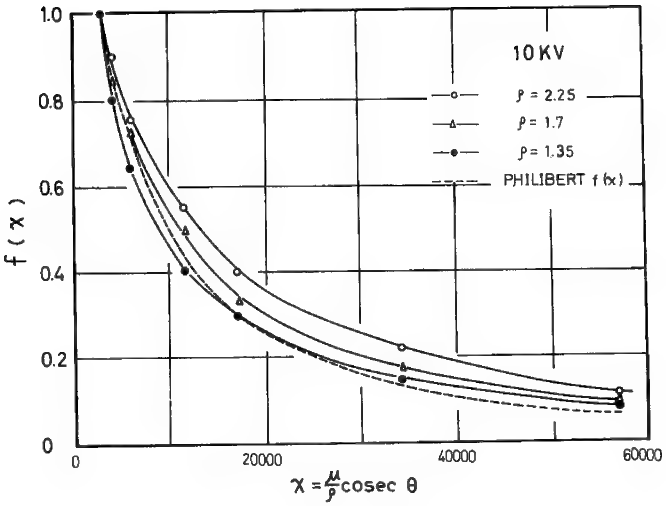

Fig. 2 Experimental f(x) curves of graphite specimens for various densities. A dotted curve shows a theoretical f(x) curve calculated from the modified Philibert formula[1].

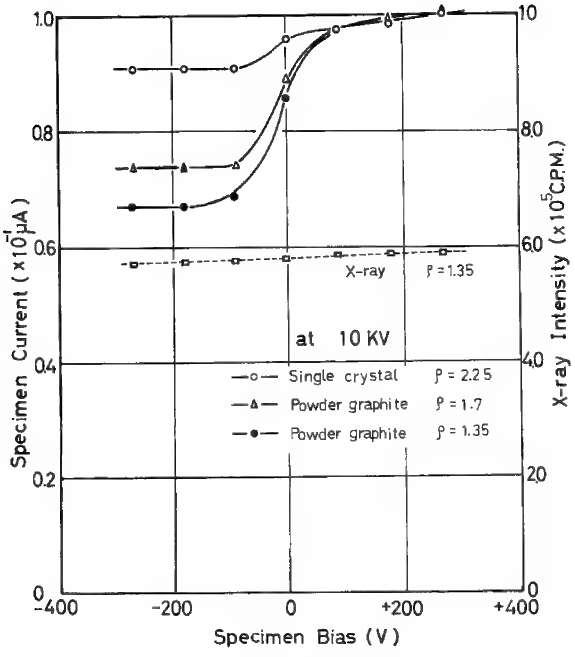

Fig. 3 Variation of specimen current and X-ray intensity for graphite specimens of various densities against the specimen bias.

DEPTH DISTRIBUTIONS OF Fe-CHARACTERISTIC X-RAY IN EPMA TARGETS OF Fe-Al ALLOYS

Ryuichi Shimizu, Kenji Murata and Masayuki Fujiwara
Osaka University, Osaka, Japan

Depth distributions $\varphi(\rho z)$ of Fe-K-radiation in Fe-Al alloys were determined by the analysis of the angular distributions which were obtained by means of the angular distribution measuring apparatus.

The apparatus was mounted in JXA-3 X-ray microanalyser so that X-ray is produced in a target under the same accelerating voltage as an usual microprobe analysis by means of this instrument is done. The experiments were carried under the conditions with specimen current $10^{-7} \sim 10^{-8}$ ampere at 20, 25 and 30 kV respectively.

Fe-K radiation was detected by means of non-dispersive method using gas flow proportional counter and the intensity of X-ray counted were kept constant at each take off angle except for the region below 2° by adjusting the specimen current so as to avoid the influence of the peak shift of the pulse height distribution.

The specimens of Fe-Al alloys of 2.0, 8.0 and 24.09 Wt% of Al content were offered by Central Research Laboratory of Fuji Iron Working Company after general survey of homogeneity and chemical analysis.

The $f(\chi)$-curves obtained for pure Fe and Fe-Al targets show distinct difference between them. And we found the remarkable discrepancy of obtained $f(\chi)$-curve from that of Philibert's formula for Fe-Al alloy as the content of aluminium in the specimen increases.

As to the analyzing process we checked the dependence of final form of $\varphi(\rho z)$ on its initial functional representation, i.e. Gaussian type $\exp -a(Z-Z_o)^2$ and $(\sum_i b_i Z^i) \exp -Hz$ that was used by Kirkpatrick et al.

The results show clear difference in their distribution as is given in Fig. 1 which shows the angular distribution of Fe-K-radiation from pure Fe- and Fe-Al 24.09 % targets af 30 kV.

Fig. 2 shows their depth distributions which were obtained by the least square method using the latter functional representation because the residual in the calculation was smaller than the other.

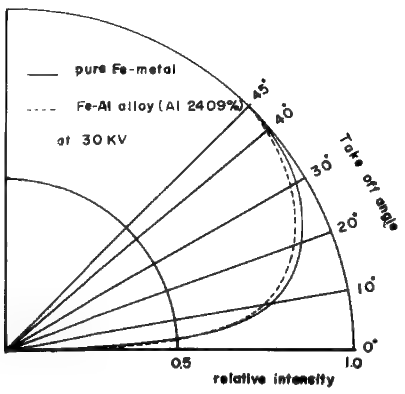

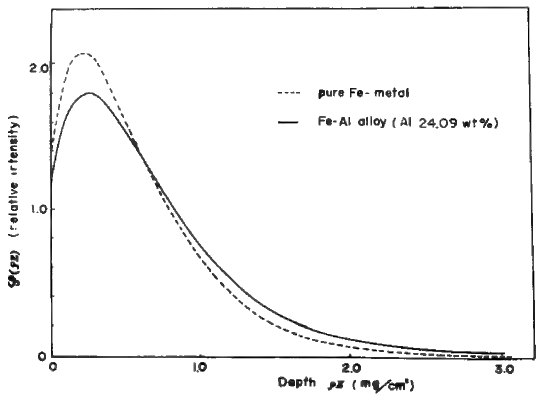

DEPTH DISTRIBUTION OF Cu- AND Au-CHARACTERISTIC X-RAY IN INCLINED EPMA TARGETS OF Au-Cu ALLOY

Ryuichi Shimizu, Kenji Murata and Norio Gennai
Osaka University, Osaka, Japan

The depth distribution $\varphi(\rho z)$ of characteristic X-ray in alloy target is determined mainly by the mean atomic number of the target as well as the accelerating voltage and its shape changes usually to take slower decrease with depth as the mean atomic number decreases. The case of Fe-K characteristic X-ray production in Fe-Al alloy-targets shows this tendency very clearly as is described in other summary. However $\varphi(\rho z)$ of Cu-K-radiation in Cu-Au alloy is quite another[1]. It shows, in this case, inverse change to the case of above Fe-Al alloys, that is, it takes more sharp shape as the mean atomic number decreases. This result that seems curious at first sight is due to indirect excitation and $f(\chi)$-curve finally obtained is, therefore, not for mere absorption correction but it already contains fluorescence correction too. The inclined rotating target technique keeps the target inclined to incident electron beam and rotates it around the axis of the electron beam with constant speed to change the take off angle which is given as a function of an angle of the rotation φ by equation

$$\sin\theta' = \cos\theta \cos\beta - \sin\theta \sin\beta \cos\varphi$$

where θ' is take off angle, β angle of inclination to the electron beam, and θ angle between the direction of X-ray detected and the axis of the beam.

This technique has some advantages. e.q. it needs not any special devices to obtain an angular distribution of reference X-ray with more accurate spectroscopic detection than the technique we adopted before etc.

In this paper we adopted the inclined rotating target technique to investigate the change of $\varphi(\rho z)$ of Cu-Kα- and Au-Lα-lines with mean atomic number and the contribution of indirect excitation to the shape of $\varphi(\rho z)$ with reference to the results obtained preliminarily by using angular distribution measuring apparatus at normal incidence.

Fig. 1 shows one of the results obtained by this technique where the speed of the rotation of the specimen stage was set synchronized with the recording chart speed.

The experiment was carried at 30 kV as to Cu-Al alloys of 20, 40, 50, 60 and 80 Wt % of Cu-content. And $\varphi(\rho z)$ of CuKα- and Au-Lα lines were obtained for the angles of inclination 15°, 30° and 45° respectively by applying the least square method to determine their functional representations

$$(\sum_i b_i z^i) \quad \exp(-Hz)$$

for $\varphi(\rho z)$.

The similar tendency of change in the shape of $\varphi(\rho z)$ to the case of normal incidence were remarked, but the change became less remarkable as an angle of incidence increased. And the change of the mean depth of X-ray source in each specimen was obtained as a function of angle of incidence.

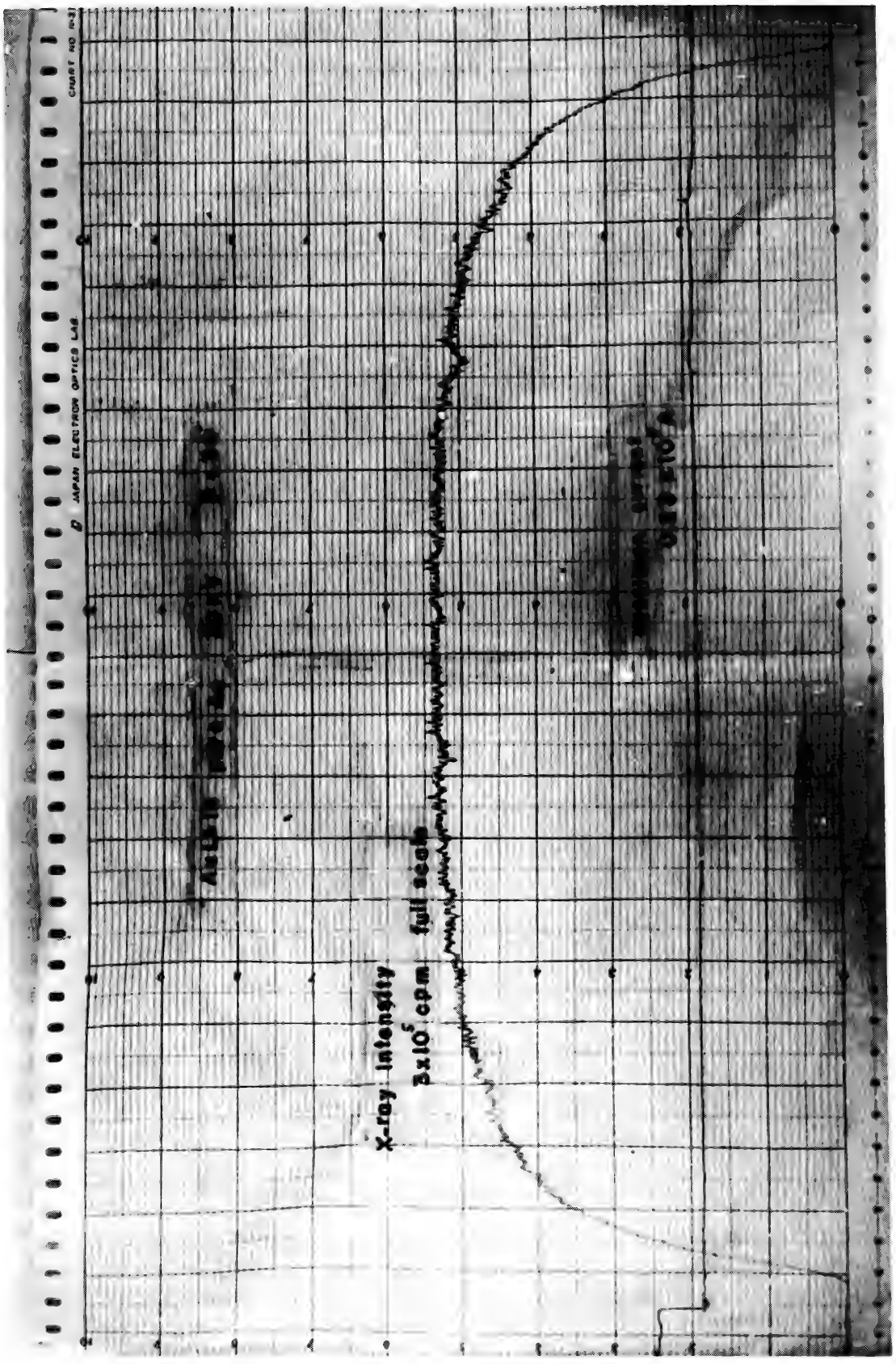
JAPAN ELECTRON OPTICS LAB.
CHART NO. R-31
X-ray intensity
3x10⁵ cpm full scale

EFFECT OF ELECTRON BOMBARDMENT ON THE MICROSCOPIC STRUCTURE OF TARGET MATERIALS

Gunji Shinoda, Masae Seki, and Michiko Kita

Japan Women's University, Tokyo, Japan

It is well known that polymerization of oils occurs when an electron beam strikes the specimen. Also sometimes in the absorbed electron image of alloys at a high temperature a metastable phase is frequently observed. In these cases information on surface structure obtained from the back-scattered or absorbed electrons should be modified by the structure change due to bombardment. On the otherhand, we have observed in a water cooled iron target of an open type X-ray tube a small grained surface layer having several irregular shaped holes and a layer of large grain beneath it. This shows that in a surface layer both mechanical and thermal effects of electron beam are active and beneath it exists a layer in which termal effects are not predominant. However, the thermal effect indicates not only temperature rise but also movement of atoms, the latter being more important. A mechanical effect is also observed in a very high melting point metal such as molybdenum in which cracks have been observed in addition to the formation of holes in the target point. Grain growth is observed even by low energy electron bombardment, i.e., few hundreds volts, even in a nickel plate. As such examples of structure change have been experienced for a prolonged exposure to electron beam, next the effect of electron beam for shorter period has been studied.

Figure 1 shows one example of the effects of 12 hours electron irradiation with accelerating voltage of 35KV on the structure of chill cast copper-5% tin alloy. Original material has an ordinary dendritic structure. After irradiation the cored structure has completely disappeared and a recrystallized structure having twins and etch pits has appeared. In the non-irradiated area only an increase in number of etch pits has been observed -- this may be due to backscattered electrons re-entering the sample. At a depth of about 100μ an enormous number of etch pits have been observed as shown in Fig. 2; this should correspond to the formation of a crack parallel to the surface. Below this depth a dendritic structure remains, although diffusion of atoms and movement of grain boundaries are taking place. Such effect has been observed up to a depth of several-tenths mm below the surface.

Even for much shorter irradiation, i.e., one hour, recrystallization begins partly and perhaps the formation of some kind of lattice defect may begin at much earlier stages. However, no appreciable change has been observed for an irradiation of several minutes.

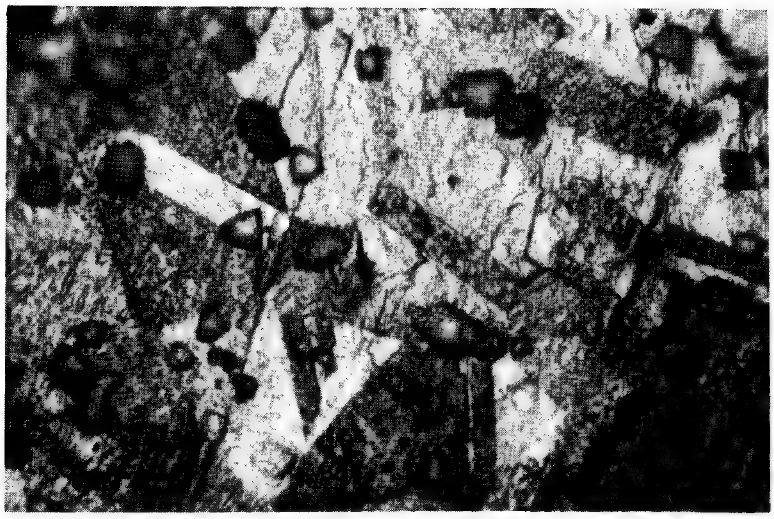

Fig.1 Cu-5% Sn alloy.
Irradiated area. Near the surface.

Fig.2 Cu-5%Sn alloy.
Irradiated area, 100μbelow the surface.

THE INFLUENCE OF TARGET ABSORPTION ON THE RELIABILITY OF QUANTITATIVE CHEMICAL ANALYSIS

Victor G. Macres
Materials Analysis Company, Palo Alto, California

The reliability of $f(\chi)$ data obtained experimentally by the direct and indirect (tracer) methods and, more generally, by the Philibert equation have been examined. General curves relating $\Delta f(\chi)/f(\chi)$ to $f(\chi)$ have been obtained which allow a direct estimate of the reliability of compositions obtained after absorption corrections. A detailed computer analysis of experimental emission distribution, $\phi(\rho x)$, curves (1-3) has also been carried out which allows: (i) examination of the emission distribution curves of measured radiation, $\phi'(\rho x)$; (ii) formulation of an analytical expression which corrects for the presence of thin surface films in applying $f(\chi)$ factors; (iii) derivation of a new empirical absorption correction equation.

The direct method for determining $f(\chi)$ curves employs experimental methods which allow variation in χ_T [$\chi = (\mu/\rho)\chi_T$, where χ_T is a geometrical factor used in describing pathlength] The effect of experimental limitations on the uncertainty of such $f(\chi)$ values is shown in Figure 1 for various targets and accelerating voltages, V_o. (The additional effect of uncertainty in the self-absorption coefficient is not included.)

An analytical expression for calculating $f(\chi)$ has an obvious utility and the Philibert equation is commonly used for this purpose (4). In certain cases, its accuracy is quite good and can be applied to instrument geometries of a wide range. Figure 2 illustrates this point for the 30 KV analysis of Ni Kα in a 66 % Fe-34 % Ni alloy. In general, however, there is a significant deviation from experimental $f(\chi)$ data as is shown in Figure 3 [Duncumb and Shields σ values (5) are used in this comparison].

The large discrepancy between experimental and Philibert (χ) values under high absorption conditions can be explained by considering the origin of measured radiation. In Figure 4, the percentage of measured radiation originating above a given value of $\rho x'$ is illustrated for various χ and V_o values in alumin um (x' is the distance below the surface). For high absorption conditions, about 50 % of the measured radiation comes from less than 1000 Å of the target surface. This circumstance is in constrast with the Philibert equation which assumes zero emission at the target surface.

In the correction for absorption, account must be taken of the effect of thin surface films on the applicability of $f(\chi)$ values. Analysis of experimental emission distribution data has shown that the following expression can be used to calculate the percent change in the $f(\chi)$ value which would otherwise be used if the effect of such film were neglected

$$\frac{\Delta f(\chi)}{f(\chi)} \cdot 100 = -0.13\sigma_L \frac{\Delta\rho x'}{\sin\gamma} \log f(\chi) \qquad (1)$$

where σ_L is the Lenard coefficient, γ is the electron incidence angle and $\Delta\rho x'$ is mass per unit area of surface film.

Uncertainty in χ can arise from uncertainties in the absorption coefficient and the geometrical factor, χ_T. In the analysis of experimental $\phi(\rho x)$ curves, a surprising and most useful result was obtained (Figure 5) which related the percentage uncertainty in $f(\chi)$ to $f(\chi)$ for various uncertainties in χ. The curves fit the experimental $\phi(\rho x)$ data (1-3) to within 10 % and allow the percentage uncertainty in $f(\chi)$ to be predicted directly. The curves are universal as indicated in the caption of Figure 5.

Figure 5 represents a differential form of an equation relating $f(\chi)$ and χ. Upon integration, the general form of the equation is

$$\frac{f(\chi)}{1-f(\chi)} = B\chi^a \qquad (2)$$

The log-log graphical presentation of $\frac{f(\chi)}{1-f(\chi)}$ vs. χ (Figure 6) using experimental $\phi(\rho x)$ data (1-3) yields an approximate linear relation for values of $f(\chi)/1-f(\chi)$ between 100 [$f(\chi) = .99$] and 1 [$f(\chi) = 0.5$]. The B factor accounts for variation in target material, accelerating voltage, and critical excitation voltage. Using Philibert h values and the general form of the Duncumb and Shields relation for σ, the expression giving the best fit is

$$\frac{f(\chi)}{1-f(\chi)} = \frac{9 \times 10^5}{\chi^{1.1}\left[\left(\frac{V_o}{V_c}\right)^{1.65} - 1\right] V_c^{1.65}(1+h)} \qquad (3)$$

Agreement of Equation 3 with experimental data is about two times better than that given by the Philibert equation.

---

1. R. Castaing and J. Descamps, J. Phys. Radium 16, 304 (1955).

2. J. D. Brown, Ph.D. Thesis, University of Maryland, 1966.

3. R. Castaing and J. Henoc, "X-Ray Optics and Microanalysis", Fourth International Symposium on X-Ray Optics & X-Ray Microanalysis, p. 120, Hermann Press, Paris, 1966.

4. J. Philibert, "X-Ray Optics and Microanalysis", Third International Symposium on X-Ray Optics & X-Ray Microanalysis, p. 379, Academic Press, New York and London, 1963.

5. P. Duncumb and P. K. Shields, "The Electron Microprobe", T. D. McKinley, K. F. J. Heinrich, and D. B. Wittry, eds., J. Wiley and Sons, Inc., New York (1966) p. 217.

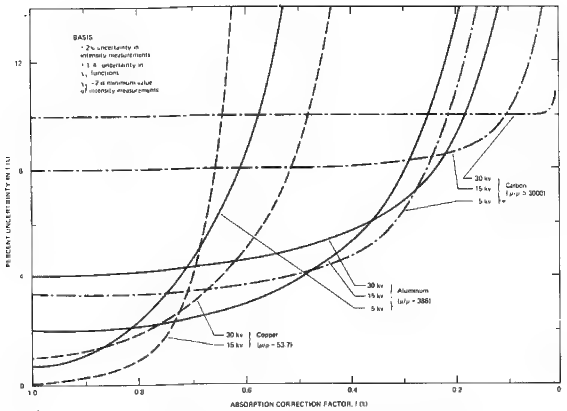

Figure 1. EFFECT OF SELF ABSORPTION AND BEAM VOLTAGE ON UNCERTAINTY IN ABSORPTION CORRECTION FACTORS BASED ON THE DIRECT METHOD FOR DETERMINING f(χ) CURVES.

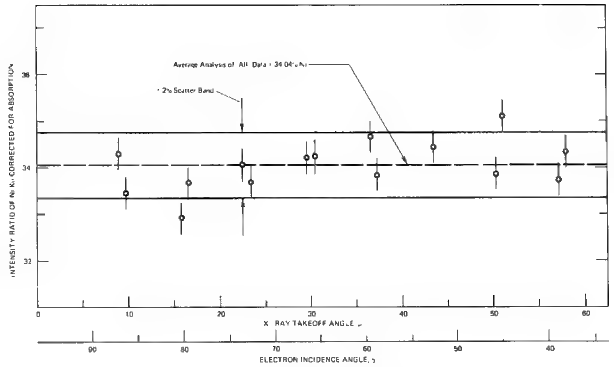

Figure 2. RESULTS OF ANALYSIS OF IRON-NICKEL ALLOY USING VARIOUS COMBINATIONS OF X-RAY TAKEOFF ANGLE AND ELECTRON INCIDENCE ANGLE

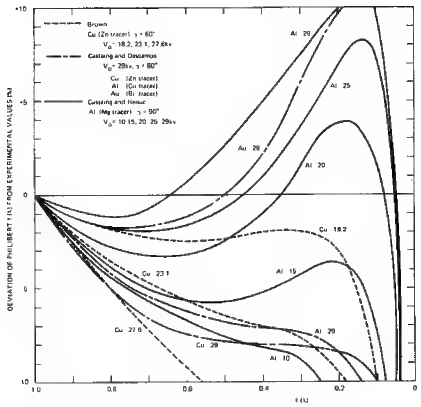

Figure 3. DEVIATION OF PHILIBERT EQUATION FROM EXPERIMENTAL f(χ) CURVES DETERMINED BY THE TRACER METHOD

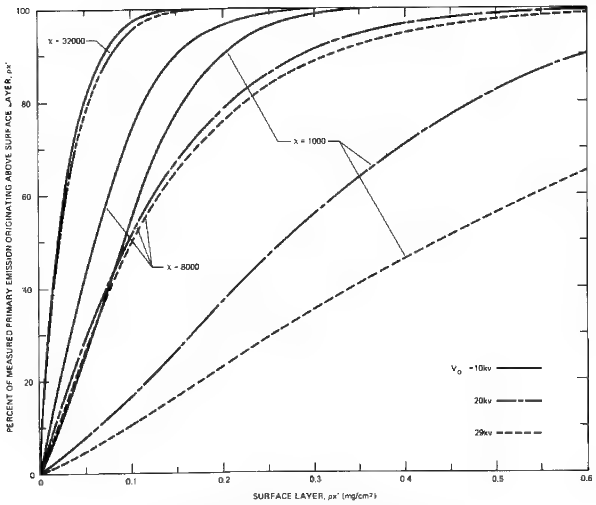

Figure 4. DEPENDENCE OF INTEGRATED INTENSITY OF MEASURED PRIMARY EMISSION ON ELECTRON ACCELERATING VOLTAGE AND ABSORPTION. ALUMINUM TARGET, V_0 = 10, 20, 29 KV.

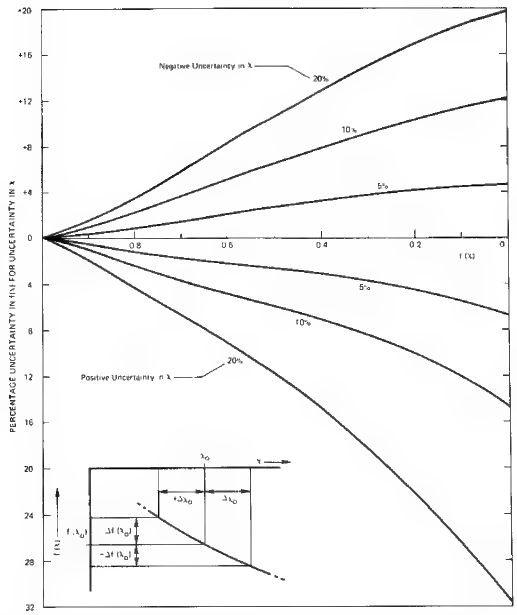

Figure 5. UNIVERSAL CURVE FOR PREDICTING PERCENTAGE UNCERTAINTY IN f(χ) FOR GIVEN UNCERTAINTY IN χ. APPLICABLE FOR ALL SPECIMEN AND INSTRUMENT VARIABLES INCLUDING COMPOSITION, ABSORPTION, ANALYZED RADIATION, ACCELERATING VOLTAGE, ELECTRON INCIDENCE ANGLE, X RAY TAKEOFF ANGLE.

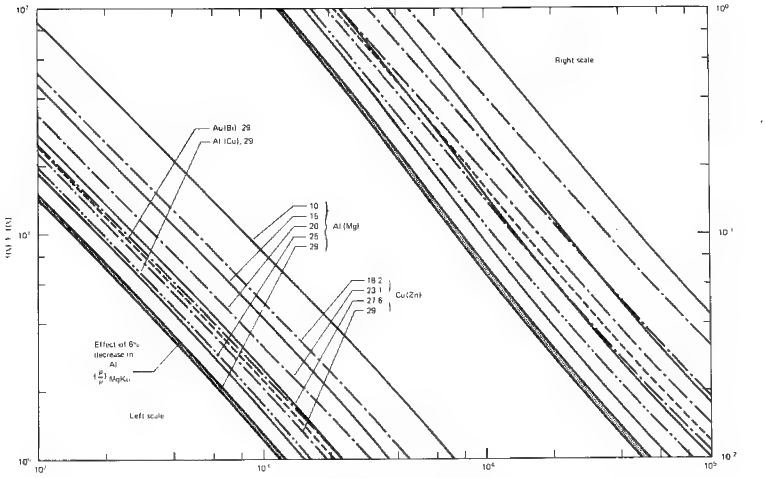

Figure 6. COMPARISON OF EXPERIMENTAL f(χ) CURVES DETERMINED BY TRACER METHOD – LOG χ VS LOG [f(χ) / f (0)] RELATIONSHIP

THE EFFECT OF ELECTRON BEAM ANGLE OF INCIDENCE IN QUANTITATIVE MICROPROBE ANALYSIS

J. W. Colby*, D. R. Wonsidler* and D. K. Conley**
*Bell Telephone Labs, Inc. **Western Electric Co.
Allentown, Pennsylvania

It has been suggested almost since the inception of the microprobe analyzer, that the effect of inclining the specimen during the analysis, would be deleterious to obtaining good quantitative results. No one has made any attempt to establish any clear cut evidence one way or the other. It is our intent and purpose in this paper to show that for all practical purposes there is no difference between corrected results obtained in microprobes in which the electron beam impringes normally on the specimen and corrected results from microprobes in which the electron beam strikes the specimen at non-normal incidence.

There are basically two ways of determining the relationships between normal and non-normal incidence. One can repeat the tracer work of Castaing, Brown and others, only over a much larger range of alloys than has been investigated to date, or one can analyze a wide range of alloys under conditions which maximuze the various effects that enter into the correction procedures. We have chosen the latter technique for reasons of simplicity and directness. Toward this end, it is not imperative that we know the composition accurately; it is only necessary that the alloys be homogeneous. We are not interested in absolutely accurate determinations of composition, but only in comparing the results obtained after corrections, from non-normal and normal incidence microprobes.

We have selected three alloy systems: (1) Fe-Cr (five compositions); (2) Cu-Au (five compositions), and (3) Ta-Al (three compositions). The Fe-Cr system (Fe Kα & Cr Kα) was analyzed at 15 kev, for which the maximum absorption correction was approximately 10 %, and the maximum fluorescence correction was approximately 20 % (both relative). The Ta-Al system (Ta Mα & Al Kα) was analyzed at 5 kev and 10 kev. At the lower accelerating potential the maximum absorption correction was less than 7 % (relative) while the back-scatter and ionization penetration corrections were as high as 40 % and 65 % respectively. At the higher accelerating potential the backscatter and ionization corrections were reduced somewhat while the absorption correction was increased to approximately 25 %. In both cases fluorescence was negligible. The Cu-Au alloys were chosen as an intermediary case and were analyzed at 20 kev for Cu Kα, Au Lα, and Au Mα radiation. Backscatter and ionization corrections were intermediate, but the maximum absorption correction was even higher, being on the order of 35 % (relative) for Au Mα radiation.

While it is not practical to prepare and analyze all possible binary systems, and composition levels over a wide range of operating conditions, it may be noted that the systems and conditions chosen above are sufficient to achieve corrections greater than those normally recommended in microprobe analysis, and cover separations in atomic number of 1 to 60.

Only small random differences are observed between corrected results from probes having normal electron beam incidence and those having non-normal beam incidence. The differences observed do not follow any trend and are well within the range expected for experimental error.

All data were corrected by conventional microprobe techniques using a computer program, MAGIC, and for the inclined specimen, the "effective" emergence angle was used for the absorption and fluorescence correction. From this study it is concluded that there are no significant differences between corrected results obtained from probes in which the electron beam strikes the sample at normal incidence and those obtained in instruments in which the electron beam impringes on the sample at other than normal incidence.

ABSORPTION CORRECTION BY THE USE OF DUAL TAKE OFF ANGLE SPECTROMETERS

P. S. Ong
Philips Electronic Instruments, Mt. Vernon, N. Y.

Quantitative analysis in an electron microprobe is based on the comparison of the intensity of X-rays generated in an unknown and the intensity generated in a pure element. Under identical excitation conditions, the relative intensity will equal the weight fraction of the element in the unknown sample. Such a comparison requires knowledge of:

1. The differences (if any), in excitation conditions of the X-rays in the pure element and the unknown, and

2. The intensities of the radiation generated within both the sample and the standard.

The first requirement included such effects as secondary fluorescence, atomic number effect, and backscatter factor of the electrons, which will not be discussed here. The subject of this paper is concerned with the second requirement i.e., the intensity as measured outside the sample and its relation to the true intensity as generated within the sample. This ratio, referred to as the $f(\chi)$ value, is a function of $\chi = \mu \operatorname{cosec} \theta$. One of the difficulties in this procedure is that μ is not always known to the required accuracy. As has been pointed out by Heinrich[1], the values of μ published by various authors often vary and moreover, the values for most elements are known only in a limited wavelength range. Another drawback of the use of $f(\chi)$ values is that χ refers to the absorption coefficient of unknown sample for the particular radiation. This means that we need to know the composition of the unknown to be able to calculate μ.

The approach to be proposed here would, in the first order approximation eliminate the use of the mass absorption coefficient of the unknown. This is accomplished by making two independent measurements and subsequently by calculating the X-ray intensity measurement at two take off angles (two values of χ). There are various ways of using the two measurements for eliminating the mass absorption coefficient. An outline of one approach will be given below.

The approach to be described here starts with avoiding the use of μ as a parameter in the consideration. Instead, we use (γ) as a variable $\gamma = \operatorname{cosec} \theta$. It is obvious that the functions $f(\gamma)$ and $f(\chi)$ are identical except for the scale value of the abcissa. Because of this, all the analytical expressions which describe the $f(\chi)$ curve, are identical to that of $f(\gamma)$, taking into consideration the different scale value. The $f(\gamma)$ can also be considered as a special case for which $\mu = 1$.

The analytical expression for $f(\chi)$ was derived by Philibert[2] and modified by Duncumb and Shields[3].

For moderate values of $1/f$, this equation can be rewritten as follows (Heinrich[4]):

$$1/f = 1 + (1+a)\ (\chi/\ ) + a\ (\chi/\sigma)^2$$

or $$1/f \simeq 1 + (\chi/\sigma)\ (1+a)$$

in which $a = 6A\ (5Z^2 + 6A)$

$$\sigma = 2.39 \times 10^5/\ (V^{1.5} - E^{1.5})$$

A = atomic weight, Z = atomic number

V = operating voltage and E excitation voltage.

Accordingly

$$1/f \simeq 1 + (\gamma/\sigma)\ (1+a)$$

which shows that for moderate values, 1/f is a linear function of γ. By plotting the inverse of the two intensities as functions of γ = cosec θ and subsequently linear extrapolation, we can obtain the reciprocal value of the intensity $1/I_o$ in absence of absorption $\gamma = 0$.

In practice it is necessary to know the relative efficiencies of the two spectrometers. This can be determined while measuring the intensity on the standard. The best way of doing so is still open for discussion.

---

1. K. F. J. Heinrich, The Electron Microprobe, p. 296.

2. J. Philibert, Third Int. Symp., (Stanford) p. 379.

3. P. Duncumb and P. K. Shields, The Electron Microprobe, p. 284.

4. K. F. J. Heinrich, Second Nat. Conference on Probe Analysis (Boston), Paper # 7.

CONTINUUM FLUORESCENCE: IS IT IMPORTANT?

J. D. Brown
University of Western Ontario, London, Ontario, Canada

Four corrections have been defined as necessary in calculating compositon from characteristic X-ray intensities measured with an electron probe microanalyzer. These four are an absorption correction, an atomic number correction, a correction due to fluorescence by characteristic radiation and a correction due to fluorescence by continuum radiation. Of the four, the latter, which has been called fluorescence due to the continuum, has been largely neglected.

Henoc[1] developed a continuum fluorescence correction based on the assumptions that the continuum radiation is generated at the surface of the specimen and that it spreads out equally in all directions from the point of generation i.e., it is isotropic. Although this equation was first published in 1962 few analysts have applied it mainly because of its complicated form. A computer program is available which makes the application of Henoc's continuum fluorescence correction feasible for routine analysis.

Springer[2] has recently modified the approach of Henoc by assuming an average value for the depth at which the continuum radiation is generated and changing the approximation used for mass absorption coefficients. The method for calculating the primary radiation intensity has also been modified. Despite the great similarity in approach of the two methods, a different dependence of continuum fluorescence on electron energy is obtained. This difference in dependence can be traced to the fact that Springer predicts that a greater fraction of the continuum radiation will be absorbed within the sample as the electron voltage is increased whereas the fraction absorbed remains constant in Henoc's treatment.

The practical importance in neglecting the continuum fluorescence correction lies in evaluations of the atomic number effect. Most authors who have claimed to have evaluated the atomic number effect, have in fact evaluated the combination of atomic number effect and continuum fluorescence. The rationale used is that continuum fluorescence is either negligible or contributes a small constant fraction to the characteristic intensity. The fact that approximately seven percent of Znkα characteristic radiation is produced by continuum fluorescence with an electron voltage of 25 Kv, and that for a similar voltage less than 0.1 percent of Alkα radiation is similarly produced should demonstrate that this rationalization rests on questionable assumptions.

The contribution of continuum fluorescence has been calculated for a number of systems which have been used to evaluate atomic number corrections. Since in these evaluations the atomic number effect has been considered as any difference remaining between known and calculated composition after all other corrections have been made, the atomic number correction is incorrect in any system where a significant continuum fluorescence correction is necessary. On the other hand, since most atomic number corrections contain variable parameters which are adjusted to obtain best agreement between known and calculated compositions, it is not surprising that improved quantitative agreement is not obtained when continuum fluorescence is considered.

To improve this situation, simplified criteria have been developed to establish if a continuum fluorescence correction is significant, and at the same time a computer program has been written for both the Henoc and Springer equations for routine use in quantitative analysis. Evaluations of quantitative analysis equations have been made on data reported in the literature.

---

1. J. Henoc, "Quantitative Electron Probe Microanalysis", N. B. S. Spec. Publ. 298, 1968, p. 197-214.

2. G. Springer, N. Jahrbuch f. Mineralogie 106, 241 (1967).

ATOMIC NUMBER CORRECTION UNCERTAINTY

Kurt F. J. Heinrich and Harvey Yakowitz
National Bureau of Standards, Washington, D.C.

This paper is a complement to the previous ones [1,2] on the propagation of error in the absorption and fluorescence corrections.

In the atomic number correction, it is difficult to separate uncertainties of the model from those of the parameters applied to the model. The calculation of the absolute intensity of primary emission within the specimen is affected by a large uncertainty, mainly due to the scarcity and poor agreement between values of parameters. There is, contrary to the cases of absorption and fluorescence, considerable compensation of error in the calculation of intensity ratios.

The customary expression for the atomic number correction factor

$$K_Z = \frac{R_{std}}{R_{spec}} \frac{\int_{E_c}^{E_o} \left(\frac{Q}{\bar{S}}\right)_{std} dE}{\int_{E_c}^{E_o} \left(\frac{Q}{\bar{S}}\right)_{spec} dE} \simeq \frac{R_{std}}{R_{spec}} \cdot \frac{\bar{S}_{spec}}{\bar{S}_{std}} \qquad (1)$$

implies the simplifying assumption that an "equivalent stopping power" at an intermediate energy level, for instance, at $E_{eq} = 1/2\,(E_c + E_o)$ [3] can be substituted for the integrals of Equation 1. Using this simplification, we can obtain the following equation for error propagation:

$$\frac{\Delta C}{C} = \frac{\Delta R_{std}}{R_{std}} - \frac{\Delta R_{spec}}{R_{spec}} - \frac{\Delta \bar{S}_{std}}{\bar{S}_{std}} + \frac{\Delta \bar{S}_{spec}}{\bar{S}_{spec}} \qquad (2)$$

A comparison of the experimental data of Dérian [4] with the values calculated by other authors [5,6,7] (Figure 1) shows that the uncertainties in the backscattering correction can amount to several percent, if the mean atomic number of standard and specimen differ significantly, and if the elements involved are of high atomic number (>40).

A calculation using the integration indicated in Equation 1 shows that the uncertainty in the ionization cross-section, Q, is negligible.

In the calculation of stopping power by the equation due to Bethe

$$S = K \cdot \frac{Z}{A} \cdot \frac{1}{E} \ln\left(\frac{1.166E}{J}\right), \qquad (3)$$

controversy centers mainly around the values of J, the mean ionization potential.

Experimentally various expressions for J - although obtained under conditions quite different from those found in electron probe microanalysis - have been reported by several authors[8,9,10]. The choice of the function for J is shown to seriously affect the calculated intensity ratio when the atomic numbers of specimen and standard differ appreciably. Duncumb and Reed[5] have proposed an empirical equation for J which optimizes the results of microprobe analysis of a large set of specimens of known composition. The results obtained with this expression differ from those obtained with the previously mentioned functions, particularly in the presence of elements of atomic number below ten. Further careful studies are needed to decide which is the best function for J. As shown in Table 1, the uncertainty caused by J can be quite considerable.

The experimental evidence concerning the stopping power and the backscatter correction factor is scanty in the case of multi-element (composite) targets. There is reason to believe that the following approximations are valid:

$$R_{comp} \simeq \Sigma\, C_i R_i \tag{4a}$$

$$S_{comp} \simeq \Sigma\, C_i S_i \tag{4b}$$

Separate averaging is preferable to and incompatible with the averaging of the factor $\alpha = R/S$.

It will also be shown that the substitution of an expression based on mean stopping power instead of the full integrations in Equation 1 may result in significant errors. Since there exists a method for formal integration[11], and since most calculations are now performed with the air of computing machines, the concept of an equivalent electron energy introduced to avoid integration should be discarded.

---

1. H. Yakowitz and K. F. J. Heinrich, Mikrochimica Acta 1968 (1) 182.

2. K. F. J. Heinrich and H. Yakowitz, Mikrochimica Acta 1968 (5) 905.

3. P. M. Thomas, AERE Report 4593 U.K. Atomic Energy Authority, (1964).

4. J. C. Dérian and R. Castaing, Optique des Rayons X et Microanalyse, Castaing, Deschamps, Philibert, Eds., (Hermann, Paris, 1966) p. 193.

5. P. Duncumb and S. J. B. Reed, Quantitative Electron Probe Microanalysis, NBS Special Publ. 298 (1968) p. 133.

6. M. Green, Thesis, Cambridge University (1964).

7. G. Springer, N. J. B. Miner, Mh. 1967, 304.

8. G. Springer, N. J. B. Miner, Mh. 1966, 113.

9. D. O. Caldwell, Phys. Rev. 100, 291 (1955).

10. M. J. Berger, S. M. Seltzer, N. Ac. Sci., Nat. Res. Council Publ. 1133 (Washington, D.C., 1964) p. 205.

11. J. Philibert and R. Tixier, Quantitative Electron Probe Microanalysis, NBS Spec. Publ. 298 (1968) p. 13.

Table I

Effect of Various J Values on the Ratio of Calculated Intensity Ratios

Operating* Voltage (kV)	Analytical Line	Composition	$\frac{k_D^+}{k_B}$	$\frac{k_{11.5Z}^+}{k_B}$	$\frac{k_S^+}{k_B}$	$\frac{k_C^+}{k_B}$
10	Ti Kα	TiC	1.015	0.978	0.988	0.974
10	Mg Kα	MgO	1.023	0.987	0.993	0.985
10	U Mα	UC	0.993	0.982	0.994	0.967
10	Pb Mα	PbO_2	0.966	0.968	0.991	0.939
10	Ca Kα	CaO	1.002	0.982	0.990	0.977
15	Ba Lα	BaO	0.986	0.984	0.994	0.975
15	Cr Kα	CrO_3	0.991	0.967	0.983	0.960
10	U Mα	0.1U-0.9Be	1.009	0.836	0.928	0.747
10	Mg Kα	0.1Mg-0.9Be	1.196	0.913	0.943	0.905

B - Berger-Seltzer, value for J [10] (chosen as reference)

+D - Duncumb-Reed [5]

11.5Z - J = 11.5Z

S - J = 9 ($Z + Z^{1/3}$) (Springer) [8]

C - Caldwell [9]

*Voltage chosen so that absorption correction factor is negligible.

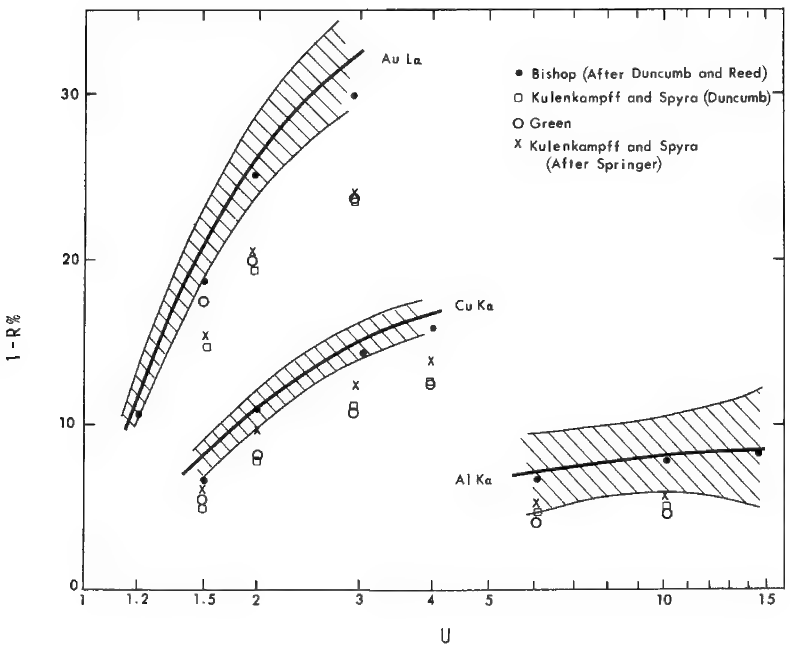

THE SOURCE AND NATURE OF DEADTIME IN ELECTRON MICROPROBE ANALYSIS

D. R. Beaman and J. A. Isasi and R. Lewis
Dow Chem. Co., Midland, Mich. Cons. Electrodynamics Corp., Monrovia, Calif.

When accurate X-ray intensity ratios are required for quantitative electron microprobe analysis, it is generally essential to correct the measured intensities for losses caused by electronic deadtime, particularly when dilute alloys are studied using pure element standards. In an earlier report [1] it was found that the experimentally measured system deadtime could be wholly accounted for in the electronic components of the counting channel, was constant and non zero over the intensity range normally encountered in microprobe analysis (<30000 cps) and was related to the amplified pulse width when this width exceeded the effective pulse width of the pulse height analyzer (PHA). The purpose of the present investigation was to extend the range of intensities previously examined to 100000 cps and to determine the source and nature of the deadtime. Such information should provide accurate deadtime values and make it possible to predict the deadtime of commercial counting systems.

Fig. 1 is a schematic diagram of the experimental arrangement, the uppermost portion representing a standard counting channel. The true counting rate, n, was provided by a pure Fe sample in a CAMECA/CEC electron microprobe operated at 25 kV. Component performance was initially examined using two single pulse generators to provide spike pulses (less than 0.1 μsec width) which could be fed to the individual components. The component output was observed on a calibrated dual trace oscilloscope. When the spike separation was sufficiently reduced amplifier pulse pileup was observed i.e., the two amplifier pulses combined to yield a single pulse of increased amplitude and width while the scaler output halved. On the other hand, reducing the spike separation caused the PHA output from the trailing pulse to disappear while the leading pulse remained unaffected. In the case where two pulses interact to create a single pulse of increased width with the subsequent loss to the second pulse to the counting system, the deadtime is of the self prolonging type [2] and the measured count rate, m, is given by $m = ne^{-n\tau}$ where n is the true count rate and τ is the deadtime associated with a single undisturbed event. When pulse interaction results in the loss of the second pulse to the counting system without affecting the initial pulse, the deadtime is of the non self prolonging type [2] where $m = n/(1 + \tau n)$.

To test the amplifier performance, amplifier pulse widths were varied from 1.2 to 8.5 μsec using the shaping amplifier while the PHA pulse width was held constant at 0.5 μsec. For each pulse width the output, m, of the Nuclear Data scaler (multiscaling input of Nuclear Data 2200 multichannel analyzer) was recorded as a function of the specimen current, i, and m/i vs. m curves (current method described by Heinrich, Vieth and Yakowitz [3]) were plotted. Curves of m/n vs. m were easily extracted from such data since $n = ki$ where k is the extrapolated value of m/i at $m = o$; thus $m/n = (m/i)/k$. In Fig. 2 experimental m/n vs. m data are compared with theoretical self prolonging (curved) and non self prolonging (linear) curves. At narrow pulse widths, the experimental precision is insufficient to distinguish between models but at wider pulse widths and high intensities it is apparent that the system is of the self prolonging type and the experimental data fit the expression $m = ne^{-n\tau}$ where τ is the amplifier pulse width. Thus, in systems where the amplifier pulse width is the predominant factor, the deadtime is of the self prolonging type and is a function

of intensity as will be shown later.

To examine the effect of the PHA, the components in the lower portion of Fig. 1 were operated simultaneously with those in the upper portion. The pulse generator with a variable delay and pulse width was triggered on the leading edge of the PHA output; thus the generator served as a PHA whose pulse width could be varied from less than the amplifier pulse width to substantially greater values. For each amplifier pulse width (τ) - PHA pulse width (λ) combination, the output of the Saphymo scaler, m', was recorded as a function of the specimen current and m'/i vs. m' data were used to obtain m'/n vs. m' data; typical data for τ = 5.6 μsec and λ = 8.0 μsec are shown in Fig. 3. It is apparent that neither a simple self prolonging nor a non self prolonging model fit the experimental data.

The inset (upper right hand corner) in Fig. 3 depicts the physical situation. The amplifier has a prolonged deadtime, τ', due to pulse pileup. The PHA output is released after τ' and triggers the scaler after time λ; however, for a period $< \tau$ before the expiration of λ the amplifier can process another counted pulse. The duration of a single counted event is then $\tau' + \lambda - \tau$. The counts lost per counted event are $n(\tau' + \lambda - \tau)$. Since the counted events per second are m, the loss per second, n - m, is m $n(\tau + \lambda - \tau)$ and

$$m/n = 1/(1 + n(\tau' + \lambda - \tau)) \qquad (1)$$

To determine τ' consider the amplifier alone. In one second the number of observed counts is m where m = n (time on); (time off) = 1 - (time on) = 1 - (m/n); τ' is the (time off)/m; $\tau' = (1-(m/n))/m$ and since $m = ne^{-n\tau}$, $\tau' = (e^{n\tau} - 1)/n$. τ' can also be obtained by determining the non self prolonging deadtime that would provide the equivalent self prolonging loss; $m/n = e^{-n\tau} = 1/(1 + \tau'n)$; $\tau' = (e^{n\tau} - 1)/n$. Substituting τ' in Equation 1 gives:

$$m/n = 1/(e^{n\tau} + n(\lambda - \tau)). \qquad (2)$$

When $\lambda = \tau$ this equation reduces to self prolonging and when $\tau = 0$ this equation reduces to non self prolonging with $m/n = 1/(1 + n\lambda)$.

In Fig. 3 Equation 2 is seen to provide a good fit to the experimental data. Plots of m'/m versus m' were linear and within experimental error gave constant deadtimes of $(\lambda - \tau)$. This was as expected since the Ortec PHA pulse width of 0.5 μsec was less than the amplifier pulse width and m represented the input to the pulse generator. A major problem involved in the collection and evaluation of such data was the pulse amplitude reduction which occurred at high intensities causing reduced pulse widths and base line clipping.

In the determination of the deadtime of a counting system on an electron probe utilizing proportional detectors, we recommend first observing the amplifier and PHA outputs with a dual trace oscilloscope. The pulse width of the amplifier output is the time between the triggering of the amplifier by the preamplifier and the point where the trailing edge of the amplifier pulse crosses the baseline voltage; the time from this latter point to the point on the trailing edge of the PHA pulse where the scaler is triggered is considered the width of the PHA pulse. If the amplifier pulse width is greater than that of the PHA the deadtime will be

related to the amplifier pulse width. Two cases are possible. If this pulse width is small, as is the usual case, and intensities are in the range normally encountered in microanalysis, the deadtime will be equal to this pulse width. This can be easily verified by performing the Heinrich[3] current measurements since under these conditions self and non self prolonging are indistinguishable. If the pulse width is moderate and high intensities are involved or if the pulse width is large, the deadtime will be given by τ' which is intensity sensitive and the fractional loss will be given by $(n - m)/n = 1 - e^{-n\tau}$. Since $m = ne^{-n\tau}$ and $n = ki$ a plot of $\ln(m/i)$ vs. i will be linear with a slope of $-k\tau$ and an intercept of $\ln k$. Corrections can be made by simply plotting m/n vs. m using $m/n = e^{-n\tau}$.

If the amplifier pulse width is less than that of the PHA Equation 2 will fit the experimental data and should be used to make the correction.

Since commercial counting channels can differ significantly, care is required in establishing the nature of the components; however, to date all amplifiers and PHA's we have examined were found to be self prolonging and non self prolonging respectively. Several commercial counting channels will be discussed.

---

1. D. R. Beaman, R. Lewis and J. A. Isasi in Transactions of 5th Internation Congress on X-ray Optics and Microanalysis, Tubingen, Sept. 1968, to be published.

2. V. I. Goldanskii, A. V. Kutsenko and M. I. Podgoretskii, Counting Statistics of Nuclear Particles (Hindustan Publishing Corporation, India, 1962), p. 190.

3. K. F. J. Heinrich, D. Vieth and H. Yakowitz in Advances in X-ray Analysis, Vol. 9, G. Mallett, M. Fay and W. Mueller, Eds. (Plenum Press, New York, 1966), p. 208.

FIGURE 1

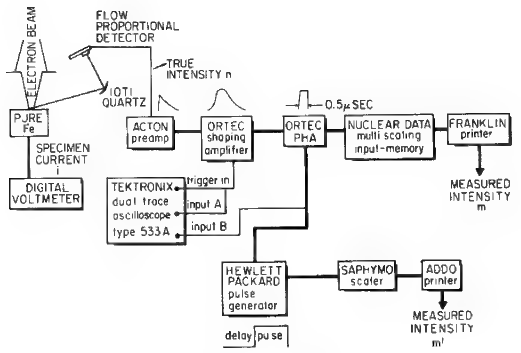

SCHEMATIC OF COMPONENTS

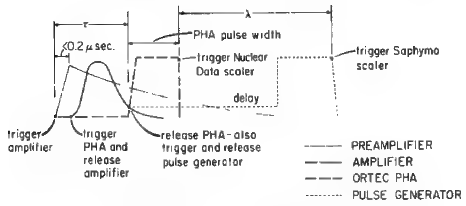

OUTPUT OBSERVED ON OSCILLOSCOPE

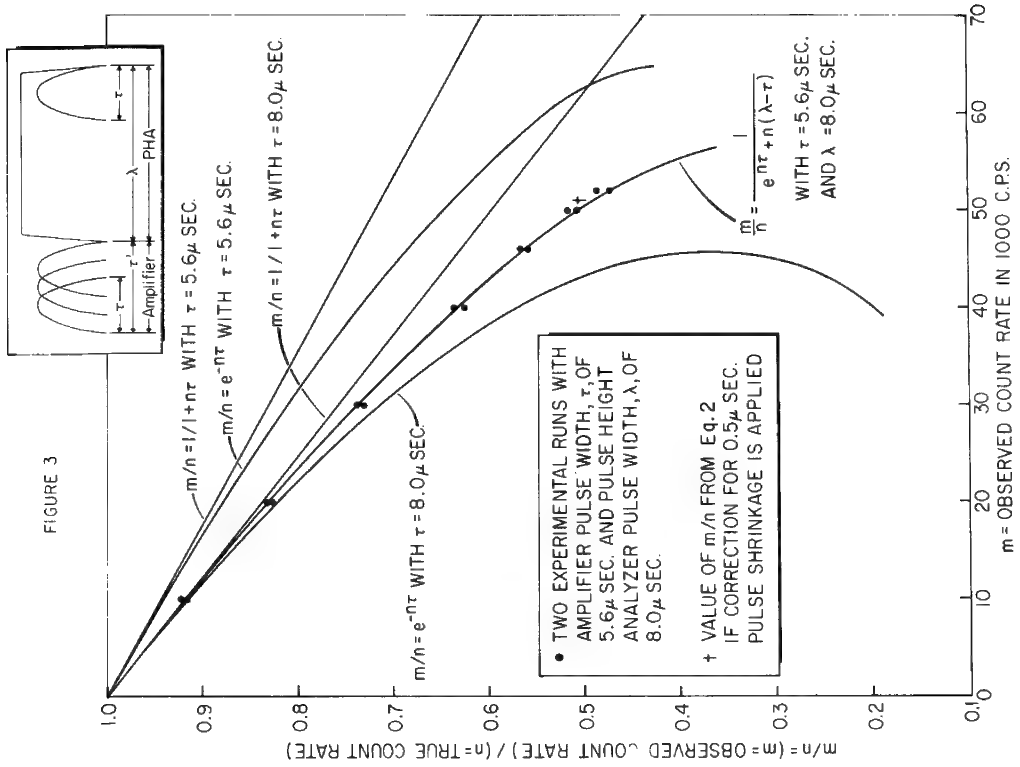

FIGURE 3

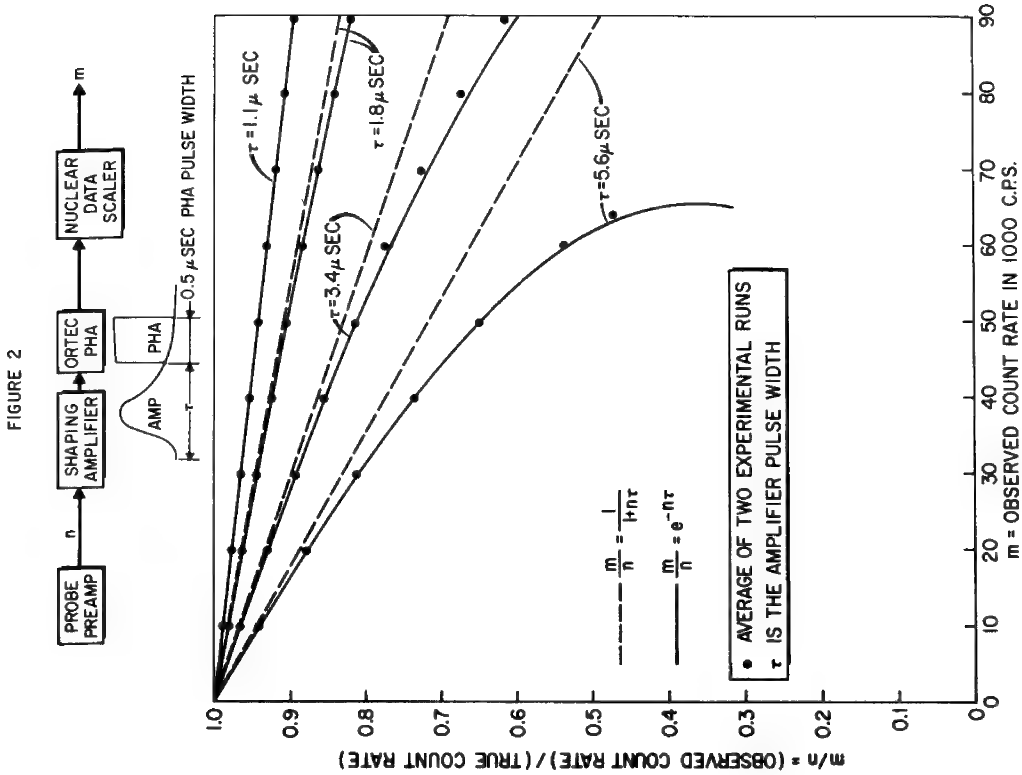

FIGURE 2

QUANTITATIVE ANALYSIS OF OXYGEN IN OXIDES

Toshio Shiraiwa and Nobukatsu Fujino
Sumitomo Metal Industries, Ltd., Amagasaki, Japan

Quantitative analysis of oxygen by means of an electron probe microanalyzer has been studied. The instrument is the ARL-Shimadzu type and the analyzing crystal is 11 inch lead stearate. The oxides examined are as follows: sintered beryllia (BeO), synthetic magnesia (MgO), titania (TiO_2), synthetic chromium oxide (Cr_2O_3), synthetic galaxite ($MnO \cdot Al_2O_3$), natural magnetite (Fe_3O_4), natural hematite (Fe_2O_3), synthetic cuprous oxide (Cu_2O), calcium aluminate (No. 1), magnesium aluminum chromite (No. 3) and manganese alumium silicate (No. 4, 5, 6).

The observed intensities of OKα from oxides are shown in Fig. 1. The accelerating voltage is from 5 KV to 30 KV and the probe current is fixed at 0.1 μA of sample current on magnesia.

Oxygen content is calculated from the observed intensity using the modified Philibert absorption correction[1,2] and the Poole-Thomas' atomic number correction[3]. The μ/ρ of lighter element ($Z \geqq 18$) are quoted from Henke's table[4]. However, the μ/ρ of heavier elements ($Z > 18$) was not given. For titanium whose L excitation energy is lower than OKα, the μ/ρ are obtained Heinrich's equation but the value near the L absorption edge is reduced according to the shape of Henke's data. For chromium, manganese, iron and copper whose L energy is higher than OKα, they are estimated as follows. For copper, it is obtained by extrapolation from Cooke's experiments[6] which give μ/ρ for shorter wavelength than 17 Å. The exponent of the absorption curve agrees with those of krypton given by Henke[4] and of Heinrich's data[5]. This absorption curve is extended to chromium, manganese and iron using Jönsson's law[7]. These estimated results are shown by solid curves in Fig. 2. Using these μ/ρ, the observed intensities are corrected. The result at 15 KV is shown in Fig. 3.

The results for oxides of heavier elements at 15 KV are incorrect. Similar errors are observed at the other accelerating voltage. It is suggested that one reason for disagreement is error in estimating μ/ρ. The μ/ρ were reversely calculated from the experimental data and the values obtained are shown by dots in Fig. 2.

---

1. J. Philibert, X-ray Optics and X-ray Microanalysis, p. 379, Academic Press, New York, 1963.

2. P. Duncumb and P. K. Shield, Electron Microprobe, p. 284, John Wiley, New York, 1966.

3. D. M. Poole and P. M. Thomas, J. Inst. Metals. 90, 288 (1961-62).

4. B. L. Henke, Norelco Reporter, 14, 112 (1967).

5. K. F. J. Heinrich, Electron Microprobe, p. 296, John Wiley, New York, 1966.

6. B. A. Cooke and E. A. Stewardson, Brit. J. Appl. Phys. 15, 1315 (1964)

7. A. H. Compton and S. K. Allison, X-rays in Theory and Experiments, p. 539, D. Van Nostrand, New York, 1935.

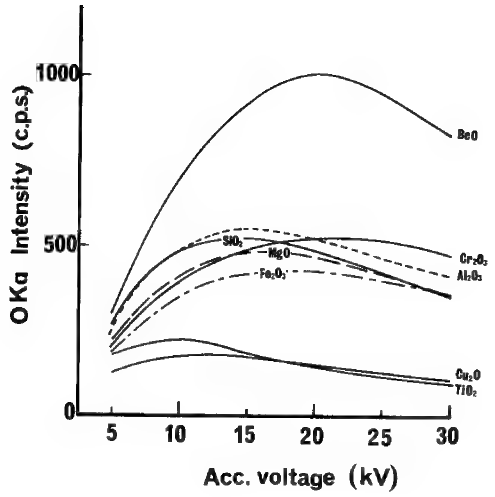

Fig. 1 Intensity of OKα from oxides

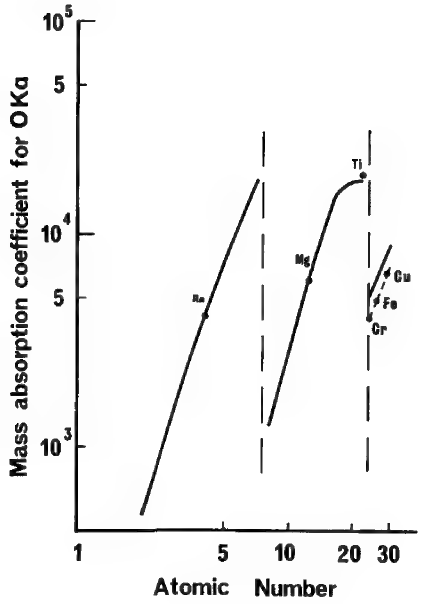

Fig. 2 Mass absorption coefficient for OKα

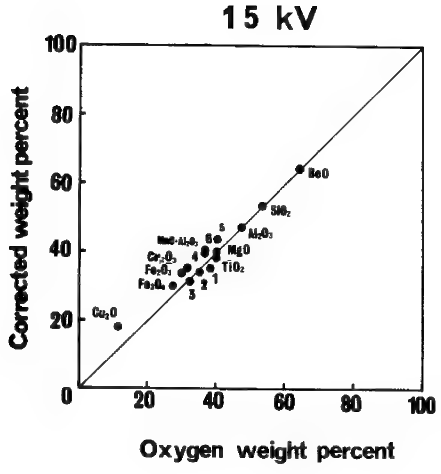

Fig. 3 Quantitative analysis of oxygen in oxides

STANDARD REFERENCE MATERIALS FOR QUANTITATIVE ELECTRON PROBE MICROANALYSIS

Kurt F. J. Heinrich
National Bureau of Standards, Washington, D.C.

The absolute measurement of the intensity of X-ray emission in the microprobe is affected by large uncertainty. Therefore, quantitative analysis is based upon the comparison of intensities obtained from the specimen and from a suitable standard.

There is controversy about standardization procedures. Practice ranges from comparison of unknown specimens with standards of very similar composition, to the use of elemental standards with extensive calculation of the corrections for matrix effects. Both approaches will be followed by the analyst, depending upon the availability of standard reference materials.

The method using simple standards and large corrections is based on our faith that the effects of composition and experimental conditions vary in a continuous and hence predictable way. In these corrections one takes into account the intensity and the primary distribution in depth of X-rays and the production of secondary X-rays. Several physical parameters are assumed to vary smoothly with atomic number and atomic weight, as well as with the weight percentage of the elemental components. The testing of a model based on such assumptions is complicated by the presence of sources of error which are not considered in the model. Among such sources of error are statistical fluctuations, measurement errors, errors in chemical analysis or inhomogeneity of the standards, and perhaps also factors related to electrical conductivity and lattice structure.

Since the precision of X-ray intensity measurement is better than the expected accuracy of the correction, the statistical error factor should not be dominant. The difficulties and pitfalls of the evaluation of models on the basis of a large number of standards and measurements have been discussed elsewhere[1]. If the assumption of continuity of the model is correct, then it is not advantageous to use a very large number of loosely screened test analyses for the comparison of the efficiency of models. Rather, it is desirable to develop a small group of standards which are very carefully chosen. These standards must

1. Represent critical tests of several aspects of the theory.
2. Be very well characterized as to composition and homogeneity, and
3. Exclude possible sources of error such as low conductivity, which were not considered in the theory behind the models.

Two series of binary alloys recently tested and certified by the National Bureau of Standards - Standard Reference Material 481 and 482 - are intended to be part of such a standard system. These alloys cover the systems Au-Ag and Au-Cu in nominal steps of 20 weight percent. The materials are offered as wires, 0.5 mm in diameter, with colored coatings for identification. They were analyzed chemically by three laboratories with the results of the analyses as shown

in Table I. Homogeneity along the wire was tested by residual electrical resistivity measurements. The variation along the total wire (hence, the variation among sub-samples) was found to be less than 0.1 % absolute. Homogeneity across diameters of wire cross-sections, and homogeneity on a microscopic scale, were tested by extensive electron probe analysis, using the matrix scanner technique[2]. On each alloy, 6-8 arrays of 10 x 10 points, from three to five cross-sections, were measured. The distance between adjacent points was 3.5 μm. Table II shows the range of the standard deviations of a single value within each of the arrays. The results do not show any inhomogeneity distinguishable from the expected precision limits of the measurement. Approximately one thousand measurements were performed at each of the eight alloys.

The systems Au-Ag and Au-Cu are of interest with regard to the following effects:

1. The measurement of the gold by means of the Au M lines, and of copper by means of the Cu L lines, is affected by strong absorption losses, which are absent for Au L lines and Cu K lines.

2. Both systems exhibit a significant atomic-number difference. The presence of a heavy element such as gold determines that the effects of both the stopping power variations and the backscatter losses will be significant.

3. The fluorescence of the copper K lines by gold L lines is significant.

Although these standards are expected to be of use in the testing of various models, for a complete testing program it will be necessary to extend the number of standards, particularly incorporating alloys containing elements of lower atomic number.

---

1. Kurt F. J. Heinrich, Adv. in X-Ray Analysis, 11, p. 40 (1968).

2. NBS Technical Note 452, (1968) p. 26.

Table I

Chemical Analysis of SRM 481 and SRM 482

SRM 481 Wire	Color Code	Nominal Composition	Cominco American[a] Au	U.S. Bureau of the Mint[b] Au	U.S. Bureau of the Mint[b] Ag	NBS[c] Au	NBS[c] Ag
			Percent by weight				
A	Gold	Au100	-	-	-	-	-
B	Gray	Au80-Ag20	80.00	80.02	20.00	80.13	19.93
C	Yellow	Au60-Ag40	60.01	60.11	39.85	60.04	39.98
D	Blue	Au40-Ag60	39.99	40.03	59.90	40.06	59.96
E	Red	Au20-Ag80	22.42	22.42	77.59	22.46	77.56
F	Silver	Ag100	-	-	-	-	-

SRM 482 Wire	Color Code	Nominal Composition	Cominco American[a] Au	U.S. Bureau of the Mint[b] Au	U.S. Bureau of the Mint[b] Cu	NBS[d] Au	NBS[d] Cu
			Percent by weight				
A	Gold	Au100	-	-	-	-	-
B	Gray	Au80-Cu20	80.1	80.13	19.81	80.21	19.85
C	Blue	Au60-Cu40	60.3	60.37	39.66	60.41	39.62
D	Yellow	Au40-Cu60	40.1	40.06	59.88	40.11	59.97
E	Red	Au20-Cu80	19.9	20.12	79.84	20.21	79.86
F	Copper	Cu100	-	-	-	-	-

---

a. The fire assay method was employed for the determination of Au by Cominco American.

b. At the U.S. Bureau of the Mint, Au was determined by fire assay, Ag was determined by titration as AgCl, and Cu by electrodeposition.

c. At NBS, Au was determined from the residue after treatment of the alloys with HNO_3. The Au residue was dissolved in aqua regia, filtered, the Au precipitated by sulfurous acid, and weighed. Ag was determined gravimetrically as AgCl in all four alloys, and also coulometrically in the 80% Ag alloy.

d. At NBS, Au was determined by precipitation from solution, and Cu was determined by electrodeposition.

Table II

Standard Deviations Obtained on 10 X 10 Arrays

Nominal Composition	Element Evaluated	Range of Standard Deviations for Arrays*
Au80-Ag20	Ag	0.09-0.15%
Au60-Ag40	Au	.18- .57
Au40-Ag60	Au	.11- .66
Au20-Ag80	Au	.19- .25
Au80-Cu20	Cu	0.09-0.24%
Au60-Cu40	Cu	.16- .27
Au40-Cu60	Au	.13- .23
Au20-Cu80	Au	.13- .20

*(Note: The ranges in this table are close to the precision of the method and should be considered upper limits of estimates of inhomogeneity.)

A CRITICAL EXAMINATION OF COMPUTER PROGRAMS USED IN QUANTITATIVE ELECTRON MICROPROBE ANALYSIS

D. R. Beaman and J. A. Isasi
Dow Chemical Company, Midland, Michigan

All of the existing computer programs used in the conversion of X-ray intensity ratios to chemical concentrations have been studied and critically evaluated. There are presently 23 such programs available to the analyst. The objectives of this investigation were as follows: 1) to provide a complete listing of the available programs including a brief description and the merits of each; 2) to provide sufficient information so that each analyst could select the program most suitable for his needs based upon the type of problem he normally encounters, the computer facilities at his disposal, his interest in different correction procedures, etc.; 3) to critically examine the program and therein provide guidelines for program selection; 4) to establish what a program should and should not contain in an attempt to diminish duplication and the proliferation of inadequate programs.

Each program was carefully studied and a description of each was written which was sent to the author for his comments. The description covered many aspects including: software information, correction procedures (range of atomic number applicability), non-normal incidence, normalization of calculated concentrations, mass absorption coefficients, drift, deadtime, background, permutation, convergence, input requirements, etc. Each author was also requested to use his program and correct specific probe intensity ratios supplied by us for three alloy systems using the same physical data. The three systems were Ti-Nb, Fe-Cr, and Cr-Co-Mo. Programs written by the following authors were evaluated: D. R. Beaman; F. Borile; J. Brown; J. W. Colby; J. W. Criss; P. Duncumb and E. M. Jones; M. Frost; J. Z. Frazer, R. W. Fitzgerald and A. M. Reid; J. I. Goldstein; T. R. Gurney and E. Bonizewski; R. E. Hanneman and E. Lifshin; C. I. Helgesson; M. G. Hobby and G. W. Wood; S. Kimoto, M. Sato and H. Ohyi; V. G. Macres and R. G. Wolf; J. Moriceau; B. Pascal; J. Rucklidge and E. L. Gasparrini; J. L. Shaw; S. S. So and H. R. Potts; G. Springer; L. T. Woodyatt and R. J. Henry; C. Zeller, J. C. Reithler and F. Zeller. Complete references will be made available.

The programs were judged using several criteria: proven usefulness of the correction schemes; completeness of the correction scheme (is an atomic number correction included ?); accuracy of the correction scheme; applicability to different disciplines; data handling capabilities; range of applicability, i.e., usefulness at very low and very high atomic numbers; limitations of the correction scheme, i.e., voltage restrictions, KL fluorescence etc.; applicability to different angles of incidence and take-off; restrictions imposed by permanent input information (physical constants); running cost and storage requirements; degrading approximations such as normalization etc.; relative ease of use (input requirements); availability of secondary information such as limits of detection, Ziebold a coefficients, etc.; calibration calculations, i.e., expected intensity ratios computed from assumed compositions; use of compound standards, number of components allowed per alloy system; etc.

Table I is typical of one of the many tables constructed to aid in the evaluation. Most of the information is self explanatory. Programs which, can only be used in binary systems, contain

incomplete fluorescence corrections, lack or contain an inappropriate atomic number correction, are not written in a common language, can only be used at a single take-off angle, etc. will be of limited usefulness. Several additional tables and a ranking of the programs with respect to overall usefulness and quality will be presented.

The results of the calculations by selected authors are presented in Table II. The variations arise primarily from the use of different mass absorption coefficients and correction schemes; incomplete and improper corrections also contribute. Additional results will be presented and discussed.

TABLE I

Author	year of publication	language	maximum no. of components	take-off angle	cards available on request	calibration k from C	KL, LL, LK fluorescence	Kβ or Lβ excitation	Correction Scheme: Atomic Number	Absorption	Characteristic Fluorescence	Continuous Fluorescence
Borile	69	Basic	any	any	no	no	yes	no	DR	DS	Reed	none
Duncumb	69	F	8	any	yes	yes	yes	no	DR	H	Reed	none
Frost	69	F-4				yes	yes		DR	DS, H	Reed	none
Kimoto	69										Reed, C	
Colby	68	F-4	8	any	yes	no	yes	no	J-S-R	DS	Reed	none
Goldstein	68	F-4	9	any	yes	yes	yes	yes	DR	H	Reed	none
Moriceau	68						no	no	S-R	P	Castaing	none
Pascal	68	F	10	any	no	yes	yes	yes	Monte-Carlo	Monte-Carlo	C, Monte-Carlo	Henoc
Rucklidge	68	F-4	15	52.5*	yes	yes	yes	no	LR	P	Reed	none
So	68	F-4	2	any	no	yes	yes	no	P	DS	C, Reed, Birks	none
Woodyatt	68	F-4	10	any	no	no	yes	no	Z	DS, P	C, W, Birks	none
Zeller	68	Algol	12						Zeller (R)	DS	C	none
Hobby	67	Algol	20	20*	no	no	LL	yes	DS-F(χ)	DS-f(χ)	Reed	none
Shaw	67	F-4	8	any	no	no	yes	yes	J-S-R	H	Reed	none
Springer	67	Algol	any	any	no	yes	yes	no	Springer	DS	Reed	Springer
Brown	66	F-4	10	any	yes	yes	yes	yes	Thomas	DS, P	C, W, Reed	Henoc
Frazer	66	F-63	18	52.5*	no	yes	no	no	none	DS	C-W	none
Helgesson	66	F	2	any		no	no	no	Tong, P	Tong, P	none	none
Lifshin	66	F	2	any	no	yes	yes	no	none	DS	Reed	none
Criss	65	F-2	any	any	yes	yes	yes	yes	Thomas	Criss	Criss	none
Macres	63	Balgol	2	38.5	no	no	no	yes	none	P	W	C
Beaman	67	Algol F-4	7	any	yes	yes	yes	yes	Tong, Thomas DR, PT, Z	Green, AW DS, H, P	Reed, C	Henoc

P= Philibert; DS = Duncumb and Shields; H = Heinrich; DR = Duncumb and Reed; LR = Long and Reed; PT= Philibert and Tixier; AW = Andersen and Wittry; Z =Ziebold; C = Castaing; W = Wittry; J-S-R - mean ionization potential from DR, stopping power from Bethe, backscatter from Bishop.

*can be easily changed to another fixed value
F = Fortran

TABLE II

RESULTS OBTAINED USING DIFFERENT COMPUTER PROGRAMS

alloy systems	Ti-Nb		Cr-Co-Mo			Fe-Ni	
element	Ti	Nb	Cr	Co	Mo	Fe	Ni
experimental concentration	32.6	62.0	11.7	79.7	7.7	49.4	52.5
true chemical concentration	35.0	65.0	9.9	80.6	9.4	43.6	56.6
Author	Calculated Concentrations						
Brown	37.9	62.7*	10.4	81.3	9.2	44.7	56.7
Colby	34.8	63.6	10.0	80.9	9.5	44.7	56.3
Frazer	37.9	63.3*	12.01	81.7	9.5	45.4	55.4
Beaman	35.3	65.5	9.9	81.0	9.9	44.7	56.7
Rucklidge	34.4	64.4	10.2	80.6	9.7	44.8	56.1
Pascal	35.1	64.9	9.9	80.5	9.5	44.1	55.9
Woodyatt*	26.3	73.6	10.6	77.6	11.6	45.2	54.7
Hobby	36.5	63.3	10.7	81.4	9.3	44.7	56.8
Shaw	34.7	65.1	10.2	80.7	9.8	45.0	55.9
Duncumb	34.7	65.3	10.3	80.7	9.9	45.0	55.9
Borile	35.3	65.4					
Mean	35.7	64.7	10.4	81.0	9.6	44.8	56.2
1σ	1.3	0.8	0.7	0.4	0.2	0.4	0.5

*omitted in calculating the mean

AN INVESTIGATION OF THE ATOMIC NUMBER EFFECT IN Cu-Ni ALLOYS

Richard M. Ingersoll*, H. Richard MacQueen** and Joel L. Solomon***
*Anaconda American Brass Co. **IBM, Endicott, New York ***IBM, Owego, New York

---

Three Cu-Ni alloys were analyzed to investigate the atomic number effect in Cu-Ni alloys as indicated by Ranzatta and Scott[1].

For this work, three Cu-Ni alloys - 90 Cu, 10 Ni - 70 Cu, 30 Ni - 10 Cu, 90 Ni - were made at the Research and Technical Center of Anaconda American Brass Company. The alloys were cast, hot and cold worked to 1/8 inch thickness, and then annealed 170 hours at 1000°C to minimize segregation which is difficult to completely eliminate in Cu-Ni alloys. The alloys were encapsulated in Vycor glass with an He atmosphere for the annealing, and no discoloration of the samples was noted after the heat treatment. The alloys were then analyzed for segregation in the probe and found to be sufficiently homogeneous for this study, except for some grain boundary precipitates in the 10 Cu, 90 Ni material. These precipitates were quite evident in the as-polished condition and the Group was told to analyze only in grain centers on this specimen.

The specimens were analyzed by 12 laboratories using probes from six manufacturers utilizing take-off angles from 15 to 52.5°. Point counting was used in all analyses. The atomic number correction was calculated using the method of Duncumb and Shields[2] and the Nelms[3] electron range; the absorption correction using that of Philibert as modified by Duncumb and Shields[4]; and the fluorescence correction using that of Reed[5]. These corrections were calculated as a function of weight fraction in increments of 0.001 weight fraction within a range of $\pm$ 0.025 from the nominal compositions of the alloys. When this data was plotted, the curves indicated the direction and magnitude of these corrections. The data in Table 1 for the 70 Cu, 30 Ni alloy illustrates this, and shows a fairly strong atomic number correction, one that certainly for Cu-Ni alloys cannot be ignored.

Data from the other two alloys will also be presented as well as the curves from which this information is derived.

---

1. G. V. T. Ranzatta and Scott, British Journal of Applied Physics 18, no. 10, p. 1403-1406.

2. P. Duncumb and P. K. Shields, British Journal of Applied Physics 14, p. 617-625.

3. A. T. Nelms, NBS Circular 577 (1956) and Supplement 1958.

4. P. Duncumb and P. K. Shields, The Electron Microprobe, McKinley et al. (eds.), Wiley and Sons, N.Y. 1966, p. 284.

5. S. J. B. Reed, British Journal of Applied Physics 16, p. 913, 1965.

TABLE I

EFFECTS OF VARIOUS CORRECTIONS ON A 70 Cu–30 Ni ALLOY

FOR Cu TAKE OFF ANGLE	I/I_o	ABSORPTION	ABSORPTION AND ATOMIC NUMBER	ABSORPTION AND FLUORESCENCE	ABSORPTION ATOMIC NUMBER FLUORESCENCE
15°	0.7051	0.7012	0.7125	0.7012	0.7125
52.5°	0.6939	0.6925	0.7038	0.6925	0.7038
FOR Ni					
15°	0.3275	0.3310	0.3200	0.3170	0.3060
52.5°	0.3091	0.3085	0.2975	0.2904	0.2804

WET CHEMISTRY

Cu 0.7005 Ni 0.299

ALL VALUES ARE IN WEIGHT FRACTION.

IMAGING PROPERTIES OF THE SECONDARY ION EMISSION MICROANALYZER

R. Lewis and A. Cambey
Bell and Howell Co., Monrovia, California

The secondary ion emission microanalyzer is an instrument that combines the features of a mass spectrometer with an ion emission microscope. This unique instrument allows a surface distribution map to be formed of any isotope of the elements making up the specimen.

In this instrument, secondary ions emitted from a specimen under ion bombardment are accelerated and focused by an electrostatic immersion lens into a beam. This beam carries a real image formed by all the ion species extracted from the specimen. This image is separated into its various elementary ion images by a special prism-mirror-prism stigmatic focusing mass spectrometer. Each elementary image, isolated by the exit window of the mass spectrometer, is projected onto the cathode of an image converter to form an electron image which is displayed on a fluorescent screen. By changing the field strength of the mass spectrometer magnet, it is possible to observe in succession chemical distribution maps provided by these elementary images formed by the emission of ions from the specimen surface. Detailed descriptions of this instrument have been published[1,2].

The imaging properties of the instrument have been investigated in detail. The converted ion to electron image can be viewed on the fluorescent screen through a teleobjective microscope over a magnification range of about 350 to 700. The maximum field of view is 225 microns. This method of viewing, together with the high sensitivity of the ion detection system, allows the areas of interest to be quickly identified while the specimen position is being varied continuously.

The electron image may also be deflected to another position where it can be recorded on a film contained in a cassette placed in the image converter section. Figure 1, A and B show typical images recorded in this manner. The specimen was a Ca-Al eutectic alloy. The bombarding beam was O^+ at 10 KeV. The exposure times required were of the order of several milliseconds. Densometric analysis of the film shows the spatial resolution to be less than one micron.

Performing accurate in-depth analysis and achieving good in-depth resolution imposes further restrictions on the operating conditions in addition to those necessary for achieving good spatial resolution. It is important that the area sputtered extends well beyond the area being imaged in order to eliminate interference from material sputtered from the sides of the eroded cavity. This effect becomes of increasing importance the deeper the depth of analysis.

The shape and the depth of cavities formed in single crystal silicon by sputtering with the primary beam have been studied with the aid of interferograms. The effects of the optical aberrations in the primary beam when present were clearly discernable. In another experiment, holes were sputtered through films of known thickness. By using both these techniques and integrating the total secondary ion current produced, the sputtering yield and the sputtered ion yield have been determined for several elements.

1. R. Castaing et al., "Focusing of Charged Particles", Academic Press, New York, 1967.

2. J. M. Rouberol et al., "Transactions of the Third National Conference on Electron Microprobe Analysis", Paper No. 28, 1968.

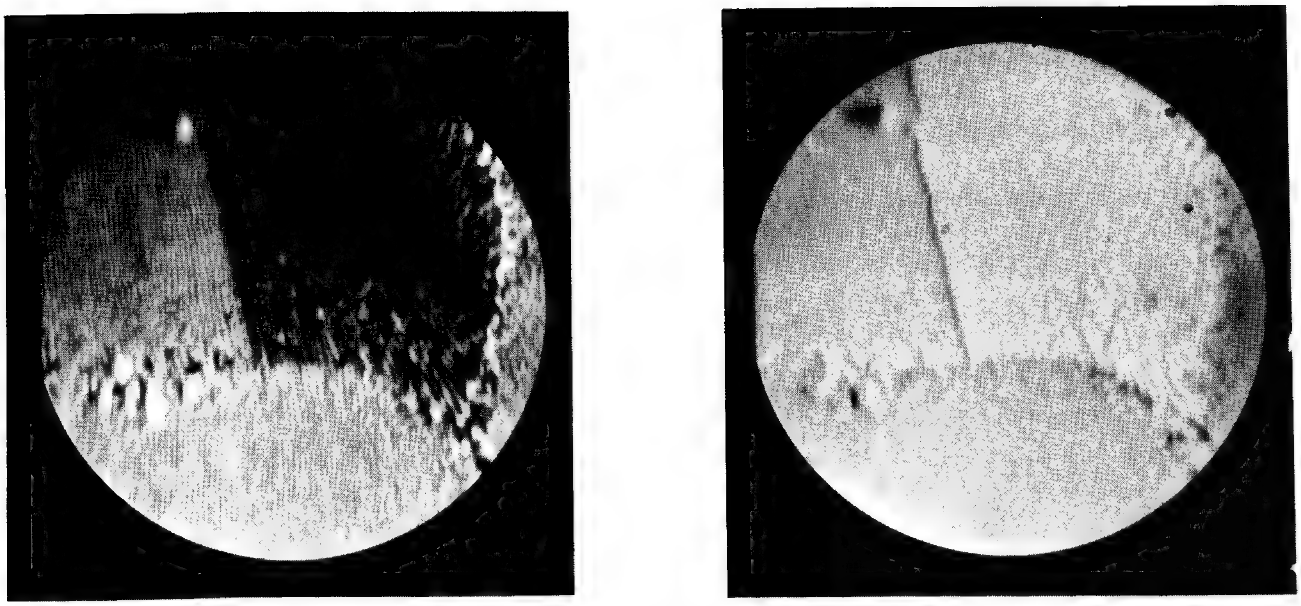

Ca^+ 350 X Al^+ 350 X

Fig.1 ION IMAGES OF A Ca-Al EUTECTIC ALLOY
PRIMARY BEAM O^+ 10 KeV

ANALYTIC METHODS FOR THE ION MICROPROBE MASS ANALYZER, PART II

C. A. Andersen
Applied Research Laboratories, Goleta, California

The ion microprobe mass analyzer utilizes the sputtering phenomena to produce a mass analysis of the surface of a solid material. The sample is bombarded with a finely focussed beam of high energy ions. The bombarding ions lose energy to the atoms in the surface of the material through a series of atomic collisions. Atoms at the surface of the sample that receive energy in excess of their binding energy are sputtered from the sample. A fraction of the sputtered atoms leave the surface as ions and these are collected and analyzed in a mass spectrometer.

It has been shown (1) that it is possible to control positive sputtered ion emission from metal samples by controlling the surface chemistry of the sample during bombardment. This is accomplished by bombarding with a highly reactive gas such as oxygen rather than an inert gas, such as argon.

The sputtered atom yield in the kilovolt bombarding energy range can, in the general case, be understood in terms of elastic, hard-sphere collision physics (2), the number of atoms sputtered from a particular sample with a given bombarding beam being proportional to the cross section for collision and to the maximum energy transferred in an elastic collision. It has also been found that the number of atoms sputtered (3) and the minimum energy necessary to initiate sputtering (4) are related to the binding energy of the atoms in the surface.

The probability that a given atom will be sputtered as a positive ion depends on the availability of electrons at the surface, being lower when loosely bound electrons become increasingly available for neutralization of positive ions as they are sputtered out of the surface. A surface layer consisting mainly of strongly bonded material contains relatively few loosely bonded electrons for ion neutralization, and such strongly bonded surface layers enhance the probability that a sputtered atom will retain a positive charge as it passes through the surface layer.

In the simple case of clean metals bombarded with inert gases the binding energy is equivalent to the measured heat of sublimation. In the case of compounds and of metals bombarded with reactive gases the binding energies are dictated by the nature of the chemical bonds, the binding energy being equal to the energy required to take an atom from the solid state of the compound to the monatomic gaseous state. The binding energy, therefore, involves the heat of formation of the compound, the heat of sublimation of the metal atom and the heat of dissociation of the gaseous anion. Standard thermodynamic values are used in these calculations. Using a model for sputtering established by sputtered atom emission it is possible to interpret the sputtered ion emission from metals bombarded with reactive gases by assuming the formation of simple compounds.

In some cases the positive sputtered ion yields from compounds and metals bombarded with reactive gases are observed to represent essentially 100% of the atom yield expected on the basis of the sputtered atom model. This high efficiency of positive ion emission is found for elements of low electron affinity sputtered from samples having strongly bonded surfaces such as highly insulating compounds and for certain electropositive metals bombarded with electronegative gases. Typical members of the first group are NaCl, KCl, LiF, BN, Al_2O_3, SiO_2 and TiO_2. Representatives of the second group are combinations such as Al, Si, Mg or Ti bombarded with C, N, O, F, or Cl. Independent surface barrier measurements (5) on thin layers of compounds produced from some of these combinations in intimate contact with the pure metal have shown the barriers to be in excess of one electron volt. This barrier height essentially precludes any appreciable electron transfer through the thin surface compound such as would be necessary for positive ion neutralization.

Isotope ratio measurements of elements in metals, alloys, and insulators show that mass discrimination effects in the sputtering and ion neutralization processes are very small, as might be expected. Thus sputtering affords a means for measuring isotope ratios of specific elements in alloyed or chemically bound form (e.g. insulators) without chemical preparation.

---

1. C. A. Andersen, Third Nat. Conf. on Electron Microprobe Analysis, Chicago, 1968; Internat. J. Mass Spect. and Ion Phys. 2, 61, 1969.
2. P. K. Rol, J. M. Fluit and J. Kistemaker, Physica, 26, 1009, 1960.
3. O. Almen and G. Bruce, Nucl. Instr. Methods, 11, 257, 1961.
4. G. K. Wehner, Adv. in Electronics and Electron Physics, VII, Academic Press, N. Y., 1955, p.239.
5. C. A. Mead, Calif. Inst. of Technology, Pasadena, Calif., personal communication.

ELECTRON BEAM MODULATED OPTICAL PROPERTIES OF SEMICONDUCTORS*

J. H. McCoy and D. B. Wittry
University of Southern California, Los Angeles, California

The electron beam and optical systems of the electron probe microanalyzer have been modified for a novel application to the study of modulated optical properties of semiconductors (1). In recent years modulated reflectance has been accomplished by the techniques of electroreflectance (6), photoreflectance (2), and thermoreflectance (3,4). These have all contributed to band theory through the measurement of critical point transition energies. The technique reported here has several advantages and produces results similar to thermoreflectance.

A commercial electron probe microanalyzer was modified for beam gating by mounting electrostatic deflection plates below the condenser lens, making it possible to sweep the beam off the lower aperture. The vertical illuminator was equipped with a quartz iodine lamp, and half angle illumination was provided on a spot of 10-20 μm. The reflected beam was analyzed by a monochromator as in cathodoluminescence studies,(5) and detected by a photomultiplier. The average output of the photomultiplier was monitored, and the output was also applied to a phase sensitive amplifier with phase reference provided by the square wave gating signal on the deflection plates. The relative reflectance $\Delta R/R$, which is the ratio of the phase sensitive amplifier output and the average photomultiplier signal, is a dimensionless quantity independent of spectral sensitivities or outputs of the optical system. An air jet was used to prevent contamination. Variables in the experiment were the modulation frequency, the electron beam size, current density and voltage, the wavelength of reflected light, and the specimen surface preparation. Measurements were made without the reflected light so that compensation for background due to cathodoluminescence could be made.

Several models have been presented for the modulation of reflectance by electron beams. The large density of excess carriers produced by the beam could change the periodic potential of the crystal or flatten the normal surface potential (2). The latter would produce a Franz-Keldysh effect similar to electroreflectance. The electron beam also causes a change in temperature of the surface and could result in a modulation similar to thermoreflectance (3).

The transient temperature response limits the modulation at high electron beam gating frequencies. From a computer solution of the heat transport equation for a disc source, the fundamental Fourier sine component of modulation was found. The amplitudes of the major peaks in $\Delta R/R$ for germanium and gallium arsenide were measured as a function of frequency, and the results agreed with the temperature modulation, assuming ΔR to be proportional to the temperature change. The response curves did not agree in shape or frequency with an excess carrier modulation model. Thus the modulation mechanism is mostly temperature change.

An attempt to obtain an estimate of carrier densities was made using infrared absorption by free carriers produced in excess by the gated beam. In high resistivity germanium a linear relationship between excess carrier concentration and beam density was found up to the highest density measured of .1 amp/cm^2 at 10 kv.

*Research sponsored by the Air Force Office of Scientific Research, Office of Aerospace Research, United States Air Force, under Grant #AF-AFOSR-68-1414.

The modulated reflectance technique was applied to gallium arsenide. The figure shows the modulated reflectance spectrum obtained near the E_1 and $E_1 + \Delta_1$ critical point transitions. The negative peaks approximate the transition energies and agree with similar results in electroreflectance (6), and the shape of the spectrum is the same as in thermoreflectance (2). The amplitude, however, is almost two orders of magnitude greater than published thermoreflectance data. Thus the electron beam modulation technique produces thermoreflectance spectra with rather high efficiency.

The results presented here demonstrate the feasibility of electron beam modulation techniques. Photoreflectance gives $\Delta R/R$ spectra which are different in shape and sign and lower in magnitude even though excess carriers are produced in both techniques. The similarity of the present results to those obtained in thermoreflectance indicates that heating effects are more important than excess carrier density effects. In contrast with other thermoreflectance techniques, the electron beam is very effective in producing large thermal modulation at reasonably high frequencies. It also places few restraints upon sample size or surface preparation and is a logical extension of electron microprobe techniques to studies in solid state physics.

---

1. J. H. McCoy and D. B. Wittry, Appl. Phys. Letters, 13, 272, 1968.
2. R. E. Nahory and J. L. Shay, Phys. Rev. Letters, 21, 1569, 1968.
3. B. Batz, Solid State Commun., 5, 985, 1967.
4. E. Matatagui, A. G. Thompson, and M. Cardona, Phy. Rev., 176, 950, 1968.
5. D. F. Kyser and D. B. Wittry in The Electron Microprobe, T. D. McKinley, et al., Eds., John Wiley and Sons, Inc., New York, 1966, pp. 691-714.
6. B. O. Seraphin, J. Appl. Phys., 37, 721, 1966.

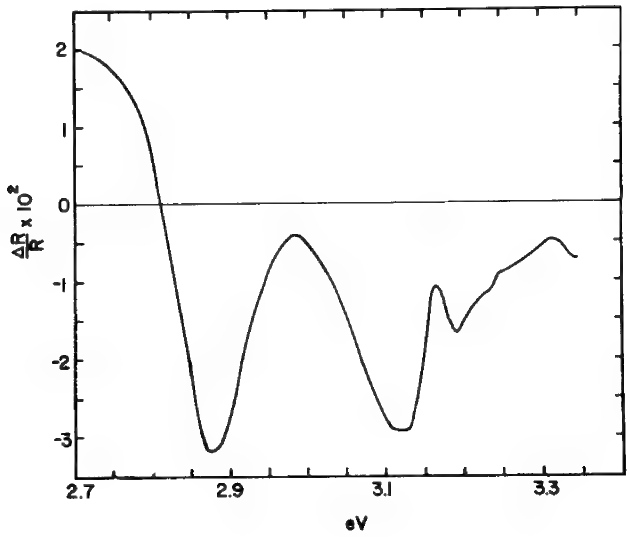

ANALYSIS OF $GaAs_xP_{1-x}$ GROWN FROM Ga-GaAs-GaP TERNARY SYSTEM: QUANTITATIVE CORRECTION AND SOLID SOLUBILITY ISOTHERMS

Chong K. Kim
Bell Telephone Laboratories, Murray Hill, New Jersey

Analysis of $GaAs_xP_{1-x}$ crystals or epitaxial layers grown from Ga-As-P solutions was performed using an electron microprobe. Combinations of raw intensity data (GaK_α and AsK_α, GaK_α and PK_α, or AsK_α and PK_α) are fed into a computer for correction for matrix absorption, backscattering effect, and fluorescence enhancement (1). The corrected results are compared with results of chemical analysis. An accelerating voltage of 25 KV, and a target current of 0.1 μA were used. For phosphorous determination both 25 KV and 15 KV were applied. The corrected data was then used to construct solid solubility isotherms for the establishment of the conditions for liquid epitaxial growth of $GaAs_xP_{1-x}$ layers on GaP and for the growth of crystallites of predictable composition.

The cross sections of the crystals were polished and three readings in different spots about fifty micron apart on each of the crystals were taken. Pure gallium phosphide and gallium arsenide were used as the binary standards for the quantitative comparison. In addition, $GaAs_xP_{1-x}$ of a known composition (X = 0.68) prepared by Monsanto Company was used for checking the correction method.

The corrected data is in good agreement with the wet analysis which is shown in Table I. In wet analysis, arsenic contents in the crystals were determined gravimetrically in the form of As_2S_5 precipitation. Those samples in which chemical analysis data are not shown in the Table are either epitaxially grown crystals or thin platelets grown on top of the heterogeneous Ga-GaAs-GaP mixture. The corrected arsenic and phosphorus data versus the raw x-ray intensity ratio were plotted in Fig. 1. It is indicative that the phosphorous data obtained at 25 KV is slightly over corrected. This might be due to the deeper penetration depth of 25 KV electrons and the subsequent large absorption of moderately soft PK_α x-rays by the matrix (1,2). Therefore, the absorption correction for PK_α at 25 KV accelerating potential in $GaAs_xP_{1-x}$ was somewhat uncertain. To avoid this difficulty, Ga and As x-ray intensities were used to evaluate the phosphorous concentration by difference. This is also shown in Fig. 1. However, if it is desirable to measure PK_α x-ray directly, this can be accomplished by reducing the accelerating potential to 15 KV for PK_α measurement, and subsequent absorption correction was then applied for the analysis of phosphorous.

The analysis was particularly suited for epitaxially grown crystals where wet chemical analysis cannot be applied due to the thin sample and irregularity of the surface.

Solid solubility isotherms were constructed by the use of the probe data listed in Tables II and III, by analysis of epitaxial layers and crystal platelets of $GaAs_xP_{1-x}$. All of the data are plotted in Fig. 2.

The crystals used for the data of Fig. 2 were grown by slowly cooling (5°/hr.) solutions of Ga-As-P (a total of 20°C) from the temperature at which the first crystals were observed. The composition (X) of the mixed crystal, as a function of liquidous

composition (as represented by X^{ℓ}_{As}) is given. The solid lines are the result of probe analysis. The data is consistent and agrees with the estimation drawn from liquid isotherms (3, 4).

---

1. J. Colby, Private Communication, June 1968.
2. H. Yakowitz and K. Heinrich, "Quantitative Electron Microprobe Analysis Absorption Correction Uncertainty", Microchim. Acta, 1968, p. 182.
3. M. B. Panish, B. T. L. MM-68-1152-14, September 1968.
4. C. D. Thurmond, J. Phys. Chem. Solids, 26, 785, 1965.

TABLE I

COMPUTER CORRECTED DATA ON ARSENIC AND PHOSPHORUS IN $GaAs_xP_{1-x}$, AND COMPARISON WITH WET CHEMICAL ANALYSIS

SAMPLE	Intensity Ratio (I_{As}/I^{o}_{As})	Computer Corrected ATOM-% (As)	(P*)	Earlier Report[3] (As)	25kV (I_p/I^{o}_p)	(P)	15kV (I_p/I^{o}_p)	(P)	Wet Analysis (As)	(P)
$GaAs_{.68}P_{.32}$	0.721	34.0	16.1	(34)	0.191	15.6	0.23	16.3	34.0	16.0
M-33	0.309	13.8	36.0	(15.0)	0.477	31.9	0.53	35.4	14.56	35.44
31-0	0.283	11.8	38.3		0.64	38.6	0.67	37.9		
32-2	0.735	35.4	14.0		0.140	12.0	0.18	13.5		
32-3	0.912	44.6	6.1		0.104	9.2	0.09	7.2		
33-1	0.115	4.5	45.0		0.71	41.6	0.76	41.2		
SG-4	0.730	35.0	15.0	(38.5)	0.24	19.0	0.20	14.6		
GaAs P(Monsanto)	0.717	33.3	17.2	(34)	0.19	15.8	0.23	16.3	-	-
477	0.66	30.3	20.0	(32)	0.27	20.9	0.306	21.0		
SG-5	0.91	44.3	5.3	(46.5)	0.09	7.9	0.066	5.2		
479	0.93	45.5	5.0	(49)	0.06	5.5	0.071	5.6		
M-108	-	-	-	(32)	0.124	18.8	0.29	20.0	30.30	19.7

* by difference.

I^{o}_{As} - Intensity of As Kα x-ray from GaAs standard.

I^{o}_{p} - Intensity of P Kα x-ray from GaP standard.

TABLE II

PROBE RESULTS IN ATOM % As IN SOLIDS. (ATOM % LIQUID DATA IS OBTAINED BY WEIGHING Ga, GaAs AND GaP CRYSTALS PRIOR TO MIXING)

Atom % - liquid			Atom % - solid	
Ga	As	P	As	T°C
98.55	0.80	0.65	7.5	913
97.50	2.00	0.50	14.0	902
95.7	4.0	0.30	32.0	903
94.4	5.5	0.10	46.0	900
84.3	13.7	2.00	--	1100
84.7	7.0	8.30	6.5	1220
79.5	14.0	6.50	17.0	1220
73.4	22.5	4.10	27.5	1210
68.3	30.0	1.70	45.5	1220
72.5	14.0	13.50	10.6	1312
61.25	30.0	8.75	26.0	1300
52.5	40.0	7.50	--	1305

TABLE III

COMPOSITION DATA FOR $GaAs_xP_{1-x}$ CRYSTALS GROWN FROM 1100 TO 1080°C

ATOM %-Liquid			ATOM %-Solid (probe results)	
Ga	As	P	As	Growth Type
94.32	1.0	4.65	2.3	platelet
91.90	4.0	4.10	8.3	epitaxial
91.90	4.0	4 10	6.3	platelet
88.75	8.0	3.25	13.5	epitaxial
88.75	8.0	3.25	15.1	platelet
85.70	12.0	2.30	25.6	platelet
82.60	16.0	1.40	32.0	epitaxial
82.60	16.0	1.40	38.5	platelet
80.40	19.0	0.60	45.5	epitaxial
80.40	19.0	0.60	46.5	platelet

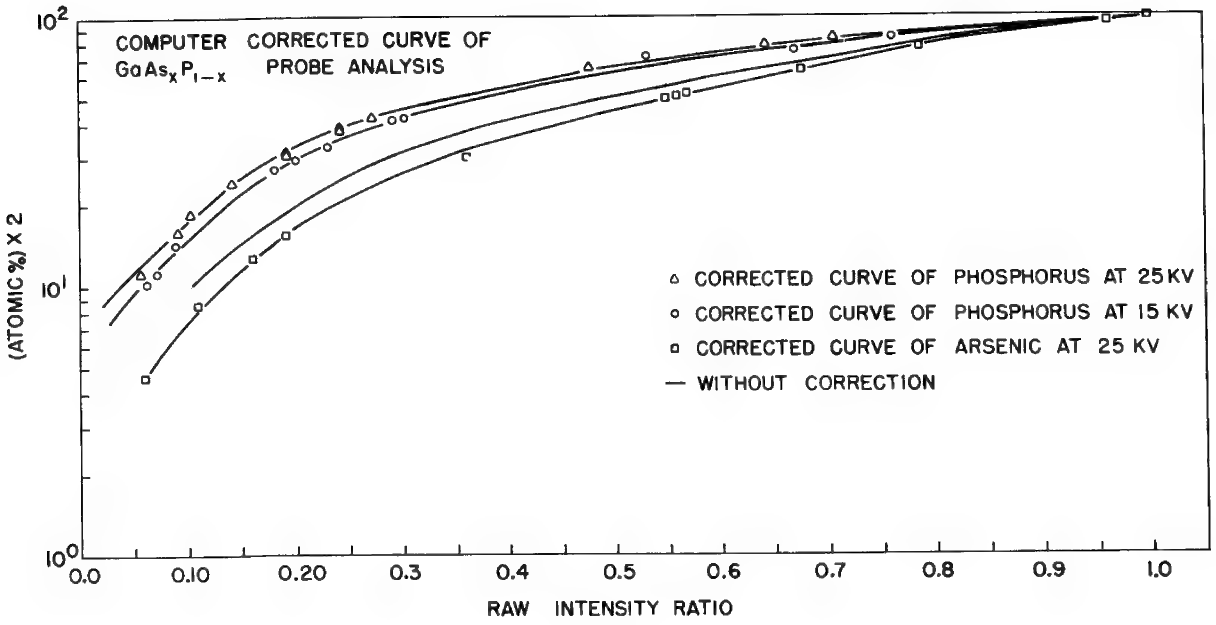
COMPUTER CORRECTED CURVE OF
GaAsxP1−x PROBE ANALYSIS
(ATOMIC %) X 2
RAW INTENSITY RATIO
CORRECTED CURVE OF PHOSPHORUS AT 25 KV
CORRECTED CURVE OF PHOSPHORUS AT 15 KV
CORRECTED CURVE OF ARSENIC AT 25 KV
WITHOUT CORRECTION

FIG 1

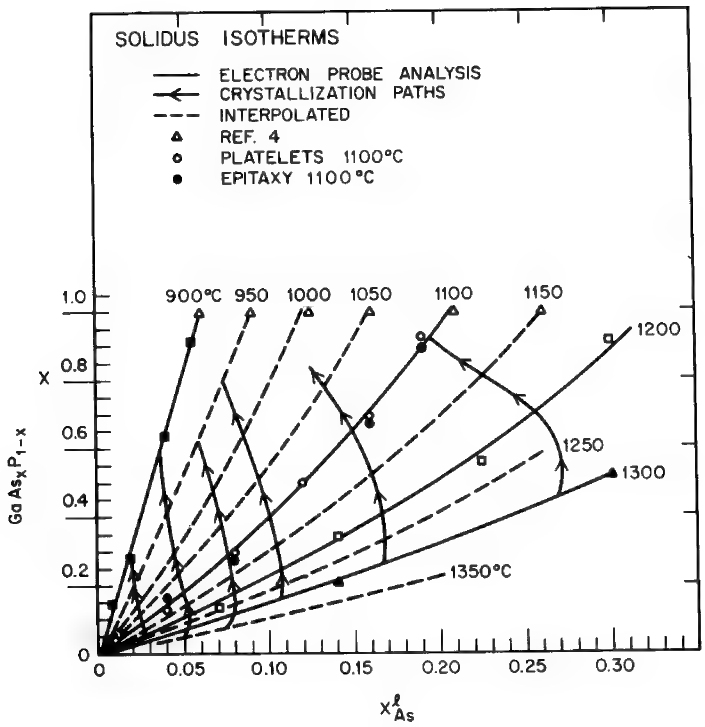
SOLIDUS ISOTHERMS
ELECTRON PROBE ANALYSIS
CRYSTALLIZATION PATHS
INTERPOLATED
REF. 4
PLATELETS 1100°C
EPITAXY 1100°C
900°C
950
1000
1050
1100
1150
1200
1250
1300
1350°C
GaAsxP1-x
X
X^ℓ As

FIG. 2

EFFECT OF SUBSTRATE CONDITION ON THE NUCLEATION AND GROWTH OF TbGe FILMS

M. A. Wilkov and W. D. Stewart
University of Texas, Austin, Texas

TbGe films were prepared by evaporation in a mechanical vacuum of 10^{-5} torr. on single crystal substrates of different crystallographic orientation, i.e., mica, quartz, NaCl and amorphous glass. Variations, in the substrate temperature from 300°C to 750°C, in the evaporation rate from 10-40 A° per min. and in the film thickness from 500-5000 A°, were studied. After evaporation, each film was divided into two parts; half for the determination of the stochiometry, using x-ray florescence in the electron microprobe and half for the study of crystal structure and character using transmission electron microscopy.

The source of evaporation consisted of a small piece of Tb_5Ge_3 of the hexagonal $D8_8$ - Maganese Silicide (Mn_5Si_3) structure mounted on a tungsten filament. The substrates used were freshly cleaved surfaces of mica and NaCl and etched surfaces of AT cut quartz and glass, heated by radiation from a surrounding coil of tantulum wire. The initial evaporation rate was determined by measurement of the optical transmission through the thin foil. All foils were annealed at 300°C for 12 hours before observation.

Upon completion of the annealing period, half of each foil and substrate was mounted inside the electron microprobe, together with pure samples of Ge and Tb. X-ray pulse counts, over a ten second period, were taken from both film and pure samples and used for the computation of the stochiometry of the alloy. Allowance was made for absorbtion using the data of Theisen[1]. The other half of the foil was stripped from the substrate by standard methods, and mounted in the electron microscope for determination of the foils' orientation and structure by selected area electron diffraction.

Microprobe measurements show that the substrate temperature was the most influential of the experimental parameters. At temperatures above 500°C, the films deposited on mica show a significantly higher than normal concentration of terbium. Below 500°C, the stochiometry of the film is independent of the substrate condition and very close to the evaporation source. Films less than 700 A° show a high concentration of terbium on both quartz and mica at temperatures above 600°C. As Tb_5Ge_3 is a very stable compound, having a single vapor pressure, the differences in stochiometry appear to arise from atomic terbium distributed interstitially in the deposit. This interstitial terbium must result from a disassociative reaction occurring when the vapor strikes the hot substrate.

At the lower substrate temperatures, the diffraction patterns indicate a fine grained randomly oriented structure. As the temperature rose, the structure became less random and occasionally, at temperatures above 700°C on the quartz, possessed large regions of epitaxial (well oriented) growth. Due to the dehydroxylation of the mica at 650°C, it was not possible to grow epitaxial films on mica.

---

1. R. Theisin, "Quantitative Electron Microprobe Analysis", Springer Verlag, New York, 1965.

QUANTITATIVE ANALYSIS OF TERNARY AND QUATERNARY SEMICONDUCTING ALLOYS*

Mary C. Finn
M.I.T. Lincoln Laboratory, Lexington, Massachusetts

This paper describes a method which uses theoretical calibration curves for independent determinations of the elements A and B in 14 ternary $A_{1-x}B_xC$ alloys, each formed by two binary semiconducting compounds AC and BC belonging to the II-VI, IV-VI, III-V, or III-VI groups. The alloys are all pseudo-binary solid solutions in which the atom fraction of element C is always 0.5 . A similar method for determining all 4 elements in the quaternary solid solution $Pb_{1-x}Sn_xTe_{1-y}Se_y$ is also described.

The standards used are the constituent binary compounds (e.g., PbTe and SnTe for $Pb_{1-x}Sn_xTe$ alloys.) It is impractical to use a number of the pure elements (e.g., Pb, Se, and As) as standards because of the difficulty of obtaining polished, flat surfaces. The calculated calibrations employ the backscattered electron correction of Duncumb and Shields (1), the absorption correction of Philibert (2), and the fluorescence correction of Wittry (3). The calibration curves for each alloy system will be available for distribution.

Table I lists the ternary alloys which have been analyzed. The quantity of material available has been insufficient to permit experimental calibration of the microprobe analysis by comparison with the results of an absolute method. For several $Pb_{1-x}Sn_xTe$ and $Pb_{1-x}Sn_xSe$ samples, however, the analysis was checked by wet chemical determinations of Pb and Sn. The results of these determinations for 4 samples of $Pb_{1-x}Sn_xTe$ are compared with the microprobe data in Table II. There is good agreement except for the low Sn samples, where the error in both analyses is large.

In analyzing the $Pb_{1-x}Sn_xTe_{1-y}Se_y$ alloys, the standards used are PbTe for Pb and Te, SnTe for Sn, and PbSe for Se. For a given value of (1-x), the calculated intensity of the Pb radiation from the sample is almost independent of the Te/Se ratio. Therefore an approximate value of (1-x) is first obtained from the sample-to-standard intensity ratio for Pb by using the calibration curve calculated for $Pb_{1-x}Sn_xTe$. Calibration curves calculated for this approximate value of (1-x) are then used to obtain independent values of y and (1-y) from the measured intensity ratios for Se and Te, respectively. A new correction factor is then calculated for each of the 4 elements, and these factors are used to obtain the respective atom fractions. This procedure is repeated until convergence occurs. Two repetitions are usually sufficient. The results obtained by this method for 4 representative quaternary alloys are given in Table III. The values of (1-x), x, (1-y), and y for each sample are listed under the heading "2 x (atom fraction)". These values have been adjusted so that their sum is 1 for Pb and Sn and also 1 for Te and Se, as required by the formula $Pb_{1-x}Sn_xTe_{1-y}Se_y$.

---

1. P. Duncumb and P.K. Shields, in The Electron Microprobe, T. D. McKinley, K. F. J. Heinrich, and D. B. Wittry, eds., John Wiley and Sons, Inc., New York, 1966, p.284.

* This work was sponsored by the U.S. Air Force.

2. J. Philibert, in Proceedings of the Third International Symposium on X-ray Optics and X-ray Microanalysis, Academic Press, Inc., New York, 1964, p.379.

3. D. B. Wittry, "Fluorescence by Characteristic Radiation in Electron Probe Microanalysis," U. of Southern California Engineering Center Report 84-204, July, 1962.

TABLE I

TERNARY ALLOYS ANALYZED

$CdTe_{1-x}Se_x$	$Pb_{1-x}Ge_xSe$	$Sn_{1-x}Ge_xTe$
$CdS_{1-x}Se_x$	$Pb_{1-x}Ge_xTe$	$GaAs_{1-x}P_x$
$Zn_{1-x}Cd_xS$	$Pb_{1-x}Sn_xS$	$Ga_{1-x}In_xP$
$Zn_{1-x}Cd_xTe$	$Pb_{1-x}Sn_xSe$	$InSb_{1-x}Te_x$
$ZnTe_{1-x}Se_x$	$Pb_{1-x}Sn_xTe$	

TABLE III

ANALYSIS OF $Pb_{1-x}Sn_xTe_{1-y}Se_y$ ALLOYS

Sample		Pb	Sn	Te	Se	Total
1	Wt. frac.	0.540	0.068	0.384	0.007	0.999
	2 x (At. frac.)	.820	.180	.974	.026	(2)
2	Wt. frac.	.535	.082	.360	.027	1.004
	2 x (At. frac.)	.789	.211	.893	.107	(2)
3	Wt. frac.	.533	.060	.326	.066	0.985
	2 x (At. frac.)	.837	.163	.754	.246	(2)
4	Wt. frac.	.573	.072	.291	.101	1.037
	2 x (At. frac.)	.820	.180	.640	.360	(2)

TABLE II

ANALYSIS OF $Pb_{1-x}Sn_xTe$ ALLOYS

Microprobe analysis (mole fraction)			Wet chemical analysis (mole fraction)		
PbTe	SnTe	Total	PbTe	SnTe	Total
0.968	0.031	0.999	0.986	0.017	1.003
0.943	0.062	1.005	0.940	0.057	0.997
0.799	0.207	1.006	0.797	0.206	1.003
0.620	0.378	0.998	0.608	0.385	1.003

THE USE OF AN INTERACTIVE COMPUTING SYSTEM IN QUANTITATIVE ELECTRON MICROPROBE SPECTROSCOPY

W. Reuter
IBM Thomas J. Watson Research Center, Yorktown Heights, New York

Programs were written in the APL language for absorption, atomic number, and fluorescence corrections in electron microprobe spectroscopy. For the absorption correction, Philibert's method was selected. For the backscatter correction in the atomic number effect we have taken data tabulated by Duncumb and Shields. The energy dependence of the backscatter coefficients was represented by a second order polynomial fit. Bethe's retardation law was chosen for the calculation of the electron range effective for X-ray excitation rather than the frequently used Nelm's equation, which neglects the range dependence on the excitation level. For the fluorescence correction, we programmed Castaing's equation, as modified by Reed.

This program was applied to the analysis of three ternary semiconductors. First in this series was $Ga_xIn_{1-x}P$. Data were taken at 6, 12, and 30 kv, using GaLa, PKa, and InLa radiation. The fluorescence correction was small and less than 1.3% for all possible radiation combinations. The absorption correction was large, particularly for GaLa and PKa radiation, and exhibited a strong voltage dependence. This correction cannot be neglected even at 6 kv. The atomic number correction decreased with increasing electron energy and must be considered for In and P over the entire concentration range. This effect is negligible for Ga. After the application of all corrections, the elemental concentrations found at the three electron energy levels agreed within 5%. Also, good agreement was found with data obtained for the concentration of Ga and In by atomic absorption spectroscopy on samples where sufficient material was available.

Next in this series was the analysis of epitaxial layers of $Al_xGa_{1-x}As$ grown on GaAs. The fluorescence correction was less than 0.4% and hence omitted. The absorption correction for AlKa and AsLa was large and about 50% in the composition range studied, using 12 kv as the primary electron energy. The atomic number correction was less than 1% for Ga and As and omitted. For Al this correction was approximately 15% in the range of interest (GaAs to $Al_{0.2}Ga_{0.8}As$). Point counts were taken in steps of 10 microns. Analytical data obtained by other techniques were not available for comparison in this study. There is, however, strong indirect evidence for the reliability of the analysis:

a) The found substrate composition is very close to the expected composition of GaAs.

b) The sum of all weight fractions is close to one.

c) The mole fraction of As is within experimental error equal to the sum of the mole fractions of Ga and Al.

In a third example $Ga_xIn_{1-x}Sb$ was analyzed using GaKa, InLa, and SbLa radiation. In spite of the high primary electron energy used (25 kv) the corrections were small and less than 6%. The microprobe data agree within ± 5% with data obtained by classical analytical techniques.

The thickness of a film of known composition can be deduced from the appearance potential of the substrate radiation. The appearance potential is defined as the primary electron energy at which the substrate radiation becomes detectable. The program executes Bethe's law in steps of 1 kv. The film thickness is then determined by the appearance potential. This is supported by data obtained by us on films of known composition and thickness. In Fig. 1 the AuMa intensity is plotted versus the primary electron energy. At 6 kv primary energy, the electrons, after penetrating a Cu layer of 1500 Å, have their energy reduced to that corresponding to the absorption edge energy of AuMa.

Range calculations and matrix correction must be applied for the analysis of thin films. We were interested in the stoichiometry of thin films (~6000 Å) of Al_2O_3 grown by vapor deposition. The experimental work must be preceded by an electron range calculation. Based on this input we selected 5 kv at which the electron energy is reduced to the absorption edge energy of AlKa after penetrating 1900 Å into the Al_2O_3 film. For the stoichiometric concentration of Al in the Al_2O_3 bulk standard we calculate at 5 kv an intensity ratio of 0.480 which is in close agreement with the measured ratio of 0.477. It has been argued by Duncumb and Shields that the validity of the assumption made in the atomic number corrections remains to be demonstrated, particularly for voltages below 10 kv, where the ratio of the stopping power in standard and sample changes more rapidly. The good agreement getween the measured and calculated ratio is retained over the entire energy range studied (Fig. 2).

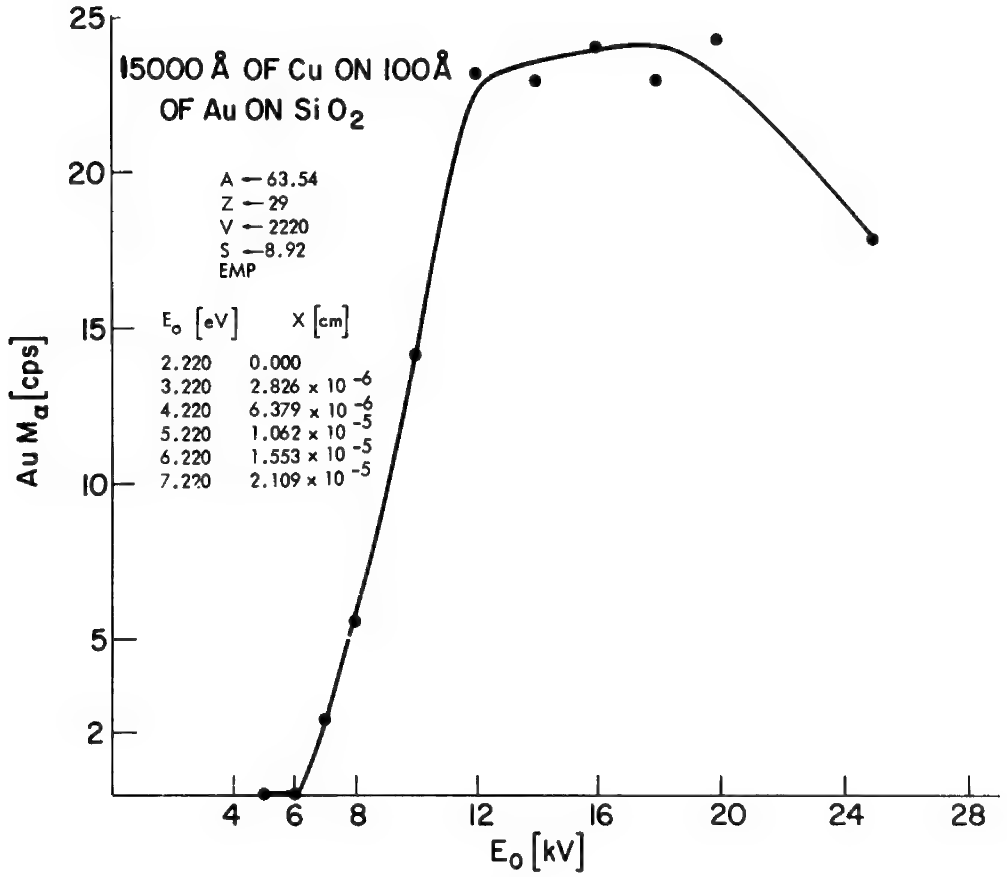

Fig 1

CALCULATION OF $k = \frac{I_{Al\ k\alpha,\ Al_2O_3}}{I_{Al\ k\alpha,\ Al\ STD}}$ FOR Al_2O_3

E_0	$k_{cal.}$	$k_{meas.}$
5	.480	.477
7	.471	.468
10	.454	.452
20	.395	.417
30	.343	.344

Fig 2

A COMPUTER-OPERATED MICROPROBE

Michael A. Bayard
Walter C. McCrone Associates, Inc., Chicago, Illinois

One of the major problems occurring in the analysis of air pollution particulates is the large number of particles which have to be analyzed from each sample in order to give an idea of the total composition of the sample. Accordingly, we decided to automate our electron microprobe. The parameters to be controlled were: the stage position in X and Y; the wavelength setting of the three spectrometers; and the beam position in X and Y. Also, it was necessary to have the computer read in from the probe, the scaler and timer data, rate meter data and sample and beam currents.

To implement these requirements, a computer with 4096 words of 16 bits each was interfaced to the analyzer with an analog to digital converter and a relay network. The relay network allows 81 separate commands to the electron probe. The position of the various mechanical devices on the probe was encoded by means of precision potentiometers. The voltage on these potentiometers is then converted into digital form by means of the analog to digital converter and fed into the computer. The computer can, of course, choose which voltage it wants to read in by simply closing one of the relays. By using a 10-turn potentiometer for coarse positioning and a continuous rotation potentiometer for fine positioning, both the spectrometers and stage can be easily controlled to one part in 20,000 accuracy. An additional advantage of using the simple potentiometer system to encode mechanical position is that the addition of other devices to the probe can be made quite easily.

Much of our work consists of analyzing particles mounted on a beryllium substrate that have been characterized beforehand by optical microscopy. One of the most time consuming aspects of this type of analysis is locating the particle. We have constructed two stages, one of which fits on the electron probe; the other, on a conventional optical microscope. These stages are encoded in the same way. It then becomes a simple matter for the person mounting the particles, or examining a metallurgical sample in other applications, to note the X and Y coordinates of points of interest. We have found in practice that the accuracy of relocation is about ± 2μm. In the case of particles on the beryllium substrate, this is more than adequate. The position can then be further refined by having the computer read in sample currents and by noting when the current deviates from the value measured on the beryllium substrate. With inclusions in metallurgical or geological samples, where an accuracy of ± 2μm can be accepted, this two-stage method seems to work quite well. For details smaller than about 2μm it is necessary for the computer-probe combination to analyze several points in order to insure that the point of

interest is indeed analyzed. This at first may appear to be more time consuming than the use of the probe alone; however, the computer has been able to operate the probe unattended for 24 hours a day. This allows us to do such things as build up a concentration map for several elements using either the spectrometer or a lithium-drifted silicon detector over an area of a few square millimeters during the evening. Also, the unit can be programmed to take many beam scanning pictures for any selected element or elements on 16mm motion picture film. This allows an entire 1 inch sample mount to be scanned in the matter of an evening.

Since the electron probe is an extremely expensive piece of machinery, it is an economic necessity that the maximum amount of data be accumulated. With computer control we have found that we can get analyses equal to those run by an experienced operator; however, with the interface we can run the machine 24 hours a day, 7 days a week, with down time only for filament changes and routine maintenance.

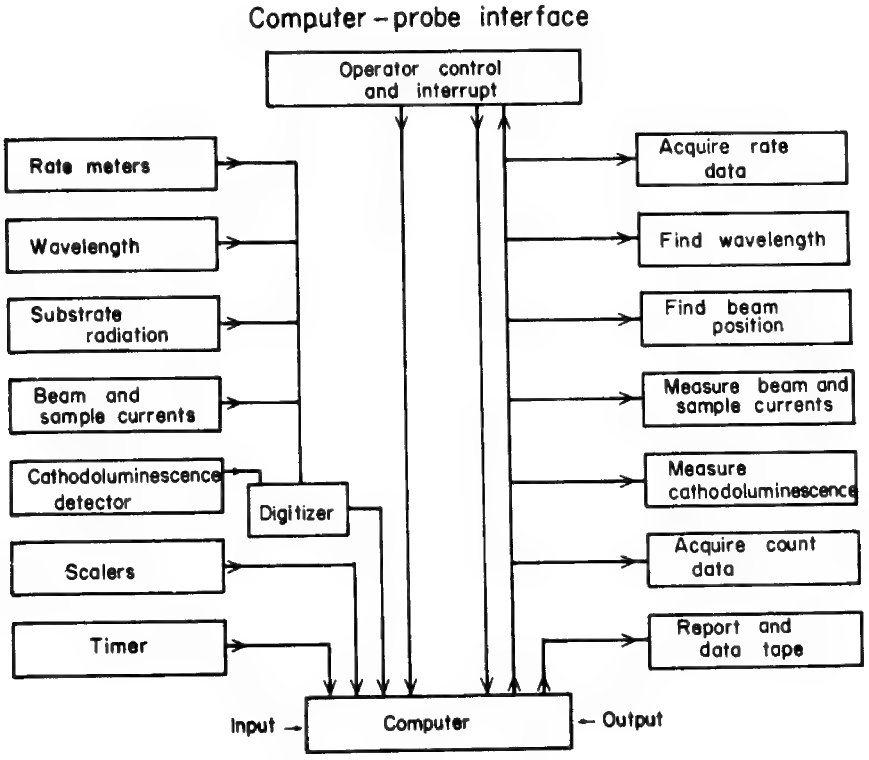

Figure 1
Block diagram of system

Figure 2
Interface unit

X-RAY EMISSION SPECTRA FOR THE ANALYSIS OF INSULATING FILMS IN THE MICROPROBE ANALYZER

J. W. Colby, D. R. Wonsidler and A. Androshuck
Bell Telephone Laboratories, Inc., Allentown, Pennsylvania

Emission spectra have been studied in the past to determine information about the nature of the chemical bond, coordination, state of oxidation, etc. . Several investigators have employed the microprobe analyzer for these studies. However, most investigators have recorded the spectra by using a ratemeter-strip chart recorder combination. This technique requires caution in choosing the proper time-constant in the ratemeter, requires some superposition of two-theta or wavelength information on the strip chart, and requires operator interpretation.

The technique used in the present work, is entirely digital, and therefore amenable to computer processing. The stepping circuitry of the microprobe has been modified such that the spectrometer may be incrementally stepped through its two-theta range, and angular position read out on a digital voltmeter. After each step, intensities are measured for a predetermined counting interval, and recorded on punched paper tape. All further data processing is done by an IBM 360 computer. The data points are plotted on a Calcomp plotter, the experimental points are fitted to a Fourier series, and the peak positions and full widths at half maximum are precisely determined. Composite spectra may be unfolded into their individual Lorentzian components, making interpretation easier. The raw data points are plotted in normalized form, as well as the fitted curve, the peak positions and the full widths at half maximum. If it is desired, the individual Lorentzians may also be plotted.

This technique has been used to study thin films deposited on silicon substrates. The films are first analyzed by conventional microprobe techniques, and then their emission spectra are studied, usually the K beta and K beta prime emission band.

Typical results are shown in Figures 1 - 5, which are the Silicon K_β emission spectra from a series of silicon oxynitrides, varying in composition from pure SiO_2 (Fig. 1) to pure Si_3N_4 (Fig. 5). It may be noted that the main band exhibits an energy shift in direct proportion to the composition, while the K_β satellites for Si_3N_4 and SiO_2 stay fixed in position but vary in intensity also in proportion to composition. The positions of the satellites, 1826.31 ± 0.11 eV for Si_3N_4 and 1821.58 ± 0.15 eV for SiO_2 may in this sense be used to establish the presence of either the oxide or nitride, in the absence of a light element analytical capability, while the shift in the main band may be used as a measure of composition.

Other systems are compared, and an explanation of the K_β' satellite is offered.

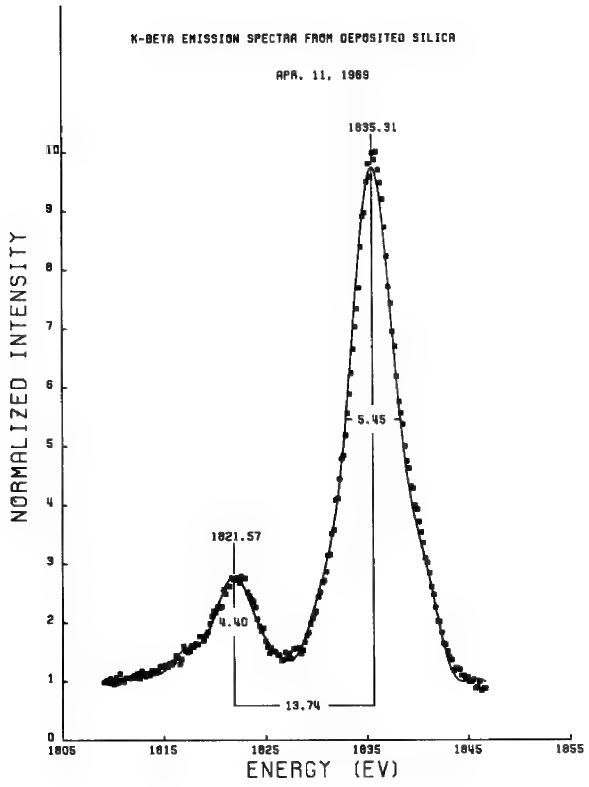
K-BETA EMISSION SPECTRA FROM DEPOSITED SILICA
APR. 11, 1969
1835.31
5.45
1821.57
4.40
13.74
NORMALIZED INTENSITY
ENERGY (EV)

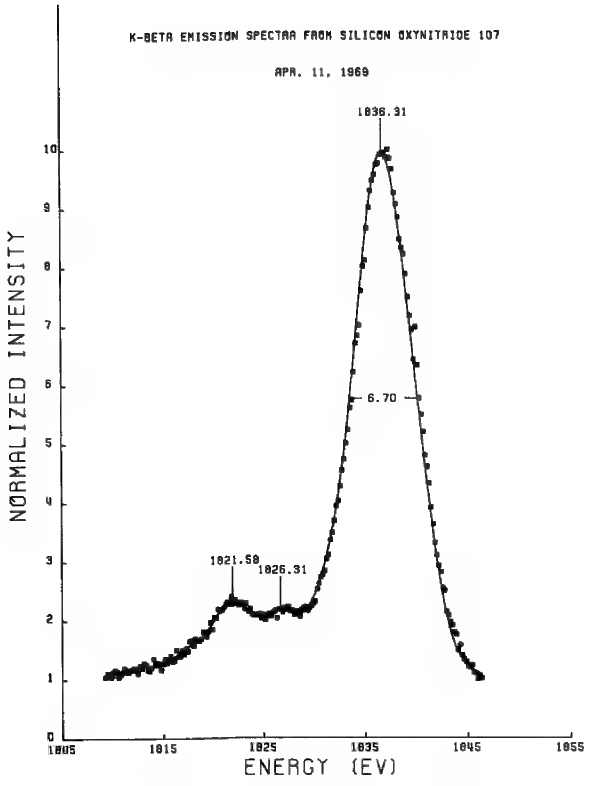
K-BETA EMISSION SPECTRA FROM SILICON OXYNITRIDE 107
APR. 11, 1969
1836.31
6.70
1821.58
1826.31
NORMALIZED INTENSITY
ENERGY (EV)

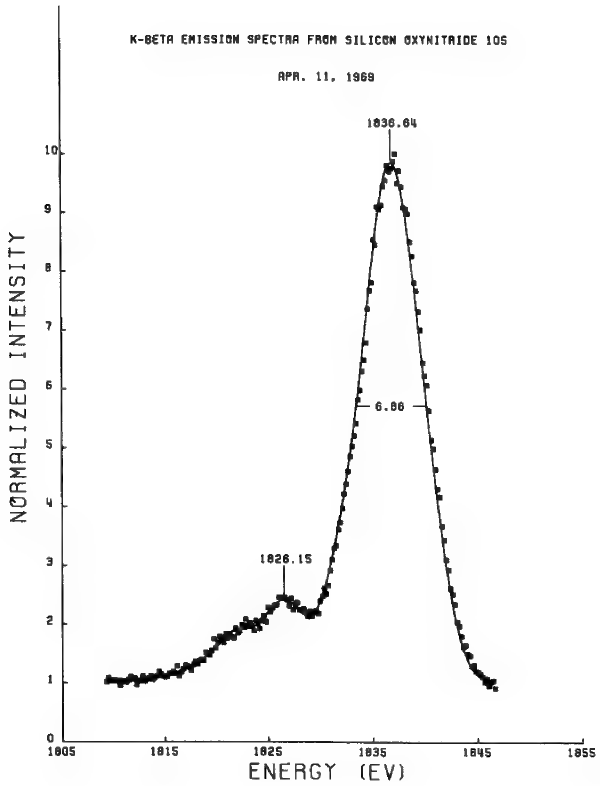
K-BETA EMISSION SPECTRA FROM SILICON OXYNITRIDE 105
APR. 11, 1969
1836.64
6.86
1826.15
NORMALIZED INTENSITY
ENERGY (EV)

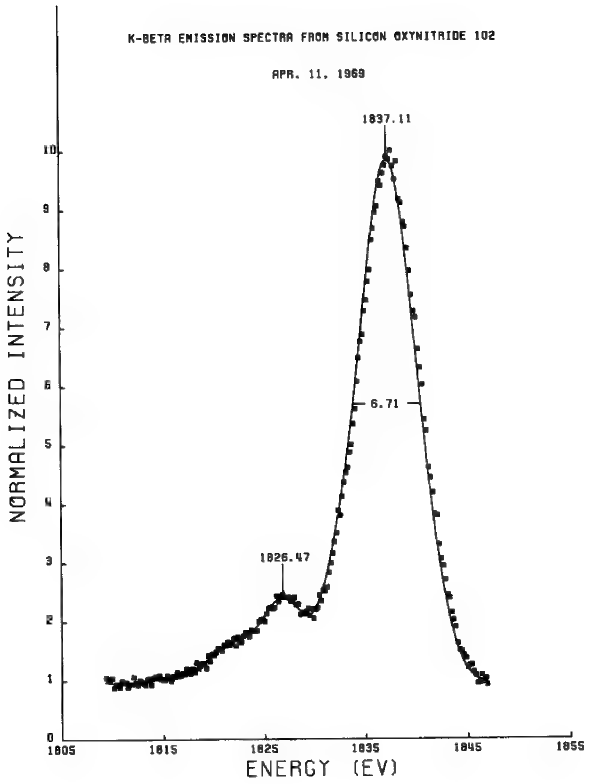
K-BETA EMISSION SPECTRA FROM SILICON OXYNITRIDE 102
APR. 11, 1969
1837.11
6.71
1826.47
NORMALIZED INTENSITY
ENERGY (EV)
1805
1815
1825
1835
1845
1855

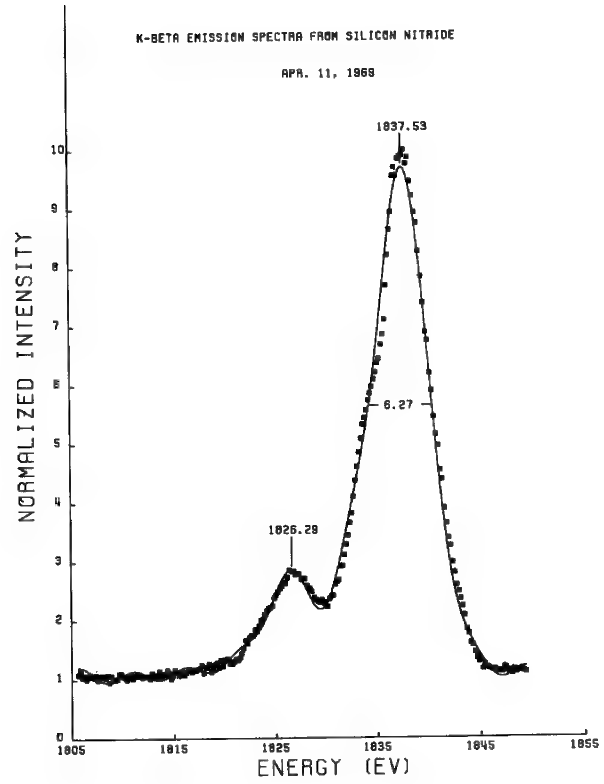
K-BETA EMISSION SPECTRA FROM SILICON NITRIDE
APR. 11, 1969
1837.53
6.27
1826.28
NORMALIZED INTENSITY
ENERGY (EV)
1805
1815
1825
1835
1845
1855

A SMALL COMPUTERIZED ON-LINE DATA GATHERING SYSTEM FOR THE ELECTRON MICROPROBE

F. Duane Ingram
University of Iowa, Iowa City, Iowa

Electrolyte concentration distributions measured with an electron microprobe across sections of soft biological tissue are presented as line scan profiles (1). The concentrations of electrolytes normally encountered in soft biological tissue are on the order of 1 to 200 mEq/1. The concentration of potassium, for example, is approximately 2.5 mEq/1 (.01 Wt. %) in interstitial fluid and approximately 120 mEq/1 (.47 Wt. %) in the cell of frog tissue. With the 1μ diameter, .05 μa, 10 keV beam often used, the counting rate is well under 100 counts per sec. The resultant low signal to noise ratio at low counting rates necessitates the use of long counting times to obtain statistically significant numbers for each data point along the line scan profiles. Also there are a number of conditions which require the rapid and efficient handling of numerous arrays of numbers, for example: rapid sample deterioration under the electron beam, the desire to study concentration distributions of more than one element, and the need to correlate the measurements with the location on the tissue section.

As an aid in gathering and manipulating the arrays of numbers encountered in electron microprobe measurements, the appropriate electronics were constructed to interface the electron microprobe (EMX) (2) to a Linc-8 computer (3). The system is currently capable of handling five data parameters with a flexibility that allows for the addition of other parameters as the situation demands. The parameters that are monitored are the signals from the three spectrometers, the backscattered electron signal, and a signal related to the position of the electron beam in the scan. Different arrangements of data parameters can usually be treated with relatively simple modifications of the interface and software.

The Linc-8 has 4096, twelve bit storage locations. The computer is located in a room near the electron microprobe laboratory. It was not installed as a machine dedicated to microprobe data handling, but as a computer for the general use of the Department of Physiology and Biophysics.

The main features of the data handling system are illustrated in Figure 1. Counting is accomplished by setting flip-flops in the interface with pulses from the detectors. The computer tallies one in the appropriate line scan profile and resets the flip-flops after each count. One of the computer's eight ADC's is used to monitor the sweep voltage ramp and present numbers to the computer that are related to the position of the beam in the sweep. Similarly, numbers related to the magnitude of the backscattered electron signal are presented with another ADC.

An example of the type of data obtained with this system is illustrated in Figure 2. It is a superposition of four data parameters that were simultaneously monitored during the scan of a myelinated frog nerve section for Na, K and Cl. Ten line scans, each 53 sec long, were taken with a .05 μa, 10 keV beam. The backscattered electron signal is displayed to help establish the physical location of the scan on the tissue. The various line scan profiles were written on magnetic tape for permanent storage.

Although the appropriate data manipulations may be performed immediately, and to some extent even while the data is coming in, we have chosen to dedicate the computer to data gathering only. The analysis is then performed at a later time by calling the data from the magnetic tape. Once the data has been stored on magnetic tape, the treatment of the final analysis is limited essentially only by the imagination of the investigator. Final analyzed data may be stored in permanent fashion either on magnetic tape, punched paper tape, photographs from the computer CRT, or as columns of numbers typed by the computer.

The system is not necessarily the most versatile data handling system one could develop, nor is it necessarily the best for our particular requirements. It is, however, an entirely adequate system which was developed with a minimum outlay of funds and the use of presently available equipment. The benefits of an on-line computer data handling system were obtained with an investment of about $100 worth of additional components.

---

1. M. J. Ingram and C. A. M. Hogben, Procedures for the Study of Biological Soft Tissue with the Electron Microprobe, Developments in Applied Spectroscopy, 6:43-64, 1968.

2. Applied Research Laboratories, Glendale, California.

3. Digital Equipment Corporation, Maynard, Massachusetts.

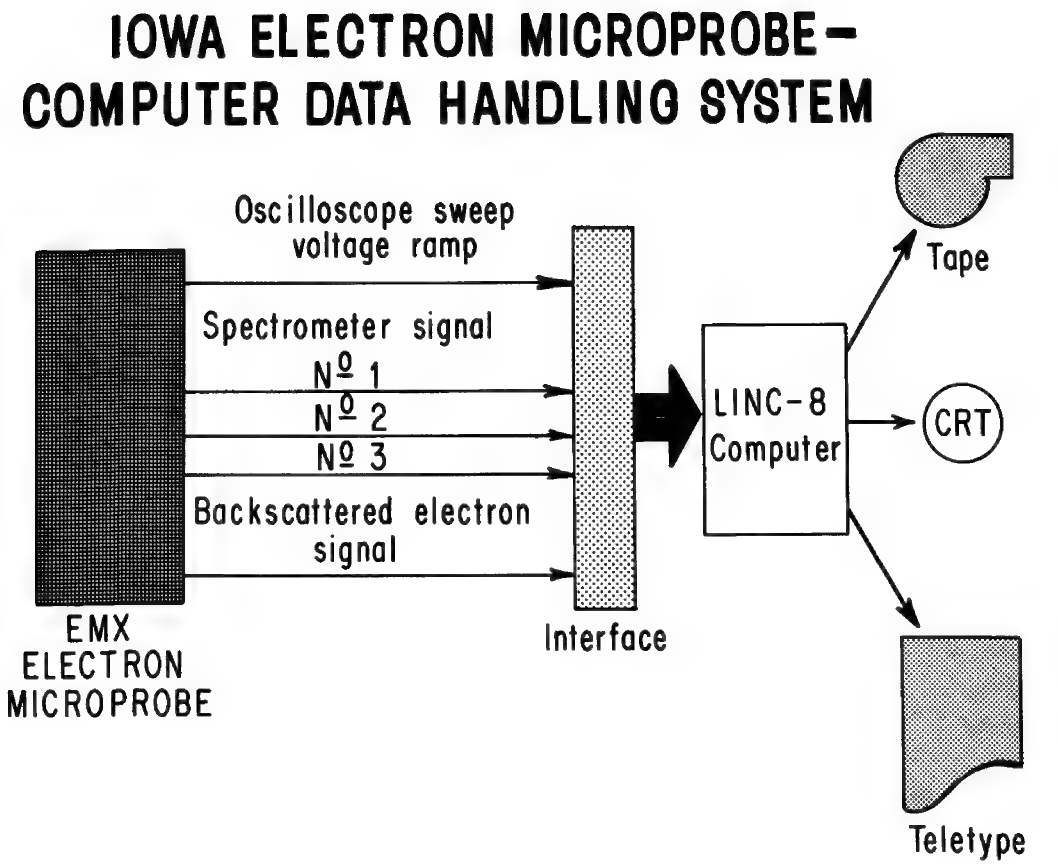

Figure 1. Block diagram of the main features of a computerized data handling system for an electron microprobe. The computer is located in another room about 75 feet from the electron microprobe.

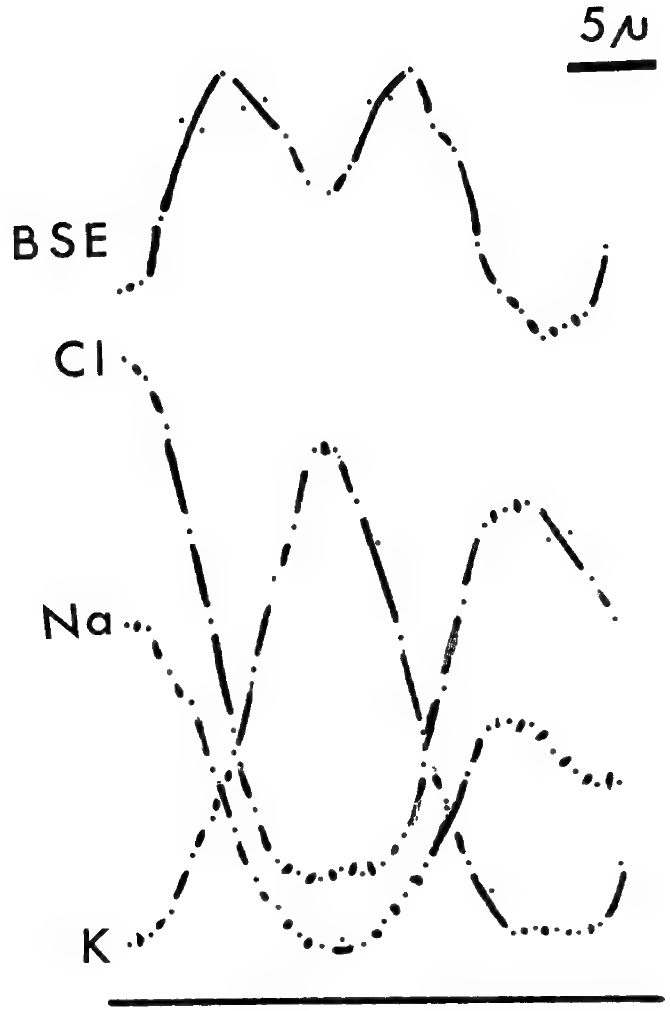

Figure 2. Reversal of polaroid photograph of the raw data from line scan profile measurements of the Na, K and Cl concentrations across a myelinated frog nerve. All the parameters shown here were taken simultaneously and superimposed later for this photograph. The lines were added later to aid the eye.

MANIP: A COMPUTER PROGRAM FOR PROCESSING X-RAY INTENSITY DATA ON PUNCHED PAPER TAPE FROM THE ELECTRON PROBE MICROANALYZER

G. L. Fisher and W. G. Wickersty, Jr.
The International Nickel Company, Inc., Suffern, New York

A computer program has been written to process X-ray intensity data on punched paper tape from an electron probe microanalyzer. The program gives unknown and standard X-ray intensities corrected for background, dead-time, and drift for as many as eight elements. An analysis can be done by point counting or step scanning and X-ray counting can be terminated either on a fixed time or fixed integrated beam current basis. The program was designed to be linked directly to J. Colby's (1) Microanalysis General Intensity Program (MAGIC) so that corrected compositions can be obtained. The program is being used in our laboratory with an ARL EMX-SM microanalyzer which has three X-ray channels and a Model 33 ASR teletype. However it should be readily adaptable to any microanalyzer having punched paper tape readout. It was written in Fortran IV for an IBM 1130 computer with 8K core storage.

The program requires only a limited amount of input information before an analysis is started. Besides information indentifying the analysis (name, problem number, date, title) only the accelerating potential, elements and lines analyzed, and two codes telling how the analysis is to be performed and how counting is to be terminated are entered. Then the X-ray intensities for the standards and unknowns are taken in the following order:

1. Background-element A, standard-element A, background-element B, standard-element B, etc.
2. Unknown intensities for elements A, B, etc. Up to 20 different points can be analyzed.
3. Recount standards for the drift correction. This step can be eliminated if no drift correction is desired.

It is often desirable to take several X-ray intensity measurements at a single point on the standards or unknowns so that a statistical analysis can be performed on the data. The program allows for this but does not require that a predetermined number of counts be taken at each point. When the analyst has finished taking measurements at a given point he prints a special character on the tape. This character tells the computer that a given counting sequence has ended. To print the special character he uses an encoder connected to the data translator. This encoder consists of a seven digit thumbwheel selector. Any digit selected on it will appear in the sixth output channel and be punched on the tape. The encoder is inexpensive to build and easy to install on the instrument.

The advantages of using preset integrated beam current to terminate X-ray counting and thus limit long time drift are preserved by the program. When this counting mode is used X-ray intensities are kept as total counts except while making the dead-time and background corrections. The drift correction is performed by taking the mean of the initial and final standard intensities.

Besides giving corrected intensities, the program gives the counting time and background intensities for the standards and the standard deviation of the standard intensities. When step scanning, the distance in microns from the start of the scan to each observation is given.

The program has been found to save about 1-1/2 hours of desk calculator computation and key punching time for an analysis of a binary alloy system with twenty observations. It should be pointed out that the program can be used with punched card input. Thus, if typewriter readout is being used, the hard copy can be key punched and used as input to the program.

---

1. J. Colby, Quantitative Microprobe Analysis of Thin Insulating Films, Advances in X-Ray Analysis, Volume 11, page 287-305, 1967.

SPATIAL CONCENTRATION DISPLAY AND MAPPING

J. L. Solomon
IBM, Owego, New York

A new method has been developed for acquiring and presenting quantitative X-ray count data on the electron microprobe analyzer. Previous methods of data acquisition had several limitations. If the X-ray information was collected using beam scanning techniques, the elemental concentration data obtained was strictly qualitative in nature and merely provided information as to whether the element was present in a particular area or not (see Figure 1). Line profiles can be run for a particular element across a sample surface, but these also have the disadvantage of being qualitative although they do indicate relative concentration levels as a function of distance across the sample surface.

Quantitative data may only be obtained by allowing the electron beam to dwell for a fixed period of time on a certain spot and recording the number of counts generated. To index the beam manually across the sample surface is extremely tedious and lacks reproducibility; step-scanning removes the tedium but is essentially unidirectional and also suffers from lack of reproducibility.

The National Bureau of Standards has developed a technique whereby a matrix of points may be quantitatively evaluated. The method to be discussed here is a logical extension of the work begun by NBS and incorporates the following instrumentation:

1. Ortec Model 701 Matrix Generator (MG)
2. Multichannel analyzer (MCA) with a 4096 word (or greater) capacity
3. Time base generator (TBG) compatible with 1. and 2. above
4. Isometric display capability (ID) and associated R/O devices

The system operates in the following manner. The MG is connected to the beam scanning system of the microprobe so that a point matrix, generated by the MG will index the electron beam across the sample surface, i.e., if a 1024 point matrix is selected, the matrix generator will be set up in a 32 x 32 point square matrix which will be reproduced by the electron beam on the sample surface. The MCA is operated as a multiscaler, receiving its count input directly from the pulse height analyzer associated with the microprobe X-ray readout system. The dwell time of both the MG and MCA is controlled by the TBG so that as the electron beam indexes from position 1 to position 2, the MCA will index from channel 1 to channel 2, and will then accumulate the X-ray count data from the new point. Dwell times may be as short as 100 msec or as long as 10 sec. depending upon the number of counts desired and the precision required by the experiment. Since we have three dispersive and one non-dispersive X-ray detectors, concentration data may be collected for four elements <u>simultaneously</u> by using four input multiscaling techniques. Since four separate add-1 registers are involved, dead time for the four input system is equivalent to that of the single input system and is about 1 usec. A block diagram is shown in Figure 2.

Since the data is accumulated serially in the MCA, in order to provide useful display, it must be unfolded by use of the ID. The ID presents the data <u>as accumulated</u>, i.e., in a 32 x 32 point matrix. X and Y directions in the display correspond to X and Y directions on the sample surface, while the 2 direction on the display corresponds to element concentration. Operation on the data as displayed can take many forms. Visual observation often is sufficient to show elemental concentration gradients. Photographic techniques produce permanent records of the data. In addition, <u>any single X or Y line</u> may be selected for readout as numerical information suitable for reduction to true concentration data by any of a number of currently available data reduction schemes.

Two examples are now shown of the use of this system. The first is the analysis of a solder joint where an unusually large amount has been allowed to form. Referring again to Figure 1, we see a conventional X-ray display for copper, tin and lead. Figure 3 shows the same X-ray count data accumulated using the spatial concentration technique described above. The ID allows manipulation of the data so that one may select different viewing angles for optimum data presentation. The intermetallic shelf of Cu_6Sn_5 is

clearly visible as well as the concentration gradient present in the tin as the copper surface is approached.

The second sample is the base junction of a transistor on an I.C. where electromigration of aluminum is suspected as a failure mode. Figure 4 shows the conventional aluminum and silicon X-ray images while Figure 5 shows the spatial concentration display. One may note the relative magnitude of the silicon inclusions on the aluminum conductor stripe as well as the fact that there is no significant change in aluminum concentration across the entire land in question.

This technique is particularly useful where concentration changes occur over a large area and are not readily observable using conventional techniques. In addition, all information acquired is quantitative in nature so that data reduction techniques may be applied at any time to the collected data.

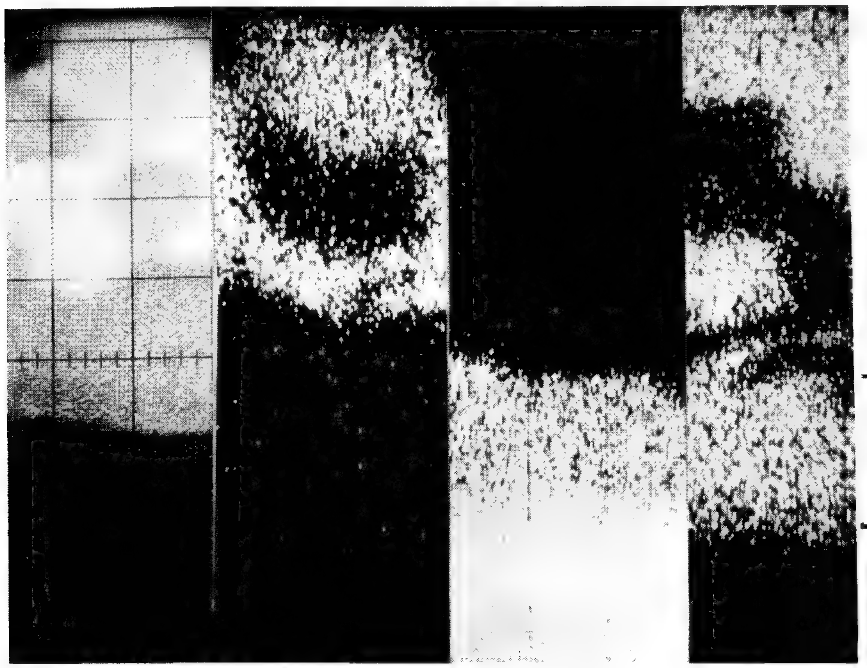

Figure 1 - Conventional Beam Scanning Images of a Solder Joint

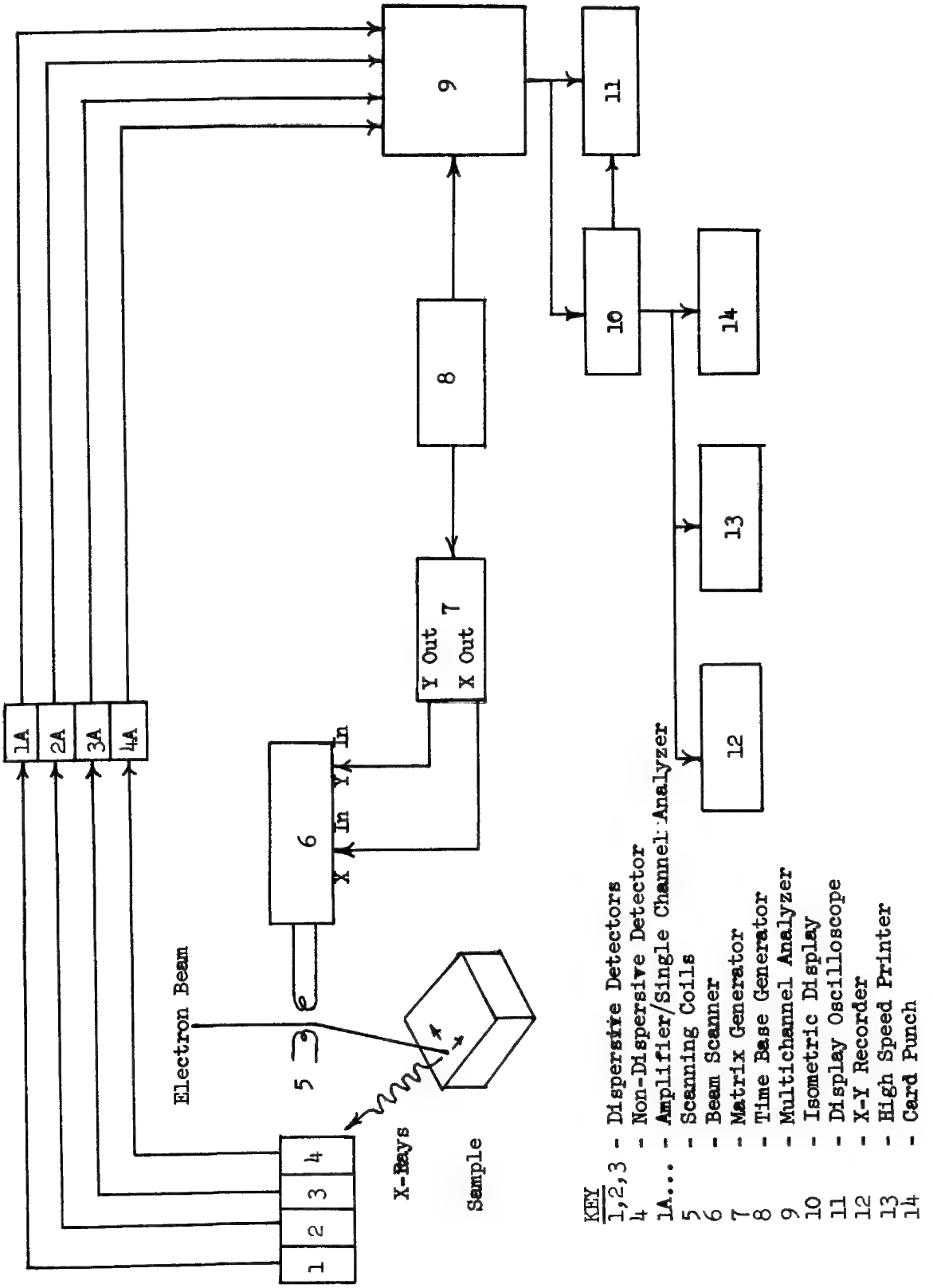

FIGURE 2 - BLOCK DIAGRAM OF SPATIAL DISPLAY SYSTEM

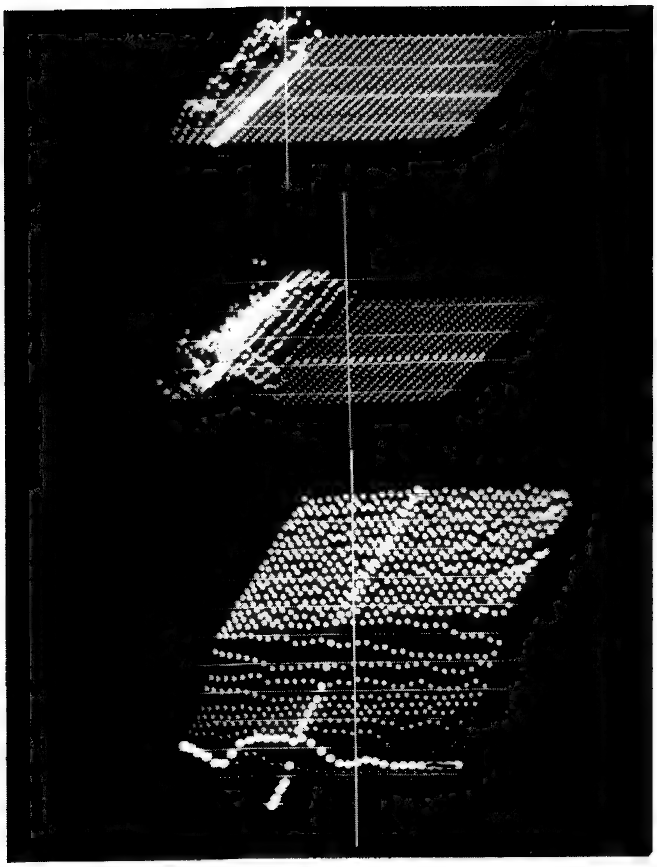

Lead Distribution Image

Tin Distribution Image

Copper Distribution Image
Note position of intensified line with respect to tin and lead images. (Rotated 90° with respect to tin and lead images).

Figure 3 - Spatial Concentration Displays for Lead, Tin, and Copper for Same Area Shown in Figure 1 (Intensified line denotes intermetallic/solder interface).

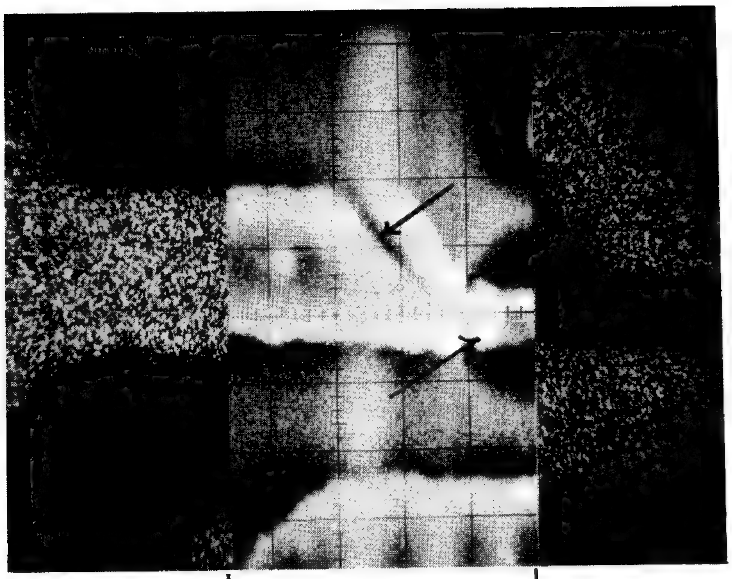

Aluminum X-Ray Image | Secondary Electron Image | Silicon X-Ray Image

Magnification: 2000 diameters
10 kV @ 0.02 uA

Figure 4 - Conventional Beam Scanning Images of Base Junction on an Integrated Circuit
(Suspected defect indicated by arrow in S.E. Image)

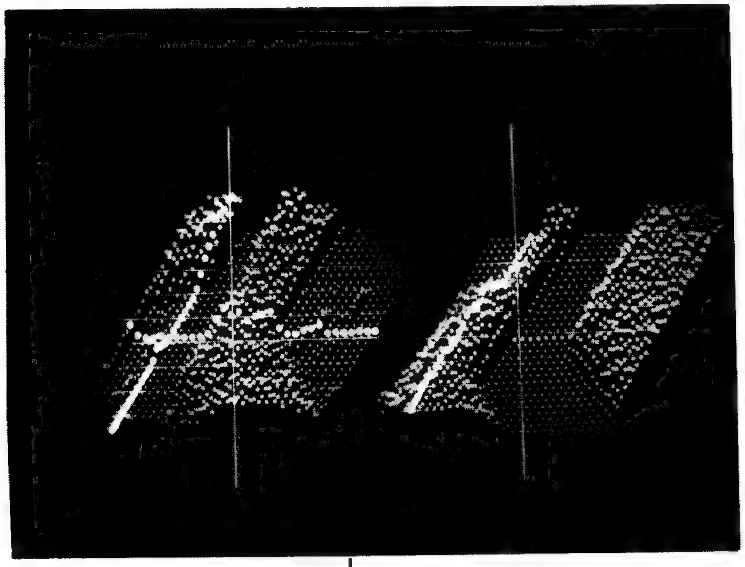

Silicon Distribution Image | Aluminum Distribution Image

(Images rotated 90° from those shown in Figure 4)

Figure 5 - Spatial Concentration Displays for Aluminum and Silicon from Same Area Shown in Figure 4.

TECHNIQUE FOR IN-SITU CHARACTERIZATION OF SURFACE SCALES

Charles J. Spengler
Westinghouse Research and Development Center, Pittsburgh, Pa.

The characterization of scales based on examination of a specimen in cross-section has several limitations. Some of them are: (1) Loss of the outer scale may occur in spite of careful mounting and polishing procedures, (2) Very thin scales cannot be resolved with the electron-beam microanalyzer, (3) Preferential patterns of scale formation that occur during the early stages of reaction are not as clearly revealed in cross-section as on the surface.

On the other hand, a characterization of the scale based on surface examination alone may be in error because it is difficult to establish the sequence of layers in a scale over 2 μm in thickness from a single-dimension analysis. Further, in the case of thin scales (<2 μm), a large X-ray contribution from the matrix masks the X-ray intensities from the scales. Therefore, the most reliable procedure is to combine both analyses of the surface and cross-sections, where practicable.

Some development work was needed to establish a satisfactory procedure for examining specimen surfaces. Most of the effort was directed at the perfection of an X-ray scanning technique of the surface of a simple 85 Ni-15 Cr alloy and a more complicated Ni-based superalloy. The alloys had been subjected to atmospheres containing various amounts of O_2, N_2, SO_2, and SO_3. The reaction times were 1, 6, and 30 hours at 1600°F (871°C).

Initially, areas representative of the distribution and thickness variations of the scales were chosen by optical examination. These areas were then examined with the electron-beam microanalyzer at acceleration potentials of 7, 10, 20, and 30 kilovolts. At each acceleration potential, the beam current and spot size were adjusted to maintain X-ray count rates of several thousand per second for the major chemical constituents.

The data were collected on film with use of the rate-metered-mode because there was a large relative difference in count rate at different points in the scanned area. The resulting X-ray scanning pictures were then evaluated in sequence on the basis of comparative change in X-ray intensity per unit area as a function of acceleration potential.

Figure 1 shows a sequence of scanning back-scattered electron and X-ray (Ti and Cr) micrographs taken on the surface of the oxidized nickel-based alloy. At 20 Kev the Ti-rich carbides as well as the Ti-rich gamma-prime phase in the alloy can be detected through the scale. At 10 and 7 Kev the Ti detected is within the scale. Similarly, at 20 Kev the Cr in the alloy can be detected but at 10 and 7 Kev the Cr detected is only that present in the scale.

Figure 2 consists of scanning electron micrographs and rate-metered X-ray (Ni and Cr) micrographs at 20 Kev of scales of different average thickness on the simple Ni-Cr alloy.

The scale formed in 1 hour in O_2 is, in general, less than 2 μm and the differentiation of the constituent oxides is not as clearly obtained as in the specimen oxidized in 30 hours where the scale is estimated to be over 2 μm thick. The scanning X-ray results can be combined into schematic diagrams as shown in Fig. 3. The microprobe results are combined with X-ray diffraction analyses.

At the lower potentials (7 and 10 Kev) where the electron penetration is less than a micron in oxides, the L-series of X-rays was used in the analyses of nickel and chromium. Operation at 7 Kev is useful to establish whether certain elements are in chemical combination on the surface of the specimen, such as sulfur and oxygen as a sulfate.

Where the scales are over 2 μm in thickness, operation to a maximum of 20 Kev is adequate to characterize the scales. This acceleration potential produces results which combine optimum spatial resolution and ease of interpretation.

The X-ray line profile technique was used in addition to the X-ray scanning method to determine more precisely the relative amount of each element on the surface. Because of relief which exceeded 1 μm, the results could not be used in any quantitative sense.

---

[1] Viswanathan, R. and C.J. Spengler, Corrosion of 85 Ni-15 Cr Alloy at 1600°F in Controlled Atmospheres Containing O_2, SO_2, SO_3, H_2S, and N_2, to be published.

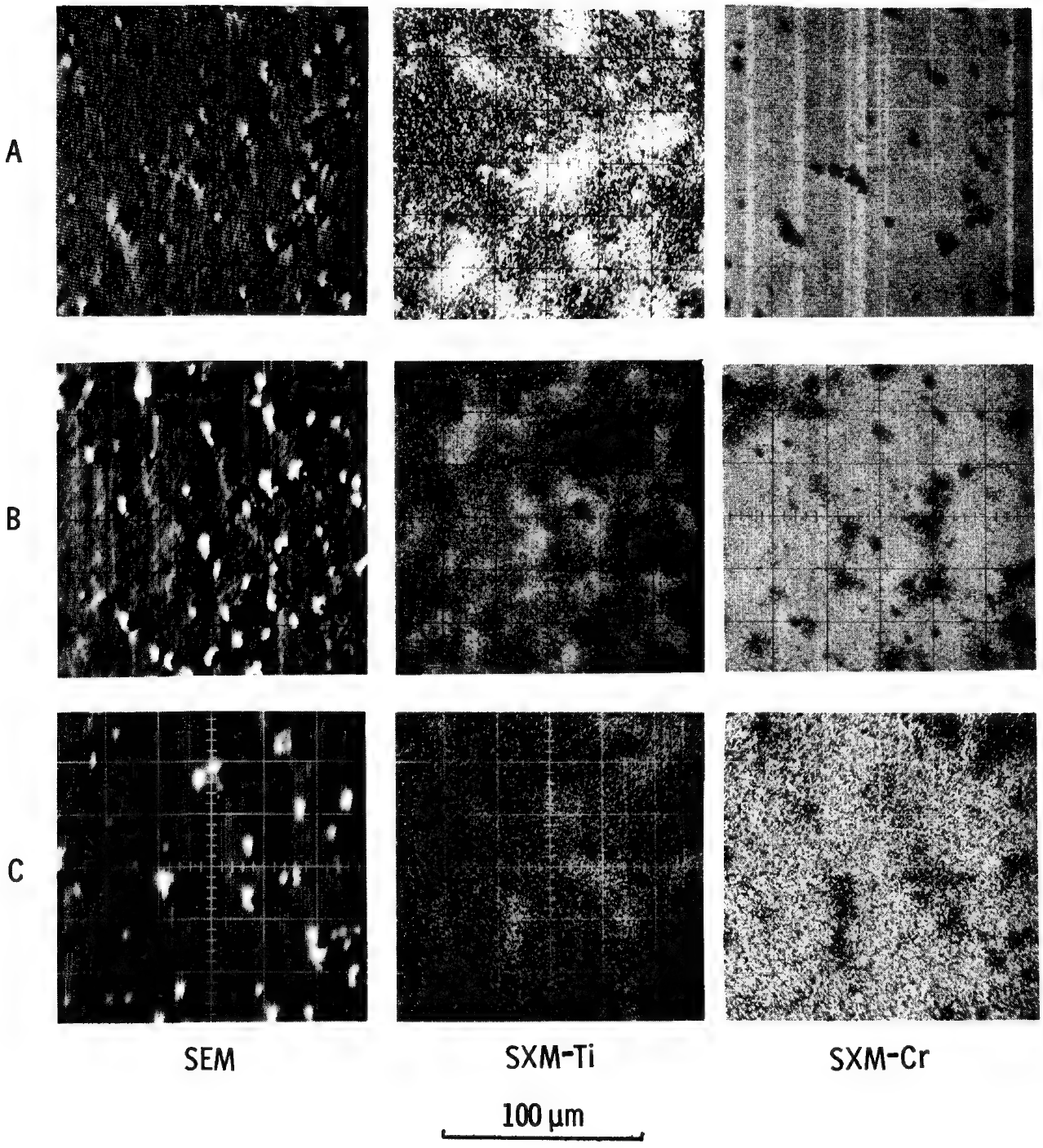

Fig. 1—Scanning electron micrographs (SEM) and scanning X-ray micrographs (SXM) of scale on Ni-based alloy at 20keV (A), 10keV (B), and 7keV (C)

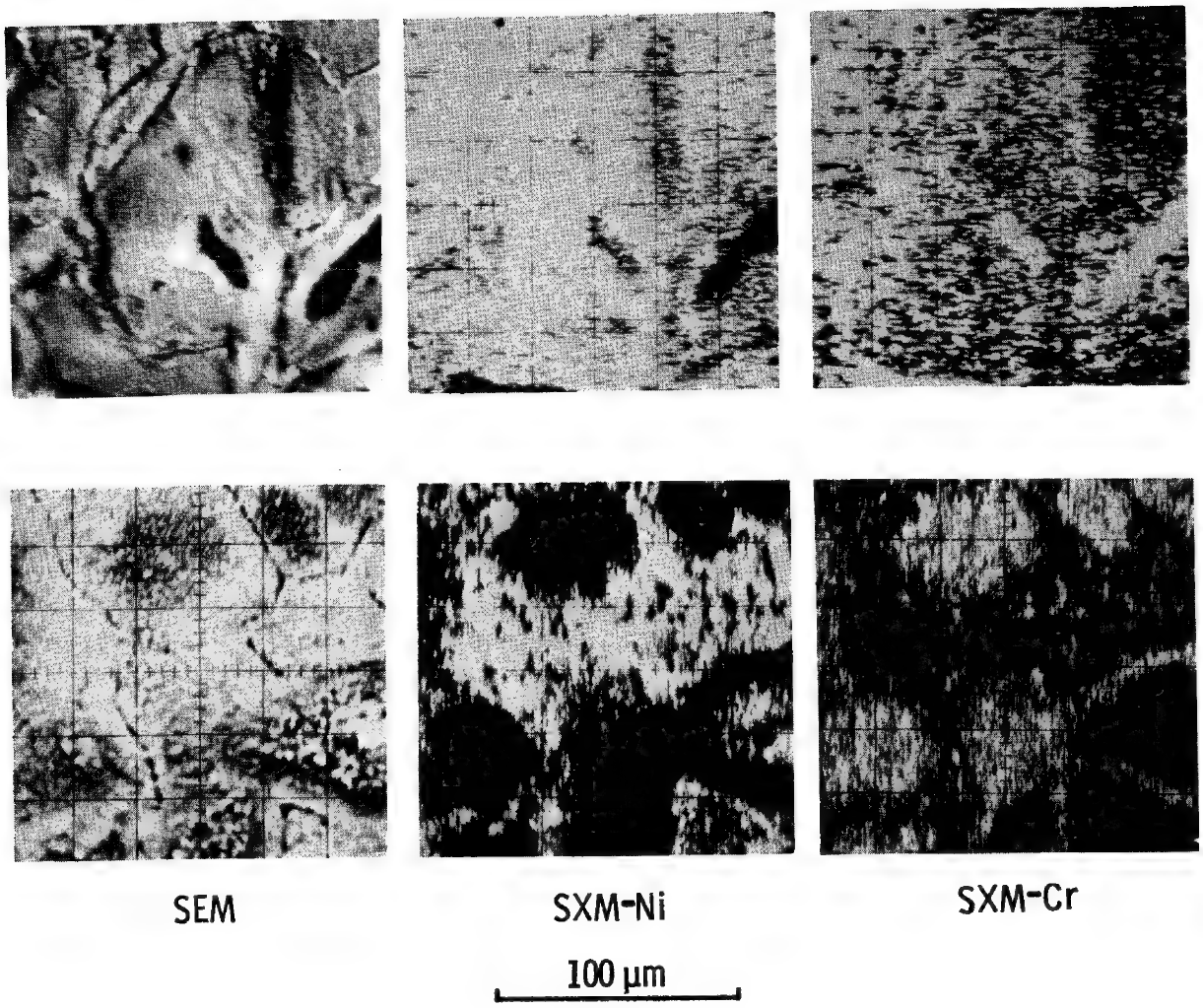

Fig. 2—Scanning electron micrographs (SEM) and scanning X-ray micrographs (SXM) - ratemetered - of scale on Ni-Cr alloy at 20 keV. Exposed 1 hour (A), and 30 hours (B) to $O_2 + N_2$

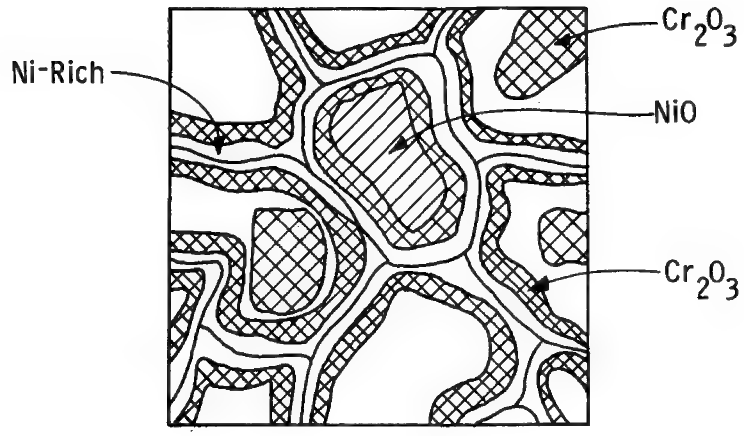

Scales on the Surface of a Sample Exposed to $O_2 + N_2$ Mixture for 1 Hour

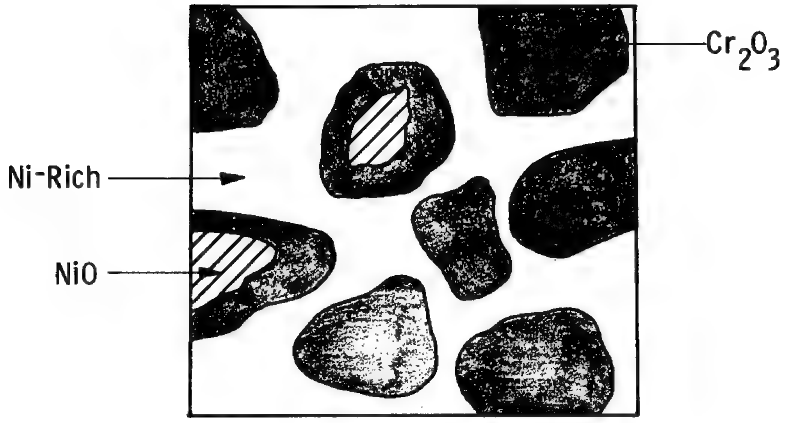

Scales on the Surface of a Sample Exposed to $O_2 + N_2$ Mixture for 30 Hours

100 μm

Fig. 3—Schematic representations of scales on 85Ni - 15Cr exposed to $O_2 + N_2$. Based on scanning X-ray micrographs shown in Fig. 2

AUTOMATED STEPPING SYSTEM FOR CARBON ANALYSIS

J. S. Duerr, J. Adario, R. E. Ogilvie
M.I.T., Cambridge, Massachusetts

The microprobe analysis of carbon, particularly in iron, presents a number of unusual obstacles to the probe operator. Fortunately, the basic techniques are known due to Ong[1] and, particularly, to Henke[2]. In our own work with a Norelco vacuum spectrometer on the MIT microprobe, a lead stearate analyzing crystal on a mica substrate is used in conjunction with a thin detector window and 75% methane - 25% argon detector gas. For low level carbon analysis, all probe operating conditons must be optimized so that the minimum detectability limit is realized. In addition, some method must be employed to eliminate the build-up of a carbon contamination layer on the sample under the electron beam.

The minimum detectable concentration is given by

$$C_{DL} \sim \sqrt{B/I_o^2}$$

where B is the background and I_o is the signal corrected for back-ground. The minimum in the curve of C_{DL} versus accelerating voltage at constant current for carbon in iron occurs near 10 kv. Since this accelerating voltage excites only a low intensity of FeK radiation, the pulse height analyzer can completely eliminate the FeK_β (fifth order) line which diffracts from the mica substrate only 0.5^o in 2θ away from the CK_α which diffracts from the lead stearate.

Carbon contamination arises from two sources: 1. adsorption of a surface layer while sitting in the atmosphere, desiccator, or microprobe, 2. decomposition of the oil diffusion pump vapor by the electron beam. A number of techniques have been tried to reduce or eliminate the contamination build-up. The most promising one is to introduce a flow of air through a fine tube directed at the probe spot[3]. Not only is the contamination rate reduced to zero, but previously adsorbed surface layers are removed.

If the sample is to be automatically traversed beneath the beam, there must be provision for introducing a period of delay before measuring the carbon intensity. For small steps (order of beam diameter), this delay time must be several minutes. On a freshly polished surface, the delay time can be eliminated; however, if the sample is in the probe for as little as an hour, the delay time again becomes mandatory.

An automated stepping system was designed to allow a step-delay-count sequence of operations as illustrated by the variation in carbon intensity with time in Figure 1. A 500 step/revolution Slo-Syn synchronous driving motor with its Preset Indexer control steps the micrometer stage traverse in multiples of 1.25 microns. A general purpose (0 to 60 minute) reset timer and other relays form part of an electronic circuit that ties together the timer scaler and stepping motor and feeds pulses to the different components in the proper sequence. Of course, the scaler can be operated manually and with either or both the stepping and delay circuits in operation.

The automated stepping system was used to measure the carbon concentration profile across the carburized case of an 8717H steel universal joint. Figure 2 shows the carbon level falling from 0.9 wgt. pct. carbon at the surface to the 0.2 wgt. pct. level of the uncarburized steel. The carburizing cycle consisted of 6 hours at 1700°F in the carburizing atmosphere followed by a quench to form martensite and a temper.

Although the feasibility of low level carbon analysis has previously been demonstrated, this capability has not been utilized to the fullest extent. The automated stepping system described here makes possible the quantitative analysis of carbon concentration profiles even for the relatively low concentrations found in steels.

---

1. P.S. Ong, "Reducing carbon contamination in an electron microprobe and measuring low energy backscattered electrons" in X-ray Optics and Microanalysis, ed. Castaing, Deschamps, and Philibert, pp. 181-192, 1966

2. B.L. Henke, "X-ray fluorescence analysis for sodium, fluorine, oxygen, nitrogen, carbon, and boron", Advances in X-ray Analysis 7, 460-488 (1964).

3. G.W. Bruno and S.H. Moll, "Gas jet sample decontamination in the electron microprobe", presented at The Second National Microprobe Conference, June, 1967.

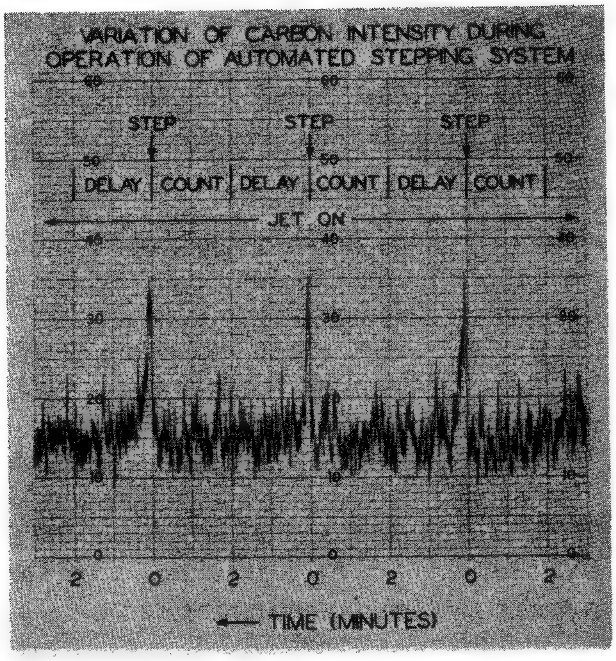

Figure 1

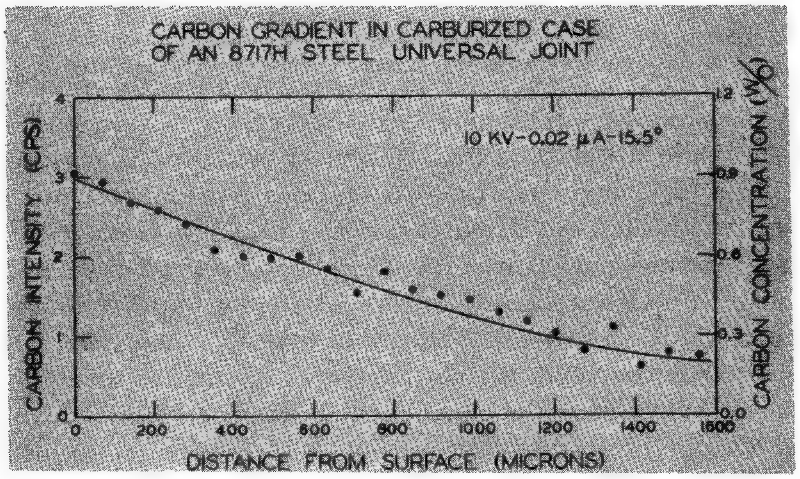

Figure 2

SEMIQUANTITATIVE ELECTRON MICROPROBE DETERMINATION OF Fe^{+2}/Fe^{+3} AND Mn^{+2}/Mn^{+3} IN OXIDES AND SILICATES AND ITS APPLICATION TO PETROLOGIC PROBLEMS

Arden L. Albee and Arthur A. Chodos
California Institute of Technology, Pasadena, California

Even semiquantitative determination of the oxidation state of Fe and Mn by electron microprobe analysis has important applications to petrologic and mineralogic problems. Andersen [1] (1966) pointed out that the relative intensities of Fe L_α and L_β x-ray emission peaks differ significantly with valence state, even though the wavelength shift is very small. The L_β/L_α intensity ratio has been measured for Fe and Mn oxides and a wide variety of Fe and Mn-bearing silicates, both natural and synthetic. As shown in fig. 1, L_β/L_α increases systematically with increase in Fe^{+2}/Fe^{+3} or Mn^{+2}/Mn^{+3} in their respective oxides. A systematic variation also occurs in the hematite-ilmenite series and the magnetite-ulvospinel series, but the Fe L_β/L_α ratios are higher for Fe-O-Ti bonds than for the Fe-O bonds. The variation is large enough to be useful in the analysis and identification of opaque minerals in petrologic and paleomagnetic studies.

The L_β/L_α values are also higher in anhydrous silicates than in oxides and are much higher for the Fe^{+2}-O-Si (or Mn^{+2}-O-Si) bond than for the Fe^{+3}-O-Si (or Mn^{+3}-O-Si) bond. The associated L_α wavelength shift is only about 0.035 Å. Most of the sample points shown on the figure are synthetic minerals with Fe or Mn in six-fold coordination with oxygen. A synthetic iron microcline ($KFeSi_3O_8$) has Fe^{+3} in four-fold coordination, but does not have a significantly different L_β/L_α value. Although relatively few anhydrous silicates have a wide continuous variation in Fe^{+2}/Fe^{+3}, the method can be useful for garnets and pyroxenes and for characterizing unknown anhydrous minerals.

Hydrous silicates, particularly layered silicates, have a wider range of Fe^{+2}/Fe^{+3}, and it is for these minerals that a microprobe technique capable of measuring this ratio would be most valuable to petrologists. However, measured L_β/L_α values are intermediate to those for anhydrous silicates, and overlap for predominantly Fe^{+2} and predominantly Fe^{+3} layered silicates and amphiboles. Fe-biotites synthesized at different oxygen activities have also been analyzed and show no significant differences. It seems probable that the valence effect in these minerals is obscured by the coordination of Fe with OH rather than O. It is possible that Fe^{+2} is oxidized by the electron beam during the analysis, but this seems unlikely because Fe^{+3} hydrous silicates show higher values than for Fe^{+3} anhydrous silicates, whereas goethite has a value similar to that in hematite. It seems more likely that the x-ray production probabilities are affected by the OH coordination, despite the small wavelength shifts.

This summary of our results is presented in part to call attention to the need of petrologists for a method of determining Fe^{+2}/Fe^{+3} on the analysis point and in the hope that some investigator can fully explain the failure of the technique for hydrous minerals and point to a better method.

---

1. C. A. Andersen, Transactions 1st National Conf. on Electron Microprobe Analysis, College Park, Maryland, 1966.

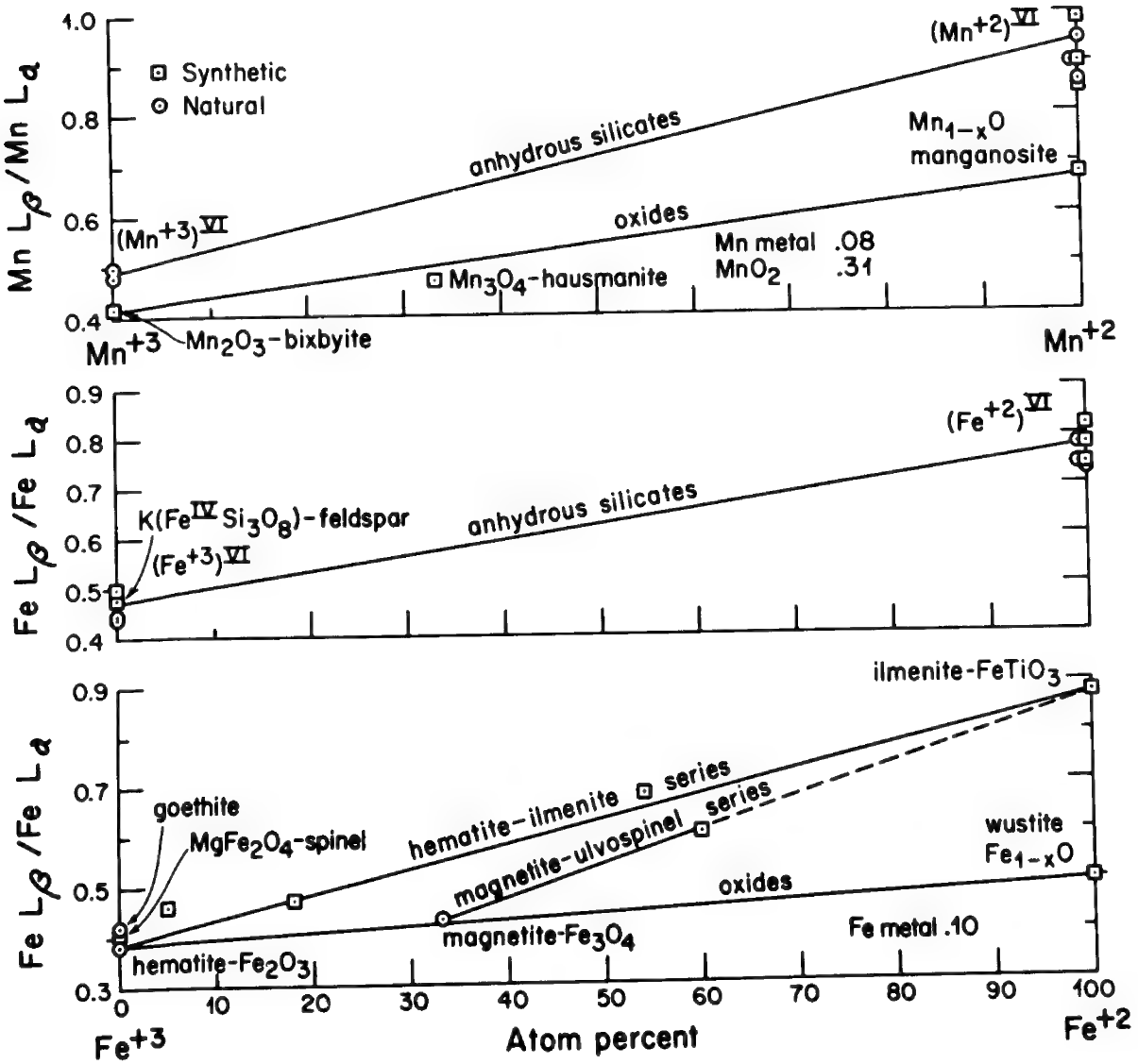

QUANTITATIVE PROCEDURE IN ELECTRON PROBE ANALYSIS OF SILICATE SERIES

Ramon Coy-yll and Jacques Soudiere
Universite de Montreal, Quebec, Canada

Recently, some authors (1)(2) have reviewed the correction models used in quantitative microprobe analysis. It appears that more reliable input parameters such as mass-absorption coefficients, fluorescence yield and electron scattering are needed. However, the correction errors that result from uncertainty in these input parameters may be minimized by the use of optimum operating conditions.

The basic problems involved in microprobe analysis of silicate series such as olivines are discussed and a new correction procedure is proposed. The use of correction curves plotted from computer-calculated absorption and atomic number corrections is suggested. These corrections depend on the concentration of variable elements in each silicate series: e.g., iron for olivines and calcium for plagioclases. The correction procedure has been perfected for an M.A.C. electron probe but the method may be extended to other probe types.

The absorption and atomic number correction for an element A may be written as follows:

$$\frac{C_A}{K_A} = \frac{1/f(\chi)_A \text{ specimen}}{1/f(\chi)_A \text{ standard}} \quad \frac{R \text{ st.}}{R \text{ sp.}} \quad \frac{S' \text{ sp.}}{S' \text{ st.}} \qquad (1)$$

The term S' describes the electron stopping power contribution to the atomic number effect as proposed by Philibert and Tixier (3). R is the electron backscatter factor given by Bishop (4). $1/f(\chi)$ is the absorption correction function given by Philibert with voltage dependence as proposed by Heinrich (1). Considering the relatively low fluorescence yield of the silicon-aluminium pair as well as the small amount of nickel present in the studied silicates, we have not taken into account the fluorescence correction.

Figures 1, 2 and 3 show the C/K ratio calculated for Fe, Mg and Si present in the olivine series. For this calculation we have applied Eqn. 1 to the olivine analyses given by Deer, Howie and Zussman (5). Using synthetic pyrite as an Fe-standard, the C/K ratio is not affected by the absorption effect at 20 Kv; but the atomic number effect is significant at this voltage for iron-poor olivines. For the correction of Mg-results, the atomic number effect reduces considerably the absorption correction; however, the large values for Mg-correction at relatively high voltage indicate the desirability of using standards of composition near to olivine or of using a lower voltage. For the Si-correction the atomic number effect is also significant. We may conclude that atomic number correction is necessary even when standards of composition similar to the analysed material are being used.

In practice, we are using the calculated correction curves to determine the composition of a few minerals which afterwards are employed as routine standards. Results

obtained using such calculated curves agree well with results given by an iterative correction program. Furthermore, our experience seems to show that analytical precision depends more on experimental errors than on the uncertainty in the correction precedure.

A collection of correction curves like figures 1, 2 and 3 have been obtained at different voltages and take-off angles for all elements present in the plagioclase, augite, diopside, hornblende and garnet series.

---

1. H. Yakowitz and K.F.J. Heinrich: "Quantitative Electron Probe Microanalysis: Absorption Correction Uncertainty". Mikrochim. Acta, in press.
2. H. E. Bishop, Brit. J. Appl. Phys. (J. Phys. D), 1, 673-683, 1968.
3. J. Philibert and R. Tixier, Brit. J. Appl. Phys. (J. Phys. D), 1, 685-694, 1968.
4. H. E. Bishop, "Optique des Rayons X et Microanalyse", Hermann, Paris, pp. 153-158, 1966.
5. W. A. Deer, R. A. Howie and J. Zussman, "Rock Forming Minerals", Longmans, London, pp. 10 - 13, 1962.

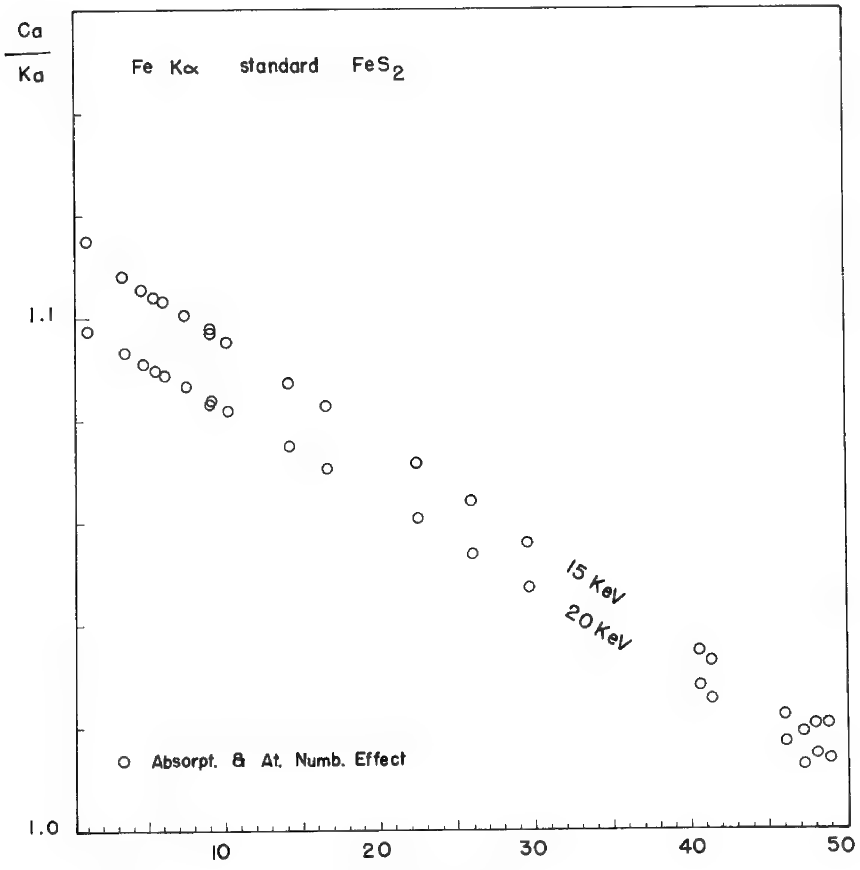

fig. 1

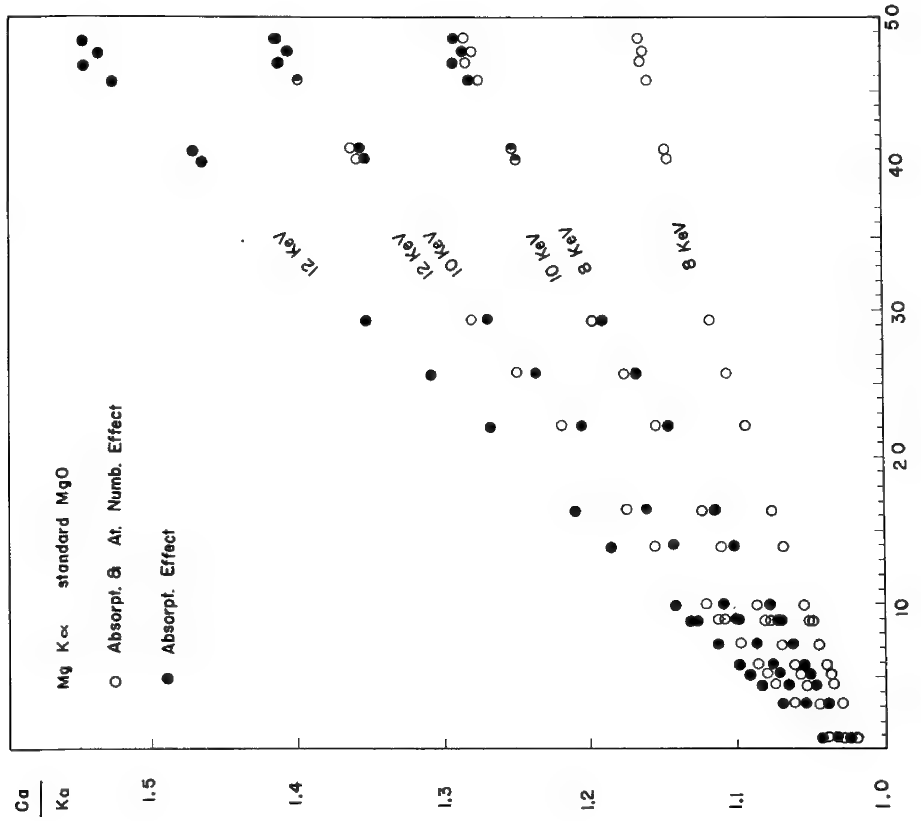
Mg Kα standard MgO
Absorpt. & At. Numb. Effect
Absorpt. Effect
12 KeV
10 KeV
8 KeV
Ca/Ka
weight per cent Fe

fig.2

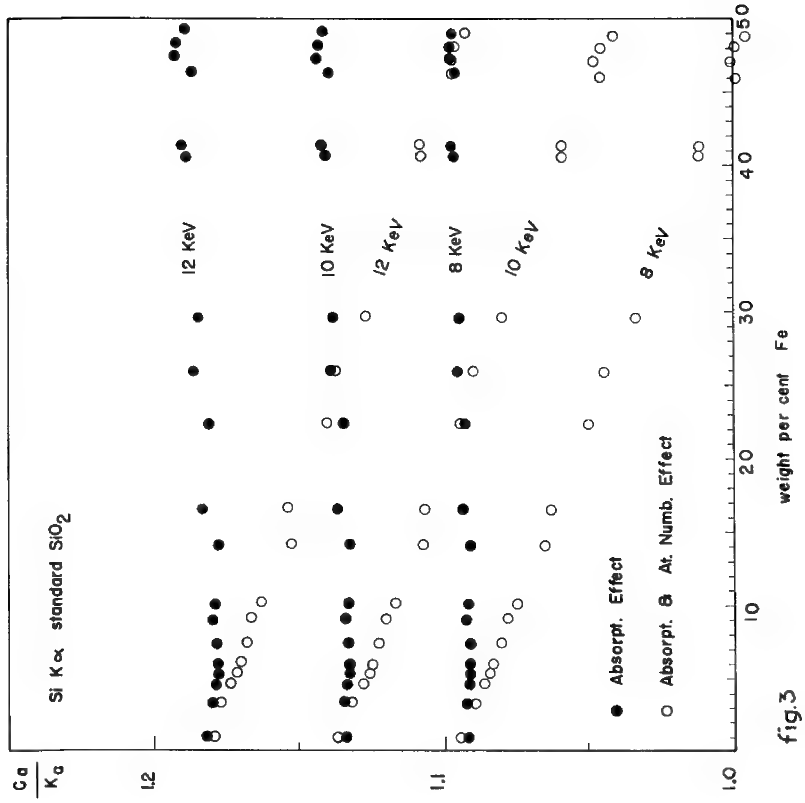
Si Kα standard SiO2
12 KeV
10 KeV
8 KeV
Absorpt. Effect
Absorpt. & At. Numb. Effect
Ca/Ka
weight per cent Fe

fig.3

CHARACTERISATION OF PYROCLASTIC UNITS - A STRATIGRAPHIC APPLICATION OF THE MICROPROBE

D. G. W. Smith, J. A. Westgate and M. C. Tomlinson
University of Alberta, Alberta, Canada

Pyroclastic layers, essentially representing time planes, have long been recognised as having great potential for long distance stratigraphic correlation -- provided that they are widespread and distinctive. Much effort has consequently been expended in developing characterisation techniques. With reference to Quaternary pyroclastics, attention has particularly centred on optical methods (e.g. Wilcox, 1965), but they have achieved only partial success. Bulk ash chemistry has proved unreliable, composition varying from locality to locality within individual layers as a result of detrital contamination, post-depositional alteration and winnowing effects during deposition. C^{14} dating of associated organic matter is again only suggestive of the affinities of an ash and is useless in old Quaternary deposits.

Refractive index measurements suggest the volcanic glass composition should be characteristic of an ash. However, it is impossible to separate from most pyroclastic materials glass that is completely free of phenocryst fragments and microlites; thus the chemistry of such glass cannot be investigated in bulk. The microprobe was therefore used to analyse pure, inclusion-free glass from individual shards, thereby avoiding problems facing bulk analysis. Shards and pumice fragments (relatively free of bubbles and inclusions) were concentrated by heavy liquids, mounted in epoxy and polished. Si, Ti, Al, Fe, Mn, Mg, Ca, Na, K, Cl, P and F were determined to establish the potentialities of each for discriminating between certain recent ashes from widespread localities in northwestern U.S.A. and southwestern Canada. Initially, 14 different samples confidently identified by various workers as "Mazama" ash were investigated to establish the consistency and range of variation to be expected of one bed (Smith and Westgate, 1969). Results were then obtained from Glacier Peak, St. Helens "Y" and Bridge River ashes: their compositions are clearly resolved by the technique; in fact, as few as 3 elements (e.g. Na, K and Fe) serve to distinguish all unequivocally.

Average compositions have now been obtained for the glasses by a refined technique involving, among other things, counting 50 shards for 20 secs. each; in some cases (e.g. Glacier Peak) these differ significantly from analyses available in the literature. Furthermore, these refinements make possible the distinction of fine structure in the chemistry of the ashes; thus it appears that Glacier Peak and possibly Bridge River ashes may have resulted from a series of closely spaced eruptions. The Waskana Creek ash from southern Saskatchewan (Christiansen, 1961) proves to be rhyolitic and completely distinct from well documented dacitic or rhyodacitic ashes of the High Cascades. The coarse grain size of this ash, which underlies a glacial till, and its thickness in Saskatchewan (well away from areas of Quaternary volcanism) suggest that it should be widespread and potentially very useful in correlation. Preliminary work on ashes from the Yukon (Table 1) shows that these are also readily distinguishable.

The technique is much quicker than optical methods of characterisation and undoubtedly more precise. However, separation of concentrates of unaltered glass may be time-consuming, particularly when an ash is composed largely of pumiceous fragments riddled with bubbles and inclusions. Alternative methods have therefore been sought which

retain the microprobe's advantages of selectivity and rapidity but eliminate separation difficulties. These methods are based on the composition of phenocrysts from the ashes and thus might be applicable to older pyroclastics where the glass has started to devitrify and perhaps change in composition. Magnetite is most easily separated and as it precipitates early from many dacitic or rhyolitic magmas, it is a common constituent of most ashes. Furthermore, as there are significant variations in Ti, Mg and Al in the glasses, it might be expected that concentrations of these elements in magnetites would also vary from ash to ash. Magnetite was therefore extracted from a series of ashes, mounted in epoxy and polished. The compositions reported in Table 1 show that in each case the magnetite is distinctive. Again, however, a considerable scatter was noted in results from Bridge River ashes. Ilmenites which coexist with the magnetites are being analysed to provide further data for characterisation and also with a view to determining temperatures and oxygen fugacities immediately prior to eruption.

---

1. E. A. Christiansen, Geology and groundwater resources of the Regina area, Saskatchewan, Sask. Res. Council Geol. Div. Rpt. 2, p.72, 1961.
2. P. Duncumb and S. J. B. Reed, The calculation of stopping power and back-scatter effects in electron probe microanalysis; in Quantitative electron probe microanalysis. Ed. K. F. J. Heinrich, Nat. Bur. Stds. Sp. Publ. 198,133,1968.
3. K. F. J. Heinrich, X-ray absorption uncertainty, in The electron microprobe, Wiley, New York, 1966, p. 296.
4. S. J. B. Reed, Characteristic fluorescence correction in electron-probe microanalysis, Brit. J. Appl. Phys., 16, 913, 1965.
5. D. G. W. Smith and J. A. Westgate, Electron probe technique for characterising pyroclastic deposits, Earth and Planet. Sci. Lett., 5, 313, 1969.
6. R. E. Wilcox, Volcanic-ash chronology, The Quaternary of the United States, Princeton University Press, 1965, p. 807.

TABLE 1: GLASS AND MAGNETITE COMPOSITIONS

	1	2	3	4	5	6	7	8
SiO_2	76.77	73.88	72.69	76.96	-	-	-	-
TiO_2	0.13	0.31	0.49	0.22	8.63	5.95	7.50	5.84
Al_2O_3	12.22	13.57	14.33	12.84	2.11	1.96	2.02	2.69
FeO	1.48	2.19	2.07	1.20	35.71	34.21	34.87	34.88
Fe_2O_3	*	*	*	*	50.74	55.61	52.32	54.67
MnO	n.d.	0.02	0.05	0.04	0.44	0.34	0.42	0.31
MgO	0.04	0.23	0.59	0.36	2.07	1.39	1.76	1.01
CaO	0.53	1.26	1.60	1.36	-	-	-	-
Na_2O	3.62	4.50	5.16	3.86	-	-	-	-
K_2O	4.99	3.63	2.72	2.94	-	-	-	-
Cl	0.16	0.24	0.18	0.19	-	-	-	-
P	0.07	0.18	0.06	0.02	-	-	-	-
F	n.d.	n.d.	0.05	0.04	-	-	-	-

nd = not detected; - = not sought; * = All Fe calc. as FeO; FeO:Fe_2O_3 of magnetites based on struct. formula; All glasses recast to 100% water-free; All detns. on an A.R.L. EMX microprobe at 15KV, 200μA emission current, 0.1μA beam current; Stds.: wet-chemically anal. obsidians for glasses; hematite, spinel and pseudobrookite for mgtes; anals. corrected for absorption fluorescence and atomic no. effects by APL language computer program incorporating recent improvements to correction formulae (Duncumb & Reed, 1968; Heinrich, 1966; Reed, 1965): Corrections small to insignificant except for Si which range up to 1% of amount present.
1 = Waskana Creek ash, glass; 2 = Gold Bottom Creek, Yukon ash, glass; 3 = Ave. of 5 Mazama glass samples; 4 = Glacier peak glass, Adrian, Washington; 5 = Ave. mgte. for 2 Mazama ashes; 6 = Ave. mgte. for 2 Glacier Peak ashes; 7 = Ave. mgte. for 9 Bridge River ashes; 8 = Ave. mgte. for 2 St. Helens "Y" ashes.

MINERAL INCLUSIONS AND MICROSTRUCTURE OF CARBONADO DIAMOND

L. F. Trueb* and C. G. Henderson**
*University of Denver, Denver, Colorado
**E. I. DuPont deNemours & Company, Wilmington, Delaware

Carbonado the so-called "black diamond" makes up only 0.1% of the world's production of natural industrial diamonds, but it is used in drill bits designed to pierce very hard rocks where its extraordinary toughness, far exceeding that of monocrystalline diamond, is advantageous.

Wentorf and Bovenkerk (1) found that under pressure and temperature conditions which are substantially above the equilibrium line between diamond and graphite, the nucleation rate of diamond is very high. This causes the growth of many small and imperfect crystallites aggregated into black lumps. Carbonado might thus have formed under the effect of rapid cooling-off processes at high pressures, or by a sudden increase in pressure at moderately high temperatures in a suitable plutonic environment.

Carbonado has been known to be a rather impure form of diamond since 1843. Inclusions of graphite and various minerals have been claimed to act as a "cement" holding the diamond crystallites together and giving the stones their dark color. However, X-ray diffraction work by Brandenberger (2) showed no evidence of the presence of graphite, and very little has been published concerning the nature and distribution of the mineral inclusions. In view of the present interest in meteoritic and shock-synthesized polycrystalline diamond, it appeared appropriate to undertake a detailed characterization of carbonado. This was done by combining light-optical, scanning and electron microscopy with electron probe microanalysis and X-ray diffraction.

The investigated carbonados came from the state of Bahia, Brazil. The stones were fractured and first examined by light- and scanning electron microscopy. Figure 1 is a representative micrograph showing a porous polycrystalline aggregate. The crystallite size varies between 0.5 and 20μ, most crystallites being in the 1 to 5μ range. Fracture is mainly transgranular and the crystallites are interlocked and have irregular shapes. Transmission electron microscopy and diffraction revealed that the diamond crystallites do not contain any foreign phases.

Mineral inclusions are visible on fractured surfaces; the contact microradiographs in Figure 2 show that they are often distributed throughout the stones in parallel layers. These inclusions are pink, white and bluish-gray crystallites measuring up to 100μ and filling many of the pores. Electron probe microanalysis was used for determining the composition of these inclusions. Goniometer scans revealed the presence of Si, Al, K and Fe in relatively large amounts. P, S, Ca, Ti, Cu Zn, Zr and Sn and traces of Mg, La, Pr, Nd and Hf were also detected. The distribution of the major elements was mapped by means of a three-color oscilloscope connected to an ARL probe as described by Ficca (3). This microprobe study showed that 15 minerals were present and greatly facilitated their identification from powder X-ray diagrams of crushed carbonado. As shown in Table 1, these inclusions consist mainly of silicates (predominantly orthoclase) and minor amounts of phosphates, carbonates, titanates, oxides and sulfides.

With the exception of pseudomalachite, covellite, rosasite and parisite, the minerals listed in Table 1 are either primary or common accessory constituents of igneous rocks, which are known to be normally associated with diamond. Copper phosphate, sulfide, copper-zinc carbonate and cerium-calcium fluorocarbonate are secondary minerals of hydrothermal origin.

The above mineral inclusions thus directly reflect the geochemical history of the carbonados.

---

1. R. N. Wentorf and H. P. Bovenkerk, Astrophys. J. 134, 995, 1961.
2. E. Brandenberger, Schweizerische Mineralogische and Petrographische Mitteilungem, 10, 490, 1930.
3. J. F. Ficca, Third National Conference on Electron Probe Microanalysis, Chicago, Ill., Paper #15, 1968.

TABLE I

Mineral Inclusions in Carbonado Diamond

Elements found by electron probe microanalysis to be associated in inclusions (Elements in parenthesis are present as traces).	Corresponding minerals identified by X-ray diffraction	Types of Rocks
Si, Al, K	Orthoclase, $KAlSi_3O_8$	Igneous
Si, Al, Ca, (Mg)	Gehlenite, $Ca_2Al_2SiO_2.H_2O$	Igneous
Si, Al, Fe	Chloritoid, $FeAl_2SiO_5(OH)_2$	Igneous
Si, Al, Ca, Fe, Ce, (Pr, Nd)	Allanite, $(Ca,Fe)_2(Al,CeFe)_3Si_3O_{12}(OH)$	Igneous
Si, Zr (Hf)	Zircon, $ZrSiO_4$	Igneous accessory
Cu, P	Pseudomalachite, $Cu_5(PO_4)_2(OH)_4$	Secondary
Cu, S	Covellite, SuS	Secondary
Cu, Zn	Rosasite, $(Cu,Zn)_2CO_3(OH)_2$	Secondary
Ca, Ce, (La)	Parisite, $2CeFCO_3$-$CaCO_3$	Secondary
Ca, Ti	Perovskite, $CaTiO_3$	Igneous
Fe	Hematite + Goethite, Fe_2O_3+$FeO(OH)$	Igneous
Ti, Al	Rutile + Corundum, TiO_2+Al_2O_3	Igneous accessory
Sn	Cassiterite, SnO_2	Igneous accessory

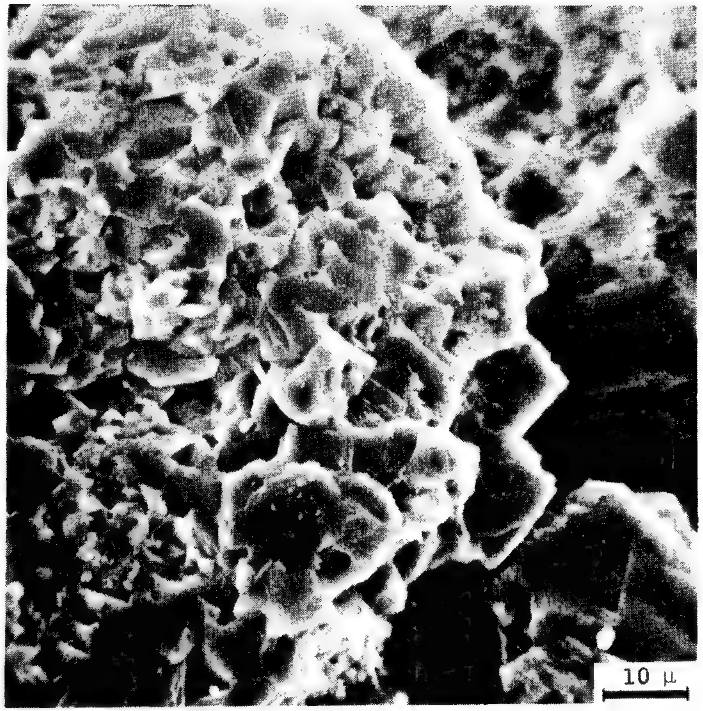

Figure 1. Scanning electron micrograph of a fractured surface of carbonado.

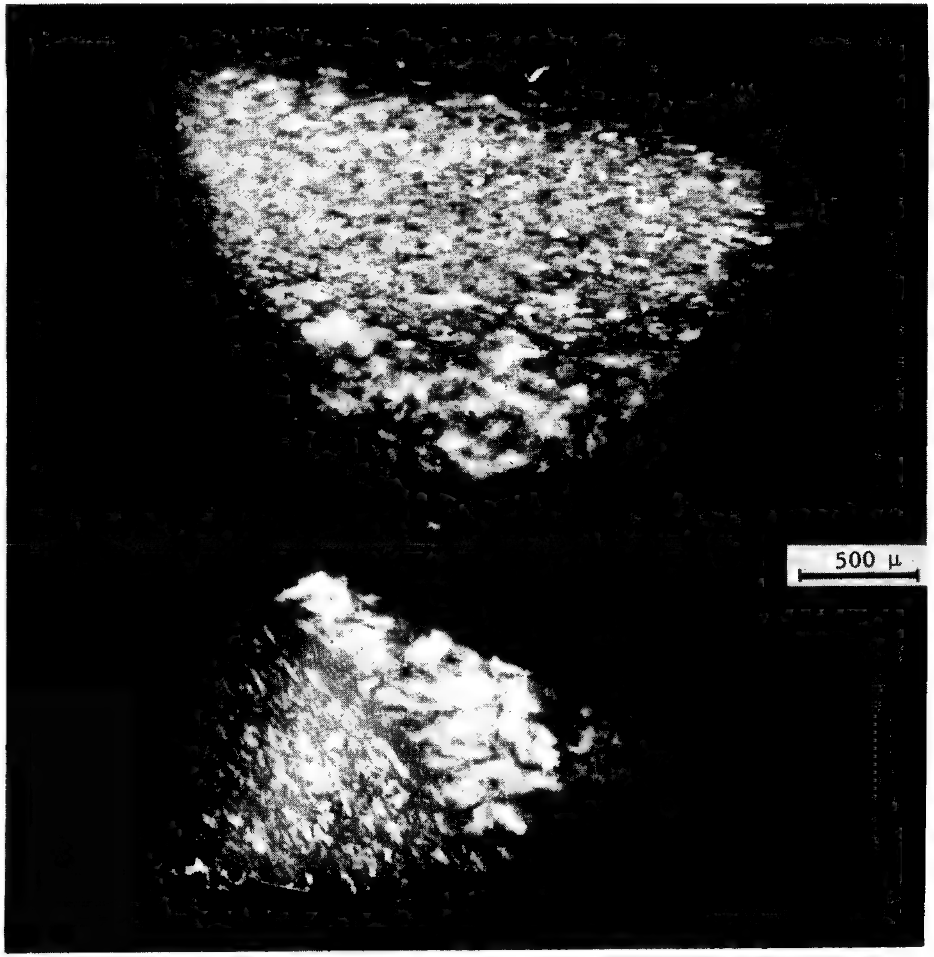

Figure 2. Contact X-Ray microradiographs(negative prints) of carbonados showing the presence of mineral inclusions.

STUDY OF DISTRIBUTION OF DIFFUSIBLE IONS IN BIOLOGICAL TISSUES USING A SECONDARY ION EMISSION MICRO-ANALYZER

P. Galle, G. Blaise and G. Slodzian
Hôpital Necker, Paris, France

Castaing's and Slodzian's Secondary Ion Emission Micro-analyzer offers the biologist new possibilities due 1°) to its very high sensitivity and 2°) to the fact that it allows separate measurements of isotopes. These possibilities are particularly interesting for the study of the distribution of diffusible ions existing in biological tissues.

The secondary ion emission of sodium and potassium has been studied from a sample of renal tissue and a smear of human red blood cells. The renal tissue has been frozen "in vivo" by means of isopentane cooled with liquid nitrogen sections three microns thick have been cut with a freezing microtome, placed on a carefully polished stainless steel support and dry-frozen; if the section is thin enough, the analysis can be carried out without difficulty although the section is a non-conducting substance. The blood smear has also been placed on a stainless steel support.

RESULTS

A) Renal tissue

In the tissue, four different parts are observed: 1°) extra-cellular space (lumen of tubules and interstitial space), 2°) nucleus, 3°) Cytoplasm and 4°) arteriolar wall.

The extra-cellular space appears very bright from the beginning of the analysis; this light however decreases within ten seconds. As soon as this light has disappeared, the intra-cellular space can be clearly seen: the nucléi then appear as very bright limited areas surrounded by less luminous areas which represent the cytoplasm. The cytoplasm remains then the only luminous part of the cell, and will remain thus for another ten minutes. Meanwhile, the arteriolar wall becomes bright for about fifteen minutes.

Thus, the disintegration speed of the different areas in the tissue varies greatly; therefore, brightness cannot be considered as a criterion for assessing the local concentration of a given element; in order to measure the concentration in a selected area, it is necessary to integrate the total number of electrons incident throughout the whole process of disintegration.

B) Red blood cells

A study of the emission of sodium shows that, in the first phase, the areas corresponding to plasma appear very bright whereas those corresponding to cytoplasm are darker (Fig. 1). After three minutes, the plasma picture vanishes and only the cells can be seen; complete disintegration of these cells has taken place within about fifteen minutes (Fig. 2).

Fig. 3 and 4, which are taken at the eighth minute of analysis show the distribution of two natural isotopes of potassium:

$$^{39}K^{+}\ (95\%)\ \text{and}\ ^{41}K^{+}\ (5\%).$$

Taking into consideration that the sodium concentration in a red blood cell is about 3.10^{-16} gram per cubic micron, that the average thickness of a cell is 1 micron, and that the disintegration time is about 900 seconds, it can be calculated that, for a surface of 1 square micron, a disintegration of $\frac{3 \times 10^{-16}}{900} = 3.3 \times 10^{-19}$ gram of Na per second takes place; the necessary exposure for a photographic picture is 0.03 sec.: thus a very small amount, i.e. as small as $3.3 \times 10^{-19} \times 0.03 = 10^{-20}$ gram of sodium (around 300 atoms), is enough to produce a significant picture.

BIBLIOGRAPHIE

1°) CASTAING (R) and SLODZIAN (G.)
J. Microscopie, 1 : 395 - 410 (1962)

2°) SLODZIAN (G.), Thèse Sci., Paris (1963).

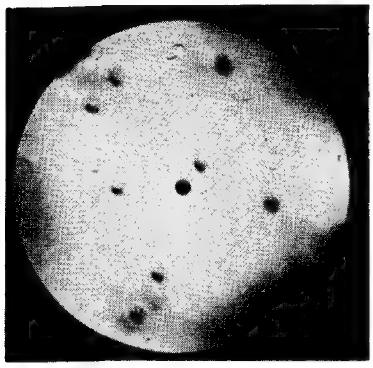

Fig. 1 : Red blood cells smear; sodium 23 distribution, tenth second

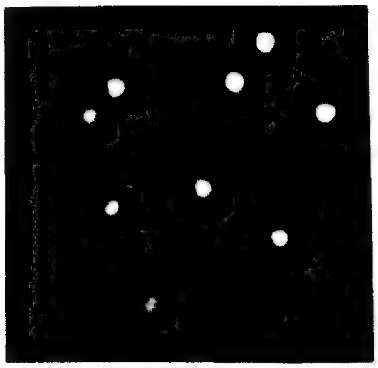

Fig. 2 : Red blood cells smear; sodium 23 distribution, tenth minute

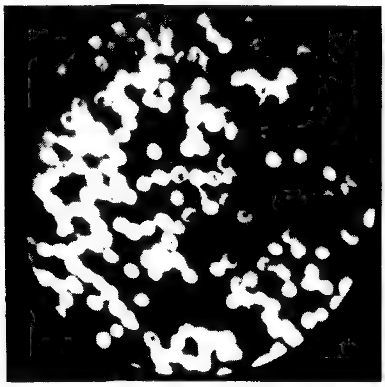

Fig. 3 : Red blood cells smear; potassium 39 distribution, eighth minute

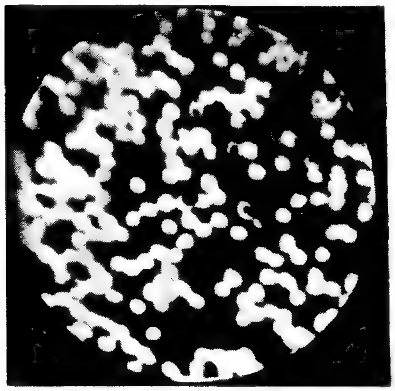

Fig. 4 : Red blood cells smear; potassium 41 distribution, ninth minute

ELECTRON MICROPROBE ANALYSIS OF THYROIDAL IODINE IN THE WHITE-THROATED SPARROW

David C. Zeigler*, W. H. Zeigler**, J. E. Harclerode*, and E. W. White**
*Bucknell University, Lewisburg, Pennsylvania
**Pennsylvania State University, University Park, Pennsylvania

---

A study was undertaken to determine the concentration and distribution of iodine within individual thyroids and variations among three groups of White-throated Sparrows. The three groups consisted of: 1) wild-netted, 2) outdoor-caged (control group), and 3) outdoor-caged White-throats fed on iodine supplemented diet (2.5 mg KI/100 gm Purina Layena). One of the objectives of the study was to establish the thyroid activity index (TAI) of the glands for each group.

The probe was operated at 15Kev, 3×10^{-8}amp. A four inch radius LiF spectrometer having a take-off angle of 52.5° was used to disperse and detect the I L_{α} line at 3.14 Å. The detector was a .001" beryllium window argon-filled proportional counter.

Standard microprobe correction techniques were applied to the count data using CdI_2 as the calibrating standard. Using the program of Colby, adapted to the Comnet Time Shared System, the corrected weight fraction of iodine was increased by a factor of eight over the observed "k" values. To circumvent the limitations inherent in the existing correctional formulas and to arrive at an acceptable calibration, a series of standards was prepared. These standards were prepared from hot aqueous solutions of Knox gelatine and KI. The resultant dense gels were subsequently freeze-dried. A vacuum evacuated die and press were used to prepare pellets having essentially zero porosity. A final assessment of this technique was not available at the time of this writing, but will be presented at the conference.

Figure 1 summarizes results of the analysis. Uncorrected values are shown but serve to illustrate the relative results for each group.

Within no group of thyroids was there significant difference in colloidal iodine content of the peripheral follicles versus the central follicles. There was, however, significant variance ($< 99\%$ level) in peripheral and central follicular iodine from group to group.

Generally, the thyroid glands of the wild-netted sparrows had the least iodine (% by weight) and the greatest TAI. The caged control group and the iodine supplemented group did not show significant difference in TAI, but the thyroids of the iodine supplemented group had the greatest iodine content of the 3 groups.

Results seem to indicate that thyroidal iodine content is inversely proportional to thyroid activity, and directly proportional to the amount of iodine ingested.

Figure 1. Follicular Iodine Content of White-throated Sparrow Thyroid Glands

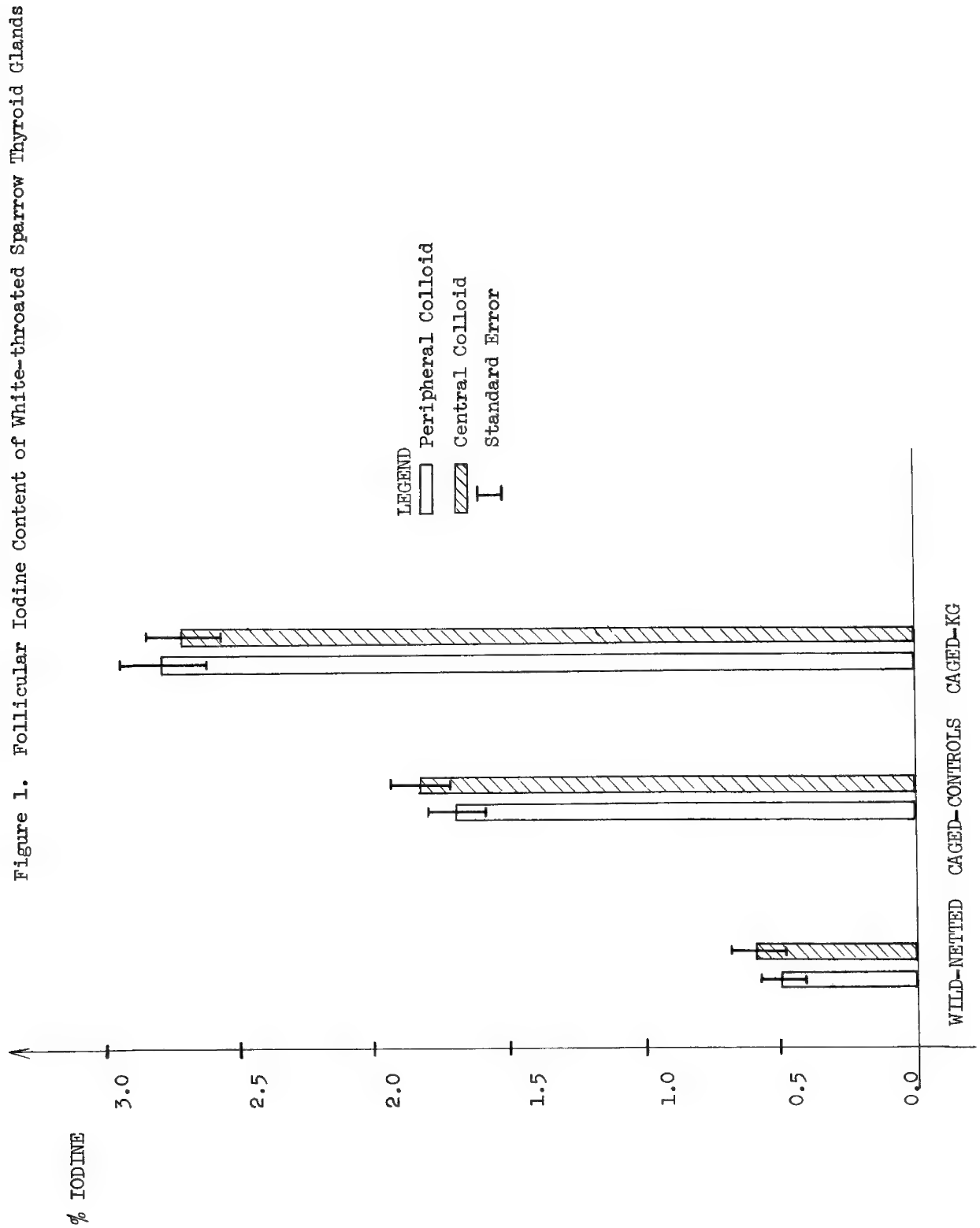

THE DISTRIBUTION OF STRONTIUM IN THE RAT FEMUR AS DETERMINED BY ELECTRON MICROPROBE ANALYSIS

A. R. Johnson
University of California, Los Angeles, California

INTRODUCTION

The distribution of mineral in bones and teeth has been investigated by a variety of techniques including x-ray microradiography, autoradiography, and electron microprobery. Of considerable interest is knowledge of the site(s) of deposition of the elements of the mineral phase and their associations. Strontium has many of the characteristics of the principal cation of the inorganic phase of hard tissues, calcium, and as such may serve two purposes, (1) to study the intrinsic characteristics of strontium metabolism under normal conditions, and (2) to alter normal functions, especially those in which calcium plays a major role, by excessive dietary loading with strontium.

The electron microprobe (EMP) was employed as instrumentation of choice to reveal the relationships of calcium and strontium in the long bones of the rat undergoing a dietary stress of high strontium intake.

MATERIALS AND METHODS

Preparation of the Tissues

Twenty-one-day-old, male, weanling, rats of the Sprague-Dawley strain were provided a diet containing approximately 0.2% Ca, 0.4% Sr, 0.4% P, and normal in other minerals, proteins, fats, and carbohydrates. Distilled water was supplied, ad lib. The rats were housed individually in a constant temperature room, provided with automatic light cycling 12 hours on and 12 hours off, for 56 days. They were sacrificed by heart puncture, the bones harvested, lipid extracted with anhydrous ether, and ethanol alternately over a period of 72 hours. The bones were then dried at 110°C overnight. Femurs were embedded in resin and cross-sections of approximately 100μ and 500μ alternately were sawn with apparatus capable of precision work. The 500μ sections were embedded in resin in brass sample holders, ground, and polished with 1μ diamond paste to a surface satisfactory for the analysis as determined at 100X under the light microscope.

Preparation of Standards

A sample of fluorapatite (FA), Saamite, with approximately the same Sr and Ca concentrations as the bone specimens, was prepared in the same manner as the hard tissues. The standard and specimens were coated with a thin layer of carbon to make them conductive.

Instrumentation

An ARL-EMX electron microprobe, Department of Geology, UCLA, was employed in this study. Instrument parameters were as follows: operating voltage 15 KV; sample current on brass 0.020 μamp, on bone 0.022 - 0.025 μamp; beam size approximately 1μ diameter. Sr Lα radiation, nominal wavelength 6.86 Å, was measured with an ADP crystal; Ca K_α, nominal wavelength 3.36 Å, radiation was measured with a LiF crystal; a window of 100-300 mv was used for each element. Data were collected for 10 second periods; in some instances repeated counts were taken at the same spot on the standard, and on the bone specimens. The standard was surveyed for homogeneity. For simplicity, background counts for each element were taken from a pure Mg standard.

Treatment of the Data

Sketches of the specimens as viewed in the EMP were made and spots analyzed were identified to be related to areas as seen on photomicrographs, which were made subsequently. The net counts/10 seconds of Sr and of Ca were determined on the specimens and on the standards. Ratios of (Sr/Ca) bone to (Sr/Ca)FA were calculated from data of spots analyzed.

RESULTS

The table summarizes data and calculations describing the spots analyzed. In general, when Sr counted very low at a spot, the Ca count approached a maximum. These low net Sr/Ca ratios appeared mainly in midcortical regions of the middle third of the femur, although isolated low spots were found in nearly every section analyzed. The high Sr/Ca ratios were especially abundant near the proximal epiphysis, and also towards the distal epiphysis. Whenever the spot was hypomineralized, a low Ca count was employed as the criterion, the Sr/Ca normalized ratios tended to be high. No region of exceptionally high Sr content with very low Ca content was found at any of the 617 spots evaluated.

CONCLUSIONS

Assessment of the data suggested that the distribution of strontium was predominantly of two types, (1) those regions of exceptionally low Sr/Ca ratios, and (2) those regions of high Sr/Ca ratios. These results imply that some regions of bone have a somewhat low rate of transformation and that the vast amount of strontium incorporated during growth is accommodated rather homogeneously. There did appear to be a gradient of increasing Sr/Ca ratios from mid-diaphysial bone towards the extremities. These suggestions must be provisional due to an insufficient number and distribution of spots analyzed in each of the sections, and the need to examine different bones to find if skeletal deposition as a whole follows the pattern as supposed here.

The technical assistance of Klaske Zeilstra and Robert Jones is gratefully acknowledged.

TYPICAL VALUES OF STRONTIUM AND CALCIUM IN REGIONS PROBED

Sample: Location	Gross C/10 Sec.		Ratio of Net C/10 Sec.
	Strontium	Calcium	$(Sr/Ca)_{bone}/(Sr/Ca)_{FA}$
Saamite[1]: Random	844 ± 32	18875 ± 563	0.0446
Femur[2]			
Lowest Ratio: Middle Third	100	19666	0.102
Median Ratio[3]	---	-----	1.55
Highest Ratio: Distal Third	983	9952	1.85
Typical Region: Middle Third	971	14015	1.55
Hypomineralized Region:			
(a) Proximal Third	219	3332	1.58
(b) Proximal Epiphysis	255	3270	1.71

1. 21 random samplings were made. Results are the mean ± s.d. (Ratio is of Sr/Ca of the mineral only.)
2. The experimental bone results were obtained on different days and the results given in the last column do not necessarily derive from calculation from tabular values.
3. Midpoint range of 1.51-1.60 is given for 617 spots analyzed.

ELECTRON MICRO-PROBE ANALYSIS AND SCANNING ELECTRON MICROSCOPY OF HUMAN TEETH

J. D. Eick, W. A. Miller and M. E. Neiders
State University of New York at Buffalo, Buffalo, New York

J. W. Leitner and C. H. Anderson
Applied Research Laboratories, Sunland, California

In order to illustrate the usefulness of the electron micro-probe with a scanning electron microscope attachment in dental research, data from three separate studies involving young human teeth will be presented. The three studies include analysis and morphological studies of cut tooth surfaces, of peritubular dentin in young human teeth, and of cementum and sublying tissues.

One of the major problems confronting dentistry is the lack of a truly adhesive restorative dental material (1). Since the condition of the prepared tooth surface affects 1. the intermolecular forces between adhesive and adherent, 2. the thermodynamic wetting characteristics of the surfaces, and 3. the mechanical properties of the constituents (2), information concerning the topographical appearance of cut tooth surfaces and the chemical nature of the surface and remaining debris is a necessity in developing an adhesive dental material. In this study six pairs of non-carious, first premolars were used. One half of the occlusal surface was cut with a 700-7P diamond and the other half with a 170 carbide burr using a cutting speed of about 200,000 rpm. One tooth of each pair was prepared using water spray and the other was cut dry. All teeth were cut *in vivo* without rubber dam and extracted within one hour. They were dried at 95°C. under clean conditions for at least three days, mounted in acrylic resin, and coated with carbon-platinum (200-400 Å) and then carbon (200-400 Å). Scanning electron microscope examination was performed at magnifications between 100X and 3300X. The surfaces cut with the diamond instrument were rougher than those cut with the carbide burr. The surfaces which were cut dry appeared rougher and were more smeared, having a disturbed layer that appeared deeper. Tooth debris and organic films containing large amounts of N, S, and C, less than $\frac{1}{2}\mu$ thick, were present on all cut surfaces. The quantity of debris did not appear to differ between the surfaces cut with the carbide and diamond nor between the surfaces cut wet or dry. No debris from the cutting instruments was found.

Practically all of the chemical analyses of dentin and of cementum have been of a qualitative or semi-qualitative nature, utilizing conventional histological methods, microradiographic techniques or wet chemical analysis of pooled samples (3,4). These techniques are unable to relate directly morphology to precise quantitative chemical analysis on the microscale. Therefore, the electron micro-probe with a scanning electron microscope attachment was utilized to correlate the morphology of dentin and of cementum and adjacent tissues with their Ca, P, and Mg content.

For both studies freshly extracted permanent premolar teeth were fixed in 100% ethanol for at least 7 days. Transverse sections were cut (a) halfway between the tip of the cusp and the cementum-enamel junction on the buccal side, (b) 2 mm. below the cementum-enamel junction on the buccal side, and (c) midway between (b) and the apex of the root. The specimens were dried at 95°C., finally polished with 1/4 μ diamond paste, and coated with a 200-400 Å layer of carbon. Scanning electron microscope pictures were taken before and after analysis. Point analysis was performed simultaneously for Ca, P, and Mg using an acceleration potential of 10 KV and a sample current of 0.01μ amperes. At least three x-ray intensity counts were obtained at each point using a constant beam current and were converted to percent composition by weight using a fluorapatite standard ($Ca_5(PO_4)_3F$) containing 39.7% Ca and 18.4% P and a 100% Mg standard.

In the dentine study, the composition of the peritubular dentine was compared with that of the intertubular dentine in the crown, (a), and root, (b), sections. In the crown section, the peritubular dentine was generally hypermineralized, with respect to the intertubular dentine. In the root section, the peritubular dentine was either hypomineralized or the same as the intertubular dentine. Statistical analysis to compare mean compositions and the variability of composition was performed and will be presented. An example of the chemical analysis obtained is presented in Table 1.

In the cementum study, four separate layers (cementum; 5μ from the cementum-dentin junction; 20μ from the cementum-dentin junction or the granular layer of Tomes; and 70μ from the cementum-dentin junction or dentin) at the cervical, (b), and midroot, (c), levels were analyzed.

In each specimen studied a layer approximately 5μ thick adjacent to the cementum-dentin junction was found to be significantly more calcified than cementum or the granular layer of Tomes. In general, the Ca and P composition paralleled one another in each layer. It was found that Mg was significantly lower in cementum, but did not follow a consistant pattern in the other layers. In general, there was no significant difference in the chemical composition of a specific layer of the cervical or midroot levels. Again, statistical analysis was performed on the data and will be presented. An example of the chemical analysis obtained is presented in Table 2.

---

1. R. W. Phillips, "Advancements in adhesive restorative dental materials," J. Dent. Res. 45: 1662, 1966.
2. A. T. DiBenedetto, The structure and properties of materials, McGraw-Hill, New York, 1967.
3. K. A. Selvig, "Studies on the genesis, composition, and fine structure of cementum," Universitets-for-laget, Bergen, 47, 1967.
4. K. A. Selvig and H. A. Zander, "Chemical analysis and microradiography of cementum and dentin from periodontally diseased human teeth," J. Periodont. 33: 303, 1962.

Table 1

Ca, P, and Mg Composition of Dentine
Upper Left First Premolar
Age 14 Years

		Intertubular Dentine % by weight	Peritubular Dentine % by weight
Ca	crown	35.1[+] ± 0.8[*]	38.0 ± 3.3
	root	33.9 ± 1.3	32.5 ± 3.4
P	crown	17.3 ± 0.3	17.5 ± 0.3
	root	16.3 ± 0.6	15.4 ± 0.8
Mg	crown	1.14 ± 0.08	0.98 ± 0.19
	root	1.01 ± 0.09	1.08 ± 0.11

[+] Average of 4 analysis points, 5 separate intensity counts (approximately 20,000 counts each) per analysis point.

[*] Standard Deviation, including instrument variation and heterogeneity of the sample.

Table 2

Ca, P, and Mg Composition
Root of an Upper Right First Premolar
Age 11 Years

Area Analyzed	Element	Cervical Area % by weight	Mid-Root Area % by weight
Cementum	Ca	26.9[+] ± 1.5[*] (1)[#]	27.8 ± 1.0 (1)
	P	13.7 ± 0.3 (1)	14.2 ± 0.5 (1)
	Mg	0.61 ± 0.05 (1)	0.59 ± 0.06 (1)
5 u from C-D Junction	Ca	30.5 ± 2.1 (3)	30.3 ± 0.6 (2)
	P	15.5 ± 1.0 (3)	15.3 ± 0.2 (2)
	Mg	1.51 ± 0.11 (3)	0.99 ± 0.11 (2)
20 u from C-D Junction	Ca	27.4 ± 1.7 (1,2)	27.6 ± 1.3 (1)
	P	13.8 ± 0.8 (1,2)	14.0 ± 0.6 (1)
	Mg	1.28 ± 0.10 (2)	1.08 ± 0.07 (3)
70 u from C-D Junction	Ca	28.5 ± 2.1 (2)	30.0 ± 1.4 (2)
	P	14.4 ± 1.0 (2)	15.3 ± 0.6 (2)
	Mg	1.23 ± 0.09 (2)	1.30 ± 0.11 (4)

[+] Average of 4 analysis points, 3 separate intensity counts (approximately 20,000 counts each) per analysis point.

[*] Standard Deviation, including instrument variation and heterogeneity of the sample.

[#] Duncan's Multiple Range Test at the 95% confidence level.

SCANNING ELECTRON MICROSCOPY OF "DENTAL CARIES" PRODUCED ENZYMATICALLY IN-VITRO

S. N. Kreitzman, A. J. Saffir, R. S. Harris and R. E. Ogilvie
Massachusetts Institute of Technology
Cambridge, Massachusetts

Dental caries is a disease process characterized by a progressive loss of tooth structure. For the past ninety years it has been generally accepted that oral bacteria produce organic acids at the tooth surface causing the dissolution of the mineral. To date, however, no one has succeeded in simulating natural caries in-vitro by acids. We have found that phosphoprotein phosphatase, an enzyme produced by cariogenic bacteria, attacks tooth structure and results in the destruction of tooth mineral in a manner characteristic of natural caries. The destruction proceeds beneath a surface layer of enamel which does not cavitate until late in the course of the disease or enzyme treatment.

The scanning electron microscope is ideally suited to the study of the pattern of destruction of these teeth, confirming our chemical evidence and revealing structural details of tooth enamel unobservable by any other method. Figure 1 is a rat molar tooth that has been subjected to enzyme attack. The appearance of the intact surface enamel is indistinguishable from untreated controls. A brief sonication removed the fragile shell of undermined enamel, but left intact tooth material undisturbed.

In Figure 2, which is a higher power view of the area enclosed in the box in Figure 1, the differences in character between the bulk of the enamel and the surface shell are clearly apparent. Note that the enzymatic attack occurs at multiple foci and spreads laterally beneath the surface shell.

The tooth in Figure 3 has been exposed to treatment for a longer period of time. The destruction has progressed far beyond the surface shell layer and the complex substructure of the underlying enamel is revealed.

Figure 4 demonstrates the surface appearance of a control tooth incubated with inactive enzyme. The apparently undisturbed ends of the enamel rods are clearly evident in this view.

The scanning electron microscope has provided evidence that dental caries lesions can be simulated in-vitro by enzymatic means. This previously unrecognized product of bacterial metabolism may well be a major factor in the progression of the natural lesion.

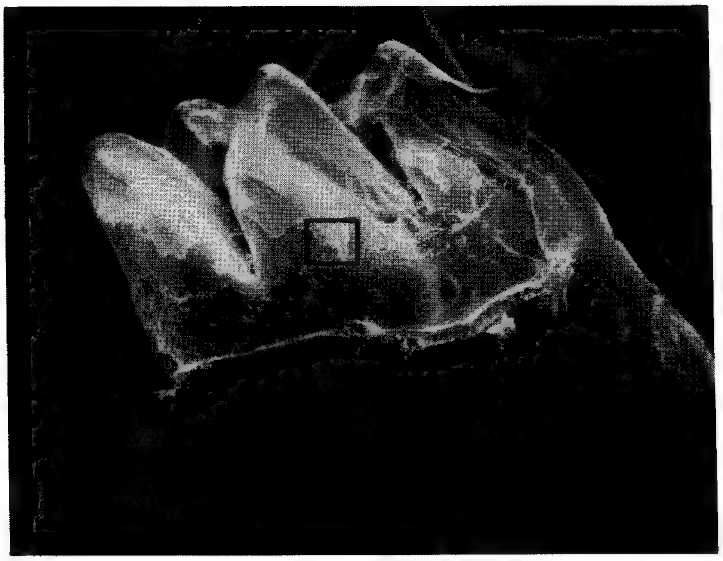

Figure 1

Simulated caries in a rat molar tooth. Surface shell of enamel has been removed to reveal substructure

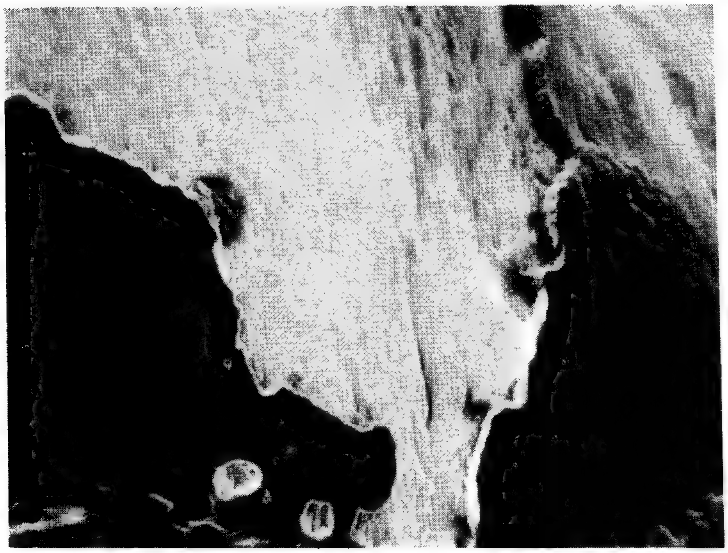

Figure 2

Surface of tooth enamel at junction of sound and attacked enamel

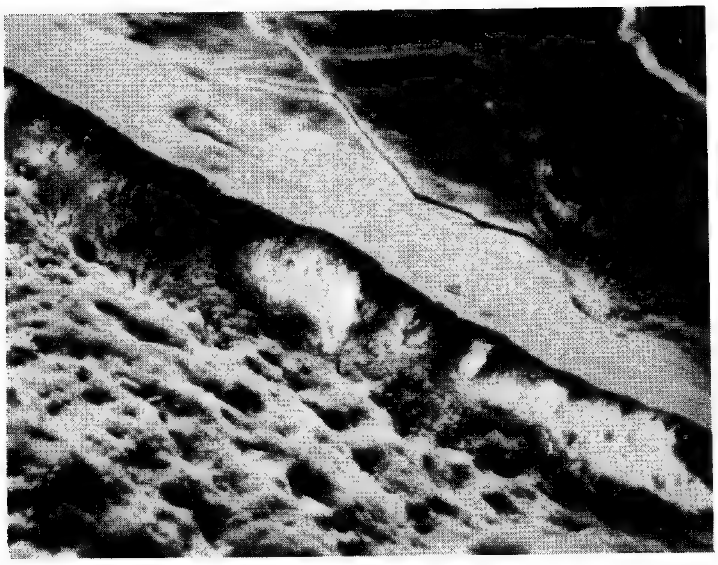

Figure 3

Advanced enzymatic lesion. Destruction has progressed far beyond the enamel shell stage.

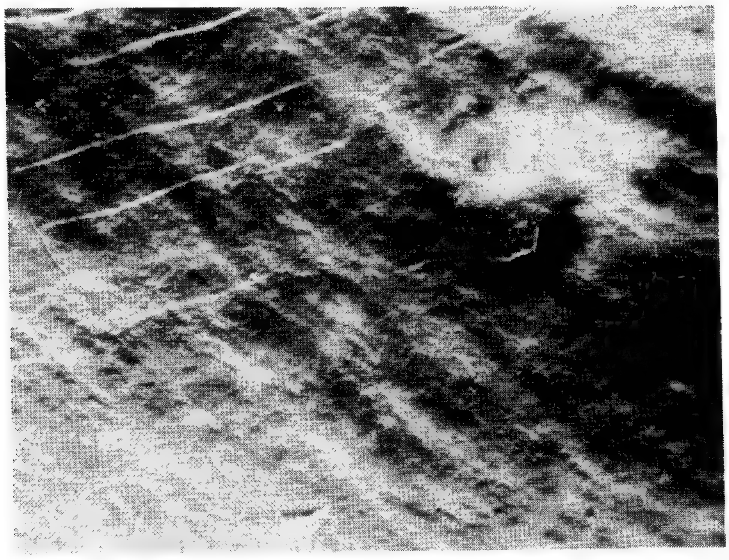

Figure 4

Surface enamel of control tooth. Inactive enzyme leaves surface intact.

MICROPROBE MEASUREMENTS OF THE DIRECT FIELD FORCE ON IMPURITY ATOMS IN METALS

Theodor Hehenkamp
Universitaet Muenster (Westf), Germany

It is well established that the microprobe is the most powerful tool to investigate transport phenomena such as electrotransport for impurity atoms in metals.[1] Earlier measurements presented in 1967 at the Boston meeting were limited to very dilute alloys because of simplicity of the solutions of the transport equations, which become non-linear even for impurity contents of the order of 1%. It was possible to solve these equations by means of a digital computer for it was to be expected that by increasing the impurity content the accuracy of the measurements could be greatly improved. Much more information is available now about the interesting physical constants as effective charges. In particular it is possible, for the first time, to discriminate clearly between friction forces (electron drag) and pure field forces which can be separated and extracted from the total effective charge of the transported species. It was necessary to evaluate the diffusion profiles and to determine not only concentration ratios, as usual for diffusion measurements in dilute alloys, but also absolute concentrations. In taking all changes of diffusion (D) (fig 1) and forces properly into account as a function of concentration, the equation

$$V = \frac{D(C)ej}{kT} (Z_o \rho (C) - K)$$

was found to be valid, V being the transport velocity at absolute temperature T, Z_o the direct charge parameter, K the electron drag parameter, ρ the total resistivity at the concentration of interest, j the current density and e the elementary charge. This is in good agreement with some theories. Diffusion is greatly enlarged by increasing the antimony content only slightly (fig 1), as might also be expected from the phase diagram (rapidly falling solidus temperature). The result of the transport measurements is given in fig (2), where a friction scattering resistivity of 6,23 $\mu\Omega$cm per atomic percent Sb impurity is found. The charge parameter could be determined precisely enough

for the first time as + 4,95 $\pm$ 0,5 e, which is, to our surprise, very close to the valence of the impurity. The absolute concentrations were determined by calibrations using very well homogenized standards, the preparation of which is difficult and will be discussed in detail.

---

1. Th. Hehenkamp; J. Appl. Phys. 39, 3928 (1968)

2. Th. Hehenkamp; Microchimica Acta Suppl. III 79 (1968)

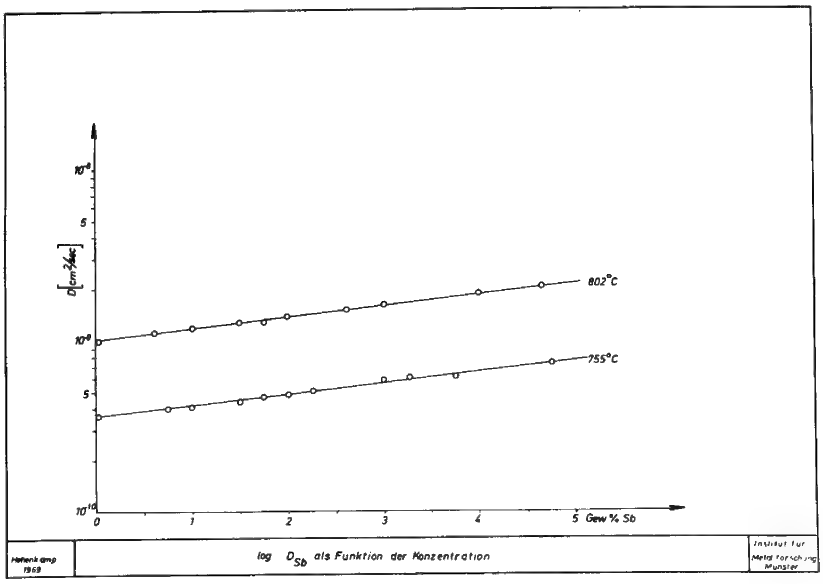

fig 1

Change of diffusivity as function of Sb-concentration

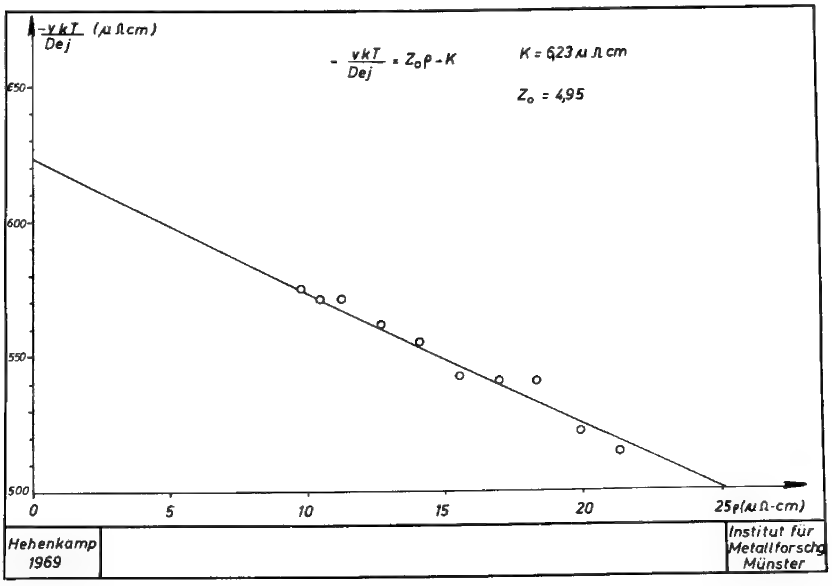

fig. 2

Plot of $\frac{vkT}{Dej}$ vs. ρ

MICROPROBE ANALYSIS OF DIFFUSION IN THIN BI-METAL FILMS OF Au-Cu

E. I. Allesandrini and J. D. Kuptsis
IBM, Yorktown Heights, New York

For the study of diffusion in thin films, bulk methods such as radioactive tracers and sectioning techniques are not readily applicable because of the limited size and thickness of the specimens. This paper describes the use of electron microprobe spectroscopy as the analytical method for the detection of diffusion of Au into Cu films.

Films were prepared by evaporating 100 Å Au onto quartz substrates followed by the deposition of 1500 Å of Cu on top of the Au. With the electron beam of the microprobe normal of the Cu film surface, the characteristic AuMα radiation was monitored at various accelerating voltages.[1] This characteristic radiation requires a minimum of 2.2 kv for excitation beam voltage. It was not observed in the case of the as-deposited sandwich films until the beam was accelerated at 6 kv. An excess of 4 kv was required in order to penetrate the 1500 Å Cu. Plotted in Fig. 1 are the number of AuMα counts/sec monitored against microprobe beam accelerating voltages in kv as a function of different annealing temperatures for a constant time. The diffusion of Au into the Cu film after various heat treatments could be detected by: first the enhancement of the AuMα intensity at a constant excitation voltage, and, second by the decrease of the minimum beam voltage ("appearance potential") necessary to produce just detectable characteristic AuMα signal. Data will be presented for varying annealing conditions. The effect of annealing time and temperature at three voltages is shown in Fig. 2. Assuming a first order process, the activation energy for the diffusion of Au into the Cu film was obtained from this type of figure by using the cross-cut technique.

At several constant values of AuMα counts/sec the temperature values T_i were interpolated for the annealing times t_i. These values were then used to calculate the activation energy E in the following form

$$\log \frac{t_1}{t_2} = - \frac{E}{k} \left[\frac{1}{T_1} - \frac{1}{T_2} \right]$$

where k is Boltzman's constant. Data were selected and taken at beam voltages below 9.5 kv to maximize the contribution of the film to the excited X-ray volume. The average value for the activation energy E of the diffusion of the Au into the Cu film was found to be 0.8 ev $\pm$ 0.2 ev[2].

---

1. J.J. Gneiwek and N.G. Koopman, "Electron Beam Microprobe Technique to Measure Phosphosilicate Glass Thickness and Composition." Paper presented at the Third National Conference on Electron Microprobe Analysis, Chicago, Ill., July 31-August 2, 1968.

2. B.Y. Pines, L.P. Grebennik, and I.P. Gribko, UKR. Fiz. ZH, 13, No. 2, 280-5 (1968); reported values in Diffusion Data 2, 116 (1968).

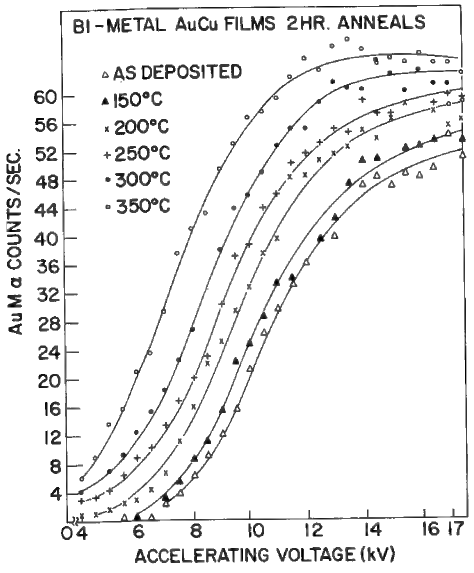

Fig. 1 Plot showing the increase in the intensity of the characteristic AuMα radiation as well as a lowering of the excitation potential as a function of annealing temperatures for a constant time.

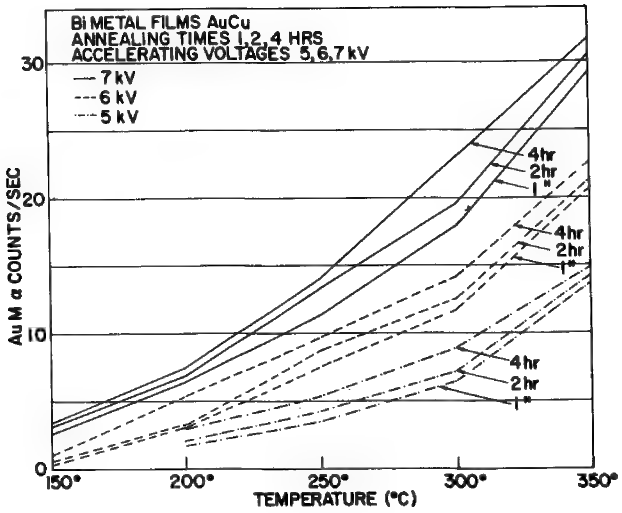

Fig. 2 Plot of number of AuMα counts/sec against annealing temperatures at various times for 5, 6, and 7 kv accelerating voltages.

ELECTRONPROBE MICROANALYSIS OF CYLINDRICAL ELECTRODEPOSITED MAGNETIC FILMS

A. Baltz
Sperry Rand Corporation, Philadelphia, Pennsylvania

We have used the electronprobe microanalyzer extensively to correlate certain magnetic effects with composition, plating deficiencies, grain boundary diffusion and surface roughness of cylindrical Ni Fe films. The films are ~ 8000Å thick and are electrodeposited onto 5 mil Be Cu wires in a vertical flow cell using a continuous plating process. In order to control the substrate surface, a layer of either Au or Cu is deposited between the Be Cu wire and the Ni Fe films. The average composition of the films is maintained near 82% Ni, the zero magnetostriction point of the alloy.

From magnetic measurements described elsewhere[1], it was inferred that a circumferential variation of the composition generally exists in the plated wires. To verify this compositional non-uniformity, the films were studied with the electron microprobe using a specially constructed specimen holder. This specimen holder enabled us to analyze the films both at 10^{o} intervals around the circumference of the wires and along the wire axis over a distance of one inch. The specimen holder consists essentially of a flexible shaft which actuates a 36 tooth gear and is brought out of the specimen stage through a vacuum seal. Thus, the films can be analyzed without breaking the vacuum during the analysis. The compositional variation was periodic with a wavelength equal to the circumference of the wire. The peak to peak deviation was approximately 4% Ni. A special problem was encountered when the grains in the films were large and the film surface was very rough. Techniques used to overcome this difficulty will be described in detail.

Magnetic measurements showed that if films having a Au intermediate layer were annealed, the magnetic easy direction, which was circumferential after deposition, reoriented perpendicular to the film surface. Electron microprobe studies showed that this phenomenon was due to diffusion of the Au into the Ni Fe grain boundaries.

Using the electron microprobe, it has also been possible to correlate low magnetic output regions with local plating deficiencies.

---

1. S. Strobl to be published.

ELECTRON MICROPROBE ANALYSIS OF THE TERNARY ALLOY SYSTEM Fe-Ni-P

A. S. Doan, Jr. and J. I. Goldstein
Goddard Space Flight Center, Greenbelt, Md., and Lehigh University, Bethlehem, Pennsylvania

---

Because of our interest in the development of the structure of iron meteorites we have studied the phase stability ranges of ferrite (α) austenite (γ) and phosphide (Ph) in the low P region of the Fe-Ni-P ternary. These three phases (α, γ and Ph) are the most commonly observed ones in iron meteorites. Comparison between meteoritic compositions and ternary alloy equilibrium data should enable one to determine the cooling times and temperatures which controlled the development of structure in iron meteorites.

Approximately 50 ternary alloys were made for this study. These alloys were heated to temperatures between 550 and 1100°C in either one, two or three phase regions of the phase diagram for varying amounts of times in order to nucleate and grow the equilibrium phases. The electron microprobe (ARL) was used to determine the compositions of the phases which formed in the ternary alloys. Data was taken at 20KV and 0.03-0.05 microamps specimen current. The data was taken using the P_K line and either the Ni_K or $_L$ line. The Ni contents were determined using nine Fe-Ni alloys as standards and the P contents were determined using a standard of natural schreibersite (15.5 wt% P) from the Odessa iron meteorite and the corresponsing Fe-Ni standard for background. The accuracy of the measurements obtained using these standards was better than 2% (rel.) except for the Ni_L radiation where the accuracy was limited to about 5% (rel).

Above 850°C the equilibrium phases were larger than 10 microns in size and homogeneous. The measurement of composition was relatively straight forward. Below 850°C the phases which formed were often small even after long heat treatments (> 6 months) and not homogeneous. The probe was still used to obtain phase equilibria data since in many cases it was possible to measure the composition of the coexisting phases at their interfaces where equilibrium is maintained.

Figure 1 shows an example of the 875°C isothermal, one of the 10 isothermal sections determined for the Fe-Ni-P system. The dashed lines represent tie lines in the 2 phase regions α + Ph, α + γ, γ + Ph and the points represent the equilibrium compositions. The equilibrium compositions in the 3 phase field at 875°C were determined by averaging the results of the measurement of α, γ and Ph in 8 different alloys in the α + γ + Ph field.

The salient features of the ternary diagram are given as follows: At high temperatures, the most important effect of phosphorus on the Fe-Ni system is the ~400°C freezing point depression caused by the addition of 1 wt% P. Liquid is still present at greater than 10 wt% Ni at 1055°C and at 100 wt% Ni at 875°C. Also the phosphorous solubility decreases below 1055°C in both α and γ . At all temperatures phosphorous is more soluble in α than in γ phase. In general the higher the nickel content, the lower is the temperature at which the α + γ + Ph ternary phase field is stable.

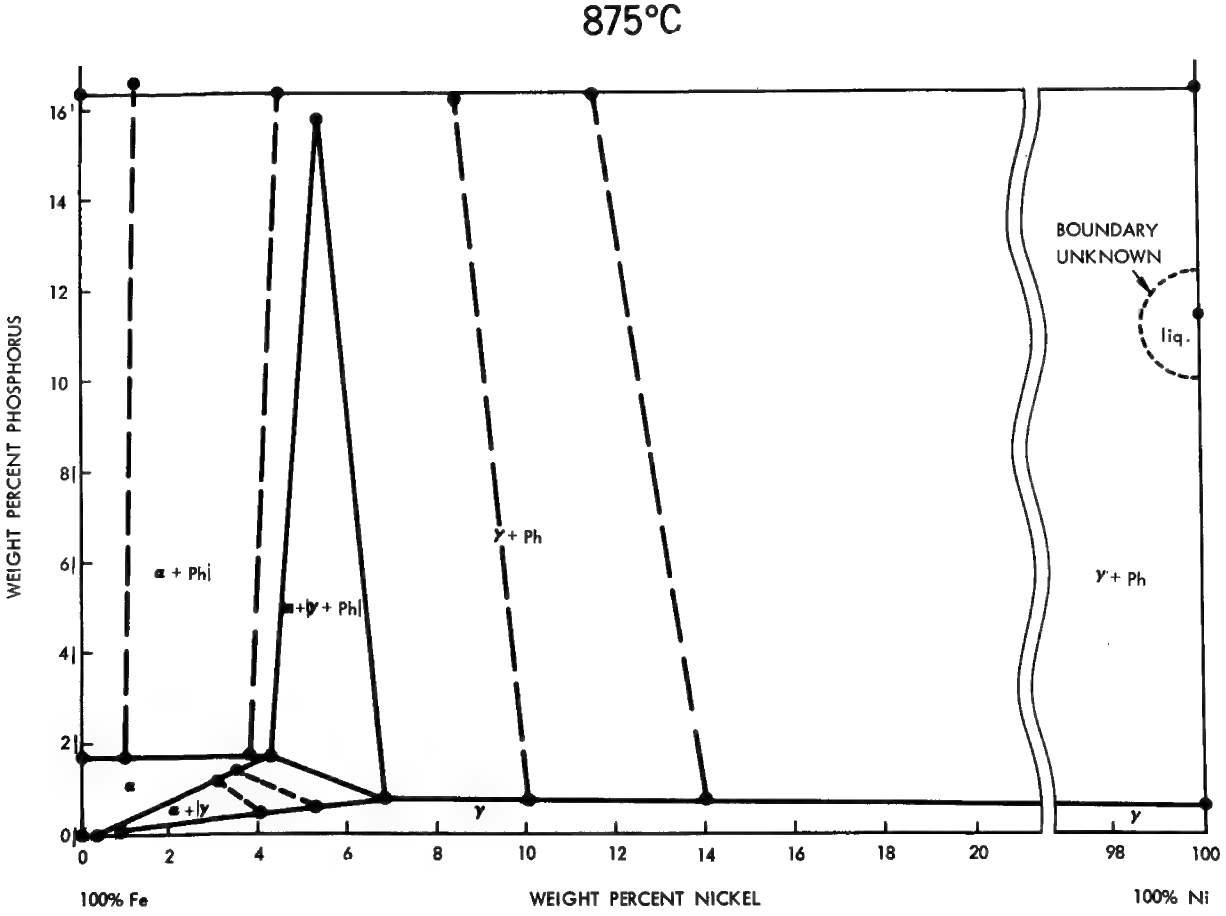

EQUILIBRIUM PHASE STUDIES IN FAST-REACTOR FUEL ALLOYS*

D. R. O'Boyle, D. E. Busch, and J. E. Sanecki
Argonne National Laboratory, Argonne, Illinois 60439

Ternary alloys that contain fissionable isotopes of uranium and plutonium are of interest as fuels for sodium-cooled fast-breeder reactors. In order to better understand their physical properties and to interpret their irradiation behavior, phase relations in the uranium-rich corner of two ternary alloy systems, uranium-plutonium-titanium and uranium-plutonium-zirconium, have been investigated by means of quantitative microprobe analysis. The microprobe data, together with optical metallography, were used to establish the phases in equilibrium in both systems at temperatures of interest.

In the uranium-rich corner of the uranium-plutonium-titanium alloy system, the major phases were found to be gamma (based on bcc gamma-uranium), orthorhombic alpha-uranium, and hexagonal $(U,Pu)_2Ti$. The binary U_2Ti intermediate phase was found to dissolve as much as 20 a/o plutonium and to extend into the ternary system as $(U,Pu)_2Ti$.

To establish the phases in equilibrium in the uranium corner of the uranium-plutonium-zirconium system, a series of high-purity binary uranium-plutonium and ternary uranium-plutonium-zirconium alloys that have a uranium-to-plutonium ratio of 4:1 were prepared by arc melting the pure elements. Following homogenization at about 1000°C in the gamma-single phase region, 27 specimens of five different ternary alloys were isothermally annealed in evacuated quartz tubes at temperatures between 590 and 700°C for times sufficiently long (up to 170 days) to allow the phases to grow large enough for accurate analysis with the microprobe. Each specimen was examined metallographically, and the compositions of the phases in equilibrium were determined by means of point counts and mechanical scans. For the analysis of specimens containing plutonium, the microprobe was modified slightly by the addition of a miniature fume hood over the specimen chamber door to prevent the spread of alpha contamination. All intensity

*This work was performed under the auspices of the United States Atomic Energy Commission.

ratios were corrected for absorption, fluorescence, and atomic-number effects using the Magic II computer program of Gray.[1]

The alloys annealed at the highest temperature (700°C) for 25 days were found to contain only the bcc gamma phase. Dilatometric measurements showed that the gamma phase is stable over a wide range of temperatures up to approximately 1100°C. Alloys annealed in the temperature range from 590 to 670°C were generally two-phase and consisted of zeta-uranium-plutonium and bcc gamma. Microprobe measurements were used to establish the zeta and gamma single-phase boundaries over the entire temperature range. In summary, it was found that (1) the γ_1 plus γ_2 uranium-zirconium miscibility gap[2] extends into the ternary system, (2) the zeta-uranium-plutonium phase[3] dissolves about 5 a/o zirconium over the temperature range from 590 to 660°C, and (3) as the temperature decreases from 660 to 590°C, the gamma single-phase boundary moves from the uranium-plutonium side of the diagram toward the zirconium-plutonium side.

An impurity phase, commonly observed in commercial-purity uranium-plutonium-zirconium alloys, was identified as oxygen-stabilized alpha-zirconium that contains some uranium and plutonium in solid solution. The solid solubility of uranium and plutonium in the alpha-zirconium phase was measured in alloys annealed at temperatures between 350 and 1000°C. The maximum solid solubility over this temperature range was 0.8 a/o for plutonium and 1.6 a/o for uranium.

In addition to the arc-melted high-purity alloys, injection-cast uranium-plutonium-zirconium alloys of commercial purity were isothermally annealed at 350, 560, 625, and 700°C for 60 and 300 days, which corresponds to burnups of 1 and 5% of the fissionable atoms, respectively. These specimens were examined metallographically and by means of microprobe analysis, and the phases identified were in agreement with those predicted from the study of the high-purity alloys. Injection-cast specimens from the same casting batch have been irradiated in the Experimental Breeder Reactor-II to 7.2-a/o burnup, and are being prepared for analysis with the shielded microprobe.

---

1. L.J. Gray, "X-ray Mass Absorption Coefficients and Quantitative Microanalysis of Metallurgical Systems, Including Refractory Metal-Interstitial Compounds," Ph.D. thesis, University of Illinois, 1969.

2. R.P. Elliott, Constitution of Binary Alloys, First Supplement, McGraw-Hill Book Company, New York, 1965, pp. 858-859.

3. F.H. Ellinger, R.O. Elliott, and E.M. Cramer, "The Plutonium-Uranium System," Journal of Nuclear Materials, 1, 233-243 (1959).

MICROANALYSIS OF HIGHLY RADIOACTIVE REACTOR FUELS*

R. Natesh, B. J. Koprowski, and E. M. Butler
Argonne National Laboratory, Argonne, Illinois 60439

Transfer of bulk radioactive samples such as irradiated reactor fuel to an electron microprobe can be time consuming since the samples are prepared in a hot cell that is physically separated from the microprobe laboratory. Another problem related to analysis of a radioactive sample is the increased intensity of the background radiation as a result of sample radioactivity. Work was done on these two problems with a shielded electron microprobe.

In order to transfer highly radioactive bulk samples more efficiently, a pneumatic transfer system was designed and built that is safe, economical, and fast. A radioactive specimen can be transferred from the hot cell to the microprobe specimen chamber in less than two minutes. The system is designed to handle uranium- and plutonium-containing fuels irradiated up to 10 at.% burnup followed by a 60-day, or longer, cooling period. Typical fission-product activity of high-burnup specimens is 100 curies with a gamma radiation dose rate of 560 R/hr at 12 in.

The irradiated specimens are prepared in the Alpha-Gamma Hot Cell by remote control. A 2-in.-diameter tube (see A-B in Fig. 1) connects the hot cell to a transfer box in the microprobe room, which is a distance of 30 ft. This tube is shielded by lead bricks 3 in. thick (see A-A in Fig. 1). A blower pump (P) is connected to the transfer tube at both ends (C and D) through valves that can be operated from the microprobe room. The mount containing the sample is introduced at A and is pneumatically transferred to B in the transfer box in about 10 sec. The transfer box is a shielded glovebox, with 9-in.-thick steel walls, which is positioned in contact with the electron microprobe. By means of a remotely controlled manipulator and a transfer slug system, the specimen is moved from the transfer box to the specimen chamber of the microprobe.

The distribution of the scattered secondary and fluorescent radiation caused by the radioactivity of the sample

*This work was performed under the auspices of the United States Atomic Energy Commission.

can be studied with the electron beam off. A UO_2-20 wt.% PuO_2 specimen, irradiated to 3.7 at.% burnup in a fast neutron flux at a maximum linear power rating of 21.3 kW/ft with an activity of 50R at 9 in., was introduced into the specimen chamber. With the electron beam off, the background intensity was found to increase as the Bragg angle (2θ) decreased. The background intensity in the 2θ range of from 40 to 80 degrees was high, necessitating the use of correction techniques to improve the peak-to-background ratio. Pulse height analysis of the background radiation at 2θ=40 degrees showed that the intensity increased as the energy of the spectrum decreased. The background intensity was found to increase rapidly below 18.0 keV, and reached a maximum at 2.1 keV. Since larger background corrections are necessary at smaller Bragg angles and lower photon energies, three methods were used that improved the peak-to-background ratio:

1) an analyzing crystal with a smaller d-spacing was used so that the characteristic line of interest was shifted to a higher Bragg angle:

2) the same crystal was used but with a characteristic line of higher order; or

3) the same crystal was used but with a characteristic line of a different series that occurs at a higher Bragg angle.

The background intensity of the specimen at 2θ=40 degrees was studied as a function of distance from the radioactive source. It was found that the intensity decreased rapidly at distances greater than 0.21 in. from the center of the radioactive sample. The intensity was only 1 cps at a distance of 0.63 in., where the standards for microprobe analysis are located. Thus, when an element A is analyzed in an irradiated matrix, the observed background of A in the radioactive matrix will be higher, and the peak-to-background ratio of A will be lower when compared with the analysis of same amount of A in a nonradioactive standard of identical composition. Improvement in the peak-to-background ratio for A in the radioactive matrix may be achieved by subtracting from the observed readings for peak and background of A, the background contribution due to the scattered secondary and fluorescent radiation. This correction becomes particularly important at Bragg angles of less than 80 degrees.

Application of the above procedure to zinc (as an example) improved the peak-to-background ratio, which was increased from 78 to 257.

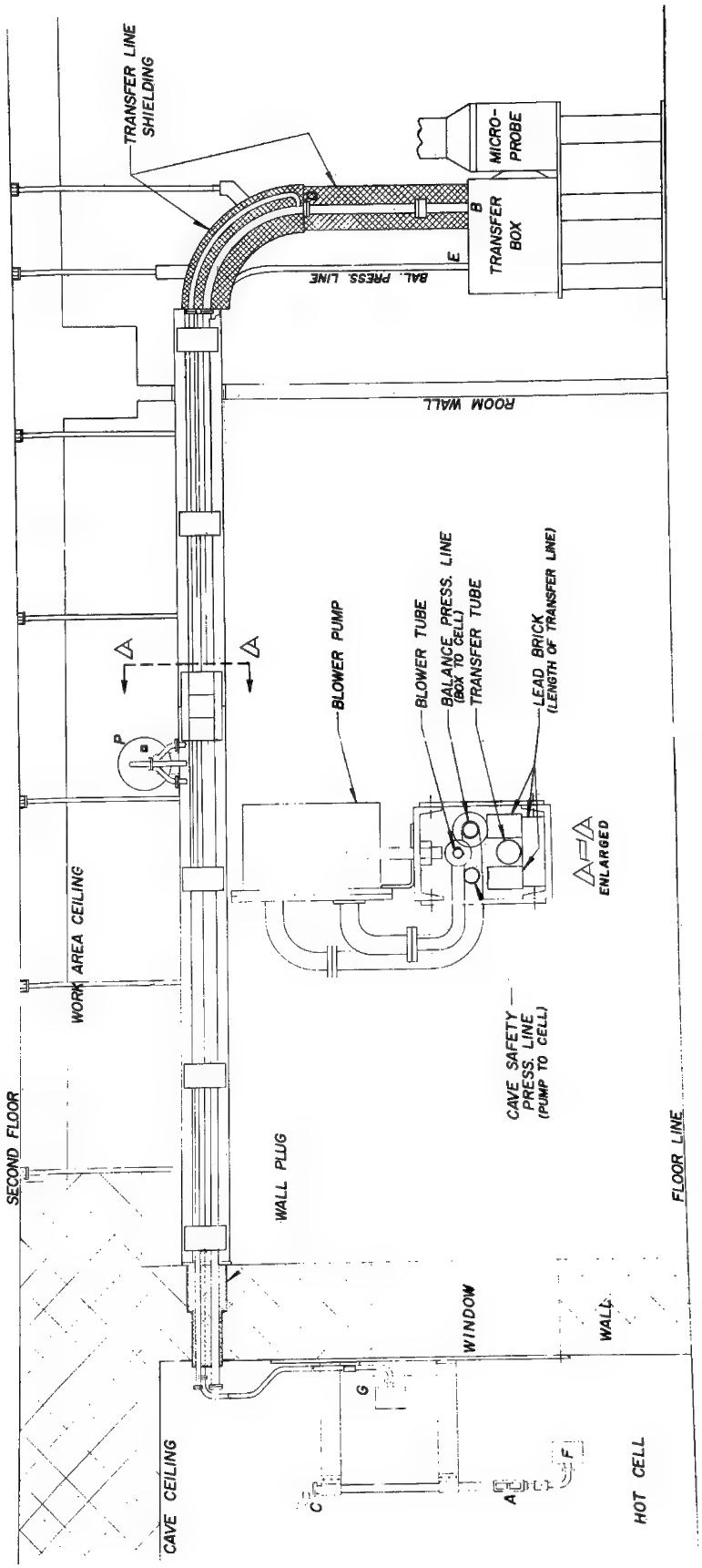

Fig. 1. The Pneumatic Transfer System for transferring radioactive solids.

DIFFUSION BEHAVIOR IN URANIUM-PLUTONIUM OXIDE FUEL IRRADIATED IN A FAST NEUTRON FLUX*

R. Natesh, D. R. O'Boyle, and E. M. Butler
Argonne National Laboratory, Argonne, Illinois 60439

Recent work by several investigators[1,2] has shown that during irradiation uranium and plutonium redistribution occurs within mixed-oxide fuels. These microprobe measurements were made on samples that had been reduced in thickness to a few mils in order to minimize the intense radioactivity emanating from the fuel so that the samples could be analyzed in a microprobe with minimum biological and instrumental shielding. In the present work a bulk UO_2-20 wt.% PuO_2 specimen, which was irradiated to a higher burnup than any previously studied, was examined in a shielded electron microprobe. The performance of this microprobe, the specimen transfer system for transporting the specimen from the hot cell to the microprobe specimen chamber, and the distribution of the scattered secondary and fluorescent radiation have been described elsewhere.[3,4]

The fuel element studied contained fully-enriched, vibratorily compacted powders of mixed-oxide fuel irradiated in a fast neutron breeder reactor (EBR-II) to 3.6 at.% burnup at a maximum linear power rating of 21.3 kW/ft. The temperature at the center of the fuel pin was estimated to be about 2800°C, and the temperature at the fuel-cladding interface was estimated to be about 605°C. The fuel had an initial effective density of 85.1% of theoretical. The diameter of the fuel was 0.25 inch, and the fuel was enclosed in Type 304 stainless steel cladding with a wall thickness of 0.021 inch.

The cross section of the unetched fuel pin is shown in Figure 1. The microstructure of the fuel matrix consists of a central void formed during irradiation, surrounded by a region of long columnar grains, encompassed by a region of equiaxed grains, which is, in turn, surrounded by an unsintered region toward the cooler regions of the fuel.

Figure 2 shows the distribution of uranium and plutonium along a radius in the columnar grain region. The plutonium

*This work was performed under the auspices of the United States Atomic Energy Commission.

concentration increases at higher irradiation temperature regions, while the uranium concentration decreases. The maximum uranium concentration and the minimum plutonium concentration occur at a distance of about 50 mils from the center of the fuel. In the region located between 68 mils and 106 mils from the center of the fuel, uranium and plutonium form a complete solid solution and the matrix is homogeneous with respect to uranium and plutonium as a result of complete sintering of the original particles of UO_2 and PuO_2. In this region the nominal concentration in the matrix is 70 wt.% uranium and 17.7 wt.% plutonium. In the cooler regions of the fuel (greater than 106 mils from the center of the fuel element), complete sintering of UO_2 and PuO_2 particle has not taken place.

Microprobe investigation of the fuel-cladding interface showed the presence of fission-product cesium in the fuel matrix, at the fuel-cladding interface, and as a grain-boundary phase (having a width of 3 μ) in Type 304 stainless steel cladding. The grain-boundary phase decreased in width as the distance from the fuel-cladding increased and became discontinuous at a distance of 200μ from the fuel-cladding interface. Figure 3 shows electron microprobe scanning images of the grain-boundary phase in the cladding. The X-ray images revealed depletion of iron, manganese, chromium, and enrichment of cesium and silicon along the grain boundaries. The concentration of nickel within the grains is nonuniform and nickel appears in small discrete areas in the grain boundaries.

---

1. D. R. O'Boyle, F.L. Brown, and J.E. Sanecki, J. Nucl. Mats. 29, 27-42 (1969).

2. N.R. Stalica and C.A. Seils, Proceedings of the Third National Conference on Electron Microprobe Analysis, p. 39 (1968).

3. R. Natesh, B.J. Koprowski, E.M. Butler, and D.A. Donahue, Proceedings of the 16th Conference on Remote Systems Technology, Am. Nucl. Soc., 243-252 (1969).

4. R. Natesh, B.J. Koprowski, and E.M. Butler, Proccedings of the Fourth National Conference on Electron Microprobe Analysis (1969).

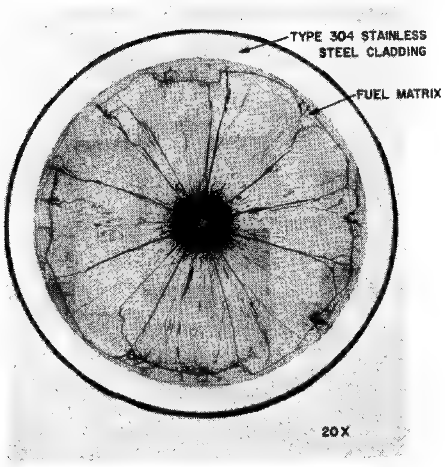

Fig. 1. Transverse cross section through a UO_2-20 wt.% PuO_2 fuel element irradiated in a fast neutron flux to a burnup of 3.6 at.%. The central void is formed during irradiation; radial cracks in the fuel are formed during cool down from the reactor operating temperature.

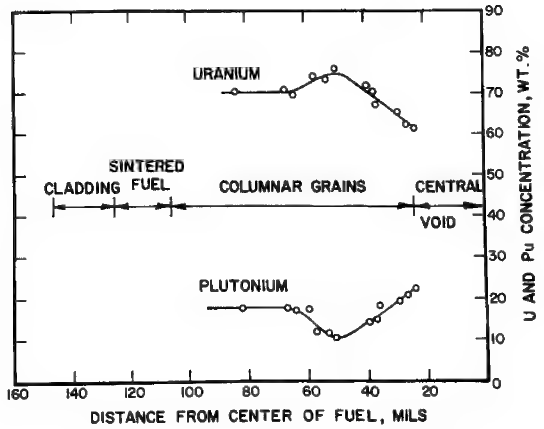

Fig. 2. Radial distribution of uranium and plutonium in the fuel element, shown in Fig. 1, after 3.6 at.% burnup at 21.3 kW/ft.

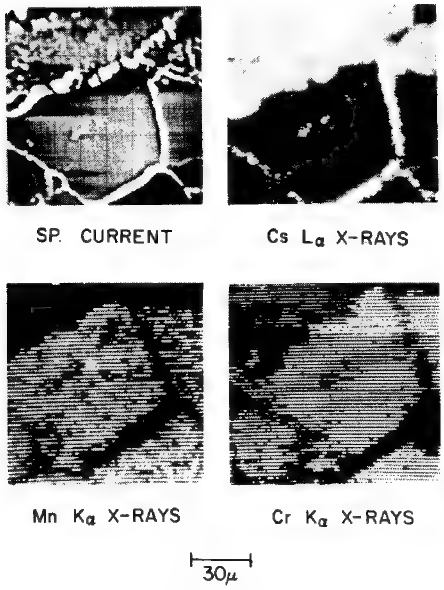

Fig. 3. Segregation of Cs, Mn, and Cr in the grain boundaries of Type 304 stainless steel cladding after irradiation.

COMBINED SCANNING ELECTRON MICROSCOPY AND X-RAY MICROANALYSIS IN METALLURGICAL NUCLEAR APPLICATIONS

L. Meny and M. Champigny

S.R.M.A. - C.E.N.
Saclay - France

The high quality of the images obtained with the S.E.M. leads to applications in many metallurgical fields. Investigations combining both S.E.M. and x-ray microprobe analysis have been made on some metallic nuclear materials, using two separate instruments. The high resolution of the S.E.M. images has been very helpful in interpreting the corresponding x-ray scanning images (or linear scans) in the 1,000 Å to 1 μ range of dimensions.

1 - Polished bulk specimens have been observed. The finest structures can be studied, which are not resolved with the optical microscope. These include the following cases:

a) Lamellar structures

The lamellar decomposition of a solid solution α (MgAl 8 %) to platelets of γ ($Mg_{17}Al_{12}$) in a magnesium rich solid solution matrix has been studied (Fig. 1).

b) Precipitates

Identification of different intermetallic compound precipitates has been made on uranium alloys (Sicral F 1 alloy, UM_oS_n alloys) (Fig. 2) and on ZrCuMo alloy. These precipitates may be dispersed in the matrix, located within the grain boundaries or may form a network within the subgrain boundaries.

2 - Fractured surfaces of bulk specimens can also be observed directly; this has been done in a prototype instrument EMMA (1), where manganese sulfide precipitates have been identified in the dimples of a ductile fracture of steel. Some good x-ray images can be obtained, as the most favorable value of the take-off angle of the analysed x-rays can be used by tilting the specimen. Since one usually knows what type of precipitates can be present in a known material, a qualitative or semi-quantitative analysis is often sufficient for their identification.

3 - In precipitation studies, it has been previously shown (2) that S.E.M. images (polished and fractured surfaces), and T.E.M. images (thin plates and replicas), give similar results for particle dimensions down to 500 Å. Hence, by using S.E.M., the analysis of precipitates can be much simplified; some of the difficulties of thin plate preparation or precipitate extraction replicas techniques (3) (4) can be avoided.

It seems that combined instruments, such as SEMMA (5), which are able at the same time to study the morphology of the fracture surface, and to analyze and identify the small particles of second phases, without any specimen preparation, are powerful tools to study kinetics of precipitation and mechanisms of deformation, including the influence of identified precipitates on the initiation and propagation of cracks.

---

1. C. J. Cooke - P. Duncumb

Performance Analysis of a Combined Electron Microscope and Electron Probe Microanalyzer "E.M.M.A."
Tubingen - Sept. 1968

2. L. Meny

Metallurgical Applications with the scanning electron microscope
Chicago - April 1969

3. R. Tixier - J. Philibert

Analyse quantitative d'echantillons minces
Tubingen - Sept. 1968

4. R. Tixier - M. Ancey - G. Henry - J. Philibert
Analyse des précipités extraits sur répliques à l'aide d'un microanalyseur équipé d'un microscope électronique
Tubingen - Sept. 1968

5. D. B. Wittry
Recent Advances in instrumentation for microprobe analysis
Tubingen - Sept. 1968

Al-Mg Alloy $(\gamma + \delta)$

γ : $Mg_{17}Al_{12}$
δ : Al-Mg sol. solution

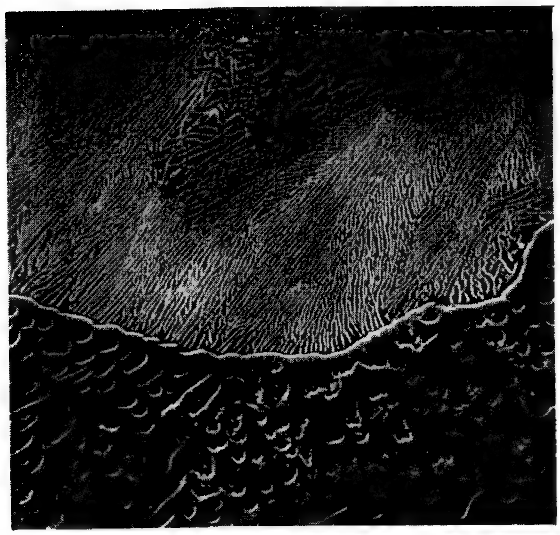

10 µ ×1400

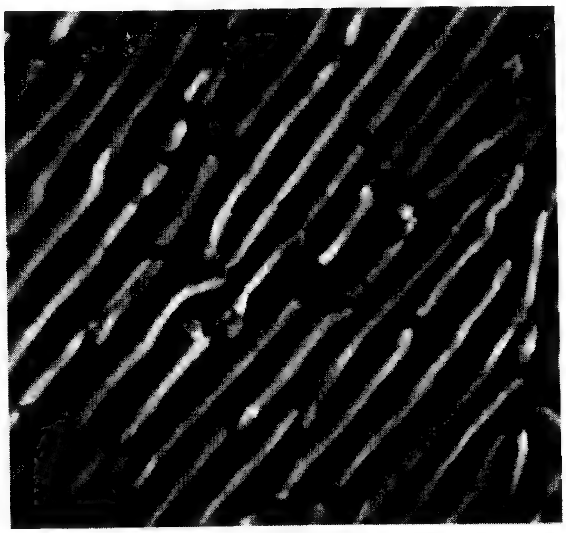

1 µ ×14000

Fig 1 : eutectic $(\gamma + \delta)$ and lamellar decomposition of δ

UMo_{10} $Sn_{0,25}$ Alloy

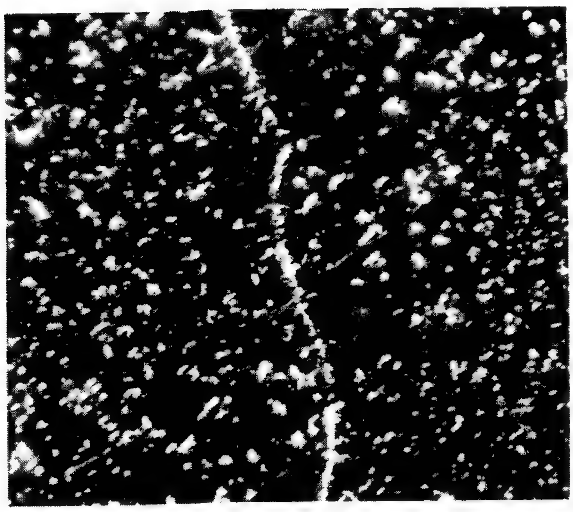

20 µ ×640

5 µ ×2600

Fig 2 : precipitates within the grains and in the grain boundaries

SCANNING ELECTRON MICROSCOPY OF SPALL FRACTURE IN ARMCO IRON

F. I. Grace and J. V. Foltz

Materials Science Division
U.S. Naval Weapons Laboratory
Dahlgren, Virginia

Brittle fractures in engineering structures have been a subject of considerable concern ever since it became the practice to weld ships and other large systems. A crack that starts in a ship's structure can pass completely around its girth, causing it to break in two. Similarly in a welded steel gas pipeline brittle fractures have been known to travel with high velocities for distances as long as half a mile. Brittle fractures in low carbon steel almost universally occur under the conditions of either low temperature or high strain rates. The purpose of the present investigation is to characterize in a qualitative fashion the nature of fractures in Armco Iron cooled to 77° Kelvin and subjected to impulsive loading.

Numerous tests have been designed within the past fifty years for the quantitative study of fracture. However, in many investigations information of a useful nature can be garnered through the study of fracture surfaces. The scanning electron microscope provides for the direct examination of fracture surfaces with a depth of focus nearly 300 times greater than optical microscopes and a resolution approaching 100A.

Fracture surfaces produced by impulsive loading are influenced not only by the material strength, but also by the stress wave pattern which develops. In this study we have chosen to investigate fracture produced by the interference of planar tensile waves during uniaxial shock loading. We have used the flying plate technique of Duvall and Fowles (1) to subject the specimen material to shock compression at 50 & 150 kilobars in these tests. Spall surfaces were produced in Armco Iron specimen plates, cooled to 77° K during the tests in an attempt to reduce the effects of shock heating in the fracture process. The Armco Iron specimen plates had a grain size of 0.018 mm and the following composition: 0.016C, 0.004P, 0.022S, 0.02Si, 0.04Mm, 0.04Mo, 0.06Ni, 0.09Cu, remainder Fe.

The fractured surfaces of the specimens were examined directly through use of a JSM-2 scanning electron microscope. The merits of the instrument have been discussed in detail by Johari (2). Microscope services were provided under contract by Dr. Ohm Johari of the Illinois Institute of Technology Research Institute.

Iron, like many other metals, exhibits a temperature dependent brittleness (3), (4). The degree of brittleness increases with a reduction in temperature and an increase of strain rate. Thus, neglecting shock effects, Armco Iron would be expected to

spall in a brittle manner under impulsive loading conditions at low temperature. Figure 1 shows a scanning electron micrograph of a typical fracture area in Armco Iron subjected to 50 kilobars at 77° Kelvin. A typical fracture zone in a second Armco Iron specimen spalled at 150 kilobars at 77° Kelvin is shown in Figure 2. Both specimens exhibit the classical cleavage fracture typical of brittle failure in polycrystalline iron (3). The second specimen also exhibits a large proportion of ductile failure which is characterized by areas of fibrious lines and dimples between cleavage planes. This observation supports the previous finding that some plastic flow and ductile behavior also accompany low temperature brittle failure in iron (3).

We conclude from these qualitative results that impulsive loading of Armco Iron at low temperature and moderate pressure produces a fracture mode typical of low temperature brittle fracture of iron. We further conclude that, as a preliminary result, the shock heating (5) and work hardening (6) associated with the preceeding shock compression play a minor role in subsequent tensile failure.

---

1. G. E. Duvall and G. R. Fowles, "High Pressure Physics and Chemistry," Vol. 2, Academic Press, New York (1963).

2. O. Johari, J. Metals 20, 26 (1968).

3. J. R. Low, Jr., Prog. Mat. Sci. 12, 1 (1963).

4. S. F. Pugh, Brit. J. Appl. Phys., 18, 129 (1967).

5. J. M. Walsh, M. H. Rice, R. G. McQueen and F. L. Yarger, Phys. Rev. 108, 196 (1957).

6. F. I. Grace, J. Appl. Phys. 40 (1969, in press.

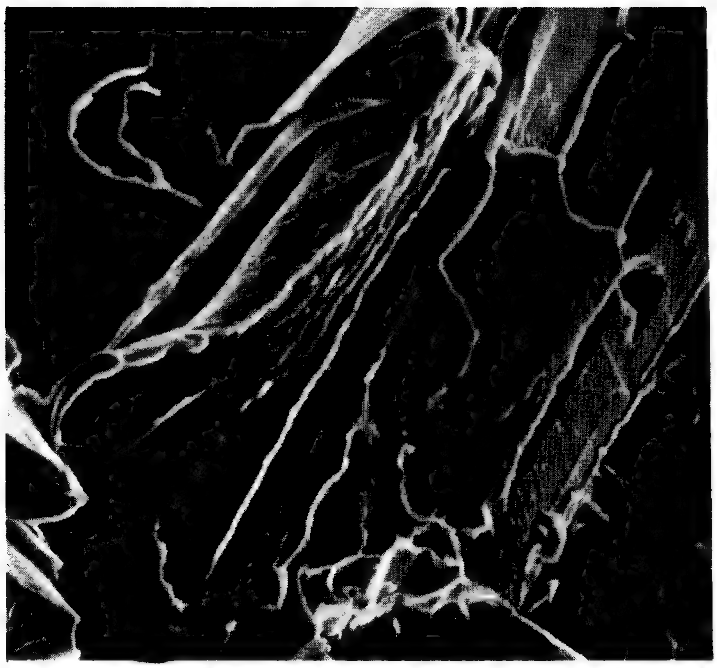

Figure 1

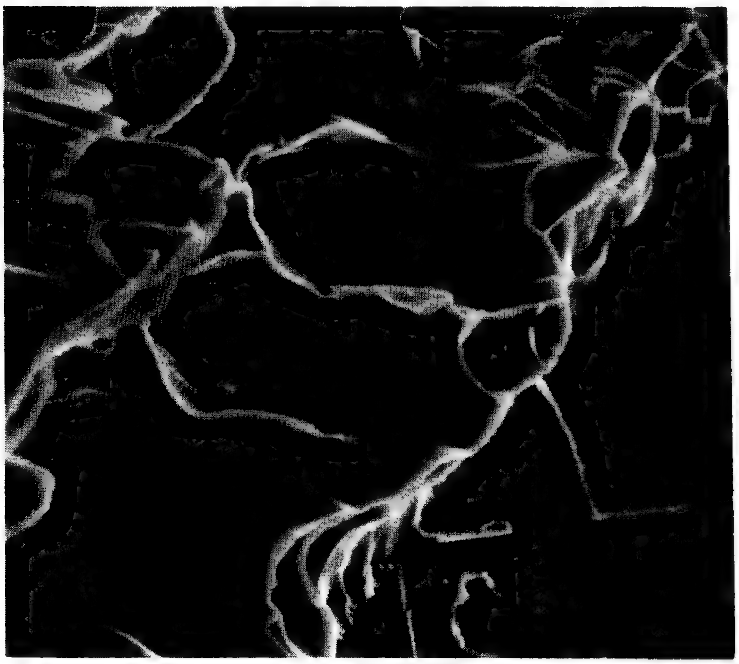

Figure 2

MICROPROBE ANALYSIS OF LIGHT ELEMENTS IN MULTI-PHASE ALLOYS

G. W. Bruno and S. H. Moll

Advanced Metals Research Corporation
Burlington, Massachusetts

In a previous study [1] it was shown that by utilizing an electron beam traversing technique, multi-phase alloys could be used as calibration standards except under certain conditions. [2] These conditions are present if: (1) the calibration curve shows a large deviation from linearity, (2) there is a very large difference in the composition of the phases in the alloy, and (3) the alloy exhibits an extremely coarse microstructure. The effects of these conditions on the analysis of Sn in the Pb-Sn system are demonstrated in Figure 1.

The beam traversing technique was recently utilized in applications involving light element analyses of multi-phase samples. In the first application it was necessary to determine the average carbon and oxygen concentrations as a function of distance from the surface (edge) in cross-sectioned cast iron samples which had been annealed.

Figure 2 shows the distributions of C and O obtained in samples annealed 1, 7 and 19 times. It is clear that O penetrates into the samples and C diffuses out of the samples as a function of the number of annealing cycles. The extent of O penetration was related to the microstructure in that it produced a very fine oxide precipitation in the areas into which it had penetrated.

In these cast iron samples it was found that the microstructure had an interesting effect on the carbon calibration curves. Normally CKα is highly absorbed in iron, yielding a large negative deviation. However, by using the as-cast sample chemistry as a standard, it was found that the CKα intensity compared to that from pyrolytic graphite was linear. This is apparently due to the fact that in cast iron the phases present are Fe and graphite. Since nearly all of the carbon x-rays produced in the sample originate in the graphite, they exit primarily through graphite which does not attenuate them. Therefore, the C intensity observed is directly (linearly) related to the amount of carbon in the sample.

A second application in which the averaging technique was utilized for light element analysis involved the study of Ta powders. Two powder samples were prepared by pressing them into high purity Al. This method of preparing the powders has proved to be very satisfactory. The average oxygen concentration in each sample was obtained, and it showed that sample "A" contained oxygen (2)

and sample "B" did not. It was found that the oxygen in sample A was related to randomly distributed particles exhibiting a thin oxide surface film.

---

(1) Moss, S. H. and Bruno, G. W., 19th Annual Pittsburgh Conference on Analytical Chemistry and Applied Spectroscopy

(2) Moss, S. H. and Bruno, G. W., Third National Conferencd on Electron Microprobe Analysis

MICROPROBE ANALYSIS OF MULTIPHASE
64-36 Sn-Pb SOLDER

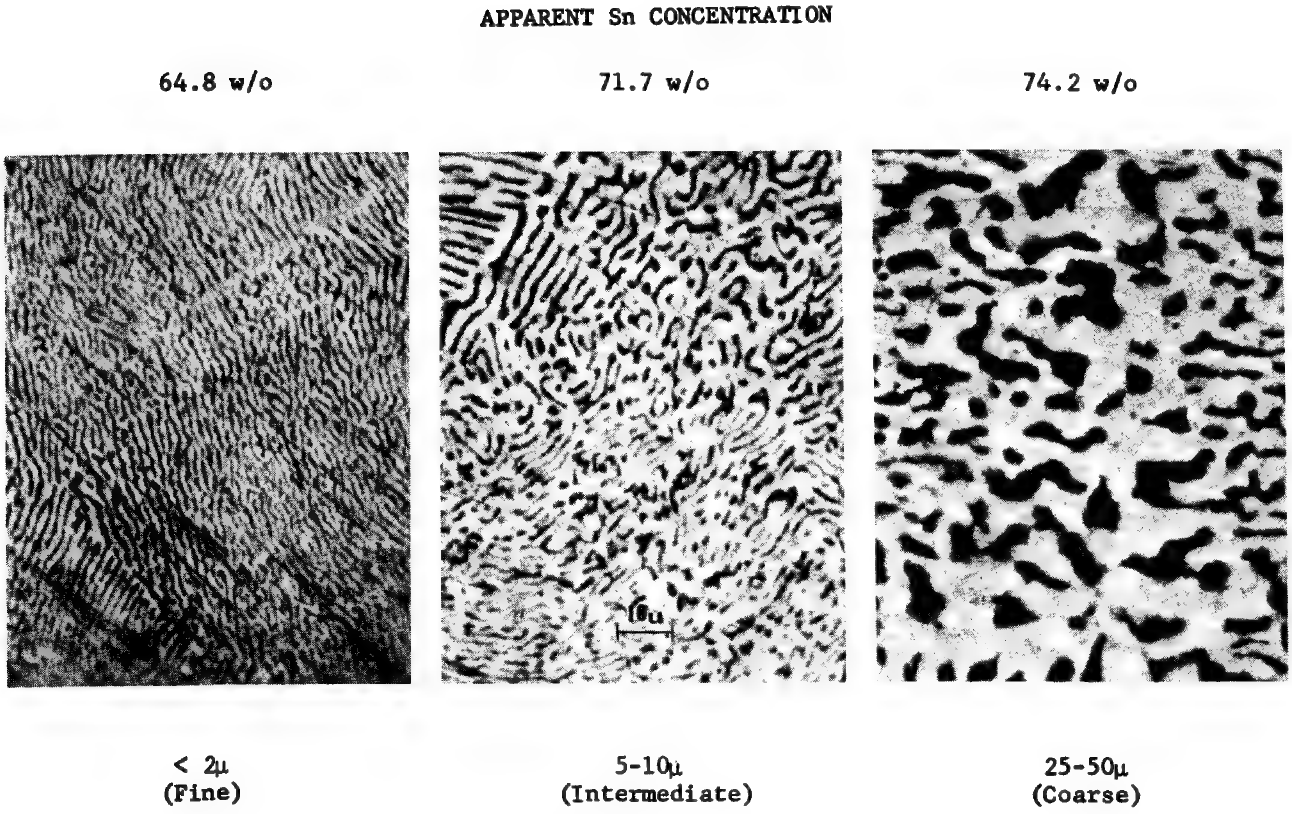

Figure 1.

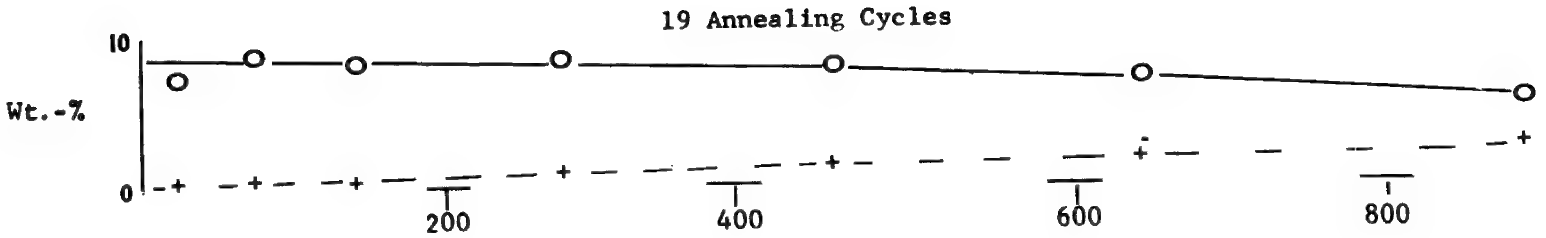

Figure 2

Average Distributions of Carbon (+) and Oxygen (o)
in Annealed in Cast Iron

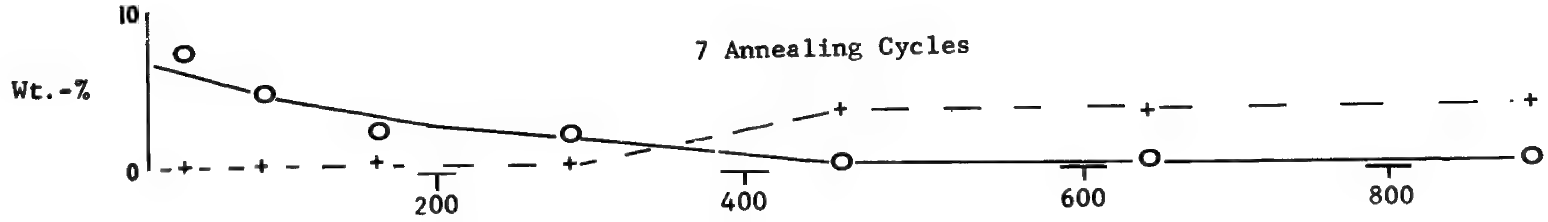

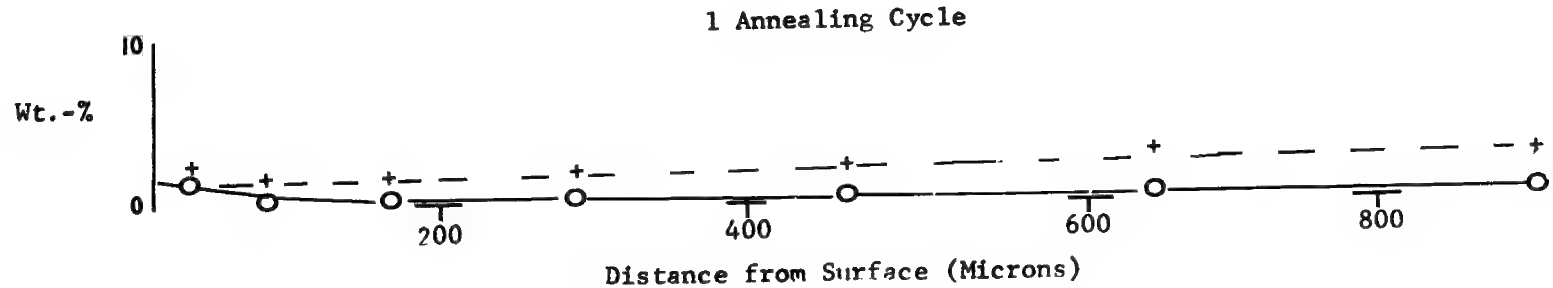

AN EVALUATION OF A SOLID-STATE X-RAY DETECTION SYSTEM FOR MICROPROBE ANALYSIS

E. Lifshin

General Electric Research and Development Center
Schenectady, New York

The resolution and sensitivity of Li drifted Si X-ray detection systems has increased significantly since their first reported application to microprobe analyzers slightly over a year ago[1]. A variety of these detectors are presently available for almost all commercial microprobes and scanning electron microscopes. In the present study a Princeton Gamma-Tech system was evaluated on a CEC/Cameca MS64 microprobe. The experimental setup is shown in figure 1. X-ray pulses from the cooled Si(Li) detector and FET preamp are transmitted to a Tennelec amplifier equipped with pole zero cancellation and a baseline restorer to minimize pulse pileup and optimize resolution. The pulses are then sorted and stored in a multichannel analyzer. Data may be read out to a teletype, X-Y recorder, or cathode ray display. With this system a resolution of better than 315ev was obtained for radiation ranging in energy from 1.254KeV (Mg Kα) to 11.103KeV (GeKα). Table I contains a list of measured peak to background ratios and integrated peak intensities for a number of elements studied at 20 KV, 10 nanoamp beam current, and 100 second counting times.

Concentrations of less than one percent of most elements with atomic number greater than Na may be detected in a matter of minutes due to the high collection efficiency of the detector and its ability to simultaneously collect an X-ray spectrum over the entire available energy range. Figure 2 shows the spectrum of a Fe-20Cr-20Ni alloy collected in one minute. Further processing of data from the multichannel analyzer can be made by a timeshared computer where spectrum stripping and statistical techniques are used to enhance sensitivity or for comparison to reference spectra. Methods for determining minimum detectability limits will be described.

---

1. R. Fitzgerald, K. Keil, K. F. J. Heinrich, Science, Vol. 159, No. 3814, pg. 528 (1968).

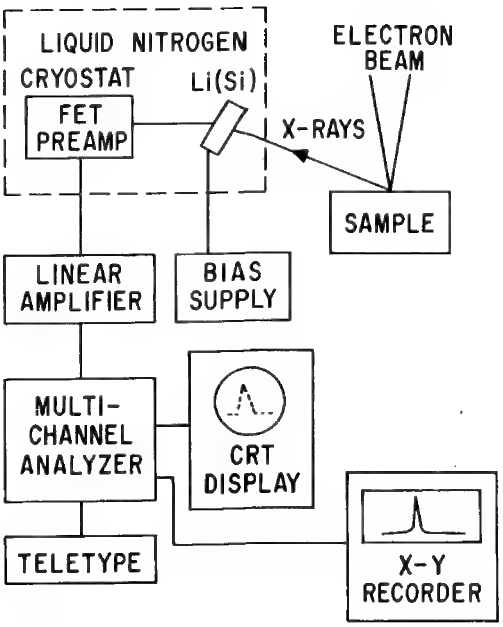

1. Schematic diagram of Li(Si) x-ray detector system

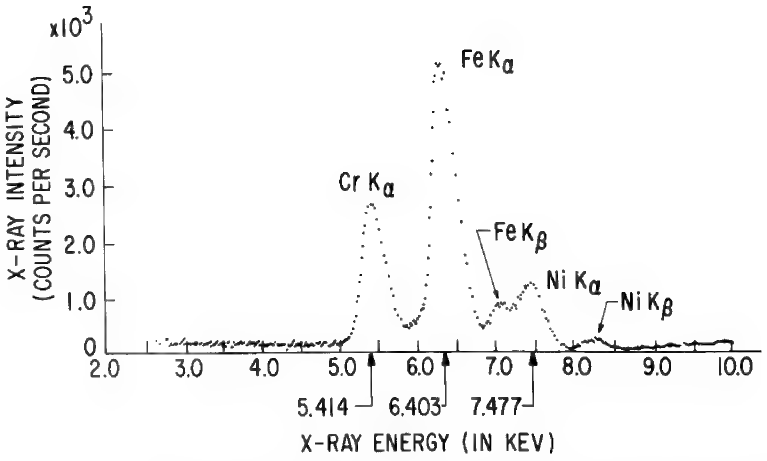

2. Spectrum obtained from Fe-20Cr-20Ni alloy

Table

SENSITIVITY OF Li(Si) DETECTOR

ATOMIC NUMBER	X-RAY LINE	ENERGY (KEV)	PEAK TO BACKGROUND RATIO	*INTEGRATED PEAK INTENSITY (C.P.S. / NANOAMP)
12	Mg Kα	1.254	15.0	157.4
13	Al Kα	1.487	31.0	287.2
14	Si Kα	1.740	39.3	379.6
22	Ti Kα	4.510	27.7	279.4
23	V Kα	4.952	25.8	243.2
24	Cr Kα	5.414	28.6	237.9
25	Mn Kα	5.898	26.6	218.2
26	Fe Kα	6.403	27.4	188.3
27	Co Kα	6.930	23.5	175.9
28	Ni Kα	7.477	25.4	162.5
29	Cu Kα	8.047	22.2	141.5
30	Zn Kα	8.636	19.2	107.2
32	Ge Kα	9.885	16.6	89.2
40	Zr Lα	2.042	15.3	204.2
42	Mo Lα	2.293	16.3	200.4
47	As Lα	2.984	15.2	225.8
50	Sn Lα	3.444	14.7	236.6
74	W Lα	8.396	5.0	165.4
82	Pb Mα	2.347	6.9	317.3
90	Th Mα	2.997	7.1	351.7

* TOTAL COUNTS CONTAINED WITHIN FWHM

1. X-ray detector sensitivity

QUALITATIVE AND SEMI-QUANTITATIVE ANALYSIS WITH NON-DISPERSIVE X-RAY DETECTORS

R. L. Myklebust and K. F. J. Heinrich

Spectrochemical Analysis Section
National Bureau of Standards
Washington, D. C.

Many problems in electron probe microanalysis can be solved with a series of qualitative or semi-quantitative analyses at various regions on a specimen. A complete wavelength scan with crystal spectrometers on an unknown specimen is time consuming, while sufficient information can frequently be obtained in a few minutes by non-dispersive analysis. A semi-quantitative determination of any element indicated in the spectrum can then be performed by comparing the peak height or the area beneath the peak in the specimen with that of a standard run under identical conditions.

Two detectors are used in our instrument to cover the x-ray spectrum. For radiation from 1 to 10 KeV, a lithium-drifted silicon detector with a 1/4 μ m beryllium window is employed. This covers the K-radiation of atomic numbers 12 to 32 and L-radiation of atomic numbers 30 to 83. A commercially available flow proportional detector with a thin nitrocellulose window is used for radiation from 0.16 to 1.5 KeV. This covers the K-radiation of atomic numbers 4 to 13 and L-radiation of atomic numbers 23 to 35, with no significant interference of M or higher lines. The spectra are sorted out into 800 channels of a multichannel analyzer and plotted with an X-Y recorder.

The success of the qualitative analysis scheme depends on selecting appropriate experimental conditions -- the detector bias, amplifier gains, pulse-shaping times, and multichannel analyzer settings -- and then maintaining them without change throughout the measurements. The peak positions of several standards are measured. From this information we derive the channel number for the peaks of all elements. These channel numbers do not shift for long periods unless the counting rate is too high: all measurements are therefore made with a dead time less than 20%. A major advantage of this technique is in the fact that the electron probe can be operated under the habitual excitation conditions of 20 KV and 30 μA target current. The time required to collect a spectrum showing the lines of the major and sub-major elements present is 1 to 2 minutes.

In our experiments, the peaks of adjacent elements in the iron group were not resolved since the peak width at half height of the silicon detector was 500 eV. Adjacent elements were detected, however, provided that their concentrations did not differ considerably. A typical series of qualitative analyses of a

steel sample (Fig. 1) shows iron in most areas, as well as manganese and sulfur in a sulfide inclusion, and the analysis of an oxidic area shows the presence of iron, silicon and manganese. An analog curve analyzer was a valuable asset in resolving overlapping peaks. (See Fig. 2)

Semi-quantitative analyses of four known gold-copper alloys were performed with the curve analyzer on non-dispersive spectra of the alloys. The area under the resolved peaks were compared to the area under the similarly resolved peaks of the standards. Table I lists the resulting k-values and the expected theoretical k-values along with the concentrations. For best accuracy, the concentrations can be calculated from the measured k-values.

Table I.

Semi-Quantitative Analysis of Au-Cu Alloys

Copper

C	$k_{calc.\ (K\alpha)}$	$k_{area\ (K\alpha+K\beta)}$	$k_{peak\ (K\alpha)}$
.80	.835	.83	.89
.60	.657	.65	.71
.40	.462	.43	.49
.20	.245	.22	.24

Gold

C	$k_{calc.\ (L\alpha)}$	$k_{area\ (L\alpha+L\beta)}$	$k_{peak\ (L\alpha)}$
.80	.748	.77	.70
.60	.528	.47	.44
.40	.333	.28	.23
.20	.158	.13	.10

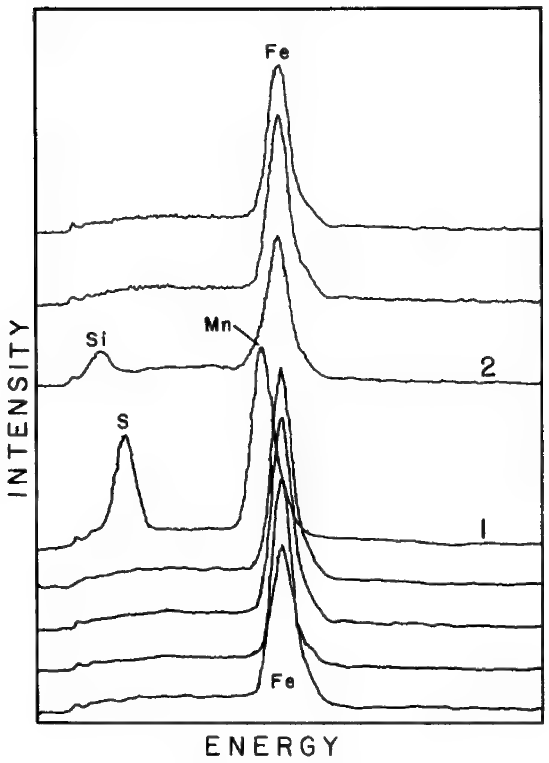

Figure 1. Qualitative analysis of steel. Spectrum 1 is of a manganese sulfide inclusion. Spectrum 2 was obtained from a slag inclusion containing silicon, iron and manganese.

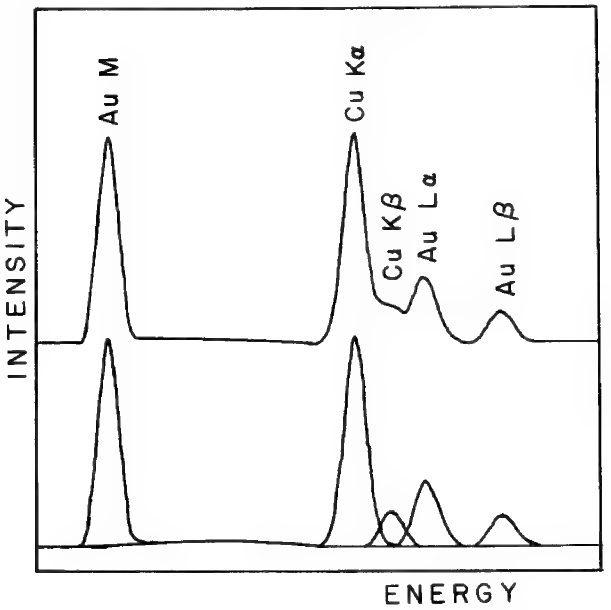

Figure 2. 40% Cu - 60% Au alloy. The upper spectrum is the original plot. The peaks are shown in the lower spectrum resolved by means of an analog spectrum analyzer.

SIMULTANEOUS MULTI-ELEMENT ANALYSIS WITH A SINGLE X-RAY SPECTROMETER

A. J. Saffir, R. E. Ogilvie and R. S. Harris

Massachusetts Institute of Technology
Cambridge, Massachusetts

In microprobe analysis one encounters the problem of spectral interference when two or more spectral lines are diffracted at the same 2θ angle. Both lines may have about the same wavelength, as do Cr Kα 2.291 Å and V Kβ 2.284 Å which can only be resolved by measuring other spectral lines. However, there is another kind of interference that results from multiple order diffraction interference that occurs when the wavelengths of two lines are not equal but are whole number multiples of each other. In this case the two spectral lines have vastly different energies. As an example, fluorine Kα, 18.31 Å, has approximately three times the wavelength of P Kα, 6.155 Å. A similar situation can result from the use of analyzing crystals composed of two diffracting media as for example in the analysis of carbon in steel with an LSD on mica crystal the 44.6 Å C Kα is diffracted at the same 2θ angle from the LSD as the fifth order of Fe Kβ, 1.756 Å, from mica. Therefore, trace analysis of carbon in iron containing alloys is very difficult with this crystal.

When sufficient dispersive resolution is impossible, reduction of the interfering signal is possible by simple pulse height analysis. For example, the first order F Kα 18.31Å is interfered with by third order P Kα 6.155Å. By careful use of a pulse height analyzer, 500 ppm of fluorine can be detected in the presence of the phosphorus of apatite, i.e., $Ca_5(PO_4)_3(OH,F)$.

This approach fails to resolve the important biological problem of measuring trace levels of fluorine in the presence of the high concentrations of phosphorus found in hard tissues, for two reasons: first, the low energy tail of the phosphorus energy distribution is large relative to the expected fluorine peak, and second, the amount of this phosphorus interference is dependent on the variable phosphorus concentration of the specimen. See Figure 1.

We have devised a new technique to overcome this problem. By means of the equipment illustrated in Figure 2, we adjust three single channel pulse height analyzers such that channel I receives the fluorine signal, and channel II receives the phosphorus signal and channel III receives the calcium signal. Since the phosphorus signal entering the fluorine channel is directly proportional to the signal measured in channel II, this interference can readily be evaluated and subtracted from the signal of channel II, giving the true fluorine signal.

The extent of the interference occuring in this particular example and the efficiency of this solution is demonstrated by the 2θ scan shown in Figure 3. This 2θ scan was obtained from fluor-apatite in the vicinity of the F Kα peak with three signal channel analyzers, one tuned to F Kα, the second to P Kα, and the third to Ca Kβ. Note the interference of first order F Kα, third order P Kα and sixth order Ca Kβ and the ability to measure three elements simultaneously from a single spectrometer.

This technique is also of great use for measuring the concentrations ratios of elements where accuracy is important. For example, in measuring the calcium:phosphorus ratio the spectrometer is tuned so that Ca Kβ second order peak overlaps P Kα first order peak to such a degree that both measured intensities are about equal at the levels expected in the sample.

Since both the Ca and P signal are attenuated by the same absorption path, the measured Ca:P ratio is not as critically affected by variable absorption paths as it would if it were measured by means of two spectrometers.

The use of this technique is illustrated by the Ca:P ratios and fluorine concentrations shown in figure three. Here the fluorine detectability limit is 100 ppm for a given point and 30 ppm for the average of twenty measurements made in the bulk of the enamel of this specimen.

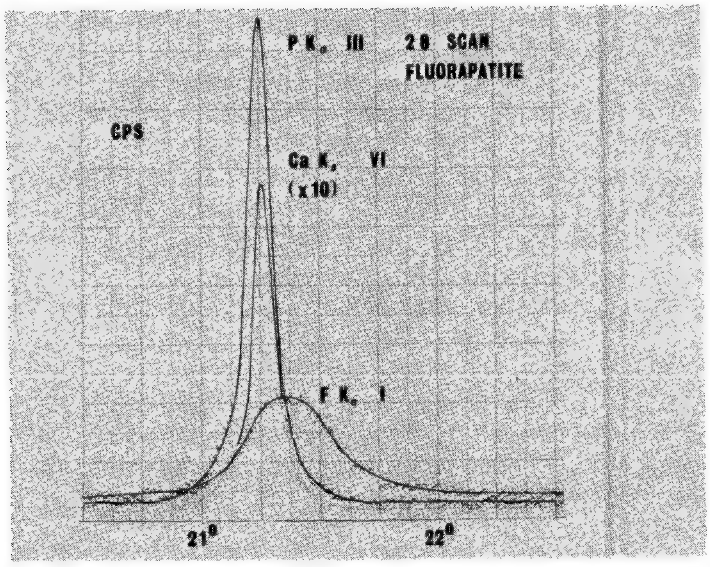

fig. 1. The pulse height distribution observed with a spectrometer tuned to the optimal position for the measurement of fluorine in apatite. A representation of the phosphorus interference is indicated.

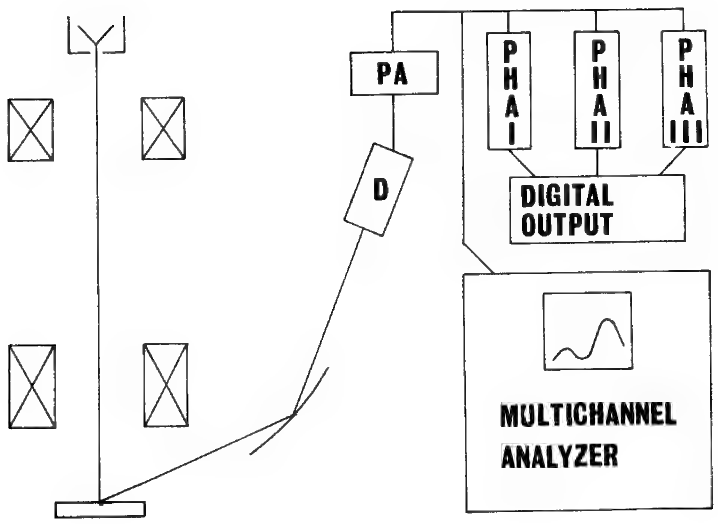

fig. 2. The aparatus to resolve multiple order interference consisting of three single channel pulse height analyzers and a multi-channel pulse height analyzer.

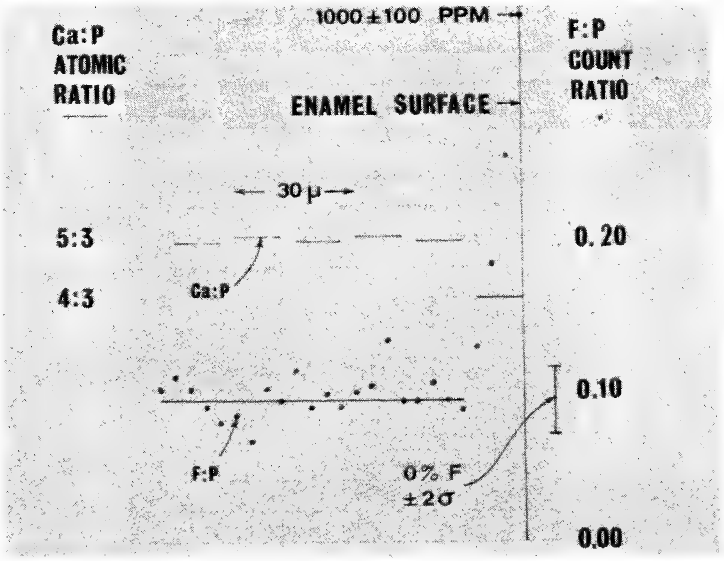

fig. 3. 2 θ scan of fluorapatite in the region of the F K_{α} peak showing that three spectral lines overlap by multiple order interference.

SELECTION OF OPTIMUM PULSE HEIGHT ANALYSIS WINDOW

L. V. Sutfin, R. E. Ogilvie and R. S. Harris

Massachusetts Institute of Technology
Cambridge, Massachusetts

The setting of a pulse height analyzer is a factor in optimizing detectability in electron microprobe analysis. With a single channel analyzer the proper window width and base line must be chosen. Similarly, with a multichannel analyzer, the channels over which one integrates to accumulate a signal must be selected.

A common feature of expressions for detectability limit published by several authors [1,2,3,4] is that

$$C_{DL} \sim \sqrt{B/I_o^2}$$

where C_{DL} is the minimum detectable concentration, B is the background, and I_o is the signal corrected for background, i.e. total counts minus background. Since a minimum value of C_{DL} is sought, all other things being held constant, a maximum value of I_o^2/B will produce the desired conditions.

Therefore it is necessary to know the shape of the pulse height distribution curve when either a single channel analyzer or a multi-channel analyzer is used. Regardless of whether one is using a crystal spectrometer, or is doing non-dispersive analysis, a proper window width can improve performance if used judiciously.

With these points in mind we have set out to develop methods whereby a proper window may be selected once the distribution of signal and noise are known.

One such method is an empirical technique in which the peak is first centered in a narrow window and then readings are taken at increasing window widths (still centered on the peak) for both a standard and a suitable background sample. A plot of I_o^2/B against window width will demonstrate a maximum at the optimum window setting. For simplicity this requires that both the characteristic and background distributions be symmetrical.

Expressions which can be used to find the optimum window have been derived for the distribution of characteristic pulses on a background which is constant over the range in question, i.e. a rectangular distribution, or for a distribution

on a uniformly increasing background, i.e. a ramp function. Using the condition that at the optimum setting a change in window width, X, produces no change in I_o^2/B, equations for the optimum window width have been derived.

For a constant background the equation is:

$$X_{opt} = \frac{\int_o^{X_{opt}} f(x)dx}{2y}$$

where X_{opt} is the window width on one side of the mode of the distribution, the integral is the area under the signal distribution curve, and y is the ordinate from the background to the signal distribution curve at X_{opt}. For a uniformly increasing background the equation is:

$$\frac{1}{X_{opt}} + \frac{1}{h/\tan\alpha - X_{opt}/2} = \frac{2y}{\int_o^{X_{opt}} f(x)dx}$$

The symbols are the same as for the previous equation, with h being the height of the background at the mode and $\tan\alpha$ the slope of the background curve. It can be seen that when $\tan\alpha$ becomes zero the latter expression reduces to that for a uniform background. Therefore this expression is general.

From an experimental pulse height distribution curve h and α can be measured and a value of X_{opt} selected which makes the right hand and left hand sides of the equation equal. Thus the optimum window can be selected by a graphical technique if the pulse height distribution is known, and a means of readily determining the area is at hand. If the curves are unsymmetrical a "right hand" window and "left hand" window can be determined independently. Therefore symmetry of the distribution is not required.

It should be noted that the optimum window will be the same regardless of the peak to background ratio if the distributions have the same dispersion. This is quite obvious in the expression for the rectangular background where no factors related to background appear. In the situation where the background is linearly increasing, for a given h and α, which should remain constant if the proper background standard is chosen, X_{opt} does not depend on the maximum value of y if y/A remains constant as Y_{max} varies. This means that a window setting determined at a higher count rate will hold at a lower count rate. However, the peak position must remain fixed or the window must be shifted accordingly.

For a Gaussian pulse height distribution of characteristic energy and a rectangular background distribution the equation predicts that the optimum

window is ± 1.4σ or approximately 1.2 times the full width at half maximum. An experimental determination done as described earlier with Cu$K\alpha$ being the characteristic line and the background determined on zinc, yielded an optimum window which was 1.23 times FWHM of the pulse height distribution curve for Cu$K\alpha$.

It can be seen from the graph of I_o^2/B vs. window width, that a wider window is a better choice than one which is narrower than the optimum. Therefore one might purposely choose a wider window to reduce the dependence on system stability.

The equations developed provide functional relationships not previously available which can be used for the setting of single channel pulse height analyzers and for region of interest selection of multichannel analyzers.

---

1. Theisen, R., Quantitative Electron Microscope Analysis, Springer-Verlag, Inc., New York, 1965.

2. Ziebold, T. O., Anal. Chem., 39, 858 (1967).

3. Andersen, C. A. in Methods of Biochemical Analysis V. 15, Glick D. ed. Interscience 1967.

4. de Ben, H. S., Paper #2, Third National Conference on Electron Microprobe Analysis, 1968.

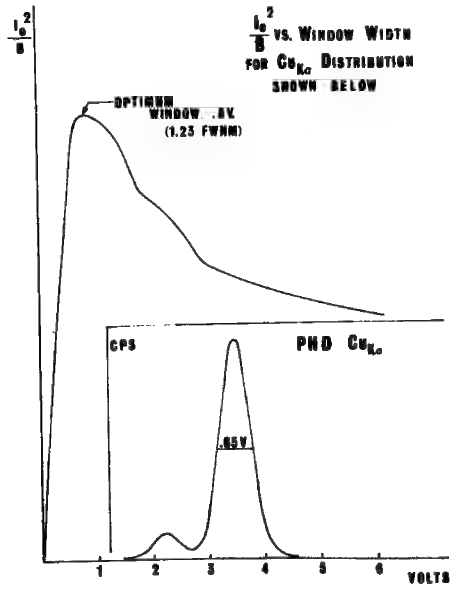

Figure 1.

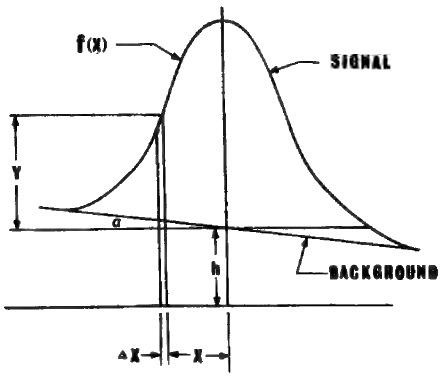

Figure 2.

CHARACTERISTICS OF MULTILAYER SOAP FILMS DEPENDING ON THE NUMBER OF LAYERS

S. Kimoto, H. Hashimoto and I. Ando

Japan Electron Optics Lab. Co., Ltd.
Tokyo, Japan

In soft X-ray analysis, the intensity and the full width half maximum of a spectrum peak depend on the number of the deposited layers of a multilayer soap film which is used as a dispersive element. [1] This relation seems to be more obvious in the case of longer wave length X-rays and the multilayer soap films with larger 2d-spacing.

This paper treats the characteristics of stearate, lignocerate, cerotate and melissate for carbon, boron and beryllium k-radiation analysis. The multilayer soap films are deposited upon mica bases by Langmuir-Blodgett technique. [2] As lignocerate, cerotate and melissate can hardly be deposited directly on mica bases, a few layers of stearate are placed upon the mica bases before the deposition of foresaid soap layers. The double monolayers excluding the predeposited stearate layers are counted.

1) Spectrum shape: When the number of the layers is small, anomalous peaks like satellites are observed. A lignocerate with 10 layers gives such anomalous peaks of beryllium k-radiation and a lignocerate with 10 to 30 layers gives those of boron or carbon k-radiation. Figure 1 shows the variation of the shape in accordance with an increase of the layers. The heights of these anomalous peak decrease with an increase in the number of layers.

2) The full width half maximum: The full width half maximum of the spectrum of a film composed of a few layers is found larger than that of a film composed of more layers. As shown in figure 2, the width is constant when a film is composed of 40 layers or more.

3) Peak intensity: As shown in figure 3 the peak intensity is maximum when a film is composed of a certain number of layers. The optimum number of layers is small if the wave length of X-rays is long.

4) Peak-to-background ratio: The P/B ratio also depends on the number of layers. The P/B ratio of beryllium k-radiation spectrum is maximum in the case of a lignocerate film of nearly 50 layers. However, in the case of boron and carbon, the P/B ratio increases with the increase of the layers up to 100. In practice, the value of B/ (P-B) indicates the efficiency of the analyzing crystal. Figure 4 shows series of these values as functions of the numbers of lignocerate layers.

These results show that a few layers nearest to the mica base are not adequate in its spacing and next 20 to 50 layers are desirable. However in the case of longer wavelength X-rays such as beryllium k-radiation, a lignocerate with 40 layers gives the optimum characteristics.

---

1. R. C. Ehlert, Advances in X-ray Analysis, 8, 328 (1965).

R. C. Ehlert and R. A. Mattson, ibid, 10, 392 (1968).

2. K. B. Blodgett, J. Amer. Chem. Soc., 57, 1007 (1935).

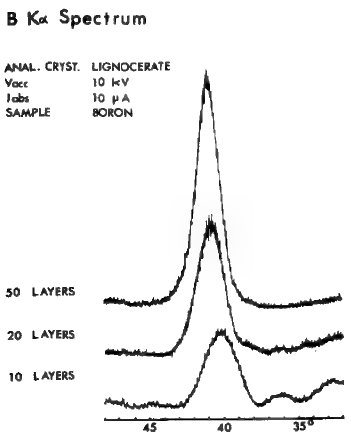

Fig.1

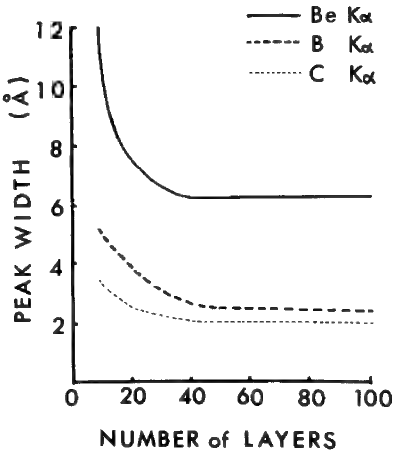

Fig. 2

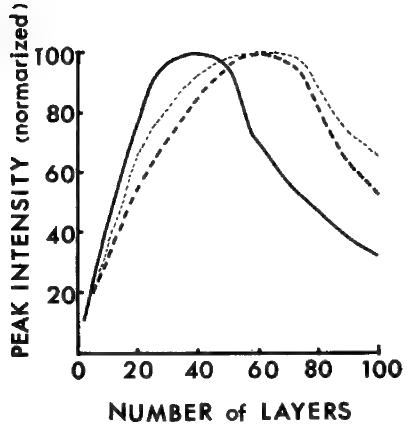

Fig. 3

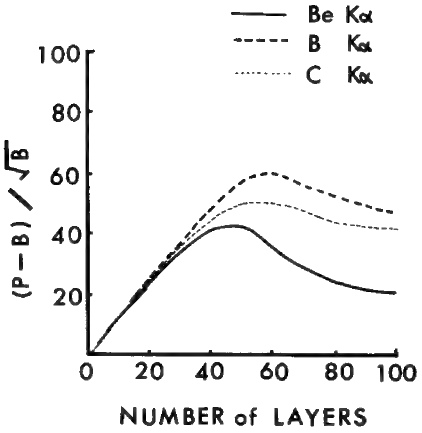

Fig. 4

SMALL ANGLE X-RAY REFLECTION

L. Marton

National Bureau of Standards
Washington, D.C.

Many measurements have been made in the last 40 years on the reflection of X-rays by different substances at varying small angles. The usual presentation of the data is either tabular, or graphical, with angle and reflectivity as ordinates, and the wavelength as variable. A survey of the literature [1] shows that it is possible to establish an empirical relationship of the following form:

$$\frac{1}{R} - 1 = \frac{\theta^{3/2}}{\text{const}\,\lambda} \qquad (1)$$

where R is the reflectivity ($0 < R = \frac{I}{I_0} < 1$), θ is the grazing angle and λ the wavelength of the radiation.

This relationship has been tested first on gold. When plotting the wavelength vs angle on a log-log scale, for constant reflectivity, the empirical law appears to be valid over more than two orders of magnitude of the wavelength, ($0.7\text{Å} < \lambda < 190\text{Å}$) (Fig. 1). The scatter of the experimental data is of the order of ± 35%, which is surprisingly low in view of the fact that the data were taken from publications ranging over the last 40 years. Many of the reflecting surfaces are badly characterized and their methods of preparation must have varied. In considering the inevitable variations of this kind the conclusion is inescapable that the three-half power law must have a sound physical background, in spite of the apparent conflict with earlier theories based on macroscopic ray optics. These earlier theories predict a dependence of the reflectivity proportional to the angle squared.

If λ is expressed in cm and the angle θ in radians, the value of the constant in Equ. 1. for gold is approximately 5.4×10^4 cm^{-1}.

Next the reflectivity of other substances has been examined. Experimental data are rather scarce, but Ni appeared to be a useful substance to test the validity of Equ. 1. At first sight there seemed to be much more scatter of the data and averaging them seemed to lead to a different power law. Closer examination of the data proved, however, that within limited wavelength regions the three-half power law applied quite well (Fig. 2) and that the break between adjacent regions occurred where the absorption edges lie for

Ni. Apparently the reflection coefficient depends only on the number of electrons per atom participating in the reflection process. If the incoming radiation is hard enough to penetrate, let us say, the L-shell, only the K-electrons will contribute to the reflection process; if it is softer, a greater number of electrons in the outer shells will participate.

Further comparison of the experimental data on Al and Pt seems to confirm the qualitative validity of the views expressed above. A really quantitative comparison is difficult because of the lack of consistent data in the literature and the experimental difficulties in measuring these small angles with the required accuracy. The empirical relationship described here points, however, to the need for a much closer examination of the reflectivities of X-rays on well defined surfaces.

Even more is to be done on the theoretical side. At present the reasons for this power law are obscure and no explanation has been offered for its existence, or for the failure of earlier theories.

---

1) A few representative papers are:

O. A. Ershov, I. A. Brytov and A. P. Lukirskii, Optics and Spectroscopy, 22, 66 (1967).

L. M. Rieser, Jr., in X-ray Microscopy and Microradiography, Cambridge 1956, Academic Press, N. Y., 1957.

J. P. Sauro, I. Fankuchen and N. Wainfan, Phys. Rev. 132, 1544 (1963)

and many others.

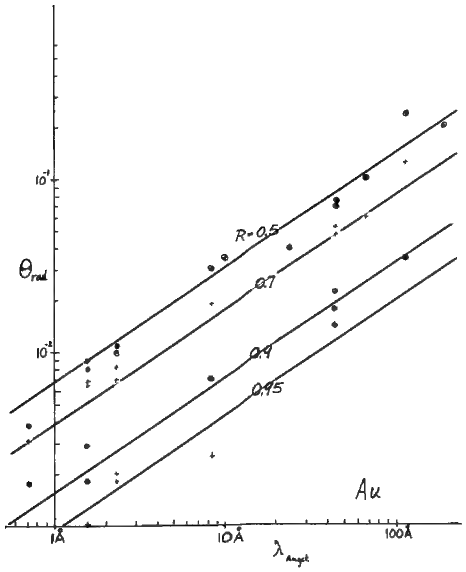

Figure 1

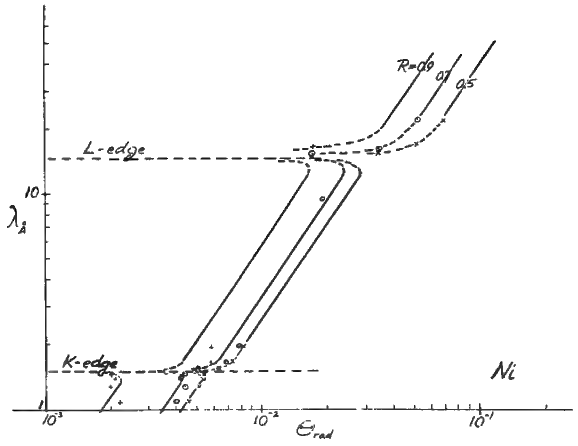

Figure 2

A GEOMETRIC METHOD FOR THE LOCATION OF THE CENTER OF KOSSEL PATTERNS

W. D. Donnelly

Materials Analysis Company
Palo Alto, California

Kossel pattern techniques have been highly developed in recent years. Much of this development may be attributed to the ability of the electron microprobe analyzer to provide a small point source of x-ray radiation. Analytical methods for determination of high precision lattice parameters and crystal orientations from Kossel patterns may be found in the literature (1,2). For the highest accuracy in lattice parameter determination, Gielen (1) has pointed out the necessity of a precise knowledge of the location of the center of the Kossel pattern for cubic crystals. Extension of the Kossel technique to less symmetric crystals has been carried out by Morris (2), where again the importance of knowing the pattern center is pointed out.

A method for precise pattern center location has been described by Vieth (3) where the crystal specimen is replaced by a small aperture where the beam strikes the sample, allowing the light from the filament of the electron gun to expose a spot on the film that locates the center of the Kossel pattern. This method of center location works only for the case where the film is normal to the electron beam. It should also be noted that in a typical case where a film to specimen distance of 10 centimeters is used and if the film is 0.1 degrees from being normal to the electron beam axis, the marked spot will be 175 microns from the true pattern center.

A method for accurate location of the center of a Kossel pattern is described below. The method described is dependent only on the two dimensional geometry of the Kossel pattern.

When a focused electron beam strikes a small crystalline sample a point source of x-rays are created. The source of radiation contains characteristic lines that diffract to form a family of conics in space, all having a common apex. When a plane of film intersects several radiation conics a Kossel pattern is formed. Since the lines observed in the Kossel pattern are the intersection of a plane and a cone, then these lines are conic sections. Also due to the nature of the family of cones causing the conic sections, the geometrical axes of the two dimensional conic sections in the Kossel pattern must all intersect at the point on the pattern that is closest to the radiation source, i.e. the center of the Kossel pattern.

Experimentally the centers of Kossel patterns have been determined in the following manner: 1) A Kossel pattern is projected on an optical comparator and ten points are measured along each of four different lines; 2) The measured data is put in a computer program that does a least-squares fit to determine the quadratic coefficients of each line measured; 3) The second part of the computer program uses the calculated coefficients to find the axis of each line and 4) A least-squares fit is found for the intersection of the several axes, i.e. the center of the pattern. Once the center of the pattern is established the methods previously mentioned (1,2) are used to calculate lattice parameters and orientation information.

Kossel patterns of Ge, Cu and TiO_2 (rutile) have been analyzed, using the method described to locate the center of the patterns with a precision of ±5 microns. The method has been used to establish sub-grain orientation differences in a 50-50, Fe-Ni alloy.

It should be noted that the method described above determines the center of a Kossel pattern independently of the film to specimen distance, the crystal used to form the pattern, the radiation used to form the pattern and the relationship between the electron beam and the film plane. In fact the only information necessary is that the pattern is a Kossel pattern and was formed on a plane film.

---

1. P. Gielen, H. Yakowitz, D. Ganon and R. E. Ogilvie, J. App. Phys., 36 (1965) 773-782.

2. W. G. Morris, J. App. Phys., 39 (1968) 1813-1823.

3. D. L. Vieth and H. Yakowitz, Rev. Sci. Inst., 37 (1966) 206-209.

THE SCANNING ELECTRON MICROSCOPY OF PERIODIC ULTRASONIC FIELDS

R. S. Gvosdover, G. V. Spivak, A. E. Lukianov,
M. V. Bicov and G. V. Saparin

University, Moscow V-234, USSR

It is well known that scanning electron microscopy may be used for observation of electric fields on the solid's surfaces (1,2).

The piezoelectric fields which appear when the ultrasonic wave propagates along the piezoelectric crystals were investigated in our laboratory. The instrument was "Stereoscan" and we used the conventional and stroboscopic regimes of operation.

The specimens were the crystals of quartz and lithium niobate, rendered conducting by the evaporation of a thin layer of Ge. The ultrasonic wave was excited by a quartz of Y-cut with the resonant frequency about 5 MHz. In the case of lithium niobate the sound was excited with the help of two copper electrodes which were applied to the opposite sides of the crystal. The frequency range was 3 - 10 MHz.

The sinewave voltage was applied simultaneously to the vibrator and the input of generator of short (10 - 20 nsec) strob-pulses. The electron beam was deflected from the aperture by the dc voltage on a pair of deflection plates. Then the strob-pulses set back the beam to the optical axis of the microscope.

The change of the delay of strob-pulses with respect to zero (or maximum) of sinewave voltage allowed to observe different phases of propagation of ultrasonic wave along the crystal.

The deformations due to the acoustic wave in piezoelectric crystal produce the electric field. The value of this field may be obtained by the measurement of the image contrast and the displacement of the electron trajectories (3).

Fig. 1 and 2 illustrate some of the images obtained.

---

1. T. E. Everhart, O. C. Wells, W. C. Oatley: J. Electronics and Control, 1959, 7, 97.

2. G. Saparin, G. Spivak, S. Stepanov: Proceed. 6-th ICEM, Kyoto, 1966, p. 609.

3. N. N. Sedov, G. V. Spivak, G. V. Saparin, V. G. Galstjan: Radiotech. i Electr., 1968, 13, 2278.

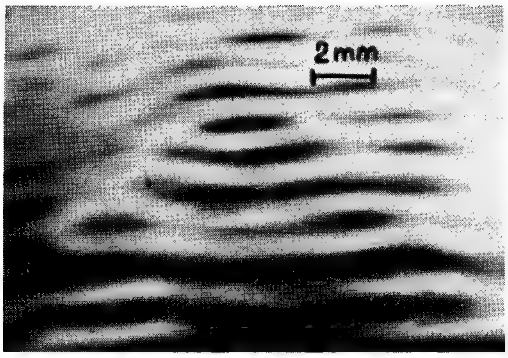

Fig. 1. The image of standing wave field in nonuniform quartz obtained in the conventional scanning electron microscope
(f = 5 MHZ)

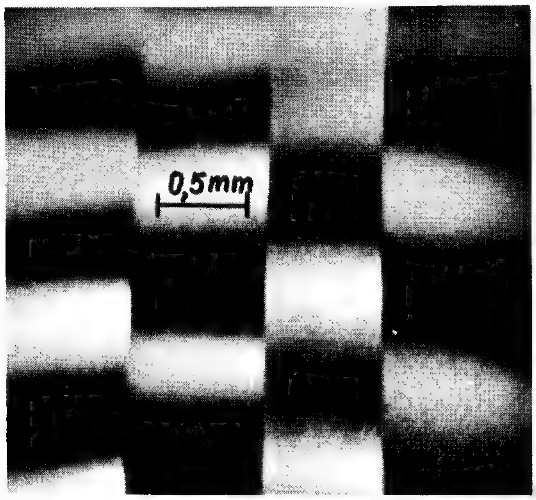

Fig. 2. The stroboscopic micrographs of the same field observed with different time delays τ (τ = 0; 0,1; 0,2; 0,3 μsec.).

SCANNING ELECTRON MICROSCOPY OF CRYSTALLOGRAPHIC DEFECTS IN SILICON *

E. K. Brandis and G. H. Schwuttke

IBM, East Fishkill Laboratories
Hopewell Junction, New York

Scanning electron microscope (SEM) observation of crystallographic defects in single crystals exploits the conductive mode of operation of the instrument. The use of the SEM to observe crystallographic defects was first reported by Lander, et al. (1) in 1963. Czaja and Wheatley (2) extended this work in 1964 and 1965. The original papers are impressive and optimistic about the future role of the SEM in the observation of crystal defects. The SEM was supposed to become the bridge between x-ray topography and transmission electron microscopy. Obviously, the SEM has not lived up to the original expectation. The question is why?

To answer this question, it is discussed how defects are actually revealed through scanning electron microscopy, and the necessary conditions for the observation of crystallographic defects in crystals through scanning electron microscopy are established.

Specific examples are presented illustrating how differently defects can influence the charge collection process. Defects in silicon are first identified through x-ray diffraction topography and then correlated with the corresponding SEM measurement. The examples presented include: diffusion-induced dislocations, process-induced dislocations and precipitation effects in silicon.

---

1. J. J. Lander, H. Schreiber, Jr., T. M. Buck, and J. R. Mathews, Appl. Phys. Letters, 3, 206 (1963).

2. W. Czaja and G. H. Wheatley, J. Appl. Phys. 35, 2782 (1964), J. Appl. Phys. 36, 1476 (1965).

* Supported in part under Contract No. AF19(628)-68-C-0196, Air Force Cambridge Research Laboratories, Bedford, Massachusetts, U.S.A.

SPECIMEN HEATING DEVICE FOR SCANNING ELECTRON MICROSCOPE

S. Kimoto, H. Hashimoto, T. Kosuge and A. Mogami

Japan Electron Optics Lab. Co., Ltd.
Tokyo, Japan

A specimen heating device has been developed for a scanning electron microscope. A similar device is used in an electron probe microanalyzer.[1] However, there are two problems in using this specimen heating device in the scanning electron microscope. It should be considered how to separate thermal electrons from secondary electrons to obtain a good quality secondary electron image. Another problem is due to the fact that the secondary electron detector is also sensitive to the light which is emitted from the specimen and the furnace at high temperature. The detector should be protected against this light.

Figure 1 shows a schematic diagram of this device. The temperature of the specimen can be changed from room temperature to 1,100°C. In order to separate the thermal electrons from secondary electrons, a nickel grid is used which is supplied with a retarding potential. The scintillator and the light pipe are housed in a metal cylinder which shields the light. The front face of the scintillator is coated with a thin aluminum film of 1,500Å.

Figure 2 shows the energy distribution of the thermal electrons and that of secondary electrons with thermal ones at 820°C. Thermal electrons have lower energy than secondary electrons. As shown in this figure, thermal electrons are completely suppressed when the grid potential is below minus 5 volts. Some of the secondary electrons are also suppressed under this condition. However, the remaining secondary electrons are enough to make a good quality image.

Figure 3 shows the image of a tip of thermocouple at room temperature and 1,065°C. The quality of the image at high temperature is the same as that at room temperature. Figure 4 shows the change of a pearlite structure of a 0.4% carbon steel at a temperature of approximately 720°C.

With this method, the observation of the specimen has become possible under high temperature without disturbance of thermal electrons. Ths installation of this specimen heating device in a TV scanning electron microscope enables a rapid dynamic transformation of a specimen due to temperature variation also to be observed.

---

1. S. Kimoto, H. Hashimoto and K. Tada, 2nd. Natl. Conf. on Electron Microprobe Analysis, 59 (1967).

FIG. 1

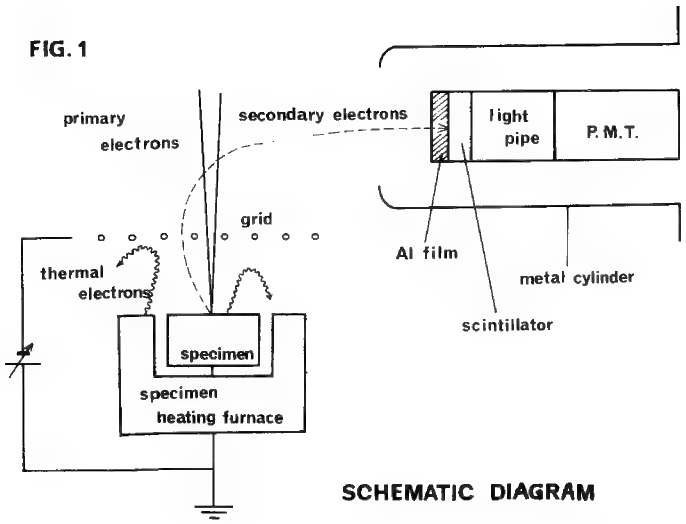

SCHEMATIC DIAGRAM

FIG. 2

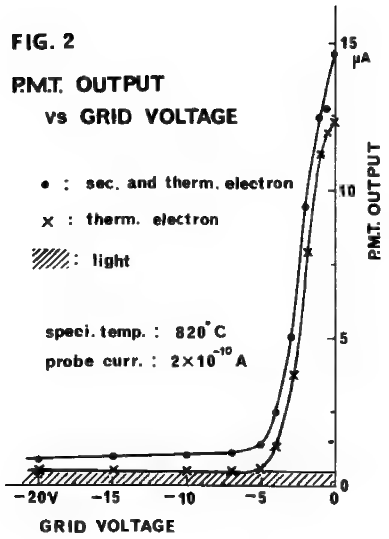

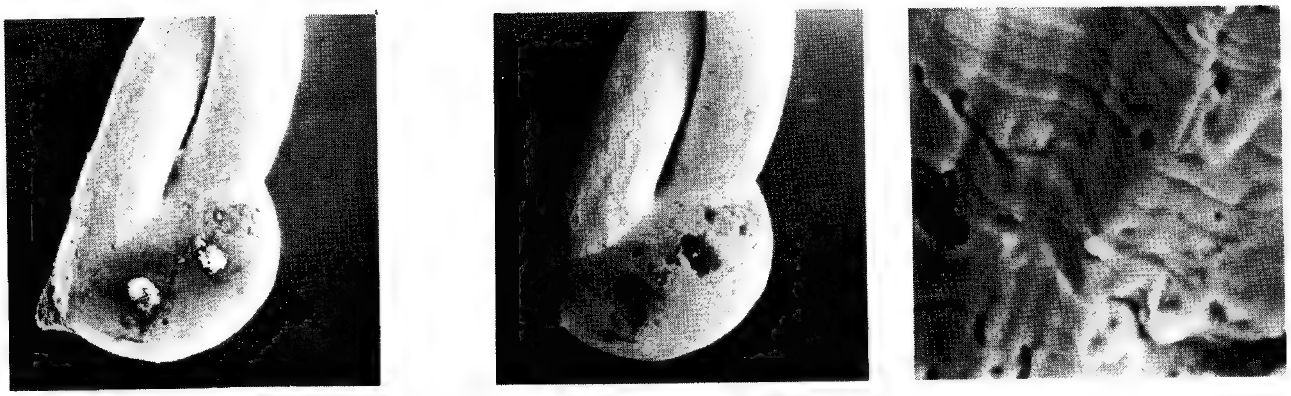

FIG. 3

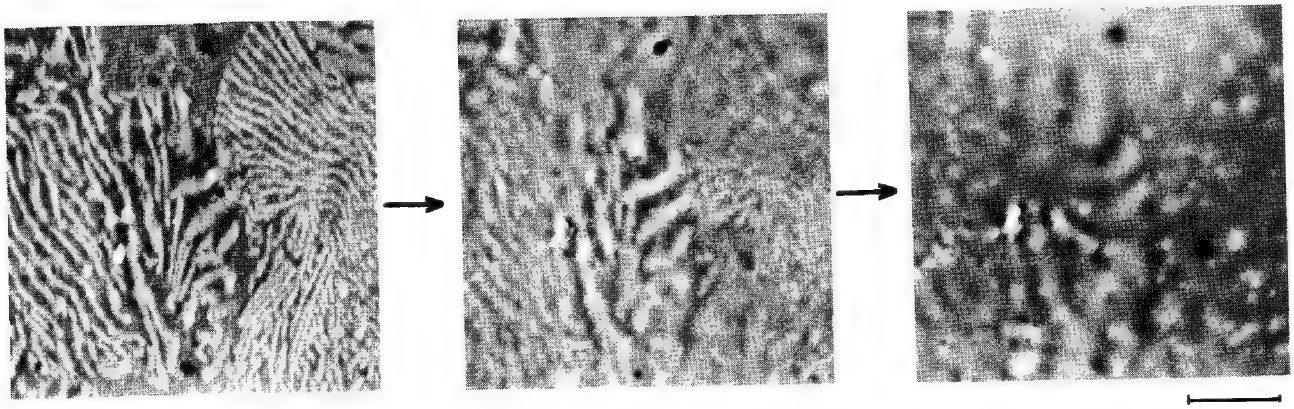

FIG. 4

COMPUTER CONTROLLED SCANNING ELECTRON MICROSCOPE

D. Yankovich, R. E. Ogilvie, R. E. Warren

Massachusetts Institute of Technology
Cambridge, Massachusetts

and

P. C. Reist

Harvard University
Boston, Massachusetts

INTRODUCTION

In 1927, a German, H. Stintzing[1] received a patent for a "Method and Device for Automatically Assessing, Measuring and Counting Particles of any Type, Shape and Size." Stintzing said that "according to the invention the individual particles are assessed by directing onto them an energy impulse in the form of waves of rays or corpuscular radiation in beams smaller than the size of the individual particles. The attenuation or deflection of the beam is then recorded by devices responding to the energy impulses."

In this paper we shall describe the use of a computer controlled scanning electron microscope which fulfills the claims and extends the concepts of the Stintzing patent.

PROCEDURE

This investigation has been directed toward the development of a completely automatic system that will rapidly count, size and classify particles whose dimensions may be as small as 0.1 micron at speeds of 1000 per minute or better. The inherent advantage of using the computer to control the microscope rather than recording data open-loop on tape is that the computer can adapt to the developing image which it sees and adjust its action accordingly.

No available single computer appears to be equally suited for image analysis as well as microscope control. A concept was therefore adapted to use two relatively inexpensive computers sharing a common memory. The larger computer will be a general purpose computer used for image analysis and a special purpose computer is being designed for microscope control. A block diagram is shown in Fig. 1.

Signal processing and pattern recognition techniques are being tested using conventional photomicrographs, some of which were reduced to digital signal by Dr. G. A. Moore of NBS and numerically reduced on an IBM 360 model 75 computer. The pattern recognition problem was divided into image parametization and object classification. Image parametization is being investigated by two accurate techniques prior to attempting rapid, more advanced methods. One of these methods requires storage of only two scan lines of picture information and the substitution of a new line each time a line of data is processed. The second method is an edge following technique which employs a counterclockwise interrogating rotation about each boundary point until a new boundary point is found. This method also requires only small computer memory. Either method allowed object parameter computation with relative ease.

Object classification is being developed using non-linear hyperplane decision surfaces. This technique allows for the classification process by differentiating between the complex pattern presented in a tabulation of object parameters.

Figure 2 shows a typical picture of aerosol particles. This picture was reduced to the parameters and classifications shown in Table I. Since no training samples for overlaps were presented, the doublet was not recognized. Further training rectified this and permitted recognition.

CONCLUSION

The results of our investigation indicate that a completely automatic computer controlled microscope can be built that will provide a tool for high speed particle counting, sizing and classification.

ACKNOWLEDGMENT

The authors wish to express their appreciation to the National Air Pollution Control Administration, Consumer Protection and Environmental Health Service, Public Health Service for the support of this work under grant numbers 3 ROI AP 00859-01 and 3 ROI AP 00860-01.

Grateful acknowledgment is also expressed to our associates on this project at the MIT Instrumentation Laboratory; Dr. J. H. Laning, J. D. Coccoli and P. D. Wolfe.

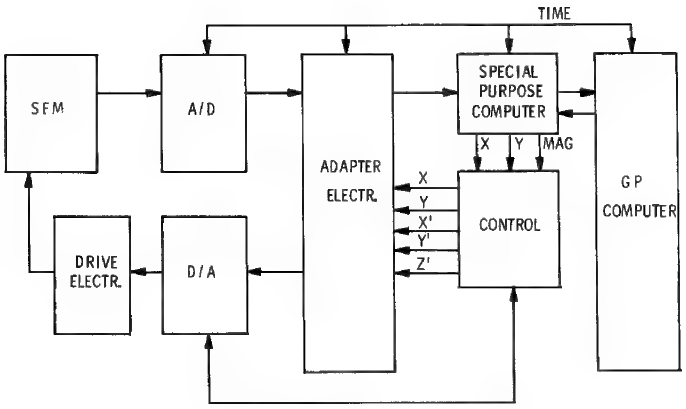

Fig. 1 System block diagram.

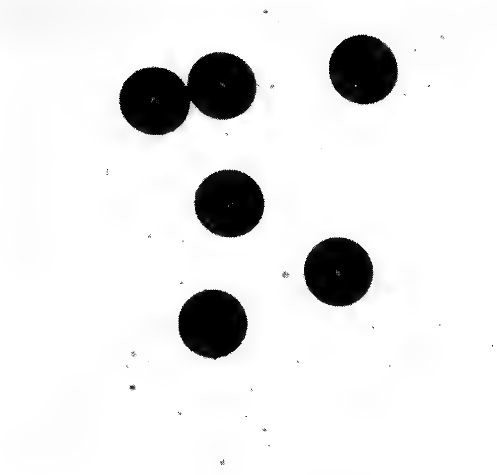

FIG. 2 TYPICAL TEST PHOTOMICROGRAPH

TABLE 1

Particle Parametization and Classification Program Results

Particle Class 1 = Single polystyrene sphere
= Two overlapping P.S. spheres
= Noise and debris

Particle Number	Area	Perimeter	Perimeter	Horiz.	Vert.	Particle Class	Computer Identification
1	11587	518	373	123	119	1	Decision: 1
2	00031	028	019	005	008	3	Decision: 3
3	00013	018	010	004	005	3	Decision: 3
4	11239	486	334	119	120	1	Decision: 1
5	10874	474	335	118	117	1	Decision: 1
6	00001	004	001	001	001	3	Decision: 3
7	00071	046	032	008	015	3	Decision: 3
8	11249	496	353	122	118	1	Decision: 1
9	00037	036	022	009	009	3	Decision: 3
10	00012	016	010	004	004	3	Decision: 3
11	00004	010	004	002	003	3	Decision: 3
12	22079	852	616	211	184	2	No Decision: 1

THE APPLICATION OF SOME NEW INSTRUMENTAL TECHNIQUES TO ELECTRON MICROPROBE ANALYSIS AND SCANNING ELECTRON MICROSCOPY

J. P. Smith and L. R. Reid

Texas Instruments Incorporated
Dallas, Texas

The electron microprobe analyzer derives great versatility from the availability of a variety of signal processing and display techniques. In the present work some new techniques for processing x-ray, secondary electron, and cathodoluminescence data have been developed. These methods can extend the sensitivity of the instrument and aid in the interpretation of the signal displays.

Photomultipliers are used in these instruments to detect the cathodoluminescence radiation excited by the primary beam or excited by secondary electrons accelerated to a scintillation phosphor. Usually these photomultiplier outputs are amplified and displayed on a CRT Z axis or integrated and recorded as a dc signal. If the radiation source can be periodically interrupted, a lock-in amplifier can be used to greatly increase the signal-to-noise ratio, however the response time is too slow for rapid displays. Digital processing of photomultiplier output pulses has the advantage of fast response times and a signal-to-noise ratio equivalent to the lock-in amplifier method (1-5). The output of a photomultiplier can be made compatible with the x-ray pulse processing and readout available on the microprobe by using a PM/x-ray compatibility interface. An x-ray channel can be selected for use as a photomultiplier channel, allowing us to record cathodoluminescence or secondary electron data at very low signal levels and with the same versatility available for x-ray readout.

The sensitivity of the secondary electron signals from a scanning electron microscope can be improved by the use of a lock-in amplifier. The periodic signal can be achieved by pulsing the electron gun or by biasing the sample with a periodic voltage (6). We have obtained a periodic signal by pulsing the high voltage on the scintillator phosphor. A synchronous high voltage modulator discriminates the secondary and backscatter electrons and greatly improves signal to noise ratios. A transistor multivibrator generates a variable frequency square wave which drives a "hard tube" modulator capable of delivering a 0-10KV output. The frequency can be varied from 30-600 Hz and a sync output is provided to trigger an oscilloscope and/or lock-in amplifier. Secondary electron signals can be readily recorded using primary beam currents in the 10^{-11} amp range. This method has been used to make quantitative measurements of the effects of sample bias and surrounding fields.

The study of active semiconductor devices in the scanning electron microscope has become a useful technique. The interpretation of the results usually involves a comparison of a photo made with the bias on, to one made with the bias off. If the bias is pulsed on and off while the scope raster displays a pattern, then this comparison can be made on one picture as shown in Figure 1. Normally one would compare the contrast exhibited by the transistor under no bias (1a) to that exhibited when bias is applied (1b). Since the secondary emission from the entire sample is altered when a part is biased and the experimental conditions might change between pictures, this direct comparison is difficult. In figure 1c the on and off condition is shown simultaneously, yielding much more information. This type of display is easily accomplished with a variable frequency square wave generator which can produce selected positive or negative voltages and can provide the current required by the device under study.

The technique of "pulse rate analysis" discriminates pulses on the basis of how soon they occur after the preceeding pulse. Coincidence counting is a special case of pulse rate analysis. Figure 2 illustrates the improvement in x-ray distribution displays which can be realized by pulse rate analysis. There are several possible methods for obtaining pulse rate analysis. We split incoming pulses into two channels. One channel goes into a variable delay and into a gated amplifier. The other goes directly to the gated amplifier. This unit, which we call a "background eliminator," passes only those pulses which occur within a certain time interval following the preceeding pulse. Thus, when the mean count rate is low, a smaller percentage of the pulses are passes than when the count rate is high. The random nature of the x-ray pulses insures that there will always be some pulses which occur within the preset time interval, therefore the background will not be completely eliminated. For the same reason very high count regions will also lose some intensity. The method of count rate analysis has great potential for pulse signal enhancement where a large difference between two signals must be observed.

ACKNOWLEDGMENTS

The authors are grateful to Ralph Tenny and Herb Bonner for contributions and assistance in building parts of the equipment.

---

1. E. H. Eberhardt, IEEE Transactions on Nuclear Science, 11, 48 (1964).

2. D. F. Kyser, J. McCoy, and D. B. Wittry, Second National Conference on Electron Microprobe Analysis, Boston (1967).

3. H. Strack and J. P. Smith, Electrochem. Soc. Meeting, Chicago (1967).

4. M. L. Franklin, Gary Horlick, and H. V. Malmstadt, Anal. Chem. 41, 2 (1969).

5. L. R. Reid and J. P. Smith, Rev. Sci. Inst. 40, 316 (1969).

6. G. A. Saparin, G. V. Spivak, and S. S. Stepanov, Proc. 6th International Congr. Electron Microscopy, pp. 609-610 (1966).

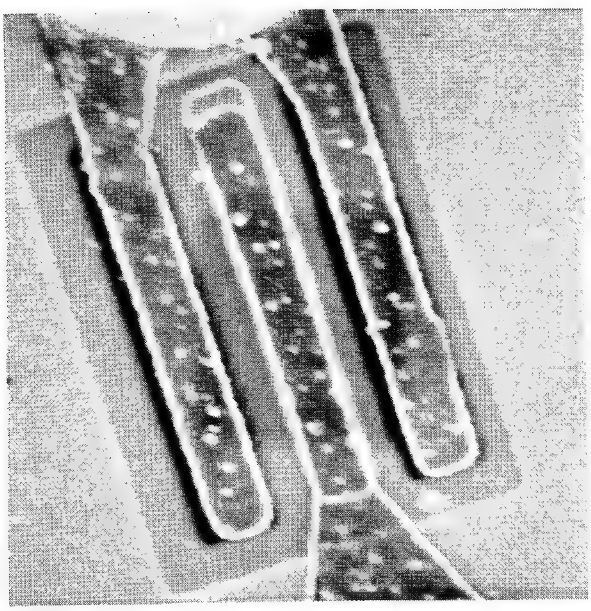

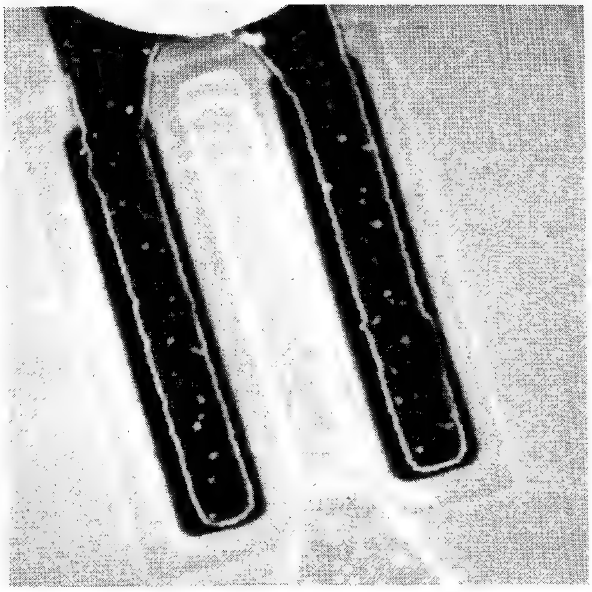

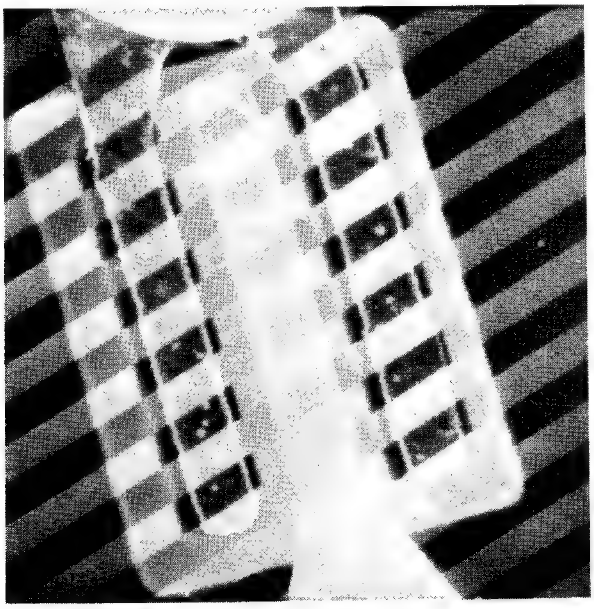

Figure 1 Illustration of the use of square wave biasing to observe voltage contrast effects on a secondary electron image on a transistor. 1(a) with no bias, 1(b) with +8 volts applied to emitter (dark), 1(c) with a +5 volt square wave applied to emitter.

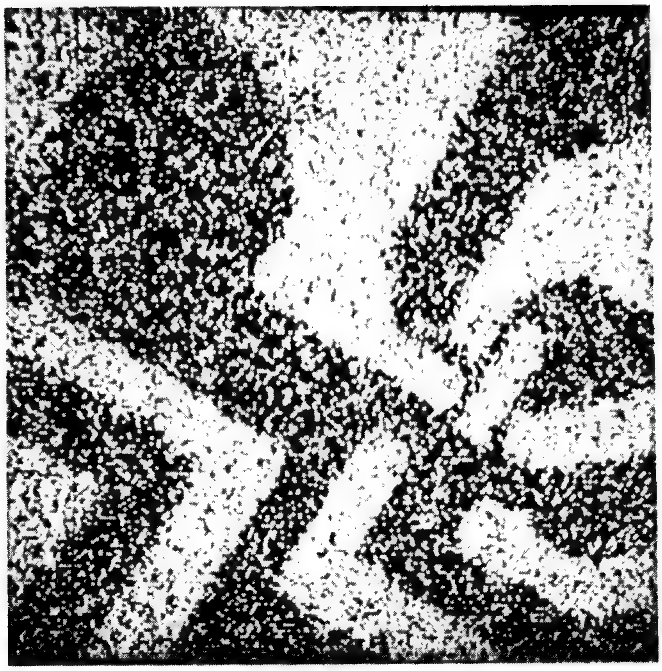

Figure 2 Illustration of the effective background reduction produced by pulse rate analysis: 2(a) without pulse rate analysis: 2(b) with pulse rate analysis.

AN ELECTRON SPECTROMETER FOR THE SCANNING ELECTRON MICROSCOPE

R. E. Ogilvie, J. Adario, and G. Sheldon

Massachusetts Institute of Technology
Cambridge, Massachusetts

The absorption of an electron beam in a specimen is usually followed by the emission of characteristic x-rays and Auger electrons. A continuum of X-rays, and primary and secondary electrons are also produced. An appreciable fraction of the Auger electrons escape from the uppermost layers of the sample without a loss in energy (except for the effective work function of the material). The application of Auger spectroscopy for macro-surface characterization has been well established by Harris [1], and Palmberg and Rhodin [2]. However, there has been little effort in employing Auger spectroscopy on a micro scale.

The purpose of this paper is to describe an electron spectrometer that was designed employing the principles described by Zashkvara et al [3]. This spectrometer, shown in Figure 1, is only 3" long and 2 3/4" in diameter. The electron detector is a Mullard B410AI channel electron multiplier used in the pulse counting mode with a Norelco panel.

The electron-optical properties of the analyzer, in which the field within a coaxial cylindrical condenser operates as an electrostatic mirror, have also been treated in detail by Sar-El [4]. The analyzer built by Sar-El was designed for a 1% energy resolution which was well documented.

The analyzer used in the scanning electron microscope was designed to meet the special limitations of the specimen stage of the Cambridge Stereoscan. In spite of the spacial restrictions, a resolution of better than 0.5% was obtained for electrons scattered elastically from a 1000A film of aluminum as shown in Figure 2. The incident current was $1 \cdot 10^{-8}$ amps and the irradiated area was less than one-micron in diameter, in contrast to the much larger incident currents and irradiated areas used by Harris [1] and Palmberg and Rhodin [2].

Very weak Auger electron peaks from NaCl have been observed. However, we have not as yet enhanced the sensitivity by electronic differentiation of the energy distribution function as described by Harris [1]. With the large solid angle that can be employed in this analyzer (3% - 4% of 4π steradians) and with incident currents of $1 \cdot 10^{-7}$ amps, it should be possible to analyze

sub-micron dust particles. By doing this type of analysis on the scanning electron microscope it is possible to select a particular particle for analysis, by examination of the sample displayed on the cathode ray tube.

---

1. L. A. Harris, J. Appl. Phys., 39, 1419, (1968).

2. P. W. Palmberg and T. N. Rhodin, J. Appl. Phys., 39, 2425, (1968).

3. V. V. Zashkvara, M. I. Korsunskii, and O. S. Kosmacker, Soviet Phys. - Tech Phys., 11, 96, (1966).

4. H. Z. Sar-El, Rev. Sci. Instr. 38, 1210, (1967).

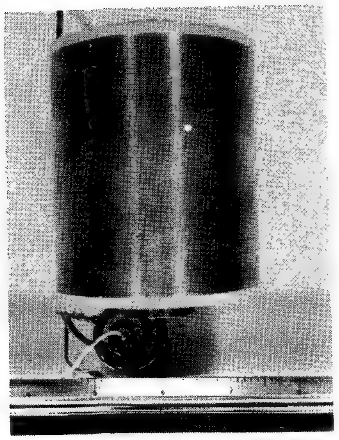

Figure 1

Electron Velocity Analyzer

for use in the scanning electron microscope

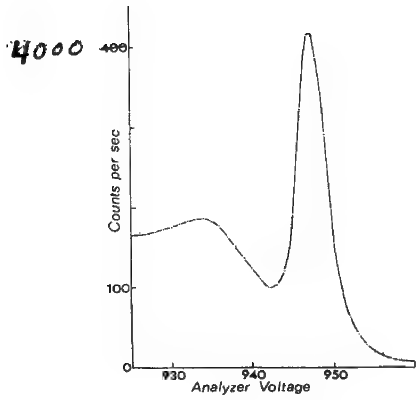

Figure 2

Tranmission electron energy distribution of 1,330 ev. The specimen was a 1000A aluminum film of a carbon cooled electron microscope grid.

A HIGH RESOLUTION ELECTRON MICROSCOPE WITH EFFICIENT X-RAY MICROANALYSIS FACILITIES

C. J. Cooke

Tube Investments Research Laboratories
Essex, England

I. K. Openshaw

GEC-AEI (Electronics) Limited
Essex, England

The advantages of combining transmission electron microscopy and electron probe microanalysis in one instrument have been described by several authors (1, 2, 3) and a number of manufacturers now offer attachments aimed at achieving this combination (4). The present instrument is based on a commercial high resolution electron microscope (AEI EM802) to which has been added a new centre section containing a probe forming lens and supporting two linear focussing spectrometers and a non-dispersive X-ray detector. The specimen is retained in the normal position inside the objective lens of the microscope with its plane at right angles to the electron beam, thus giving an aberration limited resolution in transmission of 3 AU with all the normal microscope facilities still usable.

For microanalysis, a 2000-3000 AU probe is produced by a minilens, (5), placed close above the microscope objective lens. The spherical aberration coefficient of the final probe forming lens is about 2cm. The minilens is water-cooled and capable of focussing the probe at all microscope operating voltages up to 100 kV, at which the current loading in the winding area is as high as 3000 amps/cm^2 of winding area. The optimization of the electron optics of the probe forming system will be described in some detail.

The two spectrometers are each of 6" Rowland circle radius, cover a Bragg angle range of 15-70° and have four crystals interchangeable at any angle under vacuum. The X-ray take-off angle is 45° with the spectrometers nearly horizontally opposed, the planes of the Rowland circles being vertical. The spectrometers are designed for high collection efficiency, the solid angle of acceptance of the crystal at 30° Bragg angle being .015 steradian, giving, for example, a counting rate of 1.5×10^6 counts/sec./μA probe current for $CrK\alpha$ radiation from solid chromium at 40 kV. with a LiF crystal. Steel tapes are used both to control the focussing geometry and to drive the spectrometers, which are provided with servo, as well as manual and slow scan controls.

Whilst the emphasis throughout will be on the design of the instrument, some applications will be described. These will include the analysis of asbestos particles extracted from human lungs and the examination of extraction replicas supporting particles from various steels. These applications will be used to illustrate the three advantages of the instrument:

1. The ability to analyse particles down to 1000 AU in size.

2. The ease of location of areas for analysis in a transmission image.

3. The ability to select areas as small as 2000 AU in diameter for selected area diffraction.

---

1. Duncumb, P., The Electron Microprobe, Wiley, New York, (1966), p. 490.

2. Cooke, C. J., Duncumb, P., 5th International Conference on X-Ray Optics and Microanalysis, Tubingen, 1968. Proceedings to be published by Springer-Verlag.

3. Schippert, M. A., Moll, S. H., Ogilvie, R. E., Analytical Chem., 39, 867, (July, 1967).

4. Poole, D. M., Martin, P. M., Metals and Materials Metallurgical Review No. 133, 14, 61, (1969).

5. Le Poole, J. B., Proc. 3rd. Eur. Conf. on Electron Microscopy, Publ. House Czech. Ac. Sc. Prague, Vol. A, (1964).

THE OBSERVATION OF HIGH RESOLUTION ELECTRON IMAGES IN THE HITACHI ELECTRON PROBE MICROANALYZER

H. Okano, S. Hosoki and T. Tomura

Hitachi Central Research Laboratory
Tokyo, Japan

The Hitachi Electron Probe Microanalyzer can be used in unconventional modes to present additional analytical information. The Model XMA-5 has been adapted for high resolution scanning microscopy where secondary and transmitted electrons are detected. Resolution is equal to that normally achieved with conventional scanning electron microscopes. In addition, we have investigated a new method for producing stereoscopic micrographs with the instrument.

The electron optical and display systems of the XMA-5 were modified; brightness was increased to greater than 10^5 amps/cm^2 sterad., the geometrically calculated probe was less than 100 Å in diameter, and mechanical vibration was reduced to less than 100Å. It was unnecessary to make any adjustments in the stability of either the accelerating voltage or lens current, or in the aberration constant of the objective lens. The amplifier response time was adjusted to conform to a display tube resolvable to 1000 lines/4-inch frame. A scintillation counter was located beneath the specimen for detection of transmitted electrons.

Figure 1 shows secondary electron displays of a fracture surface of a vinyl tube and wild flower pollen. Figure 2 is a pair of stereoscopic micrographs of a renal calculus obtained by the new method. Both left-hand and right-hand images of precisely the same field are easily produced with no tilting of the specimen required. Figure 3 shows transmitted electron images of evaporated gold particles and a molybdenite film which is 3000Å thick. Metallic specimens of this thickness are difficult to image in conventional transmission electron microscopes when working at lower accelerating voltages. In the above figures, the accelerating voltage is 30kV.

In summary, the Hitachi Electron Probe Microanalyzer has the capability for observing specimens with resolution and quality of images equal to those of conventional scanning electron microscopes. The combination of x-ray detection and scanning electron imaging provides much additional information about the specimen.

Fracture surface of vinyl tube

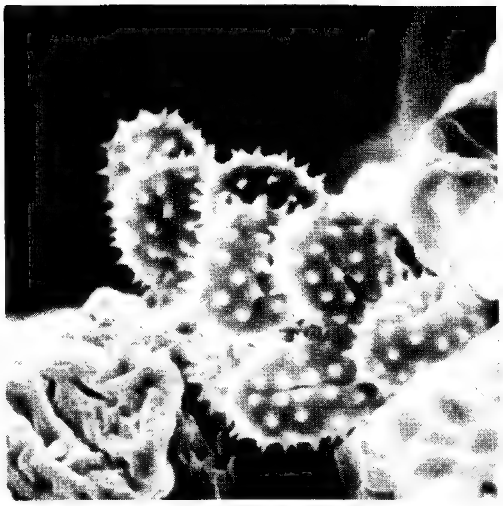

Pollen of wild flower

Fig. 1

Stereoscopic micrographs of a renal calculus

Fig. 2

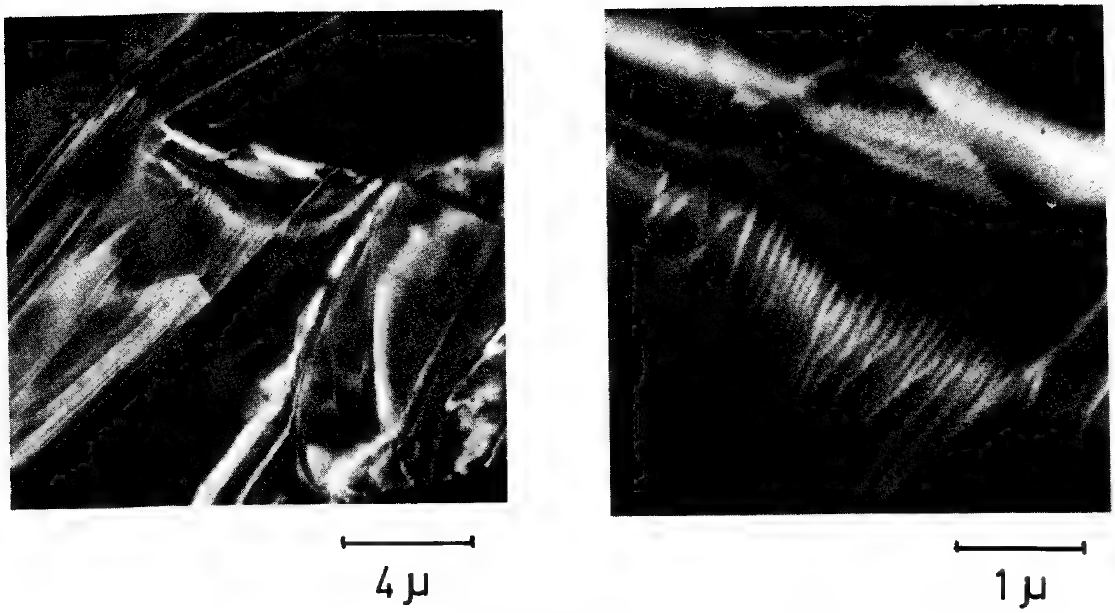

Molybdenite film

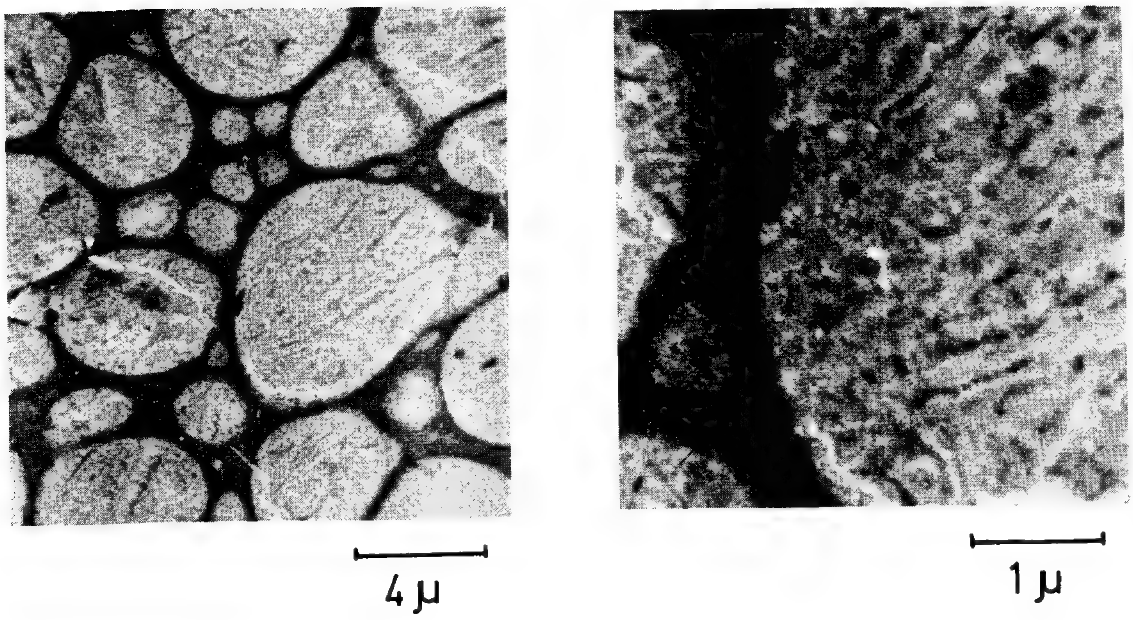

Evaporated gold particles

Fig. 3 Transmission scanning electron micrograph

A NEW SCANNING ELECTRON MICROSCOPE WITH X-RAY MICRO-ANALYTICAL CAPABILITY

R. Buchanan and N. Yew

Materials Analysis Company
Palo Alto, California

With the recent introduction of commercially available scanning electron microscopes, there has been much interest in both improving the scanned imaging capabilities of the x-ray microprobe analyzer, and in adding analytical capability to the scanning electron microscope. The instrument described here adopts the latter approach, namely that of adding elemental analysis to the already numerous capabilities of the scanning electron microscope.

The electron optical column of the microscope comprises a triode electron gun, unitized double condenser lens and objective lens. An adjustable aperture mechanism holding three apertures is located below the double condenser lens which allows the easy selection of optimum beam convergence angles for analysis and image formation. The final probe-forming lens is movable so that the working distance can be varied from zero to two inches. This allows the magnification of the instrument to be varied from 20X to 100,000X without having to break vacuum or resort to deflecting the electron beam through excessively large angles at low magnification, which would result in peripheral defocusing of the image.

A further advantage of the adjustable lens is that it allows the incorporation of a light microscope in the instrument. With the lens in its uppermost position, the light microscope objective can be lowered into position. In addition to being useful for general area selection on the specimen, the light microscope can be used to adjust the height of the specimen so that the point impacted by the electron probe lies on the Rowland Circle of the spectrometer. The microscope objective can then be withdrawn, and the final probe-forming lens lowered for analysis.

As with the rest of the instrument, the x-ray spectrometer is modular in design and is easily attached to or removed from the column as desired. Fully focusing Johansson x-ray optics are used, the Rowland circle radius being 7.75" and the 2θ coverage 40° to 140°. The spectrometer can be operated in vacuum or air and is provided with access ports for changing crystals and detectors. With the range of available crystals all elements in the Periodic Table between Boron and Uranium can be detected. An electron trapping and

baffle system at the entrance to the spectrometer prevents scattered electrons from entering the spectrometer housing, thus assuring good peak to background ratios, especially at low 2θ angles, where the x-ray detector approaches line of sight with the specimen.

The specimen stage, which is completely removed from the instrument for loading, accommodates specimens up to 1" in diameter. Orthogonal linear adjustments are provided which allow any point within a 1" diameter circle to be brought under the beam. In addition, 360° rotation, 0° to 60° tilt and 1/4" height adjustment are provided.

Care has been given to minimizing vibration problems. The instrument column and spectrometer are bolted to a 1" thick steel plate, which is supported on an air isolated anti-vibration system. The vacuum system is held by members attached to the table legs, the only connection to the column being via a flexible metal bellows.

A column isolation valve located below the condenser lens allows the gun to be kept on during specimen exchange, or crystal and detector exchange in the spectrometer. Low specimen contamination is assured by the provision of a multi-coolant baffle on top of the oil diffusion pump and a zeolite vapor trap in the roughing line.

A NEW MICROPROBE

P. S. Ong, C. D. Rudd, N. Galetta and A. Juner

Philips Electronic Instruments
Mount Vernon, New York

The Philips 4500 is a new electron microprobe designed with the following goals in mind:

1. Great flexibility in placing the emphasis on either electron probe microanalysis or on scanning microscopy.

2. Dual take off angle capability to utilize the inherent merits of the low and the high take off angle, and also to allow more accurate quantitative analysis.

3. Future use with a computer.

The electron optical column, shown in Fig. 1, consists of, from top to bottom, an electron gun with adjustable anode distance, an air lock, a double condensor (single for microprobe operation), a variable aperture and the probe forming lens. The distinctive features of the instrument are:

1. A reflective light optic with a N.A. of 0.4, located between the pole piece of the objective lens, looking at normal incidence on the sample and a low power refractive optic looking at 45° at the sample.

2. The X-rays are picked up between the pole pieces at a take off angle of 50°, and also from under the lower pole piece at a 15° take off angle.

3. A variable x-ray slit is located between sample and crystal and in a certain position acts as an airlock with a mylar window. This allows the spectrometer to be operated in air.

4. Two pairs of diametrically located linear spectrometers (with fixed curvature crystals) at 50° take off angle, or one spectrometer at 15° (variable curvature), and one pair at high take off angle, or two low take off spectrometers.

5. The two spectrometers in a pair are spaced 15° apart. A single spectrometer with 50° take off angle is shown in Fig. 2.

6. Scanning microscopy features with either backscatter, secondary emission images, or x-rays.

7. The pumping system consists of a 4" manifold connected at 4 places to the column. The manifold may contain a molecular sieve cooled with liquid nitrogen.

8. Spectrometers are driven by stepping motors and can have a shaft encoder readout.

9. Sample current meter is a digital micro amp meter.

10. The complete instrument is shown in Fig. 2. On the right, resting on the desk, is the control module for the electron column.

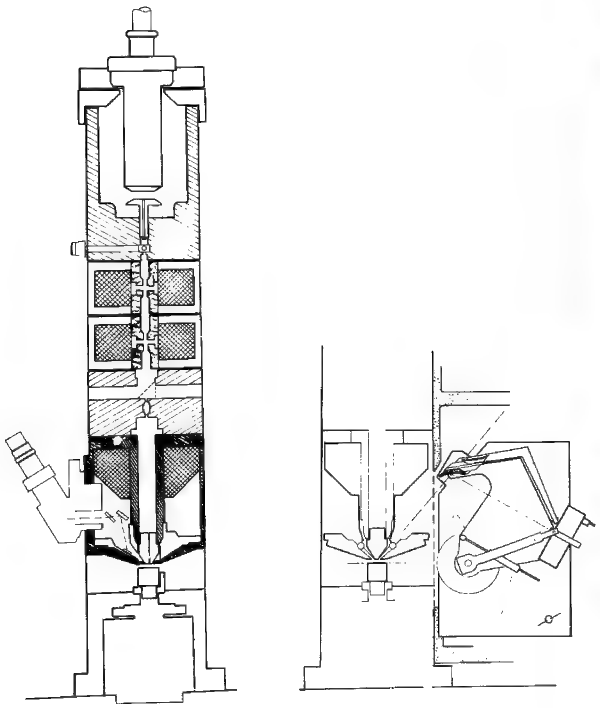

Figure 1

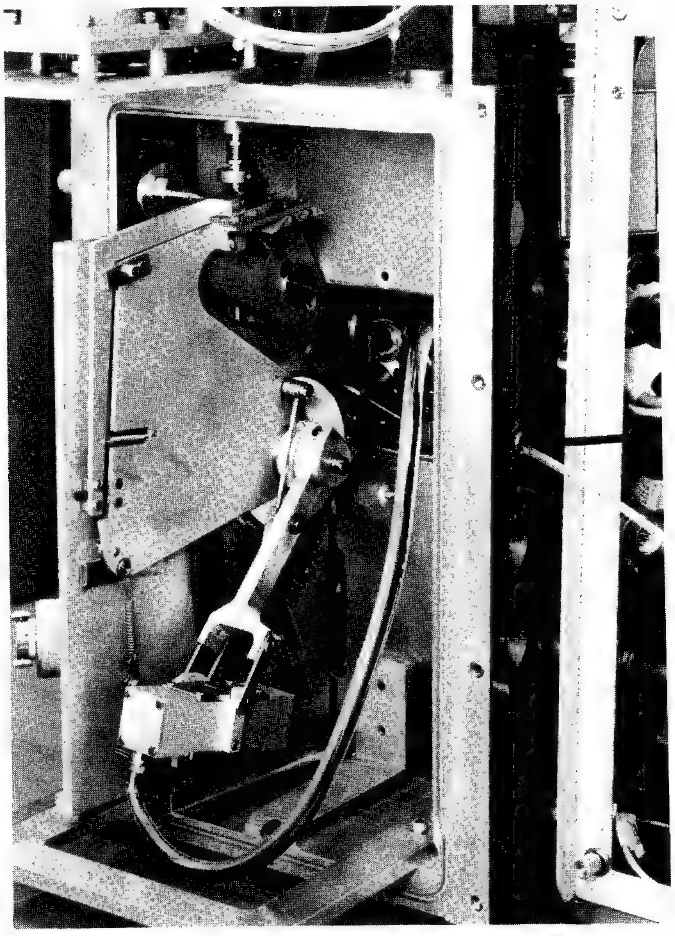

Figure 2

INDEX OF AUTHORS

AND

THEIR AFFILIATIONS

INDEX OF AUTHORS AND THEIR AFFILIATIONS

INDEX OF AUTHORS AND THEIR AFFILIATIONS

INDEX OF AUTHORS AND THEIR AFFILIATIONS

INDEX OF AUTHORS AND THEIR AFFILIATIONS

INDEX OF AUTHORS AND THEIR AFFILIATIONS

INDEX OF AUTHORS AND THEIR AFFILIATIONS

INDEX OF AUTHORS AND THEIR AFFILIATIONS

INDEX OF AUTHORS AND THEIR AFFILIATIONS